FINAL REPORT

RESISTOJET RESEARCH AND DEVELOPMENT - PHASE II

DESIGN, DEVELOPMENT AND FABRICATION OF AN
AMMONIA-FUELED RESISTOJET THRUSTOR SYSTEM

prepared for

NATIONAL AERONAUTICS AND SPACE ADMINISTRATION

December 1966

Contract NAS3-5908

AVCO MISSILES, SPACE AND ELECTRONICS GROUP
MISSILE AND SPACE SYSTEMS DIVISION
RESEARCH AND TECHNOLOGY LABORATORIES
201 Lowell Street
Wilmington, Massachusetts

N67-15847

FINAL REPORT

RESISTOJET RESEARCH AND DEVELOPMENT - PHASE II

DESIGN, DEVELOPMENT AND FABRICATION OF AN
AMMONIA-FUELED RESISTOJET THRUSTOR SYSTEM

prepared for

NATIONAL AERONAUTICS AND SPACE ADMINISTRATION
by
Richard R. John

December 1966

Contract NAS3-5908

Technical Management
NASA Lewis Research Center
Cleveland, Ohio
Electric Propulsion Office
Henry Hunczak

AVCO MISSILES, SPACE AND ELECTRONICS GROUP
MISSILE AND SPACE SYSTEMS DIVISION
RESEARCH AND TECHNOLOGY LABORATORIES
201 Lowell Street
Wilmington, Massachusetts

CONTENTS

CONTENTS (Cont'd)

CONTENTS (Cont'd)

CONTENTS (Concl'd)

Appendixes

ILLUSTRATIONS

ILLUSTRATIONS (Concl'd)

TABLES

TABLES (Concl'd)

I. INTRODUCTION

A. PROGRAM OBJECTIVES

The over-all objectives of this program have been to pursue research and development on ammonia-fueled electrothermal thrustor systems of the resistance type. The resistojet thrustor system under investigation has been defined to include the propellant feed, power conditioning, control logic, sensor, and thrustor subsystems. Thrustor systems were investigated for operation at thrust levels 100 to 1000 micropounds and power levels (to 50 watts) to be compatible with the control requirements and power limitations of satellites in the 1000-pound class. The ultimate objective of the program was to provide the technology required to develop a complete flight-qualified, three-axis resistojet attitude control system.

B. PROGRAM ORGANIZATION

This program originated from the Electric Propulsion Office of the NASA Lewis Research Center. Mr. Henry Hunczak was Project Manager for the NASA Lewis Research Center. The Project Director at Avco/SSD was Dr. R. R. John. The other participants in this program and their principal areas of contribution were: Dr. S. Bennett and Dr. D. Morgan, Mr. W. Huss, Mr. J. Malenda, and Mr. W. Davis, Thrustor and Test System Design and Development; Mr. R. Coulombre, Mr. H. D'Auriol, and Mr. J. Olbrych, System Design and Development.

C. PROGRAM SCHEDULING

This is the final report on Contract NAS 3-5908.

D. SUMMARY

The over-all objective of this program has been to carry-out research and development on resistojet thrustor systems for the attitude and orbit control of satellites in the 500- to 1000-pound class. Program emphasis has been on the development of thrustors for operation at the 100- to 1000-micropound thrust level, and for operation at input power levels of the order of 10 watts.

There are two basic concepts for the low-power resistojet thrustor. These are thermal storage and fast heat-up. In the thermal storage resistojet, thrustor power is continuously supplied to the heater element and only the propellant flow is pulsed. The heat capacity of the thermal storage unit is sufficiently great that the temperature of the heater element remains essentially constant during short propellant pulses. In the fast heat-up resistojet thrustor both the power and the propellant flow are pulsed. In contrast to the thermal storage

device, the heat capacity of the fast heat-up device is held to a minimum. The advantages of the thermal storage device include no thermal cycling, minimum time delay between input signal and resulting impulse bit, and constant power input, which reduces system complexity; the main disadvantage of the thermal storage unit is the high average power consumption, and the resulting large system weight. The primary advantage of the fast heat-up unit is low average power consumption; disadvantages include the necessity for frequent thermal cycling and the existence of a delay time between the input signal and the time that the thrustor is at operating temperature. In the present program primary emphasis has been on the development of the fast heat-up resistojet.

A critical problem in the evaluation of low thrust propulsion devices is the measurement of engine thrust at thrust levels below 10^{-3} pound. During the course of the program two separate thrust measurement techniques have been developed. There are a wire-in-tension thrust stand and an impulse table. The thrust stand has a thrust measurement capability of ± 5 micropounds, and the impulse table has an impulse bit capability of $\pm 10^{-6}$ lb-sec. The basic measurement device for the wire-in-tension thrust stand is a direct measurement displacement transducer; the angular velocity change of the impulse table is measured with on-board rate gyroscopes. Steady-state thrust data for a simple orifice have been obtained on both the wire-in-tension thrust stand and the single-axis wire table; the results from the two facilities were found, within the limits of experimental error, to be in agreement over the thrust range from 50 to 1000 micropounds.

An 11-mil diameter orifice has been operated with cold ammonia at thrust levels from 5 to 1000 micropounds. Although both the orifice coefficient and nozzle thrust coefficient decreased with decrease in thrust level or throat Reynolds number, the measured specific impulse, proportional to the ratio of nozzle thrust coefficient to orifice coefficient, was relatively insensitive to thrust level, down to thrust levels of the order of 5 micropounds. The orifice performance data were obtained at a back pressure of less than 1 micron. At back-pressure levels greater than 1 micron the thrust level was found to decrease with increase in back pressure. The cause of this effect is not clear and is still under investigation.

Experimental studies of a single-pass rhenium heater element indicate that it has a heat transfer capability of greater than 5 watt/cm and an ammonia temperature capability of at least 2000° K (3140° F). The electric-to-gas power efficiency varies from about 75 percent at engine temperatures of 750° K to about 20 percent at engine temperatures of 2000° K. On the basis of mass flow and chamber pressure measurements it is estimated that ammonia dissociation is initiated at about 1250° K and is completed at about 1750° K.

The rhenium fast heat-up thrustor has a maximum specific impulse capability of at least 300 seconds using ammonia as a working fluid. The cold ammonia

specific impulse is about 95 seconds. At the high (300-second) specific impulse levels the over-all electric to thrust power efficiency for the engine is, however, less than 10 percent. The fast heat-up thrustor is thus primarily of interest for low duty cycle applications, or for applications involving very low thrust and power levels.

A single-axis resistojet attitude control and station keeping system has been designed, developed, constructed, and evaluated on the air-bearing attitude control system test bed located at the NASA/Lewis Electric Propulsion Test Facility. The air-bearing attitude control system test bed has a moment of inertia about the vertical axis of about 30 slug-ft^2. The test bed is completely isolated from the laboratory and is selfcontained. Power is supplied by on-board batteries, and communication from the test bed is accomplished by an on-board telemetry system. The over-all purpose of the initial fast heat-up resistojet system tests has been to hold the test bed to 0.50 degree for extended time periods and to thereby demonstrate the feasibility of the fast heat-up resistojet control system concept for an ACS.

The single-axis resistojet control system contains an ammonia feed system, control logic package, power and signal conditioning package, and an on-board position sensor. The propulsion system contains three 10-watt, fast heat-up resistojet engines; two for attitude control and one for station keeping. The telemetry system contains eight input command channels and twenty-four output channels. The control logic package contains circuitry for estimating vehicle angular rate from the position output of the sensor; the control logic is therefore based on both vehicle angular position and angular rate.

The resistojet ACS has been successfully operated on the air-bearing altitude control system test bed located at NASA Lewis. The resistojet ACS has demonstrated acquisition, and both soft and hard limit cycle operation over a range of input disturbance torques from 200 to 1000 dyne-cm.

Preliminary studies have been completed on a three-axis ACS for application to satellites in the 500- to 1000-pound class. Power conditioning for the low-resistance (order of 0.10 ohm) resistojet engines is accomplished by inverting the direct-current power from the power supply into 1000-Hz alternating current, and stepping down the voltage (24 volts to 1 volt) with a lightweight transformer located at the thrustor.

II. RESISTOJET ENGINE DEVELOPMENT

A. REQUIRED ENGINE PROPULSION PERFORMANCE CHARACTERISTICS

1. Minimum Propellant Requirements

In the evaluation of electric or other propulsion devices for the attitude control and station keeping of satellites the main criteria to be considered are system reliability and weight. Further, the relative weights and reliability of the different systems can be compared only within the constraints established by a particular mission. The operating principles of a thrustor can be generalized; however, the propulsion performance required of an attitude control and station keeping thrustor system must be associated with a particular mission.

The major portion of the over-all program effort is currently being concentrated on the development of resistojets suitable for the attitude control and station keeping of a satellite with specifications similar to those shown in Table I.

TABLE I

SATELLITE MISSION AND DESIGN REQUIREMENTS

a.	Satellite Type	Synchronous
b.	Satellite Size	
	Configuration	Right Circular Cylinder
	Weight	500 lbs.
	Roll Moment of Inertia	41.2 slug-ft^2
	Pitch and Yaw Moment of Inertia	32.7 slug-ft^2
	Moment Arm	2 feet
c.	Attitude and Station Tolerances	
	Attitude	± 0.5 degree
	Station	± 0.1 degree
d.	Attitude Disturbance Torques	
	Disturbance Torques	0 to 500 dyne-cm
e.	Lifetime	1 to 3 years

The major vehicle attitude disturbance torque at the 24-hour altitude is due to solar radiation pressure (ref. 1); other torques result from gravity gradient, interaction of on-board electromagnetic fields with external fields, etc. If the assumed 500 dyne-cm disturbance torque acts for 1 year, $(3.15 \times 10^7$ seconds) the minimum required correction angular impulse for a single axis is (500 dyne-cm) x $(3.15 \times 10^7$ seconds) $= 15.7 \times 10^9$ dyne-cm-sec/year/axis or 1170 lb-ft-sec/year/axis. Assuming a 2-foot moment arm for the attitude control thrustors, the minimum required impulse for attitude control is 585 lb-sec/year/axis.

The minimum possible value for the control thrust is given by (500 dyne-cm) / (2 feet) (30.4 cm/ft) = 8.24 dynes or (8.24 dynes) x $(2.248 \times 10^{-6}$ lb/dyne) $= 0.0185 \times 10^{-3}$ lb. The vehicle must thus be controlled by a series of impulse bits, each of which has a greater amplitude than the 1.85×10^{-5} pound required for minimal control of the 500-pound satellite.

The major perturbations on the vehicle orbit are due to earth triaxiality and the sun-moon perturbation (ref. 2). Correction for the sun-moon gravitational perturbations is 163 ft/sec/year, assuming an optimum thrust mode of two nodal firings per day (ref. 3) the earth's triaxiality requires (ref. 3) a correction of 7 ft/sec/year. Thus, the minimum required velocity correction for station keeping is about 170 ft/sec/year. For non-optimum applied thrust modes, this value might increase to 270 ft/sec/year (ref. 2). The minimum impulse to maintain the 500-pound satellite on station for one year is ΔVM = (170 ft/sec) (500 lb/32.2 ft/sec^2) = 2640 lb-sec/year. This value of impulse required for station keeping is to be compared to the 1755 lb-sec/year required for three-axis attitude control. The minimum impulse requirement for the 500-pound satellite is then 4395 lb-sec/year.

The fuel required to produce a given impulse $\int F dt$ is, of course, a function of the specific impulse and is given by $\int F dt / I_{sp}$. Values of the minimum amount of propellant required during a three-year time period for the attitude control and station keeping of the design satellite are presented in Table II and Figure 1. The total effective impulse is 4395 lb-sec/year or 13,200 lb-sec for three years.

It is to be stressed that the preceding propellant requirements are "ideal" values. The "actual" propellant requirements depend on the type of control logic, and the nature and frequency of the applied impulse bits. It is unlikely however, that the actual propellant requirements will be more than a factor of 2 or 3 greater than the values shown in Table II and Figure 1. In the idealized case it is noted that the absolute weight saving in propellant obtained by increasing the specific impulse from 50 to 300 seconds is 220 pounds; this is a considerable fraction of the total 500-pound weight of the satellite. If the weight of the power supply and other equipment required to attain 300 seconds in the attitude control and station keeping
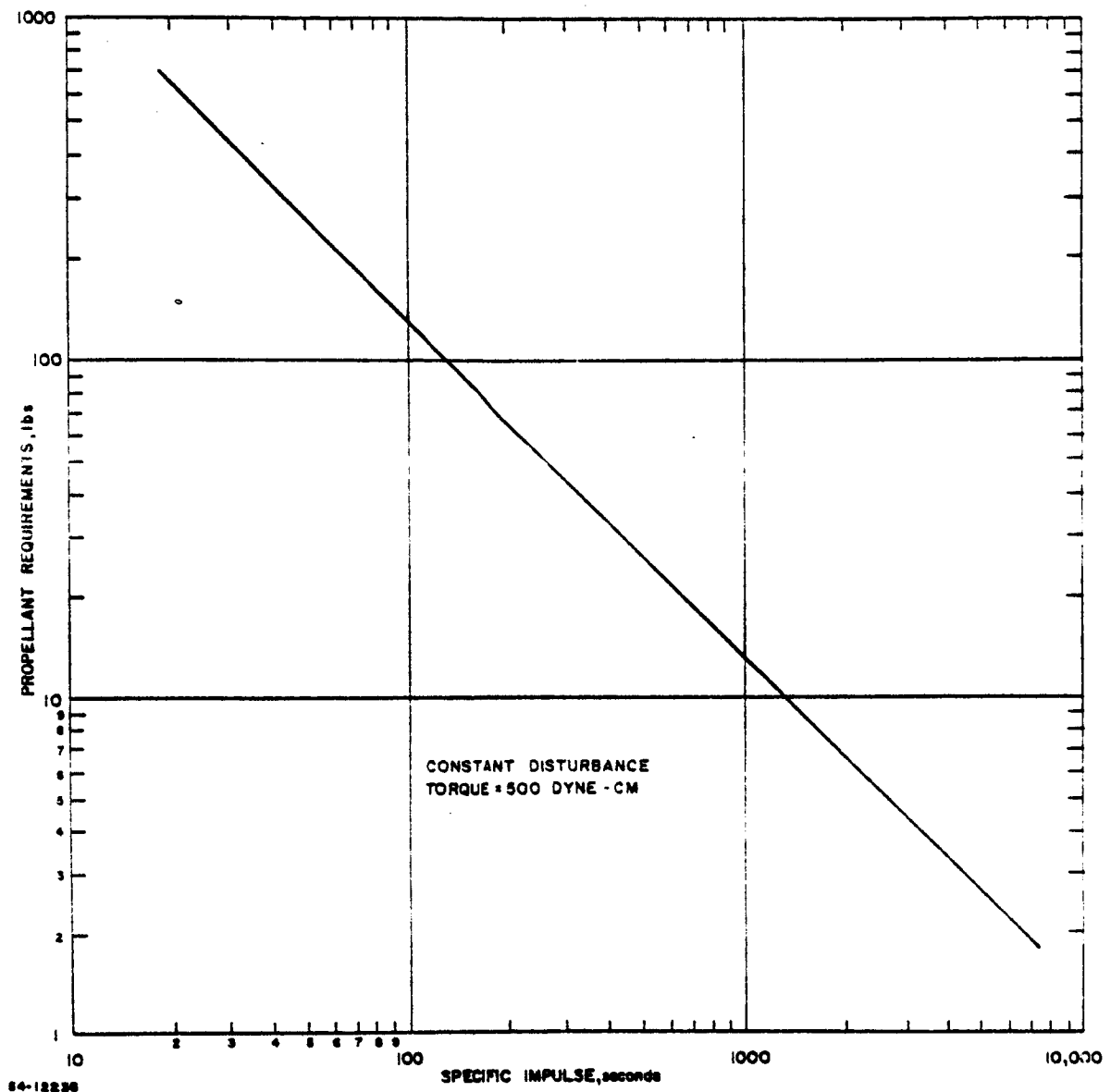
Figure 1 MINIMUM PROPELLANT REQUIREMENTS FOR 3-YEAR ATTITUDE AND ORBIT CONTROL OF A
500-POUND SATELLITE

TABLE II

SATELLITE PROPELLANT REQUIREMENTS (MINIMUM)
(Total Required Impulse 13,200 seconds)

Specific Impulse I_{sp} (seconds)	Propellant Weight for Attitude Control $W_{Prop. AC}$ (pounds)	Propellant Weight for Station Keeping $W_{Prop. SK}$ (pounds)	Total Propellant Weight $W_{Prop., total}$ (pounds)
50	105	159	264
100	52.5	79.5	132
200	26.3	39.7	66
300	17.5	26.5	44
500	10.5	15.9	26.4
1000	5.3	7.9	13.2
5000	1.05	1.59	2.64
10000	.53	.79	1.32

thrustors is considerably less than 220 pounds, there will, of course, be considerable motivation to use the 300-second system.

Thus far attention has been focused on idealized attitude control and station keeping systems. No mention has been made of the size, i. e, thrust and duration, and the frequency of the impulse bits required for actual satellite control. The following sections present a highly simplified discussion of satellite control logic with the purpose of establishing the width, amplitude, and frequency of the applied impulse bits required for satellite attitude and orbit control.

2. Soft Versus Hard Cycle Operation

For a given disturbance torque on the satellite, r_d, there are two basic control cycles for applying the control impulse bit, K_c; these are the soft cycle and the hard cycle. In the soft cycle the disturbance torque, r_d, pushes the vehicle in one direction and the control impulse bit, K_c, pushes it back the other way. The control impulse bits are scheduled such that all the control impulse goes into countering the disturbance impulse. All the propellant is used to counterbalance the disturbance torque. In the hard cycle, on the other hand, some of the delivered impulse counters impulse delivered at the other end of the cycle as well as the applied disturbance impulse. As a result, the propellant consumption in the hard cycle is greater than that for soft cycle operation at a given disturbance torque level. It is, therefore, advantageous to control the attitude of a satellite by means of soft as opposed to hard cycle operation

-8-

In order that soft cycle operation be attained it is sufficient that the control impulse bit be equal to or less than the impulse bit given by the equation (ref. 1) (also see Equation 52).

$$FT_{thrust_{max}} = K_{c_{max}} = \frac{2}{l} [\theta^* I r_d]^{1/2} \tag{1}$$

where, l is the thrustor moment arm, θ^* is the attitude angular accuracy, I is the vehicle inertia, and r_d is the disturbance torque. Thus, the maximum impulse bit which can be used and still have soft cycle operation increases with increase in the attitude angular accuracy, with increase in vehicle inertia and increase in disturbance torque. Values of the maximum impulse bit which can be tolerated for soft cycle operation of the design satellite as a function of disturbance torque are presented in Figure 2.

Referring to Figure 2, assuming a maximum disturbance torque of 500 dyne-cm the control impulse bit must be less than about 5×10^{-3} lb-sec. On the other hand, if the disturbance torque is only 5 dyne-cm, the control impulse bit must be reduced by a factor of 10 to 5×10^{-4} lb-sec in order to assure soft cycle operation.

From Equation (1) it immediately follows that, for a given impulse bit and vehicle, the disturbance torque must be greater than a critical value in order to establish a soft limit cycle. The minimum value of the disturbance torque required to establish soft cycle is given by the equation

$$r_{d)_{min}} = \frac{K_c^2 l^2}{4} \frac{1}{\theta^* I} \tag{2}$$

As might be expected the larger the applied control impulse bit the larger the applied disturbance torque sufficient to bring about a soft limit cycle.

3. Soft and Hard Cycle Propellant Requirements

As indicated, in the soft limit cycle the input disturbance, r_d, is exactly counterbalanced by the average torque introduced by the attitude control thrustors. The basic equation for the total impulse required for soft limit cycle operation is given by

$$\int_{mission} r_d \, dt = \sum_{\substack{all \\ pulses}} l \int F \, dt = N l K_c \tag{3}$$

where, N, is the total number of impulse bits per mission and F is the amplitude of the thrust pulse. The propellant flow during an impulse bit
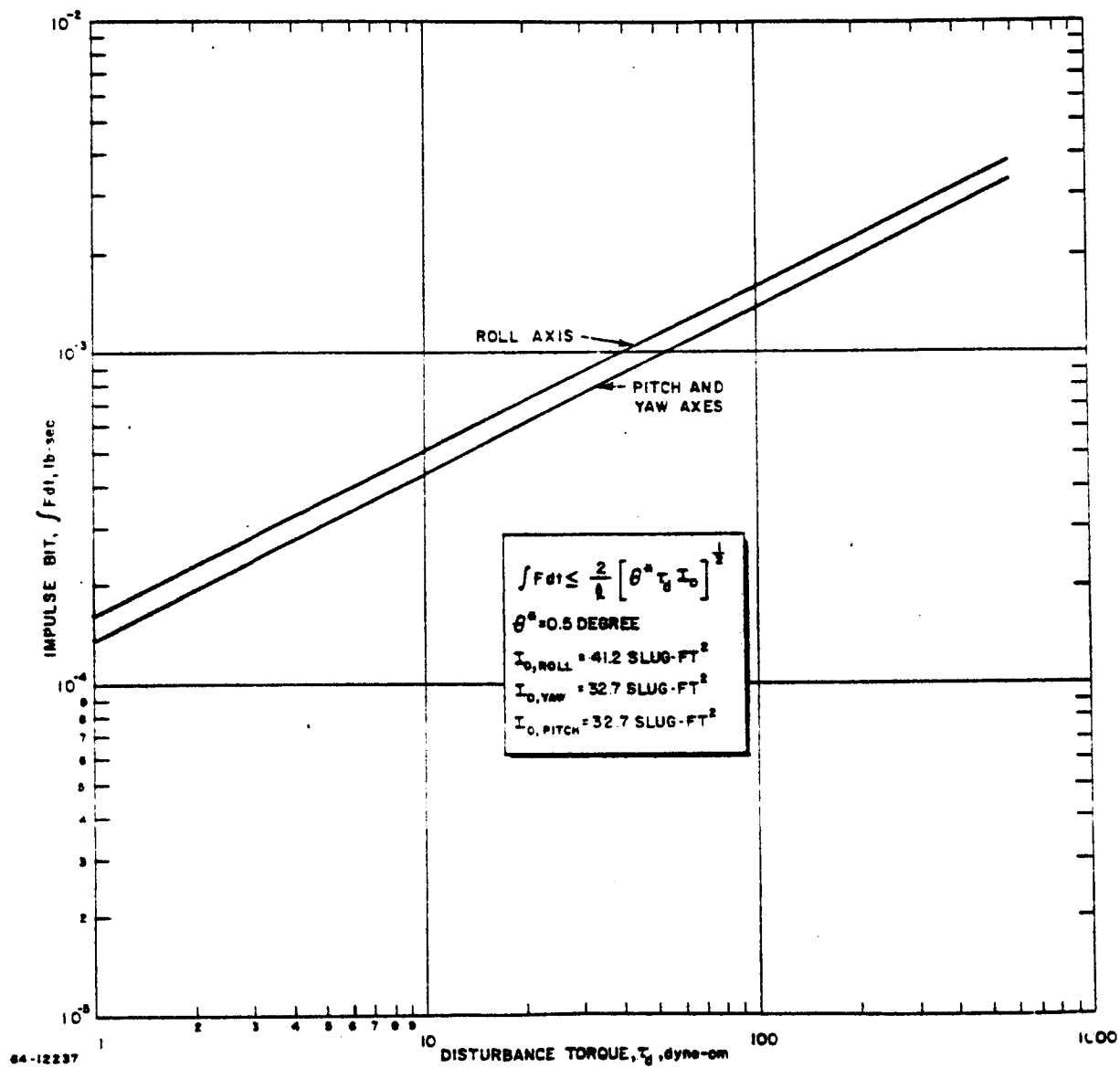
Figure 2 MAXIMUM IMPULSE BIT FOR A SOFT LIMIT CYCLE AS A FUNCTION OF DISTURBANCE TORQUE

is given by F/I_{sp}, the total propellant used during an impulse bit is $\int F dt/I_{sp} = K_c/I_{sp}$. The propellant used during a mission is NK/I_{sp}. Therefore, the propellant weight is given by

$$W_{prop} = \frac{N K_c}{I_{sp}} = \frac{\int_{mission} r_d \, dt}{l \, I_{sp}} = \frac{r_d \, T_m}{l \, I_{sp}} \tag{4}$$

where,

T_m is the total mission time.

The number of cycles is immediately given by

$$N = \frac{r_d \, T_m}{l \, K_c} \tag{5}$$

Referring to Equation (4), the required weight of propellant for soft cycle operation increases linearly with the disturbance torque and mission time and is inversely proportional to the specific impulse. Values of the fuel consumption per axis for a 3-year mission as a function of disturbance torque and engine specific impulse are shown in Figure 3. It is noted that the propellant consumption for soft cycle operation is independent of the absolute magnitude, length or amplitude of the impulse bit, and is only a function of the total value of the disturbance impulse, $r_d T_m$ and not of the individual values of the disturbance torque or mission time. This is not the case, as will be discussed below, for hard limit cycle operation.

In the hard limit cycle the time averaged applied control torque is much greater than the disturbance torque, r_d. The limiting case, of course, occurs when the disturbing torque is zero; in this situation there will always be a hard limit cycle. For the case of zero disturbance it can be shown that the required propellant weight is given by the equation

$$W_{prop} = \frac{l \, K_c^2 \, T_m}{4 \, I \, \theta^* \, I_{sp}} \tag{6}$$

and the number of cycles/mission is given by

$$N = \frac{l \, K_c \, T_m}{4 I \, \theta^*} \tag{7}$$

The hard limit cycle fuel consumption ($r_d = 0$) is thus

proportional to the square of the control impulse bit and inversely proportional to the attitude angular accuracy and vehicle inertia. Clearly, to
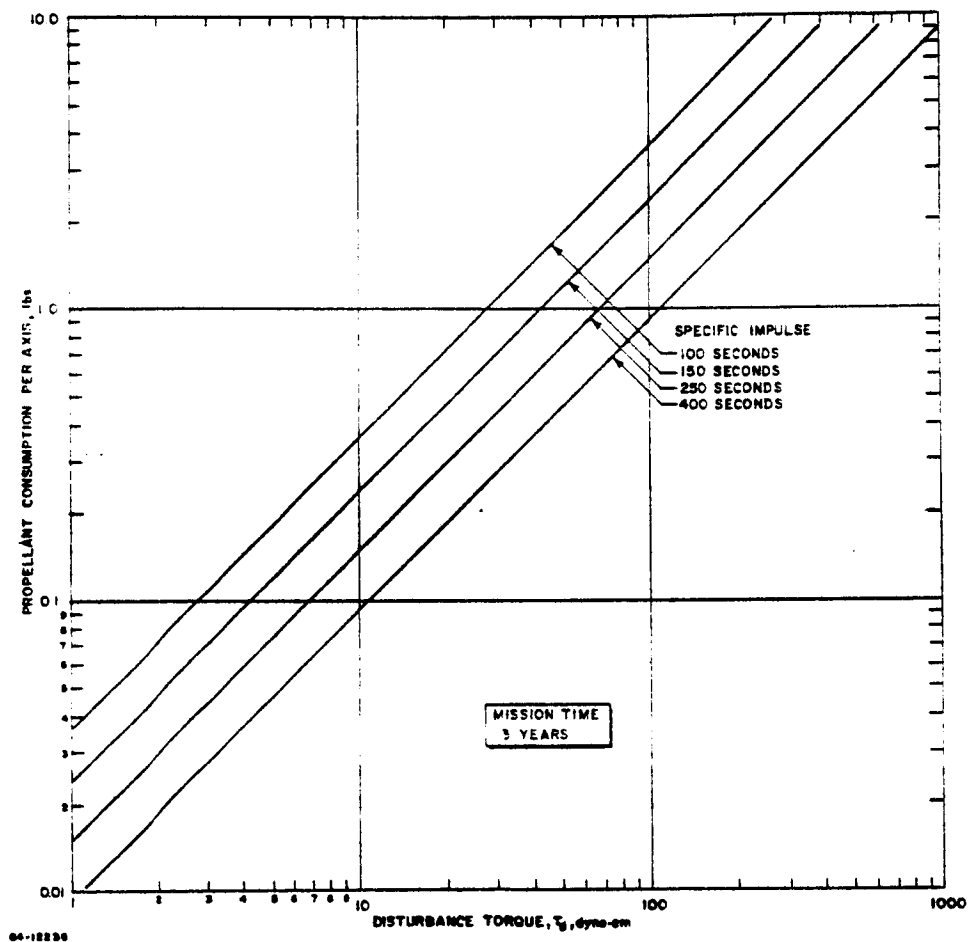
Figure 3 PROPELLANT CONSUMPTION VERSUS DISTURBANCE TORQUE AND THRUSTOR SPECIFIC IMPULSE

-12-

reduce the hard limit cycle fuel consumption the applied control impulse bit must be kept small. An increase in the control impulse bit by a factor of 10 will increase the fuel consumption by a factor of 100.

For example, if l = 2 feet, K_c = 10^{-3} lb-sec, T_m = 9.45 x 10^7 seconds (3 years), I = 41.2 slug-ft^2, θ^* = 0.5 degrees (0.00875 radians) and I_{sp} = 300 seconds, the required propellant weight for zero disturbance torque is 0.44 lb/axis. If the control impulse torque were increased to 10^{-2} lb-sec the propellant weight would rise to 44 pounds.

It is difficult to write a general relation for propellant consumption in the hard limit cycle when $r_d \neq 0$; however, Equation (6) gives a reasonable estimate of the fuel consumption between the disturbance torque at which the system goes into a hard limit cycle and zero disturbance torque.

4. __Duty Cycle Requirements (No Warmup Period)__

The duty cycle is of interest since it affects the demands on the power supply. The duty cycle is defined as the ratio of the time when power is being delivered to the engine to the total mission time. In the case of the resistojet it is possible that the engine will be heated close to operating temperature before the gas is turned on; in this situation the thrust time is less than the power-on time. The present section contains an analysis of the case in which the power-on and thrust times are equal (T_{warmup} = 0) ; in the following section the power-on time is assumed to be greater than the thrust time ($T_{warmup} \neq 0$).

In the soft limit cycle the total impulse delivered in the course of the mission exactly counterbalances the disturbance impulse. From Equation (5) the duty cycle, η, is given by

$$\eta = \frac{NT_{thrust}}{T_m} \frac{r_d}{lF} \tag{8}$$

The duty cycle is independent of the width of the impulse bit, t_{thrust}, and depends only on the amplitude, F. If the applied torque, F, is large the duty cycle is small.

In the hard limit cycle with r_d = 0 the duty cycle becomes, from Equations (6) and (7),

$$\eta = \frac{FT_{thrust}^2}{4I\theta^*} \tag{9}$$

The duty cycle thus increases with the thrust level and with the square of the thrusting time.

The power input to an electric propulsion thrustor is given by

$$P_{input} = \frac{2.18 \times 10^{-2} \, T \, I_{sp} \text{ watts}}{\epsilon_o} \tag{10}$$

where, T is the thrust in millipounds and ϵ_o is the ratio of thrust power to electric input power. For example, at a thrust of 1 millipound, a specific impulse of 300 seconds, and an overall efficiency of 25 percent the required input electrical power is 26 watts.

In the attitude control thrustor system for a satellite there may be at least nine thrustors. If the duty cycle for each of the individual thrustors is greater than 100/9 or 11.1 percent the basic power supply output must be increased beyond that required for a single thrustor.

5. Duty Cycle Requirements (Warmup Period)

When the thrustor warmup time is not negligible, the duty cycle becomes

$$\eta = \frac{N \, (T_{thrust} + T_{warmup})}{T_m} \tag{11}$$

Therefore, for the soft limit cycle, from Equations (8) and (11) the duty cycle becomes

$$\eta = \frac{r_d}{lF} + \frac{r_d}{l \, K_c} \, T_{warmup} \tag{12}$$

or

$$\eta = \frac{r_d}{lF} \left(1 - \frac{T_{warmup}}{T_{thrust}} \right) \tag{13}$$

If T_{warmup} is small compared to T_{thrust} the duty cycle is unchanged. However, if T_{thrust} is increased to make this the case then either F must be decreased or the impulse bit increases. If F is decreased too much η will become large at large r_d. If the impulse bit is increased too much the hard cycle will occur for larger r_d and propellant consumption will increase.

In the case of $r_d = 0$ with a hard limit cycle Equation (9) becomes

$$\eta = \frac{lF \, T_{thrust}^2}{4 l \theta^*} \left(1 + \frac{T_{warmup}}{T_{thrust}} \right) \tag{14}$$

-14-

Thus, for the hard duty cycle, if the warmup time is equal to the thrust time the duty cycle is increased by a factor of 2.

6. **Impulse Bit Length and Thrust Amplitude Requirements for Satellite Attitude Control**

From the relations presented in the preceding sections it is possible to bracket the values of the thrust amplitude and impulse bit length required for satellite attitude control. The satellite under consideration will be that described in Table I.

    a. The minimum tolerable thrust level is a function of duty cycle and disturbance torque and can be determined from Equation (8) for zero warmup time and Equation (13) for positive warmup time. The required duty cycle for any individual thrustor is assumed to be equal to or less than 5 percent, i. e., ≤ 0.05. The maximum disturbance torque is 500 dyne-cm.

    b. At the other extreme one upper thrust limit is fixed by the duty cycle for hard cycle operation at zero disturbance torque; this limit can be determined from Equation (10) for zero warmup period and from Equation (14) for a positive warmup period.

    c. Finally, another upper thrust limit is fixed by the requirement that it is advisable, from the viewpoint of propellant consumption, to hold soft cycle operation to as low a disturbance torque level as possible. The minimum thrust requirement is given by Equation (1); for purposes of calculation it is assumed that the soft cycle is to be held to a disturbance torque of 50 dyne-cm.

Results of calculations from the preceding relations are presented in Figures 4 through 8. Figure 4 presents a curve of thrust amplitude, F, versus impulse bit length, T_{thrust}, for zero warmup time. The lowest horizontal line corresponds to the minimum thrust $(0.37 \times 10^{-3}$ pound) compatible with a 5-percent duty cycle and a 500-dyne-cm disturbance torque. A lower value of the applied thrust will result in duty cycle greater than 5 percent per thrustor. The upper value of the applied thrust is fixed either by the requirement for a soft limit cycle or a 5-percent duty cycle at zero disturbance torque. This situation is illustrated in Figure 4. In order to hold a soft limit cycle down to 50-dyne-cm disturbance the applied thrust must be below values given on the curve $FT_{thrust} = 1.15 \times 10^{-3}$ lb-sec. The requirement for a 5-percent duty cycle at zero disturbance torque is less severe and can be established by having the control thrusts below values on the curve given by $FT_{thrust} = 3.55 \times 10^{-2}$ lb-sec. The useful operating area is given by the shaded area in Figure 4. For
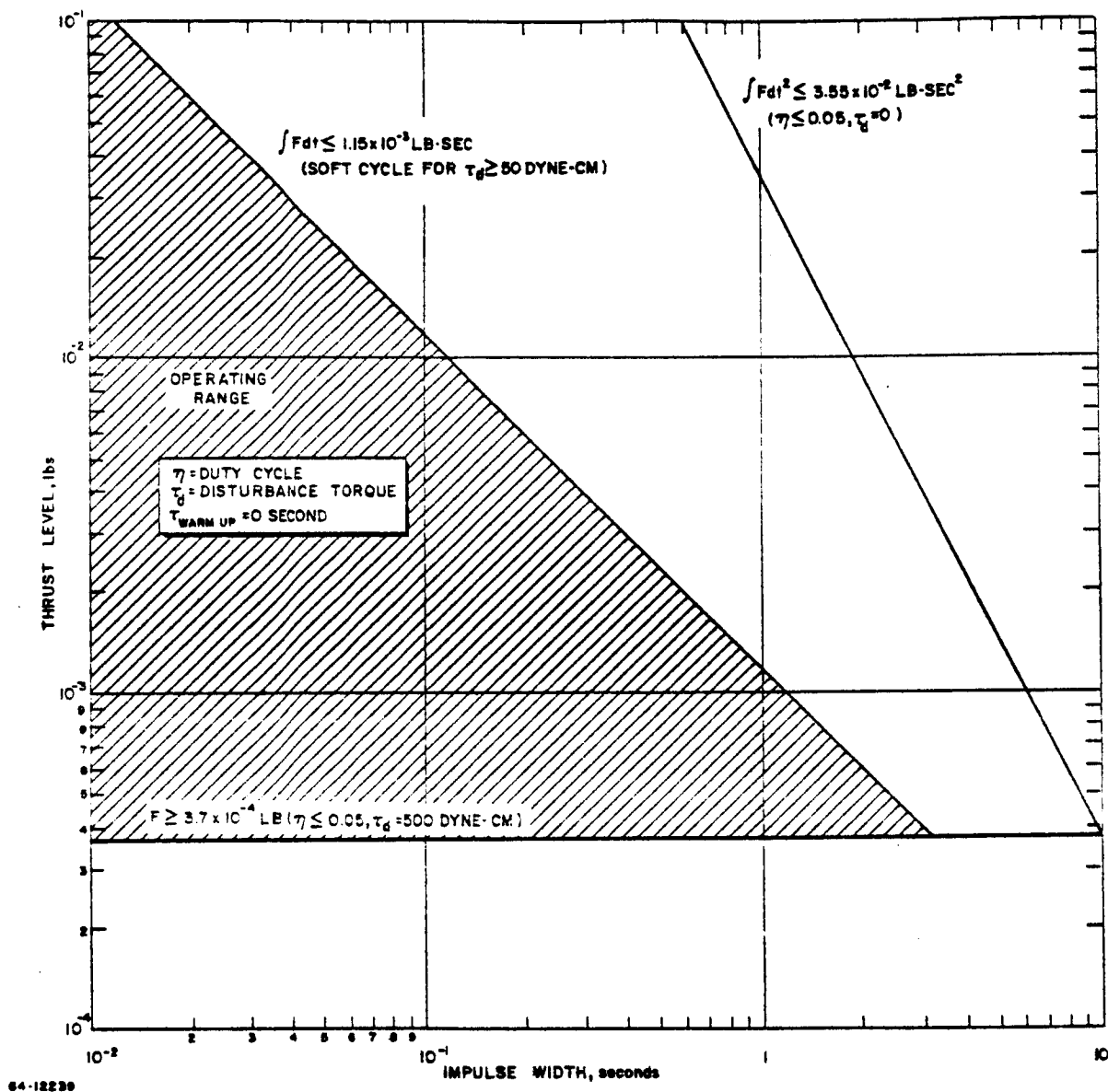
Figure 4 THRUST LEVEL VERSUS IMPULSE BIT WIDTH FOR 0-SECOND WARMUP TIME

64-12239

-16-
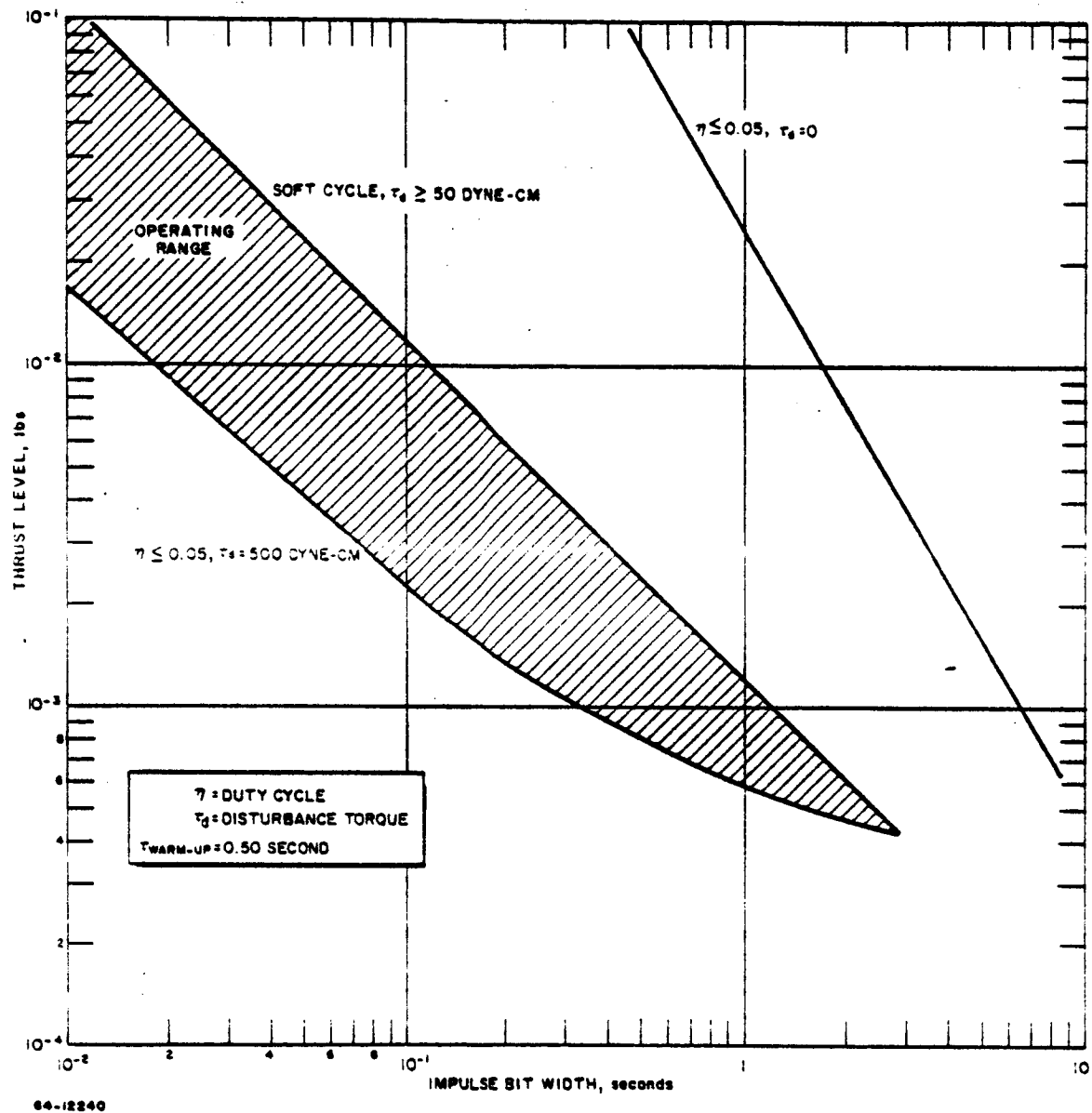
Figure 5 THRUST LEVEL VERSUS IMPULSE BIT WIDTH FOR 0.50-SECOND WARMUP TIME

64-12240

-17-
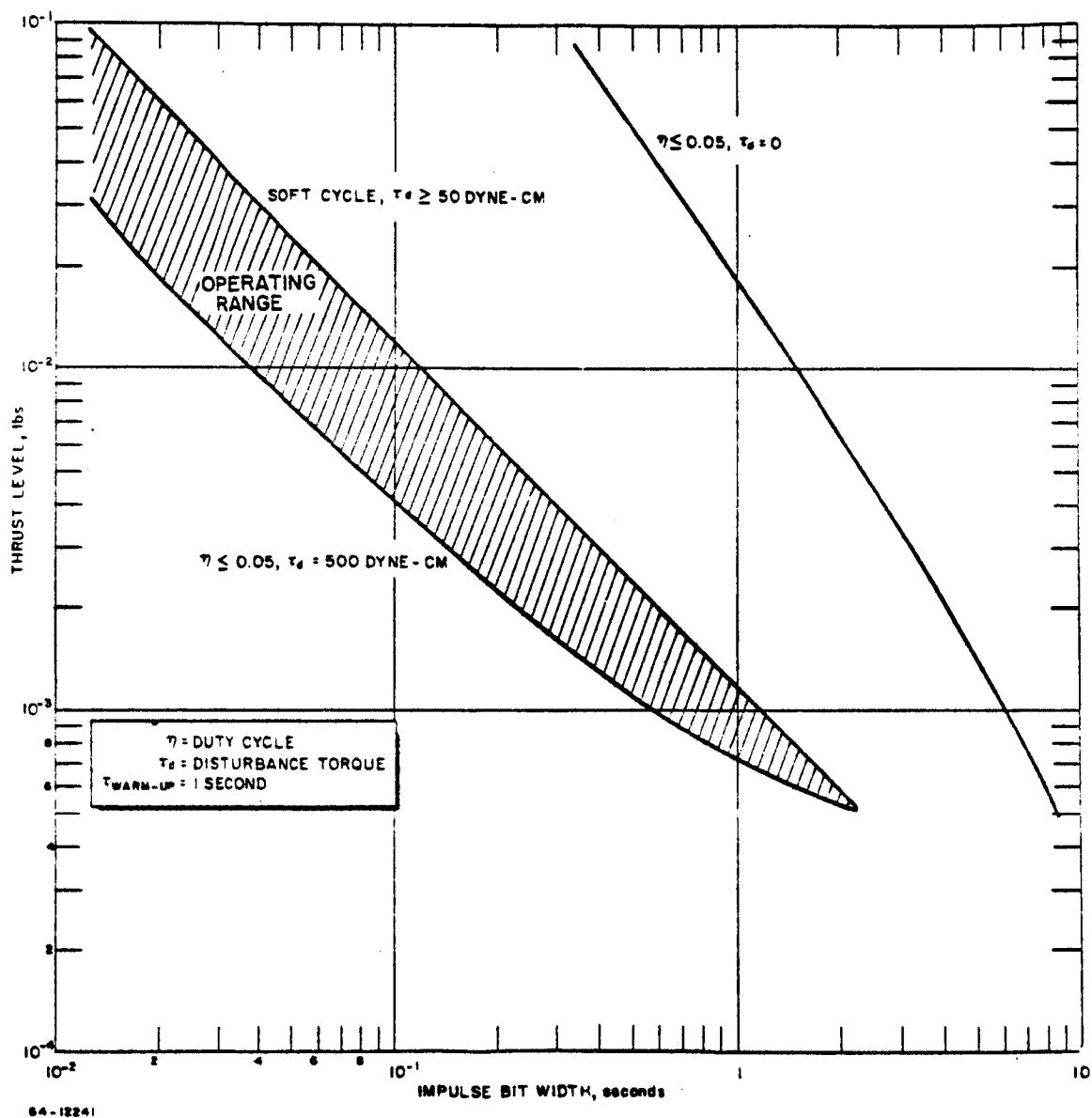
Figure 6 THRUST LEVEL VERSUS IMPULSE BIT WIDTH FOR 1-SECOND WARMUP TIME

64-12241

-18-
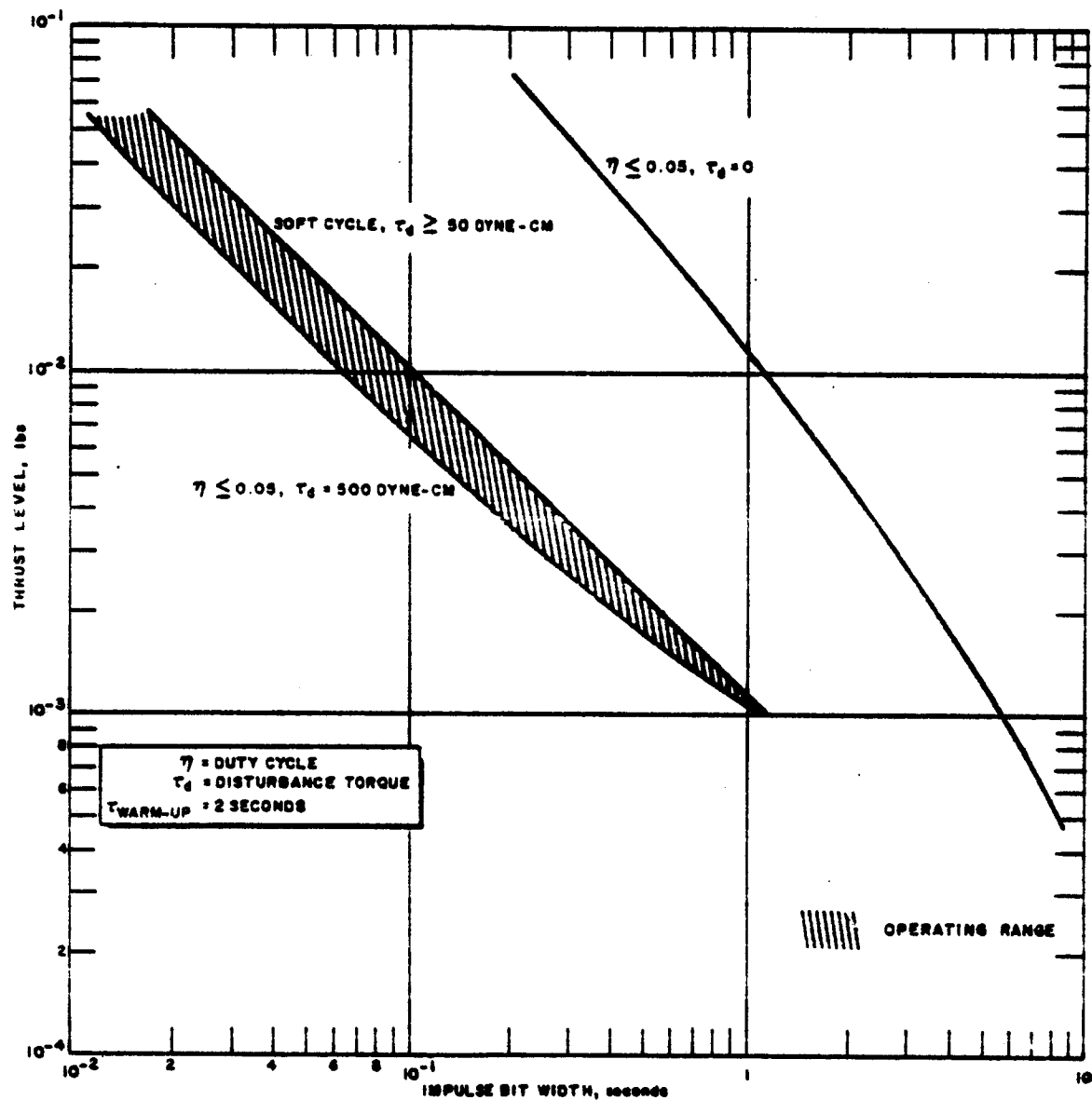
Figure 7 THRUST LEVEL VERSUS IMPULSE BIT WIDTH FOR 2-SECOND WARMUP TIME

64-12242

-19-
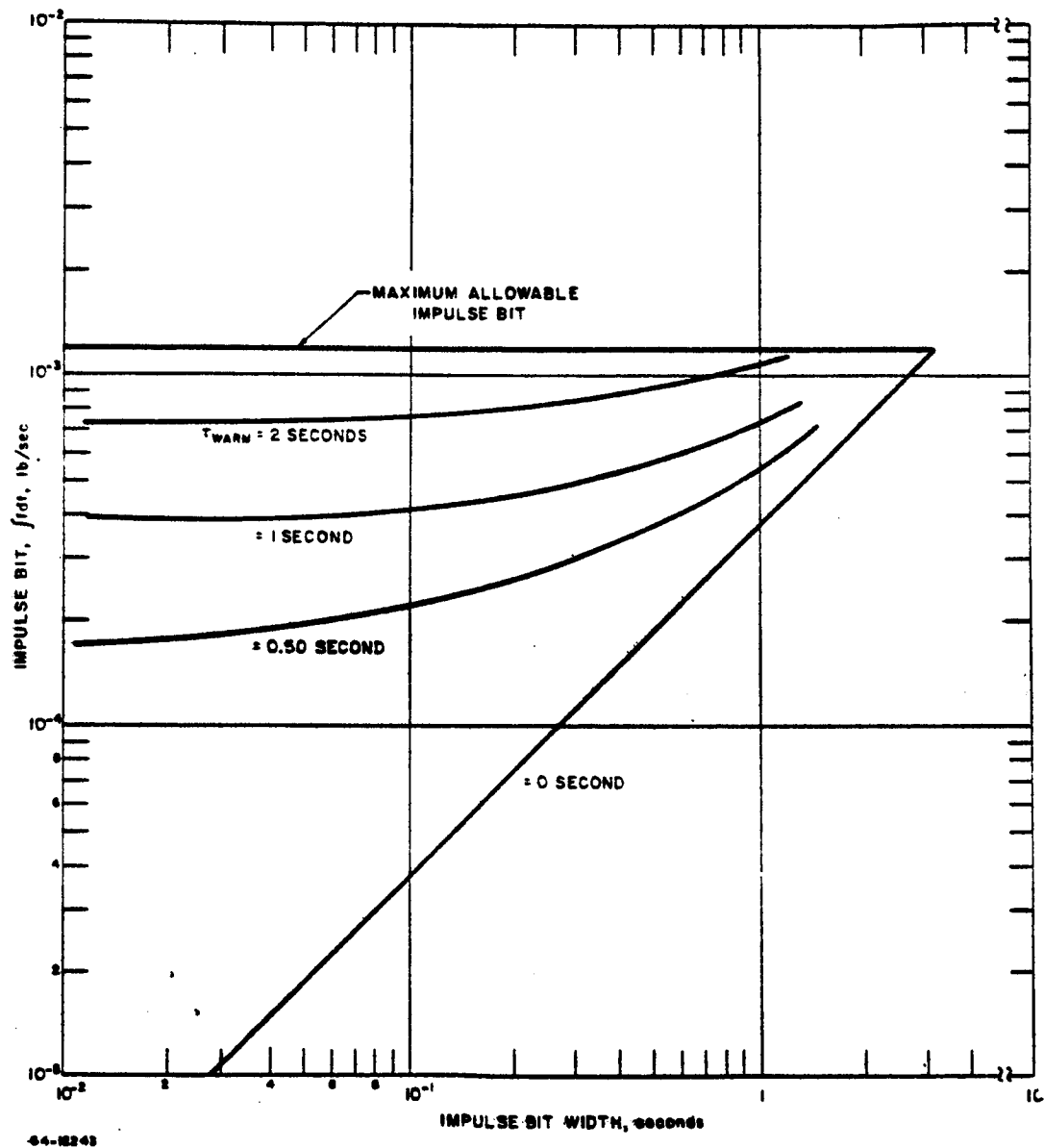
Figure 8 MINIMUM ALLOWABLE IMPULSE BIT VERSUS IMPULSE BIT WIDTH AND WARMUP TIME

64-18243

zero warmup time the thrust should be of the order of 1 millipound, the thrust time of the order of 1 second, and the impulse bit about 10^{-3} lb-sec. At 300 seconds and 25-percent over-all energy conversion efficiency, the power input would be 26 watts.

Figures 5 through 7 present values of thrust amplitude versus impulse bit length for thrustor warmup times of 0.50, 1.0, and 2.0 seconds. In comparison with the results shown in Figure 3 for zero warmup time, the operating range is greatly reduced with increase in warmup time. In particular the very small impulse bits have been eliminated since they would result in excessive duty cycles at the larger disturbance torques. In all cases, up to 2 seconds warmup time, the allowable operating range is determined by the requirements that a soft cycle can be maintained for $r_d \geq 50$ dyne-cm and a duty cycle smaller than 5 percent at a disturbance torque of 500 dyne-cm.

The results are summarized in Figure 8. Impulse bit size is plotted as a function of thrust time. The horizontal lines give the maximum allowable impulse bit in order to maintain a soft limit cycle for $r_d \geq$ 50 dyne-cm. The other lines indicate for warmup times of 0, 1/2, 1, and 2 seconds the minimum impulse bit to keep the duty cycle of each thrustor less than 5 percent at a disturbance torque level of 500 dyne-cm. The following conclusions can be reached from Figure 8.

1) Increase in warmup time increases the minimum allowable values of the control impulse bits. Since small input bits are desirable to maintain a soft cycle at the lowest values of the disturbance torque, r_d , and to reduce the propellant consumption, it is desirable to minimize the warmup time.

2) At a given warmup time, some reduction in impulse bit can be achieved by reduction in the thrust time. For warmup times in excess of 0.50 second, however, little reduction can be achieved in the size of the minimum impulse bit by reduction in the thrust time below 500 milliseconds.

3) Thrust times in excess of 3 seconds and warmup times much greater than 2 seconds will violate either the duty or soft cycle boundary conditions. The maximum allowable power on time will thus be about 5 seconds per pulse. Assuming an upper power limit of 100 watts per thrustor, an operating temperature of 2000° K, and a tungsten thrustor, the thrustor will have to weigh much less than 250×10^{-3} grams to permit it to come up to operating temperature in the allowable time.

4) It appears clear that with anticipated warmup times of the order of 1-second duty cycles substantially less than 5 percent will be hard to achieve.

7. Impulse Bit Length and Thrust Amplitude Requirements for Satellite Station Keeping

The station keeping system operates in a substantially different mode than the attitude control system. The major contribution to the total impulse required to maintain the orbit of a stationary satellite is the effect of solar-lunar attraction. The total impulse required each day to correct the solar lunar-perturbations is 7.2 lb-sec/day ($M\Delta V$ = 15.6 slugs x .461 ft/sec/day) assuming two nodal firings per day. If the thrust is applied continuously the total impulse required to correct the solar lunar perturbations can be as much as 11.7 lb-sec/day. At a specific impulse of 300 seconds 7.2 lb-sec of impulse/day requires 26.2 lbs of propellant for a 3 year mission, while 11.7 lb-sec/day of impulse requires 42.6 lbs of propellant. Including a tankage factor the propellant weight penalty for continuous rather than impulsive thrusting can be as much as 20 pounds.

Table III presents values of the total thrusting time per day as a function of thrust level to obtain the required 7.2 lb-sec of impulse. Also included in Table III are values of the required thrustor power assuming a 300 second specific impulse level and an overall energy conversion efficiency of 25 percent.

TABLE III

REQUIRED THRUST TIME VERSUS THRUST LEVEL
(Total Impulse 7.2 lb-sec)

Thrust Level (millipounds)	Total Thrust Time (hours)	Nodal Thrust Time (hours)	Thrustor Power (watts)
0.50	4.00	2.00	13.1
1.00	2.00	1.00	26.2
5.00	0.40	0.20	131
10.00	0.20	0.10	262

Referring to Table III it is likely that at thrust levels greater than 1×10^{-3} to 2×10^{-3} pounds the input ΔV can generally be considered to be impulsive; at thrust values less than 1×10^{-3} more than 7.2 lb-sec of impulse will probably be required to make the North-South correction. Exact calculations, presently in progress, will be required to evaluate the magnitude

-22-

of the increase in required impulse. From the results obtained to date, however, it appears that station keeping thrustor will operate at between 1 and 2 millipounds, power levels between 25 and 50 watts, and for time periods of the order of 30 to 60 minutes.

The total energy requirement per station keeping pulse is about 25 watt-hours. The batteries required to store 25 watt-hours of energy (assuming 50-percent depth of discharge and 10 watt-hours/lb) weigh about 5 pounds. The batteries can be charged with about 2 watts of solar cells which at 0.25 lb/watt (ref. 4) weigh only about 0.50 pound. Thus, the station keeping requirement appears quite feasible.

8. **Summary of Resistojet Performance Characteristics Required for Satellite Attitude and Orbit Control**

The resistojet performance characteristics required for the attitude and orbit control of a 500-pound satellite (see Table I) assuming a maximum disturbance torque of 500 dyne-cm, soft limit cycle operation at disturbance torques greater than 30 dyne-cm, and a maximum 5-percent electric power input duty cycle per axis is presented in Table IV.

TABLE IV

RESISTOJET PERFORMANCE CHARACTERISTICS REQUIRED FOR
SATELLITE ATTITUDE AND ORBIT CONTROL

	Attitude Control	Station Keeping
Thrust Level, millipounds	0.50-1.0	1.0-2.0
Thrust Time, seconds	0.50-1.00	1000-5000
Impulse bit, pound-second	$0.50\text{-}1.00 \times 10^{-3}$	1-10
Warmup Time, seconds	1	--
Power Level, watts	10-30	25-75

The thrustor requirements for attitude control and the requirements for orbit control tend to some extent to overlap each other. Only detailed studies will show whether they should be the same or separate thrustors. In the case of the attitude control thrustors by reducing the thrust level and increasing the thrust time, the operational requirements on the propellant control values are minimized.

B. RESISTOJET DESIGN PHILOSOPHY

There are two basic concepts for the pulsed, low power resistojet thrustor. These are thermal storage and fast heat-up. Schematic diagrams of the two basic thrustor types are shown in Figure 9.

A. THERMAL STORAGE RESISTOJET THRUSTOR

EXIT NOZZLE

SHIELDS

GAS FLOW

GAS INLET

(1) CONTINUOUS POWER

(2) HIGH THERMAL STO-RAGE CAPACITY

(3) HIGH AVERAGE SYS-TEM POWER CON-SUMPTION

B. FAST HEATUP RESISTOJET THRUSTOR

GAS FLOW

GAS INLET

(1) PULSED POWER

(2) LOW THERMAL STORAGE CAPACITY

(3) LOW AVERAGE SYS-TEM POWER CON-SUMPTION
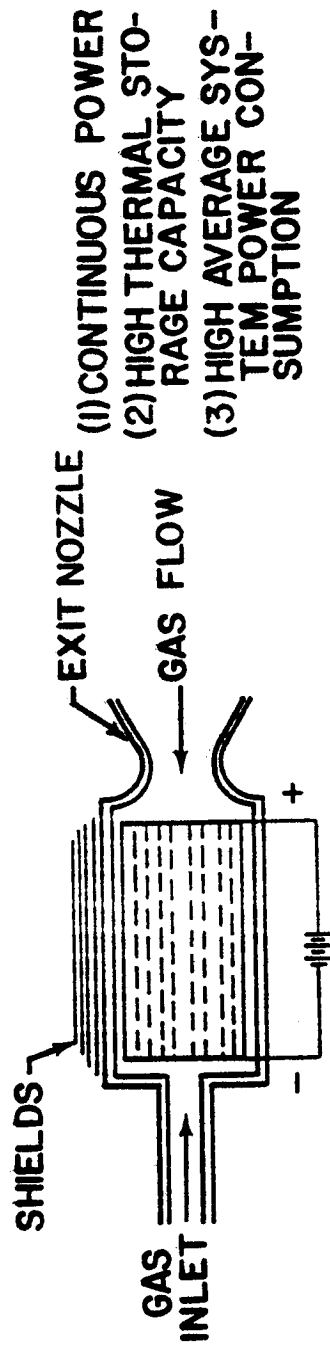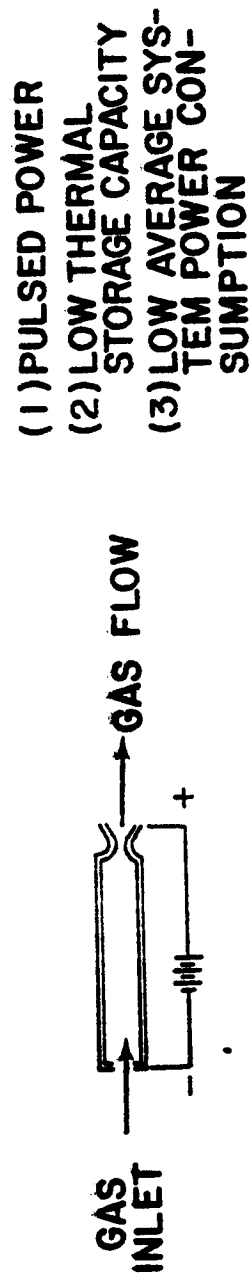
Figure 9 PULSES RESISTOJET CONCEPTS

65-1192

-24-

The thermal storage pulsed resistojet consists of a refractory heater element with a high heat capacity. Power is continuously supplied to the heater element and only the propellant flow is pulsed. The heat capacity of the thermal storage unit is sufficiently great that the temperature of the heater element remains essentially constant during short propellant pulses. The advantages of the thermal storage concept include no thermal cycling, minimum time delay between the input signal and resulting impulse bit, and constant power input which reduces system complexity. A complete satellite attitude control and station keeping system will probably contain ten or more engines. If the engines are thermal storage resistojets they will all have to be continuously supplied with electrical energy. The main disadvantage of the thermal storage engine for attitude control and station keeping is thus the high average system power consumption and the resulting large system weight.

The fast heat-up resistojet consists of a light-weight heater element with a low thermal heat capacity. The heater element of the typical fast heat-up engine shown in Figure 9 consists of a thin-walled, high-temperature metal tube with an integral exit nozzle. The working fluid passes through the electrically heated tube and out of the engine through the exit nozzle. In the fast heat-up thrustor both the power and propellant flow are pulsed. In contrast to the thermal storage device the heat capacity of the fast heat-up unit is held to a minimum. The primary advantage of the fast heat-up engine is that the input electric power does not have to be supplied continuously, and thus there is a relatively low average system power consumption. Disadvantages include the necessity for thermal cycling and the existence of a delay time between the input signal and the time at which the thrustor is at operating temperature.

During the course of the present program, exploratory experiments have been carried out with both fast heat-up and thermal storage units.

The prototype thermal storage unit consisted of a composite tungsten-zirconia heater with axial gas flow passages. The heater was surrounded by radiation shields. The unit weighed approximately 10 grams and at 2000° K had a heat content of 6000 joules. The minimum power input to maintain the thermal storage unit at an operating temperature of 2000° K was established to be of the order of 10 watts (see Appendix C).

The prototype fast heat-up resistojet consisted of a thin-wall rhenium tube which had a 0.38 mm (15 mil) inside diameter, a 0.70 mm (28 mil) outside diameter and was 2 cm long. The fast heat-up thrustor weighed approximately 50×10^{-3} gram and had a heat content of only about 40 joules at 2000° K. (See Appendix B for estimates of the heat-up time.) Operation of the fast heat-up engine at a temperature of 2000° K required a power input of the order of 25 watts. It is important to note, however, that the thermal storage resistojet must be on continuously, whereas, the fast heat-up resistojet must have power on only during the thrust period.

The present program is directed to the development of a combined single-axis attitude control and station keeping system for satellites in the 1000-pound class. The average power level for a fast heat-up thrustor attitude control system operated at a 5-percent duty cycle was estimated to be an order of magnitude lower than for a thermal storage thrustor attitude control system. The thrust level was assumed to be of the order of 500 micropounds and the specific impulse about 150 seconds. Based on these results the major portion of the thrustor experimental effort has been concentrated on the design and development of fast heat-up thrustors.

C. FAST HEAT-UP THRUSTOR--CONFIGURATION AND OPERATING VARIABLES

1. Engine Configuration

A schematic of an experimental fast heat-up thrustor configuration is shown in Figure 10, and a photograph of the unit is presented in Figure 11. The prototype engine consists of a solenoid type gas valve, a pressure transducer, a heating element, and an exit nozzle. The heating element is surrounded by a concentric support tube; the support tube is electrically connected to the nozzle end of the heater element through four support tabs. The support tube is, in turn, separated from the main engine body by an electric insulator. The engine power connections are located respectively on the heater support tube and on the main engine body.

2. Engine Propellant Feed System

A schematic of the propellant feed system is shown in Figure 12. The resistojet gas inlet, located upstream of the solenoid gas valve, is connected to a constant pressure or essentially infinite gas reservoir. Referring to Figure 12, in the case of a propellant which can be stored as a liquid, e.g., ammonia, the reservoir tank pressure is held at a constant value by means of the pressure regulator located between the liquid and gaseous ammonia reservoirs. The liquid reservoir could, of course, easily be replaced by a gas or subliming solid reservoir. During a typical run the power is turned on and the heater element is brought up to temperature; after the element has been brought to temperature and while the power is still on the propellant valve is opened and the propellant is heated as it passes through the tubular heater element and out through the exit nozzle.

It is important to distinguish between the flow system shown in Figure 12 and the flow system shown in Figure 13. The system in Figure 13 was used in the initial heater experiments. In the initial heater experiments, which were carried out with the flow system shown in Figure 13, the propellant flow was choked across the flow metering orifice. The pressure upstream of the flow metering orifice and the area of the flow metering orifice were such that the propellant flow rate was independent of the energy

GAS
IN

PRESSURE
TRANSDUCER

HEATER
TUBE

CURRENT
CONNECTION

EXIT
NOZZLE
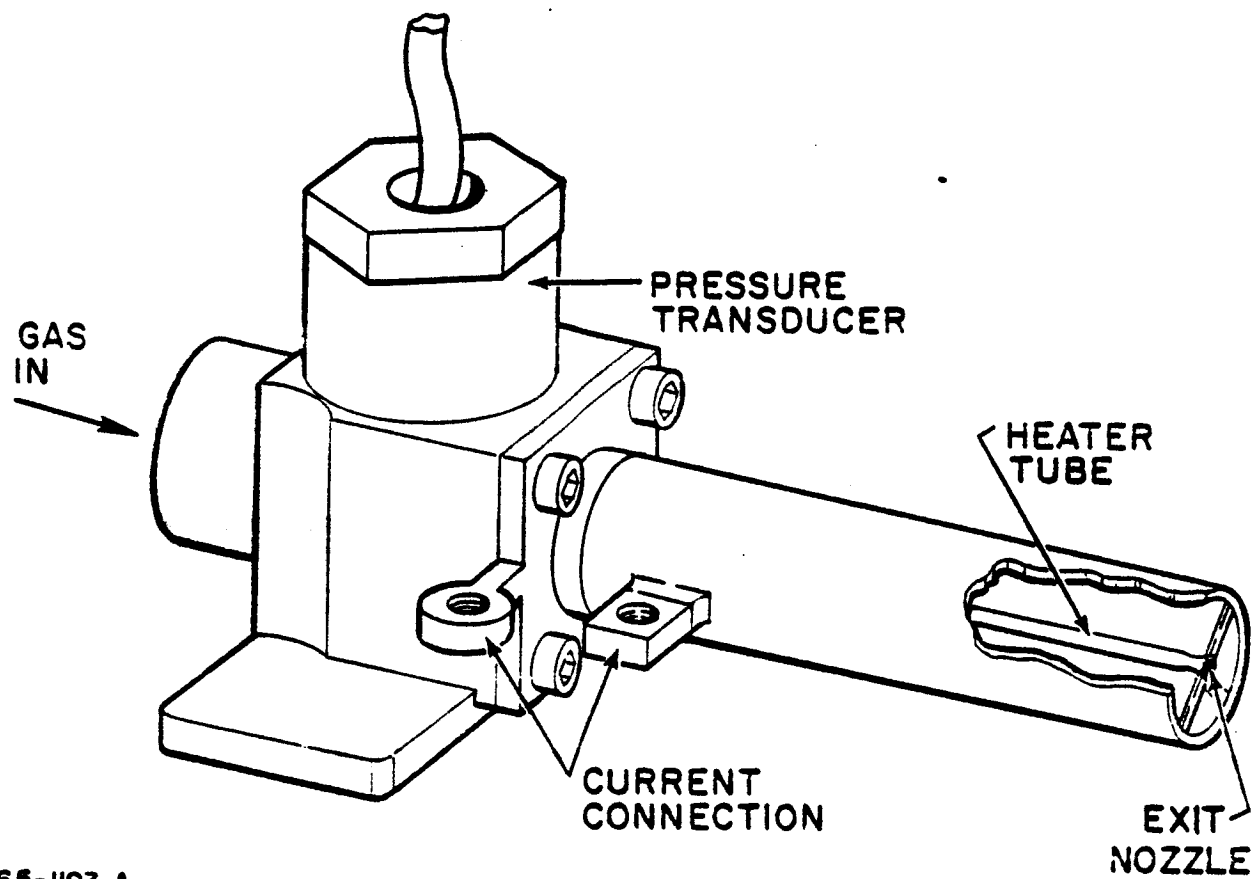
65-1193-A

Figure 10 SCHEMATIC OF AN EXPERIMENTAL FAST HEAT-UP THRUSTOR

LEAD CABLE FROM
PRESSURE TRANSDUCER

SOLENOID OPERATED ON-OFF
CONTROL VALVE

TRANSITION SECTION
CONTAINING PRESSURE
TRANSDUCER

SUPPORT TUBE
SURROUNDING
20 MIL OD RESISTOJET

TABS FOR ELECTRICAL
HOOKUP OF RESISTOJET
HEATER

INCHES
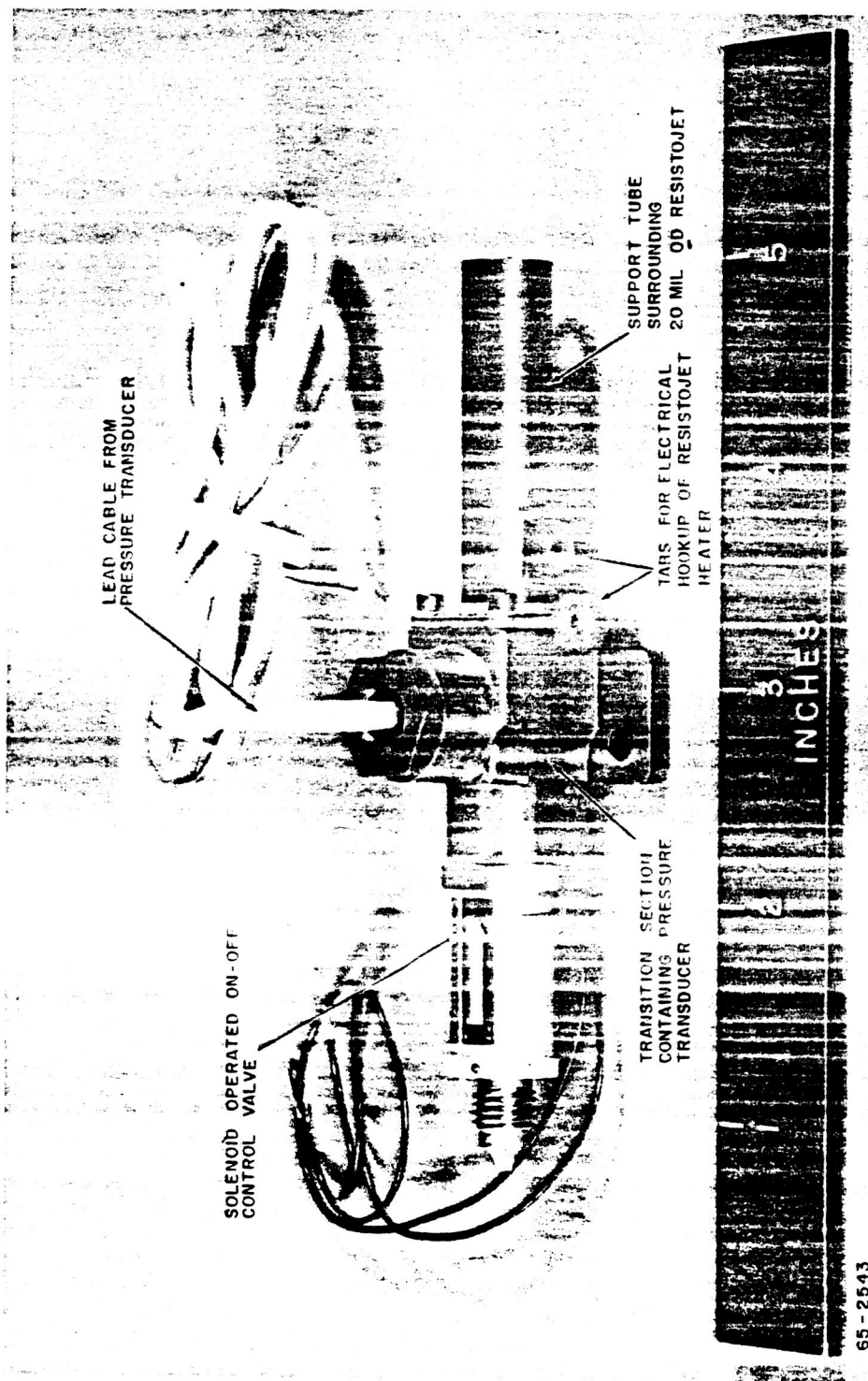
65-2543

Figure 11 PHOTOGRAPH OF A FAST HEAT-UP THRUSTOR

GAS FLOW

PROPELLANT VALVE

$A_{orifice} \gg A_{throat}$

CONSTANT CHAMBER PRESSURE VARIABLE MASS FLOW

FLOW ORIFICE

GASEOUS AMMONIA

SOLENOID

LIQUID AMMONIA

66-2644
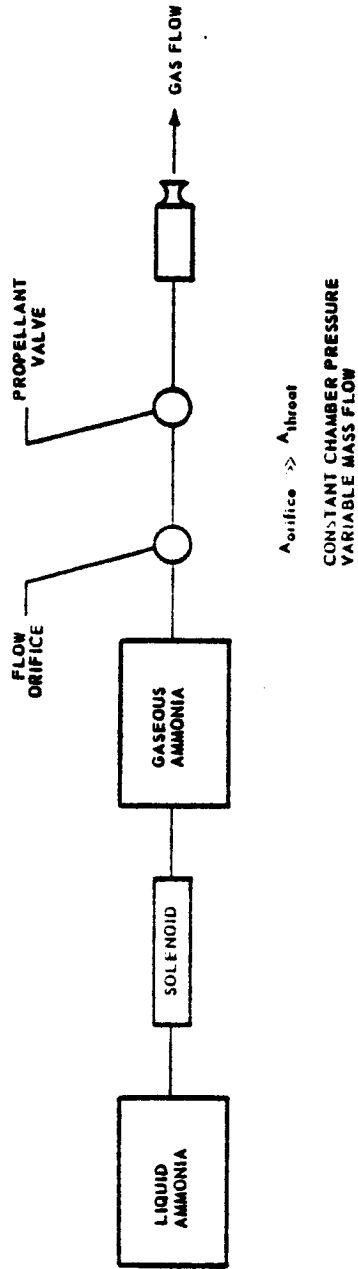
Figure 12   SCHEMATIC DIAGRAM OF A CONSTANT PRESSURE VARIABLE MASS FLOW PROPELLANT FEED SYSTEM
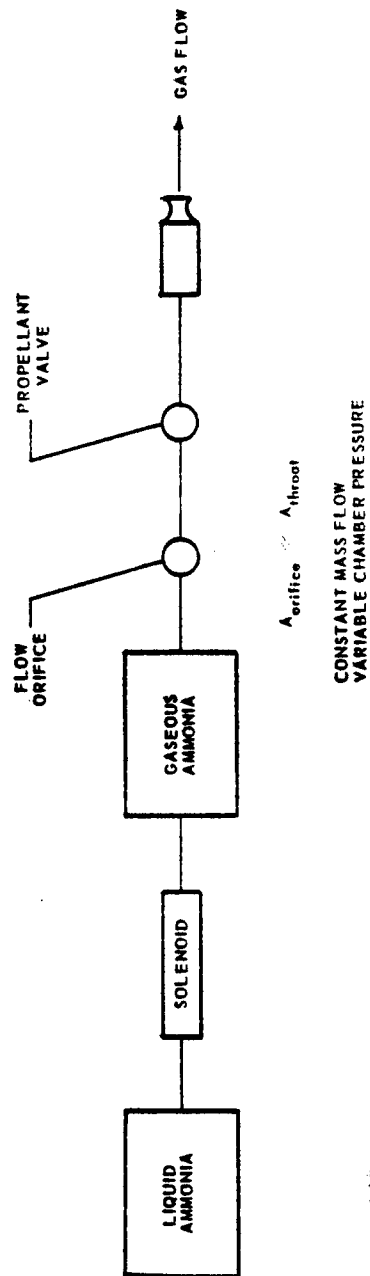
Figure 13 SCHEMATIC DIAGRAM OF A CONSTANT PRESSURE VARIABLE MASS FLOW PROPELLANT FEED SYSTEM

65-2545

added downstream of the critical flow orifice. Energy addition in the heater tube thus results in an increase in engine chamber pressure and thrust level but the flow rate remains unchanged. The pressure buildup time in this system was found to be excessive; further, and probably more important the thrust level varied markedly during a typical power-on pulse.

In the flow system shown in Figure 12 the propellant flow was choked across the exit nozzle throat; the metering orifice area was larger than the exit nozzle area. In this case, the engine chamber pressure was constant and the mass flow variable as energy was added to the gas passing through the tubular heat exchanger. Thus, for the constant chamber pressure case, the addition of energy to the gas flowing through the heater has the same effect on the propellant flow rate as would be obtained by reducing the nozzle throat area. For this mode of operation the thrust level remains essentially constant and the mass flow is reduced as energy is added to the gas stream.

3. Engine Heat-Up and Electrical Characteristics

An important parameter in the design of the fast heat-up resistojet is the response time of the heater element or the time that the heater element requires to come to operating temperature. The response time of the heater element can be obtained from an expression of the form $t_{heat-up} = M C_p \Delta T/P_{input}$ where M is the mass of the heater element, C_p is the specific heat of the heater material, ΔT is the required temperature rise, and P_{input} is the input power. A heat-up time of the order of 1 second is required to hold the power-on duty cycle for the individual engines in a 500-pound satellite resistojet attitude control system to about 5 percent. Assuming a ΔT of $1000°$ K, specific heat of 0.10 cal/$°$ C-gm, and a power input of 10 watts or 2.4 cal/sec the required thrustor mass is of the order of $M = t_{heat-up} \cdot P_{input} \cdot C_p \Delta T = (1 \text{ second}) (2.4 \text{ cal/sec})/(0.10 \text{ cal/}° \text{ C-gm}) (1000° \text{ K}) = 24 \times 10^{-3}$ gram . Thus, the required thrustor mass for a fast heat-up resistojet at the 10-watt power level is of the order of tens of milligrams.

The need for keeping the thrustor mass to a minimum is further emphasized by the results on heater resistance presented in Table V. Estimates are presented of the cold and hot resistances of a typical resistojet. The resistances in this table are based on a heater tube length of 1 inch and an inside diameter of 14 mils with wall thickness as given. It is noted that the heater resistance level is relatively low (order of 0.10 to 1 ohm) and that the cold resistance is significantly lower than the hot resistance. Further, the ratio of hot to cold resistance is strikingly sensitive to heater material varying from nearly 15 to 1 for tungsten to only 2 to 1 for stainless steel. The combination of low resistance and wide variation in resistance between hot and cold flow must be integrated with the power conditioning

TABLE V

RESISTANCE OF TYPICAL RESISTOJET

(t = wall thickness, I.D. = 14 mils, length = 1 inch)

A. Cold Resistance			
Cold Resistance at 20° C, Ohms			
Material	t = 7 mils	t = 3 mils	t = 1 mil
Tungsten	0.0047	0.014	0.046
Tungsten -26% Rhenium	0.027	0.076	0.26
Rhenium	0.017	0.048	0.16
Molybdenum	0.0049	0.014	0.048
Stainless Steel	0.041 - 0.066	0.12 - 0.18	0.40 - 0.63

B. Hot Resistance for Uniform Temperature				
Material	Maximum Operating Temp., ° C	Resistance, Ohms		
		t = 7 mils	t = 3 mils	t = 1 mil
Tungsten	2500	0.068	0.20	0.68
Tungsten -26% Rhenium	2300	0.082	0.24	0.82
Rhenium	2300	0.094	0.27	0.91
Molybdenum	1950	0.059	0.17	0.58
Stainless Steel	1100	0.099 - 0.12	0.29 - 0.35	0.97 - 1.2

equipment. Clearly, however, the resistance of the engine connections must be held to a minimum and the output of the power conditioner must be closer to constant power rather than constant current.

4.   Propellant Selection

Initial program emphasis has been on ammonia as the working fluid because of potential ease of storage for long duration missions. It is to be stressed, however, that the only real limitation on working fluid selection is that the working fluid be compatible with the heater material. Other propellants can be used equally well as resistojet propellants. Table VI presents the results of thermochemical calculations on the idealized frozen flow performance of a series of potential low molecular weight propellants.

5.   Fast Heat-Up Resistojet Operating Variables

To summarize, for constant pressure (variable mass flow) operation, and a fixed configuration, there are five basic operating variables: (a) engine reservoir pressure; (b) engine power input; (c) engine heat-up time; (d) engine solenoid valve on-time; and (e) propellant.

The engine reservoir pressure is fixed by the setting on the regulator located between the main propellant supply and the gas reservoir upstream of the engine. In the case of liquid propellant storage the gas reservoir pressure must, of course, be a value less than the vapor pressure of the propellant at the nominal propellant supply pressure. For storage of the propellant as a solid the gas reservoir tank and regulator can, in some cases, be eliminated and the engine connected directly to the supply tank. The engine thrust level is directly proportional to the gas reservoir pressure level, and thus variation of engine reservoir pressure permits a direct control over engine thrust level.

The engine power input, to a first order, permits control over the propellant flow rate at constant engine thrust level. Increase in the engine power input increases the temperature of the gas flowing through the engine; the gas temperature increase, in turn, decreases the flow rate. The maximum attainable gas temperature is limited by the temperature capability of the heater and by the required input power. The weight saving in propellant must, of course, be balanced against the weight of the required resistojet power supply.

The engine heat-up time is the time required for the engine to come to operating temperature. The heat-up time must be held to a minimum (e.g., 1 second) in order to hold the average power consumption of the resistojet attitude control system to a minimum. The required heat-up time is a function of the heater mass and heater resistance. In order to

TABLE VI

IDEAL PROPULSION PERFORMANCE OF POTENTIAL RESISTOJET WORKING FLUIDS

Temp., °K	Liquid				Solid						Gas			
	Ammonia NH$_3$ - 1 atm (I_{sp})ideal	(M)avg	Ammonium Sulfide (NH$_4$)$_2$S-1/2 atm (I_{sp})ideal	(M)avg	Ammonium Hydrosulfide NH$_4$ HS - 1/2 atm (I_{sp})ideal	(M)avg	Ammonium Carbamate NH$_4$CO$_2$NH$_2$-0.1 atm (I_{sp})ideal	(M)avg	Ammonium Carbamate (NH$_4$)$_2$CO$_3$-0.05 atm (I_{sp})ideal	(M)avg	Hydrogen H$_2$ - 1 atm (I_{sp})ideal	(M)avg	Nitrogen N$_2$ - 1 atm (I_{sp})ideal	(M)avg
298	113	17.032	98	22.71	92	25.55	92	26	95	24	296	2.016	80	28.02
500	185	9.267	152	14.05	139	17.41	132	21.83	134	20.91	389	2.016	105	28.02
1000	274	8.518	228	13.63	210	17.04	214	15.62	216	16.02	558	2.016	156	28.02
1500	347	8.516	290	13.47	267	16.48	270	15.61	274	16.01	706	2.016	197	28.02
2000	411	8.510	342	12.79	316	15.22	320	15.59	324	15.98	840	2.014	231	28.02
2500	470	8.425	392	12.27	360	14.48	366	15.19	371	15.37	961	1.991	260	28.02

VAPOR PRESSURE AT 65° F

A. Liquid

NH$_3$ 115 psia

B. Solid

(NH$_4$)$_2$S   7.0 psia

NH$_4$HS   6.4 psia

NH$_4$CO$_2$NH$_2$ 1.2 psia

(NH$_4$)$_2$CO$_3$ 0.60 psia

keep the heater warmup time at a minimum it is necessary to closely match the design of the power conditioning equipment with the wide anticipated variation in heater resistance between cold and hot flow.

The engine solenoid valve on-time is established by control logic considerations.

Finally, propellant selection is based on a variety of considerations including ease of storage and handling, weight of tankage, and material compatibility. It is important to note that the fast heat-up resistojet concept is not limited to ammonia but can be applied to a variety of propellants and is not dependent on the storage state (i.e., gas, liquid, or solid).

6. Engine Fabrication Techniques

A major problem in the development of the fast heat-up resistojet has been the fabrication of the relatively small heater nozzle elements. In the initial engines the heater-nozzle elements were fabricated directly from thin wall tubing. The nozzle shape was pressed directly into the thin wall tubing; this procedure made it very difficult to control the critical heater-nozzle dimensions.

During the course of the program a process has been developed for the reliable fabrication of the heater-nozzle units. The process consists of deposition of a refractory metal onto a mandrel of the desired shape and dissolving the mandrel in an acid. Close control can be obtained on the resistojet dimensions by machining the mandrel to the desired shape before plating. Molybdenum, which can be dissolved in hot nitric acid has been used as the mandrel for tungsten; titanium, which can be dissolved in hydrofluoric acid, has been used for rhenium. Fused salt electrolysis was used to deposit the tungsten; vapor deposition was used for the rhenium and tungsten-rhenium alloy. Details are presented below.

a. Mandrel Fabrication

Material selection for mandrel fabrication was influenced by operating temperature of the deposition process and acid resistance of the deposited metal. Operating temperatures of the fused salt plating and vapor plating processes were in the range 800-1000° C. Thus, molybdenum, which retains strength at these temperatures was chosen as a substrate for tungsten. However, molybdenum could not be used for rhenium coatings for both are attacked by the same acids. Hence, titanium was chosen as mandrel material for vapor deposited rhenium.

The mandrel is made by cutting 2-inch lengths of 0.070-inch wire, slitting 1/4-inch tabs in the wire, then machining the nozzle, constriction, and shaft on a jewelers lathe using a carbide tipped cutting tool. Figure 14 shows the various machining steps. After machining, the mandrel is polished electro-chemically in an alcohol-sulfuric acid solution using 20 volts of direct current for 1 minute. Dimensions are shown in Figure 15.

b.   Fused Salt Electrolysis

This is a proprietary process developed by the Parma Research Division of Union Carbide Corporation. The electroplating solution consists of motion tungsten fluoride, sodium fluoride, and potassium fluoride salts. The operating temperature is 800° C. Many articles can be plated simultaneously, as in regular plating. Thickness of the coatings can be controlled from a fraction of a thousandth of an inch to heavy deposits up to 1/4 inch thick or more. The tungsten coatings used in this investigation were 0.003 to 0.004 inch thick and were fully dense and free of pinholes; the crystal structure is columnar and radially oriented. At present, rhenium or alloys of rhenium cannot be deposited by this method.

c.   Vapor Deposition

This process operates on the principle of thermal decomposition of metal halides or carbonyls onto a heated substrate. Operating temperature of the substrate is 900 to 1000° C. Tungsten, rhenium and alloys of tungsten/rhenium are among the metals which can be deposited. These coatings also are fully dense and free from pinholes. San Fernando Laboratories of Pacoima, California, supplied the coatings for this investigation. Figure 16 shows samples of rhenium and rhenium-tungsten alloy deposited by vapor deposition. At present, the process is relatively expensive as only one mandrel at a time can be coated.

d.   Dissolving the Mandrel

Molybdenum mandrels were dissolved in a nitric acid (85 percent) sulfuric (15 percent) acid solution operated at 70° C under a pulsating negative pressure cycle as shown in Figure 17. The time required to dissolve a 1-inch-long mandrel is 16 to 20 hours. It is interesting to note that the dissolution rate of bare molybdenum wire in this solution is very rapid (see Figure 18).

Titanium mandrels are dissolved in a 50-percent solution of hydrofluoric acid (48-percent HF) at room temperature. In this case the

-36-
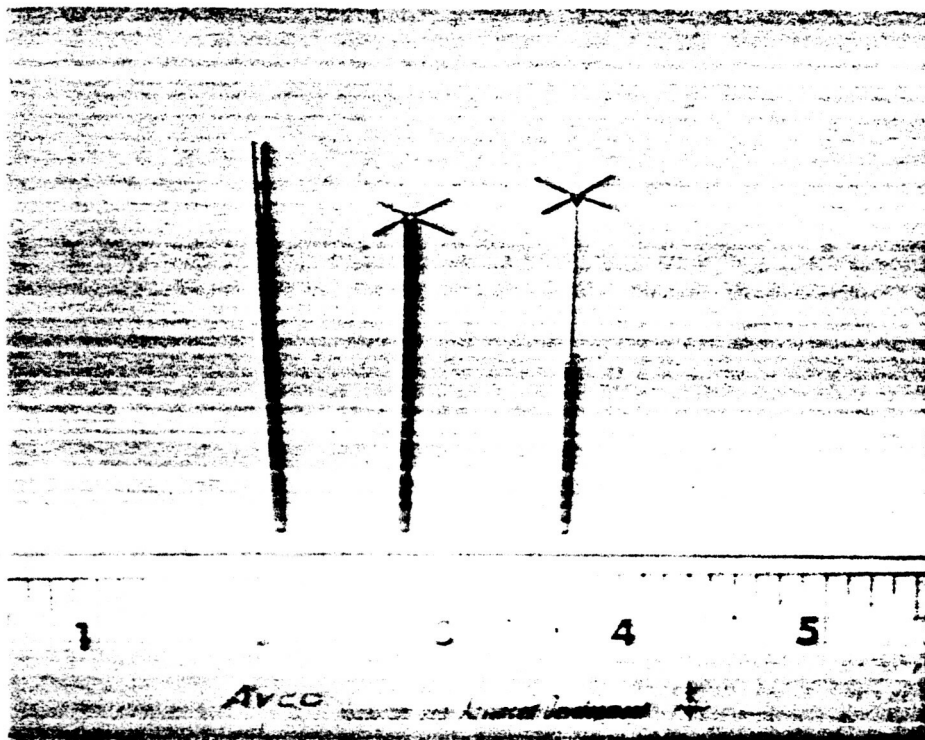
65-816

Figure 14 MANDREL FABRICATION
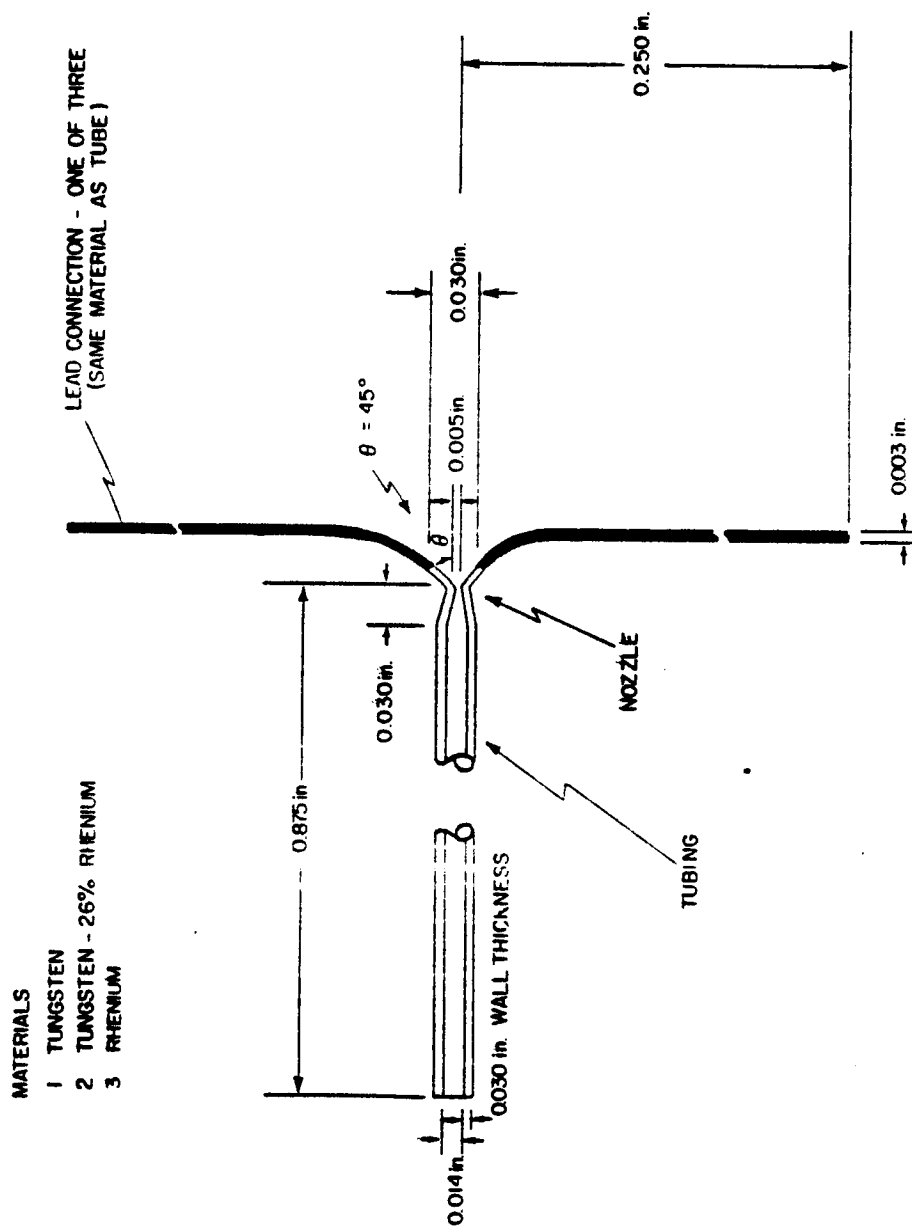
Figure 15 MANDREL DIMENSIONS

MATERIALS

1 TUNGSTEN
2 TUNGSTEN - 26% RHENIUM
3 RHENIUM

LEAD CONNECTION - ONE OF THREE
(SAME MATERIAL AS TUBE)

$\theta = 45°$

0.030in.

0.250 in.

0.005in.

0003 in.

0.030in.

0.875in.

NOZZLE

TUBING

0.030 in. WALL THICKNESS

0.014in.
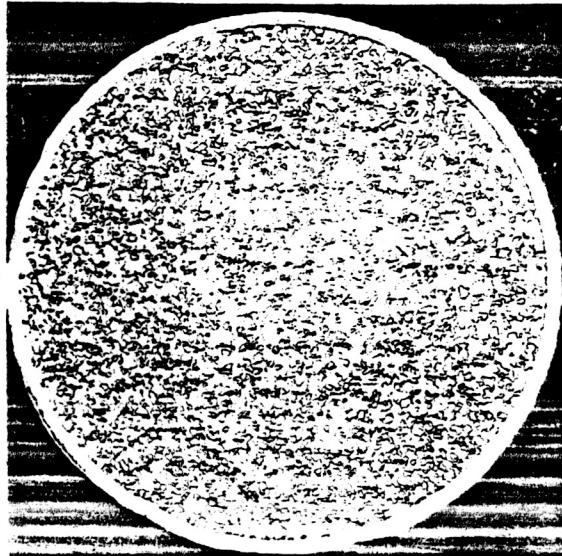
(A)   RHENIUM DEPOSITED ON TITANIUM MANDREL, MAGNIFICATION = 50 X
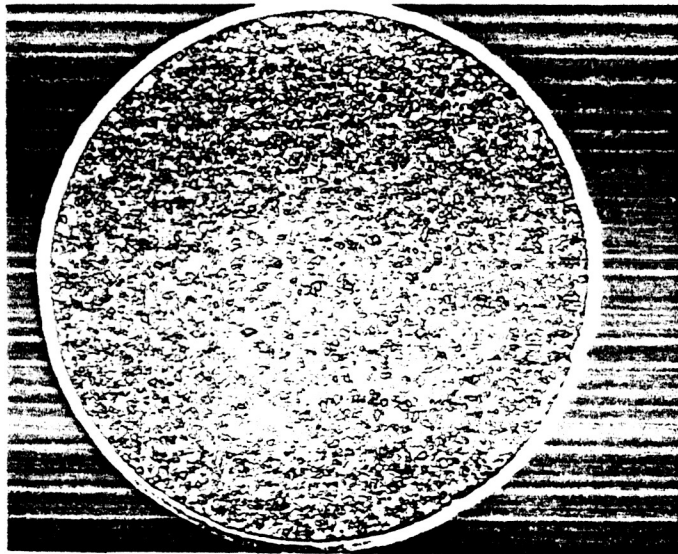
(B)   26% RHENIUM/TUNGSTEN ALLOY DEPOSITED ON TITANIUM MANDREL,
MAGNIFICATION = 50 X

Figure 16 PHOTOMICROGRAPHS OF VAPOR-DEPOSITED RHENIUM AND RHENIUM/TUNGSTEN

65-8169
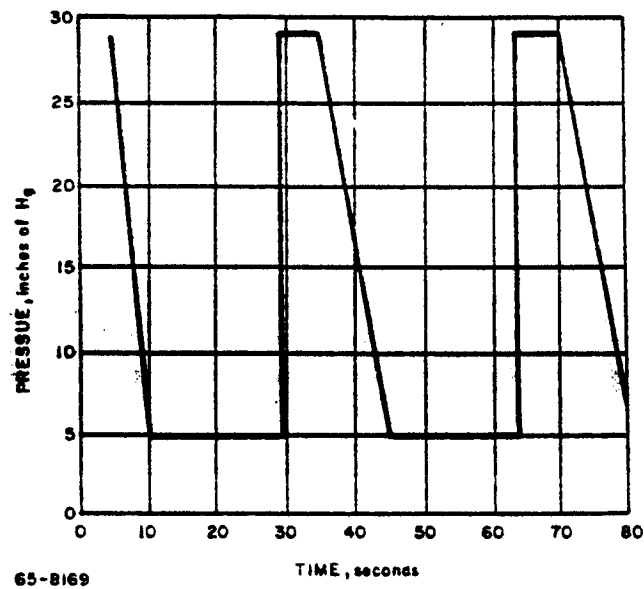
Figure 17 PULSATING PRESSURE CYCLE OF DISSOLVING THE MOLYBDENUM MANDREL

-40-
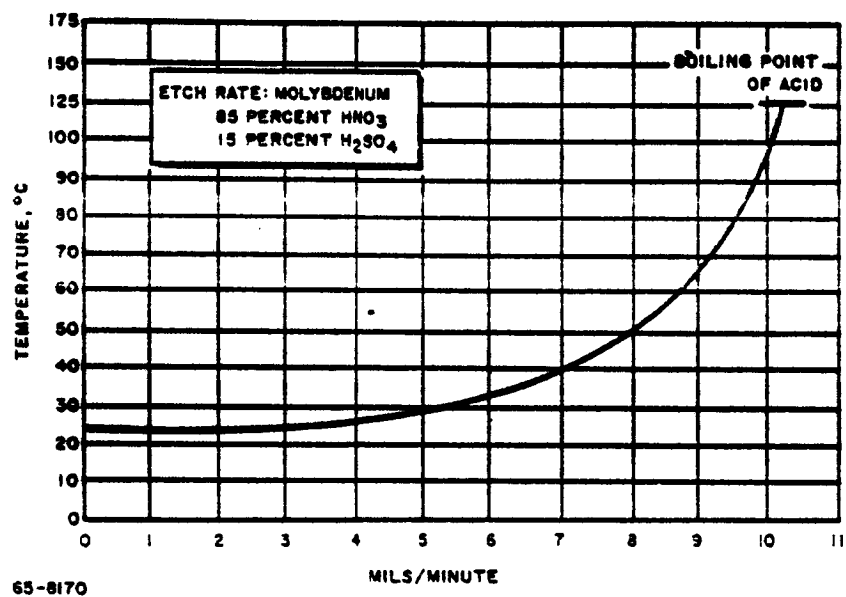
Figure 18 DISSOLUTION RATE OF BARE MOLYBDENUM WIRE

65-8170

-41-

reaction product is titanium trifluoride (red-violet). The same techniques mentioned above must be used, i. e., pulsating vacuum and careful rinsing. The dissolution rate of exposed titanium wire is shown in Figure 19. The time required to remove a 1-inch mandrel is, like molybdenum, 16 to 20 hours.

The long acid leaching time required in the case of the enclosed mandrel is due to the entrapment of hydrogen gas bubbles and reaction products in a very small diameter tube. In the case of molybdenum, the reaction products precipitated on drying out were observed to be a mixture of molybdenum dioxide (lead gray), molybdenum trioxide (whitish yellow) and molybdenum pentoxide (violet blue). These products are formed on the face of the mandrel inside the tube if the tube is allowed to dry without efficiency rinsing. If this occurs, re-starting the dissolution process becomes very difficult and even impossible in severe cases. During the course of this investigation, it was found necessary to rinse out the tubes with hot distilled water followed by a rinse in concentrated hydrochloric acid. Both rinses must be carried out under vacuum using the pressure cycle shown in Figure 17.

7. Reliability of Potential Heater Materials

Thrustor performance data have been obtained with stainless steel, molybdenum, rhenium and tungsten heater elements. Major problem areas include engine fabrication and thermal cycling capability. Extended thermal cycling (10,000 cycles) appears to be no problem for stainless steel (m. p. 1500° C), rhenium, or tungsten but is a serious problem for molybdenum (m. p. 2620° C) which has a higher temperature capability. To extend the upper temperature range of the heater element an effort has been made to fabricate the basic heater-nozzle structure from vapor deposited tungsten. This technique appears quite promising and it appears possible to fabricate tungsten heater elements with a wall thickness of only 1 to 2 mils.

In order to check the thermal cycling capability of the vapor-deposited tungsten, a sample tube of the material (25-mil inside diameter, 3-mil wall thickness, 3/4 inch long) was cycled through a typical resistojet heating cycle 40,000 times. The tube was placed in a 1-micron vacuum for the test. The ammonia flow entered from each end of the tube and passed out through an orifice at the tube center. The interior pressure was about 1 atmosphere. The operating cycle was: Power-on(no flow) 0.8 second; Power-on (with flow) 1.0 second; Power-off 2.2 seconds. During the power-on, no-flow, phase, the tube was heated to 2200° K. This temperature was maintained during the power-on, with-flow phase, after which the power was turned off and the tube cooled before beginning the next cycle. The heater was thermally cycled 40,000 times.

-42-
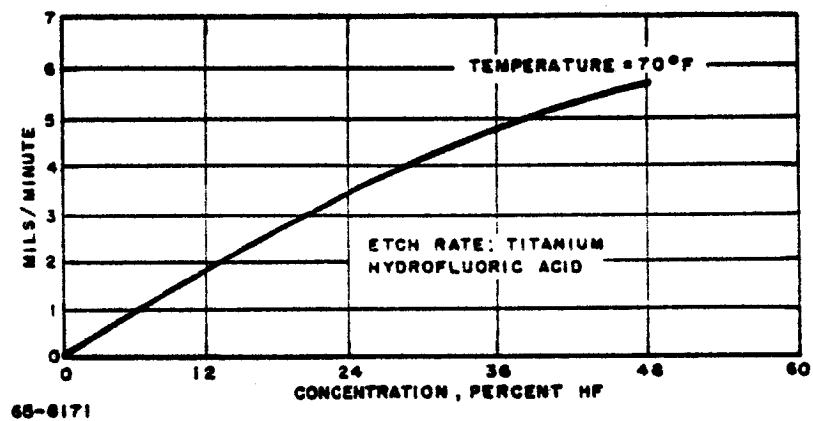
Figure 19 DISSOLUTION RATE OF BARE TITANIUM WIRE

At the completion of the test, visual examination indicated no apparent changes in the sample. Photomicrographs of the wall cross section before and after the test were prepared at 500X and indicated that there was a change in crystal structure. The material, however, appeared structurally sound, and the structural changes which did occur evidently do not affect the integrity of the material.

D. FAST HEAT-UP THRUSTOR MASS FLOW, HEAT TRANSFER, AND ELECTRICAL CHARACTERISTICS

The purpose of the present section is to present experimental data on the mass flow, heat transfer, and electrical characteristics of a fast heat-up thrustor. The propulsion performance of the thrustor is presented in Section II. E. A schematic diagram of the thrustor (heater element and exit nozzle) is shown in Figure 20. The nozzle has a 10×10^{-3}-inch throat, a 600-to-1 area ratio, and a half-angle of 45 degrees. The heater-exit nozzle combination is fabricated of vapor-deposited rhenium. The engine has been operated over the range of conditions shown in Table VII.

TABLE VII

OPERATING CONDITIONS FOR FAST HEAT-UP RHENIUM THRUSTOR

Chamber Pressure	0. 20 to 10 psia
Electric Input Power	0 to 50 watts
Ammonia Flow Rate	0. 01 to 12×10^{-6} lbs/sec
Maximum Thrustor Temperature	2000° K (3140° F)
Maximum Current	25 amperes
Maximum Voltage	2 volts
Thrust Level	1 to 1200 micropounds
Maximum Specific Impulse	300 seconds
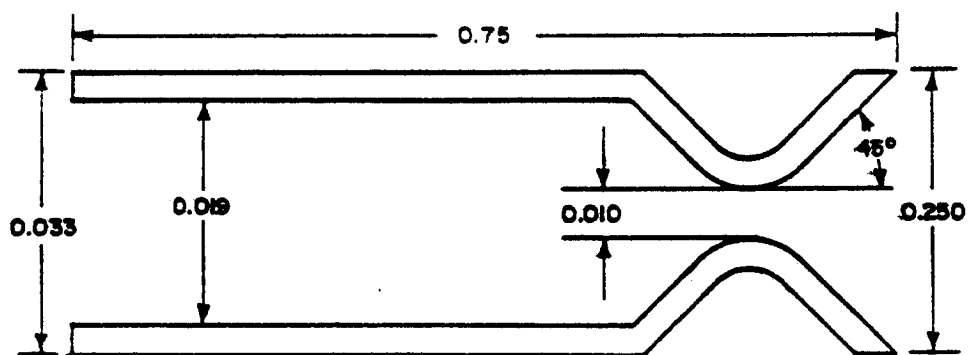
86-11978

Figure 20 RHENIUM HEATER-NOZZLE CONFIGURATION USED FOR EVALUATION OF THRUSTOR PERFORMANCE

The two critical items in the evaluation of engine performance have been the measurement of gas flow rates as low as 10^{-8} lb/sec and thrust levels as low as 1 micropound. In each case the measurement of both the gas flow rate and the engine thrust level were made by two independent techniques. The gas flow rate measurement techniques are described below and the thrust measurement techniques are described in the next section.

1. Mass Flow Measurement

The ammonia flow rate passing through the thrustor was determined by means of a calibrated orifice. The pressure drop, ΔP, across the orifice, was less than 1 percent of the pressure, $P_{orifice}$, upstream of the orifice. In this case, it can be shown that the mass flow rate, $\dot{m}$, is a function of $\sqrt{P_{orifice} \Delta P}$

The absolute flow rate was, in turn, established both by direct weight measurement and by the measurement of the pressure change in a known volume. In the first case, the mass flow rate, $\dot{M}$, through the metering orifice was held constant for a fixed time, Δt, and the corresponding weight change, ΔM, in the gas supply was recorded by weighing the propellant tank before and after the run. The run time, Δt, was of the order of one hour to permit the propellant weight loss to be measured with an accuracy of at least 0.5 percent. In the second case, the flow rate, $\dot{M}$, was held constant for a time Δt and the corresponding pressure, change ΔP_v, in a known volume, v was recorded. The corresponding weight change, ΔM, was in this case determined from the perfect law. Figures 21 and 22 show the mass flow rate, $\dot{M}$ as a function of $\sqrt{P \Delta P}$. Figure 21 covers the mass flow range from 0 to 14×10^{-6} lb/sec, and Figure 22 is an expanded portion of the calibration curve from 0 to 0.60×10^{-6} lb/sec. Figure 21 also compares mass flow rates determined from the direct weight measurement and the tank pressure change techniques. There is no substantial difference in the mass flow rates established by the two techniques. It is estimated that an individual measurement of the mass flow rate is accurate to ± 5 percent over the range from 10^{-7} to 10^{-3} lb/sec.

2. Orifice Coefficient versus Reynolds Numbers

The orifice coefficient is defined as the ratio of the actual mass flow, $\dot{M}_{actual}$ to the mass flow, $\dot{M}_{ideal}$, through the orifice, or

$$C_D = \dot{M}_{actual} / \dot{M}_{ideal} \tag{15}$$

where

$$\dot{M}_{ideal} = \frac{P_c A_t}{\sqrt{\gamma RT}} \, \gamma \sqrt{\left(\frac{2}{\gamma+1}\right)^{\frac{\gamma+1}{\gamma-1}}} \tag{16}$$

-46-
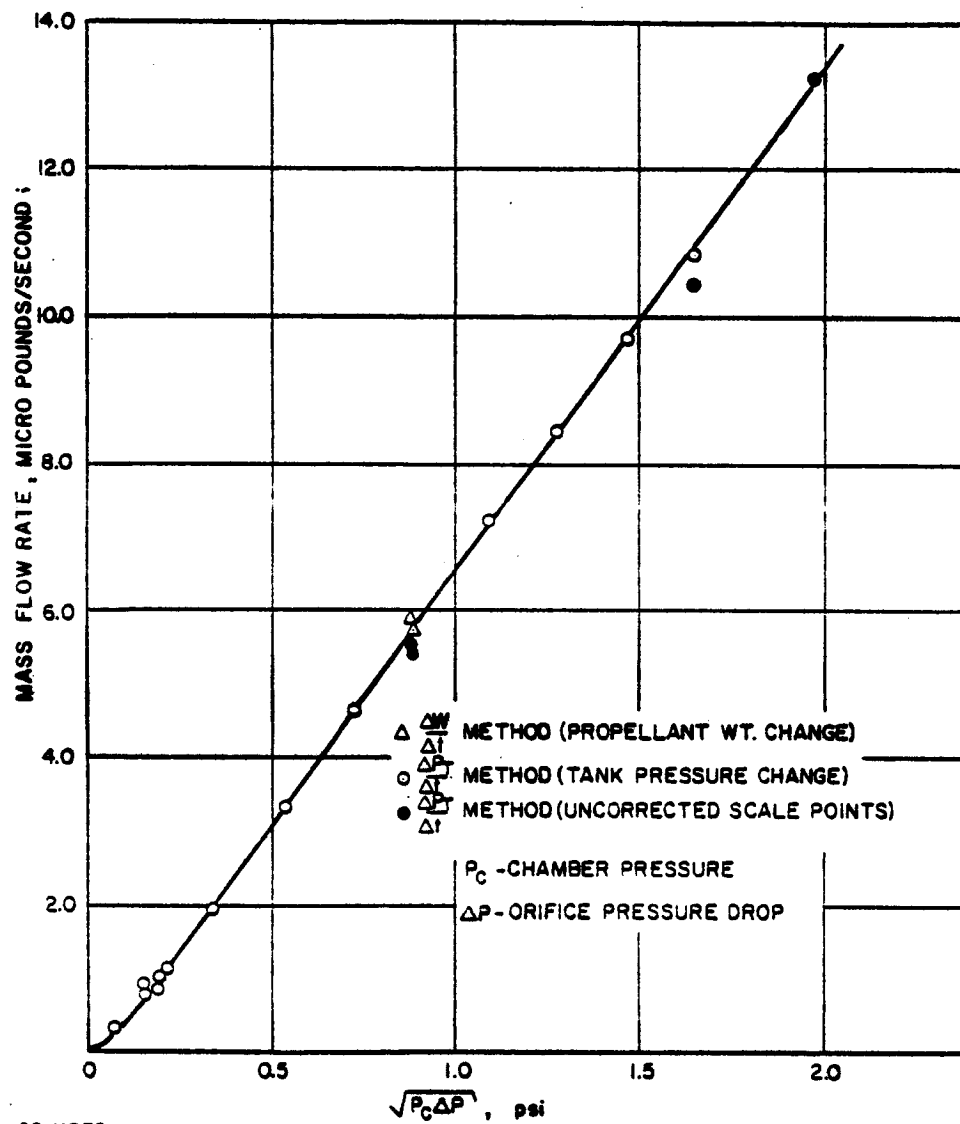
Figure 21 FLOW ORIFICE CALIBRATION — MASS FLOW RATE VERSUS PRESSURE
DIFFERENTIAL PARAMETER (0 TO 14 X 10^{-6} LB/SEC)
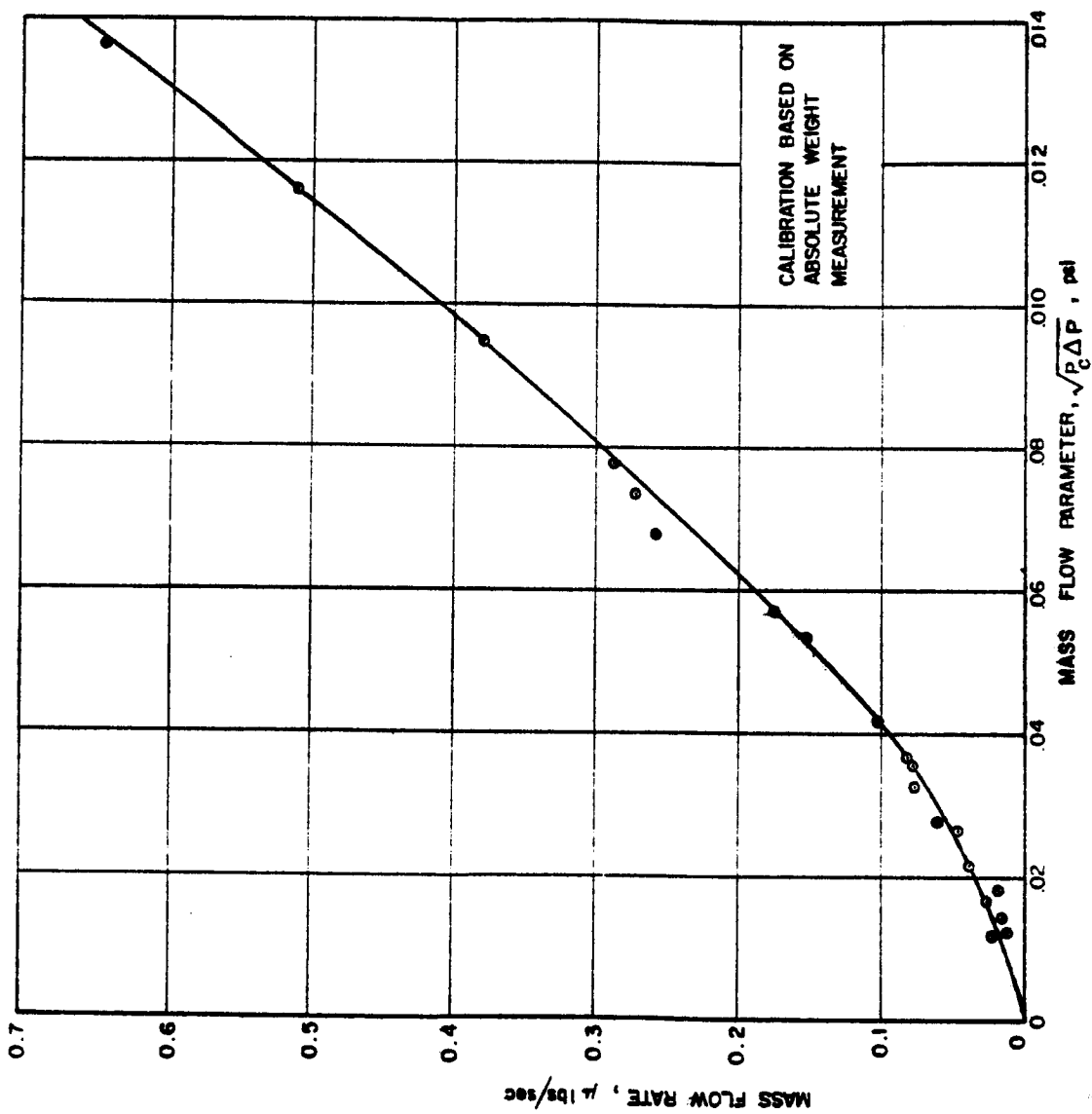
Figure 22 FLOW ORIFICE CALIBRATION -- MASS FLOW RATE VERSUS PRESSURE
DIFFERENTIAL PARAMETER (0 to 0.60 x 10^{-6} lb/sec)

86-11980

-48-

During the course of the present study considerable mass flow and thrust data has been gathered on the orifice shown in Figure 23. The orifice has a throat diameter of 11×10^{-3} inches, an area ratio of 100 to 1, and a nozzle half-angle of 45 degrees. Figure 24 shows the orifice coefficient as a function of throat Reynolds number. The results are quite similar to those of Milligan (ref. 4) in that the discharge coefficient begins to decrease rather sharply at Reynolds numbers below 100. The results on the orifice discharge coefficient will be used subsequently in the interpretation of the thrustor heat transfer data.

3. Heater Performance Data

The following data have been obtained on the thrustor shown in Figure 20. Figures 25 and 26 show ammonia flow rate as a function of power input for fixed chamber pressures of, respectively, 5 and 9 psia. At zero electric input power the ammonia flow rate for the 5-psia chamber pressure is 6.2×10^{-6} lb/sec and for 9 psia it is about 11.8×10^{-6} lb/sec. In each case as the electric power input is increased the ammonia flow rate is decreased. Figures 27 and 28 show the corresponding maximum engine temperature versus electric power input. The engine brightness temperature was obtained with an optical pyrometer; the brightness temperatures were, in turn, converted into true temperatures by assuming that the emissivity characteristics of rhenium were the same as those of tungsten.

The mass flow through the thrustor can be analytically established by the conditions at the nozzle inlet. From Equations (15) and (16) the thrustor mass flow is given by

$$\dot{M}_{actual} = C_D \, P_{nozzle} \, f(\gamma) \, A_t \sqrt{\frac{W_{nozzle}}{T_{nozzle}}} \qquad (17)$$

Referring to Equation (17), as electric power input and correspondingly the thrustor temperature are increased the mass flow tends to be reduced for the following reasons:

a. The gas temperature, T_{nozzle}, will increase due to energy addition and decrease the temperature term $\sqrt{W_{nozzle}/T_{nozzle}}$.

b. The increase in temperature will also cause a decrease in flow Reynolds number and a corresponding decrease in the orifice coefficient, C_D, (see Figure 24).

c. Because of friction and momentum losses through the heater tube, the nozzle inlet pressure, P_{nozzle}, will be less than the pressure at the entrance to the thrustor, P_{inlet}. Thus, even though P_{inlet} is fixed, P_{nozzle} will tend to decrease with increase in electric power.

0.060

45°

0.011

0.110
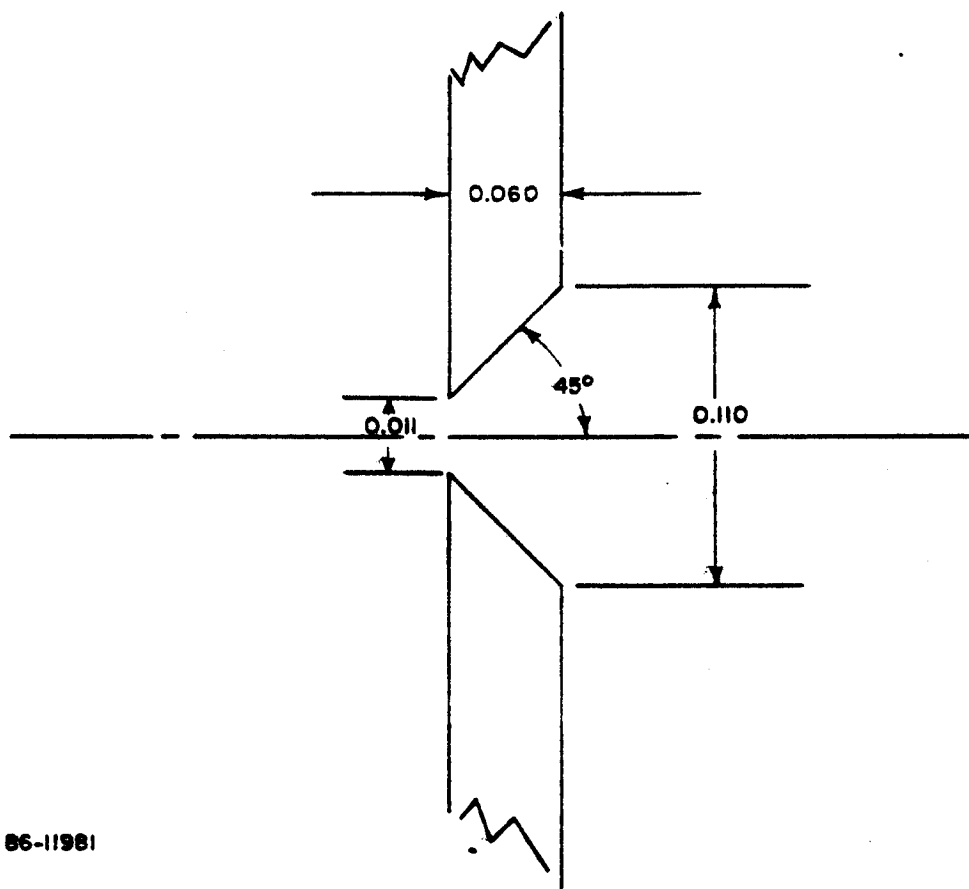
86-11981

Figure 23 CONFIGURATION OF THE 11—MIL ORIFICE
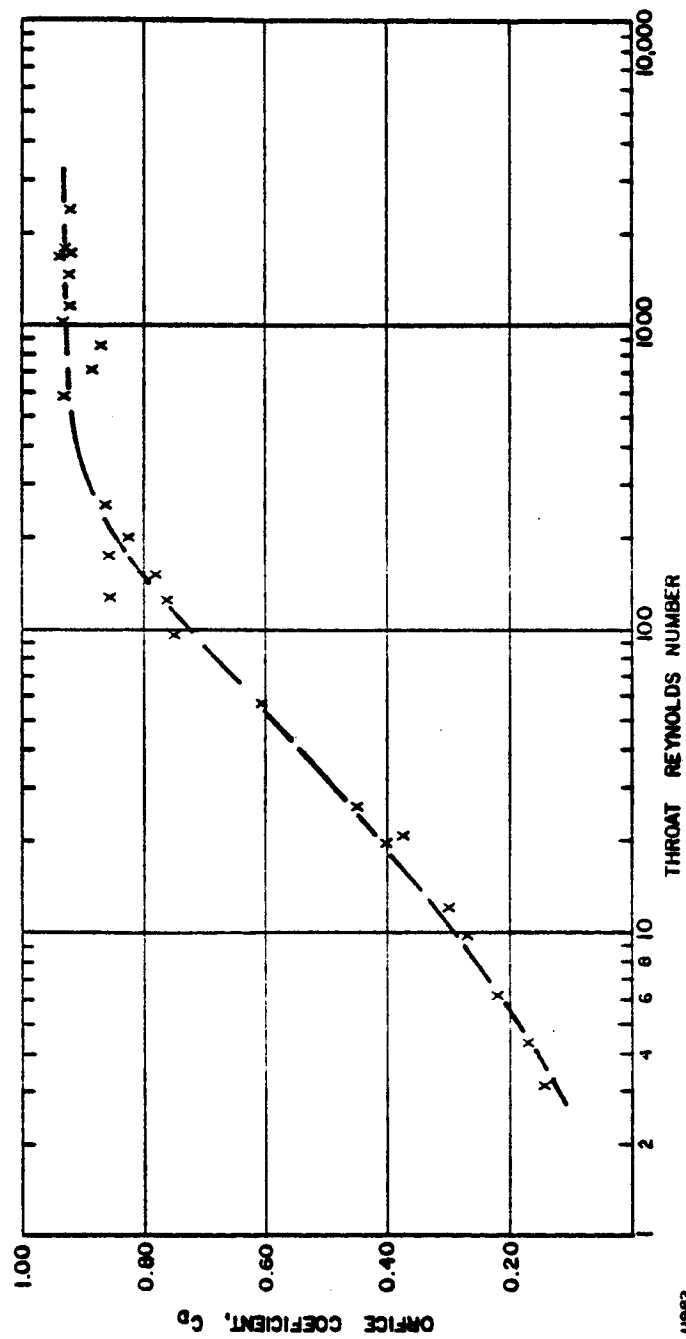
Figure 24 ORIFICE COEFFICIENT VERSUS THRUST REYNOLDS NUMBER 11-
MIL ORIFICE
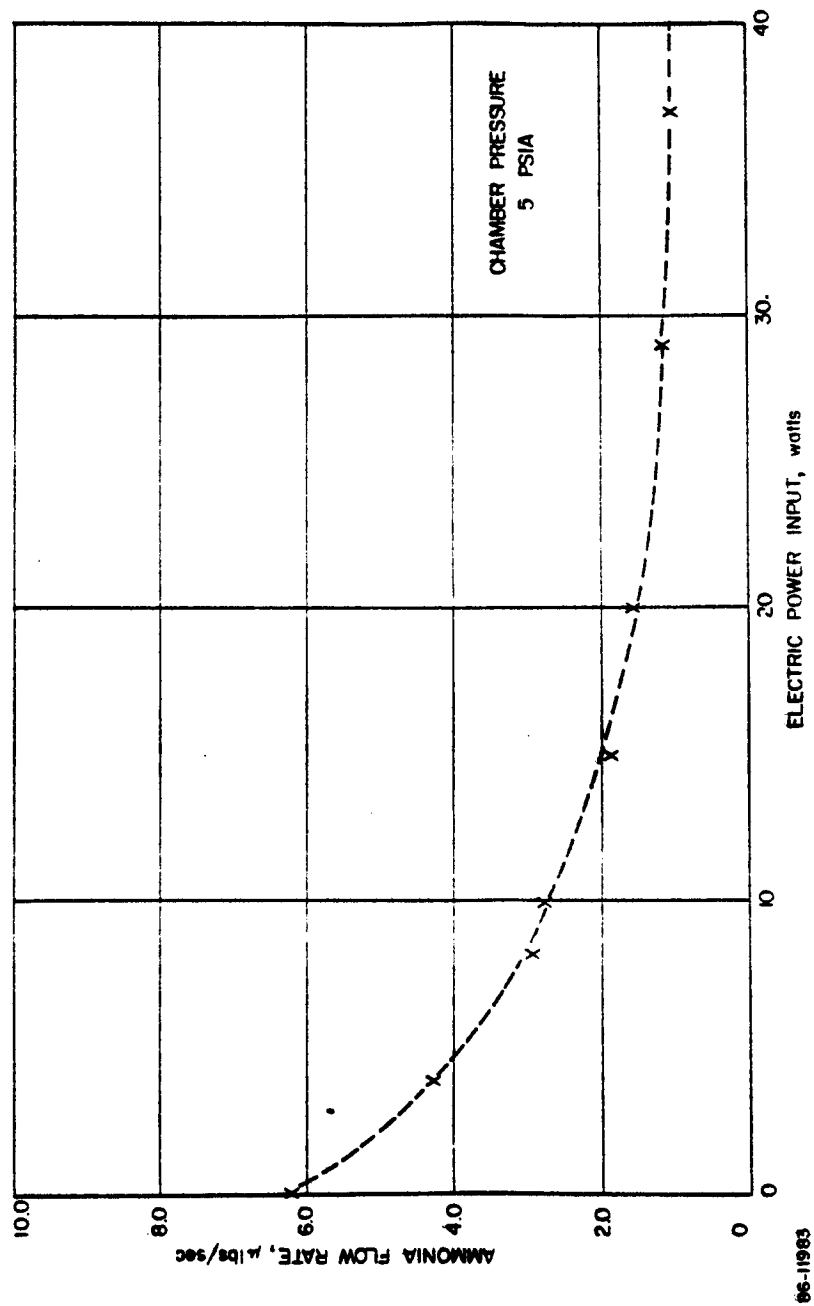
Figure 25 AMMONIA FLOW RATE VERSUS ELECTRIC POWER INPUT -- RHENIUM HEATER-NOZZLE -- 5-PSIA CHAMBER PRESSURE

66-11983
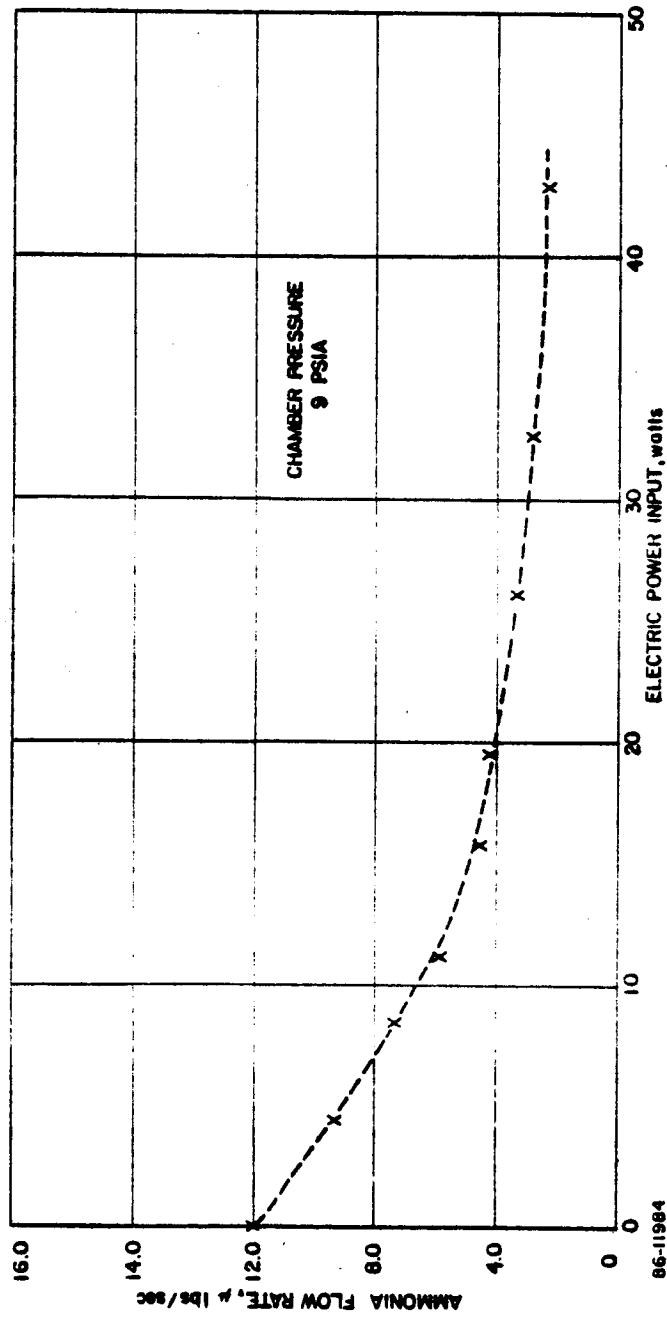
Figure 26 AMMONIA FLOW RATE VERSUS ELECTRIC POWER INPUT -- RHENIUM
HEATER-NOZZLE -- 9-PSIA CHAMBER PRESSURE
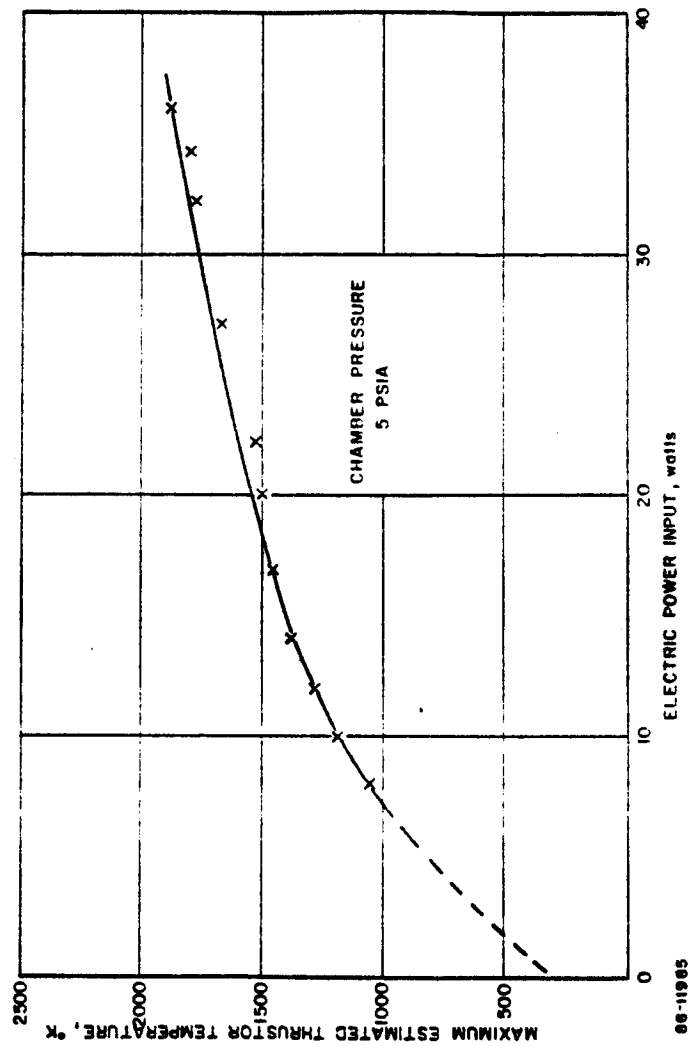
Figure 27 MAXIMUM ESTIMATED THRUSTOR TEMPERATURE VERSUS ELECTRIC
POWER INPUT -- 5-PSIA CHAMBER PRESSURE

-54-
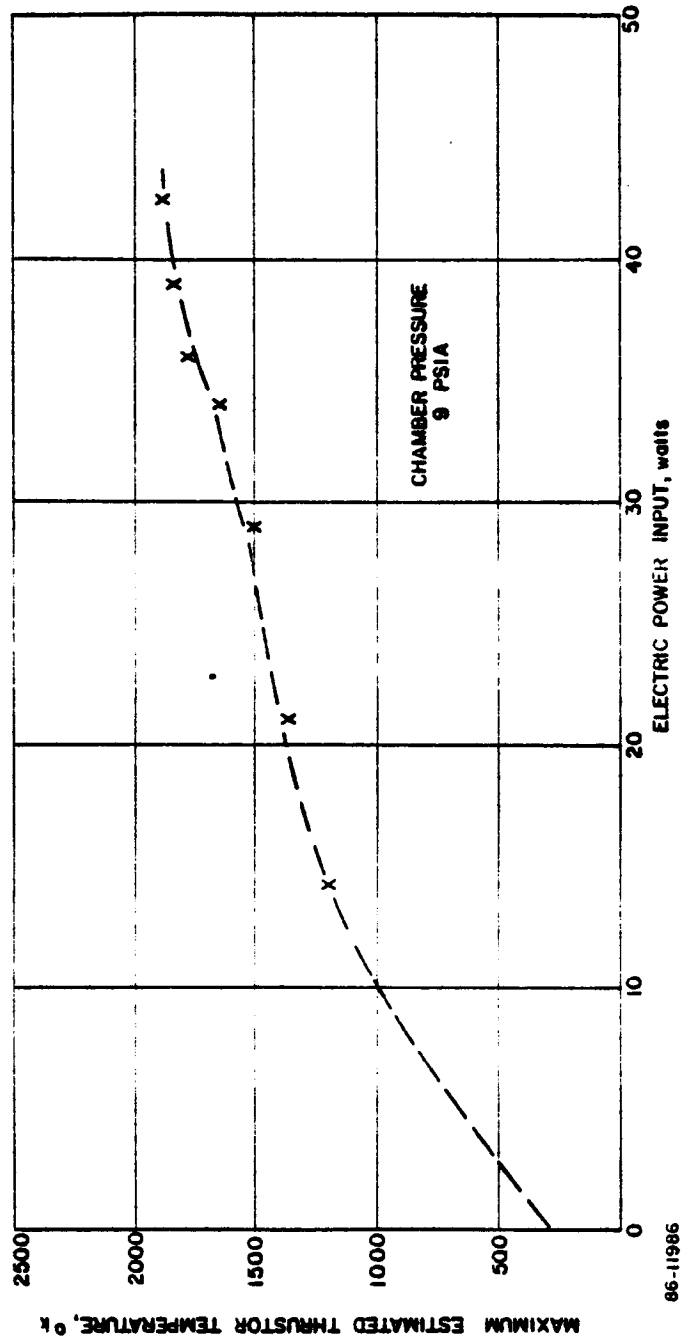
Figure 28 MAXIMUM ESTIMATED THRUSTOR TEMPERATURE VERSUS ELECTRIC POWER INPUT -- 9-PSIA CHAMBER PRESSURE

86-11986

The heater tube friction drops, $\Delta P_{friction}$, is proportional to $l \mu U_{mean}/D^2$ where, l is the heater tube length, μ is the viscosity, U_{mean} is the mean velocity, and D is the heater tube diameter.

d. Finally, as the temperature is increased there is the possibility that the ammonia will dissociate and this, in turn, will result in a decrease in the ammonia flow rate due again to the drecrease in the temperature term $\sqrt{M_{nozzle}/T_{nozzle}}$.

An attempt has been made to estimate the gas temperature at the inlet to the thrustor exist nozzle by simultaneously solving the momentum and continuity equations along the heater tube. Account has been taken of both the pressure drop due to heat addition and the friction drop. The estimated gas temperatures versus the electric power input for 5-psia and 9-psia inlet pressure are shown, respectively, in Figures 29 and 30. Curves are presented for both the case of dissociated and non-dissociated ammonia. Curves of maximum thrustor temperature as a function of electric input power are superimposed on the estimated gas temperature values. The estimated gas temperatures, based on the non-dissociation assumption, exceed the maximum thrustor temperature at an estimated non-dissociated gas temperature of about 1250° K (or 1800° F). Thus, it is concluded that the dissociation of ammonia is initiated at about 1250° K and that the dissociation is nearly complete at about 1750° K.

Figures 31 and 32 show the estimated heater pressure drop as a function of electric input power for respectively the case of 5-psia and 9-psia chamber pressure. As in the preceding figures the calculations have been carried out on the assumption that the flow is either dissociated or not dissociated. The pressure drop is higher for the non-dissociated case than the dissociated case because the estimated gas temperatures and thus the gas viscosities are higher. The estimated pressure drops for the 9-psia case are higher than those for the 5-psia case, since there is a corresponding higher gas flow. The pressure drop through the heater tube can, of course, be reduced by operating at a larger tube diameter, D. At a constant mass flow the heater pressure drop is inversely proportional to the fourth power of the tube diameter.

Figures 33 and 34 show the thrustor power distribution as a function of maximum thrustor temperature again for chamber pressures of, respectively, 5- and 9-psia. The estimated power to the gas for dissociated ammonia is, of course, higher than that for non-dissociated ammonia because
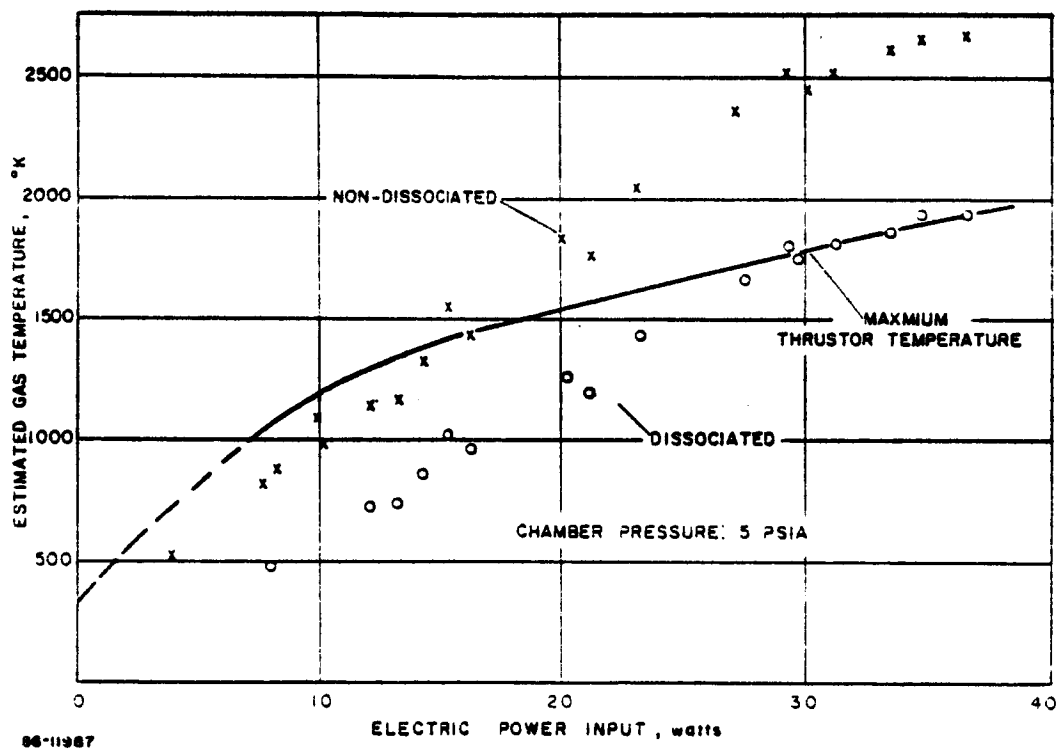
Figure 29 ESTIMATED GAS TEMPERATURE VERSUS ELECTRIC POWER INPUT —
5-PSIA CHAMBER PRESSURE
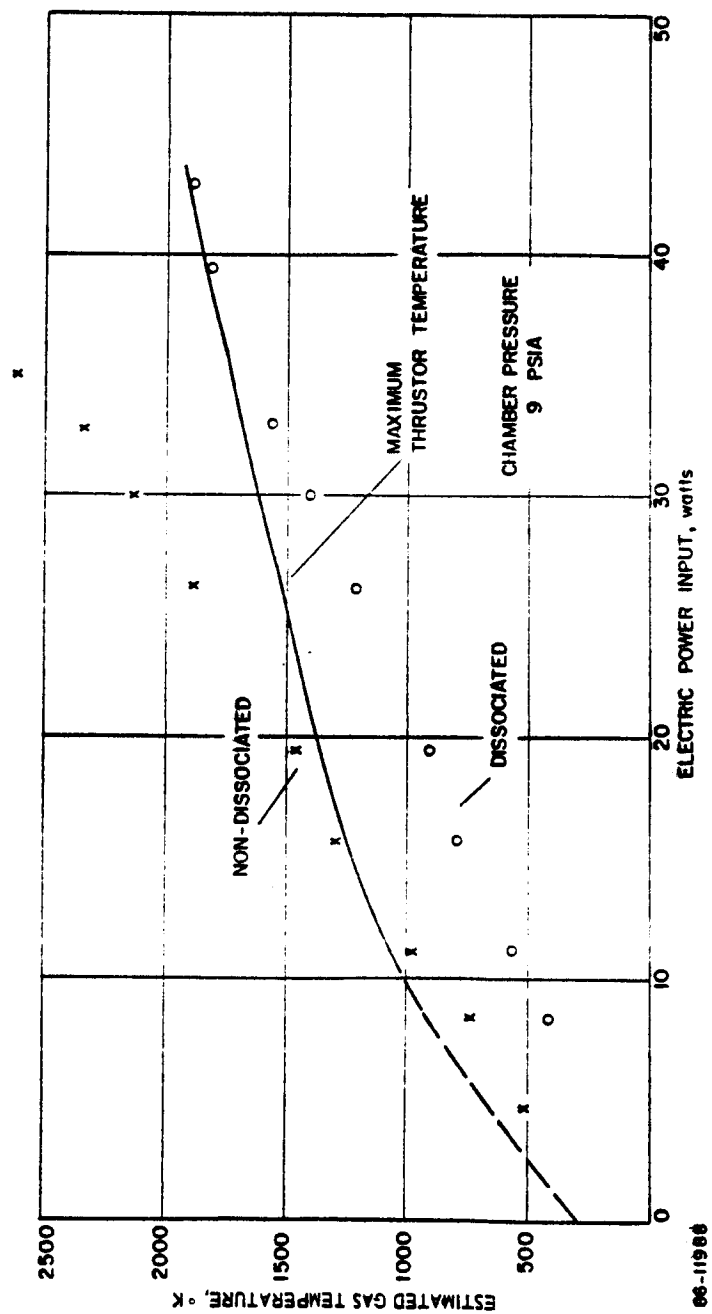
Figure 30 ESTIMATED GAS TEMPERATURE VERSUS ELECTRIC POWER INPUT --
9-PSIA CHAMBER PRESSURE

66-11988

-58-
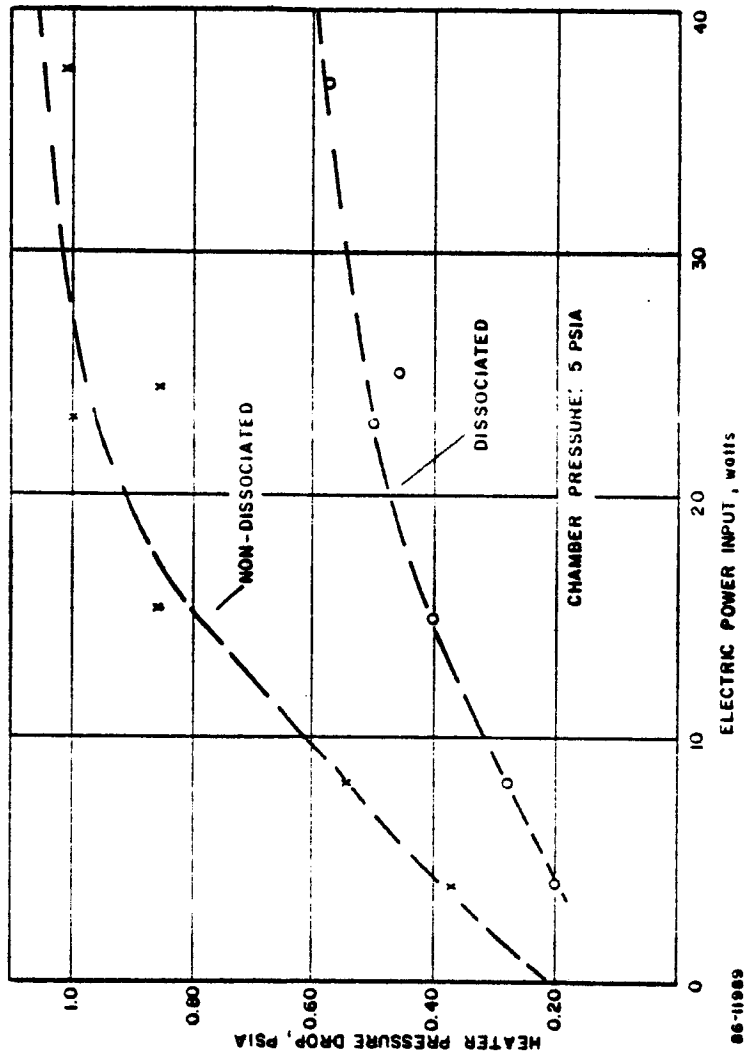
Figure 31 HEATER PRESSURE DROP VERSUS ELECTRIC POWER INPUT -- 5-PSIA CHAMBER PRESSURE

86-11969

-59-
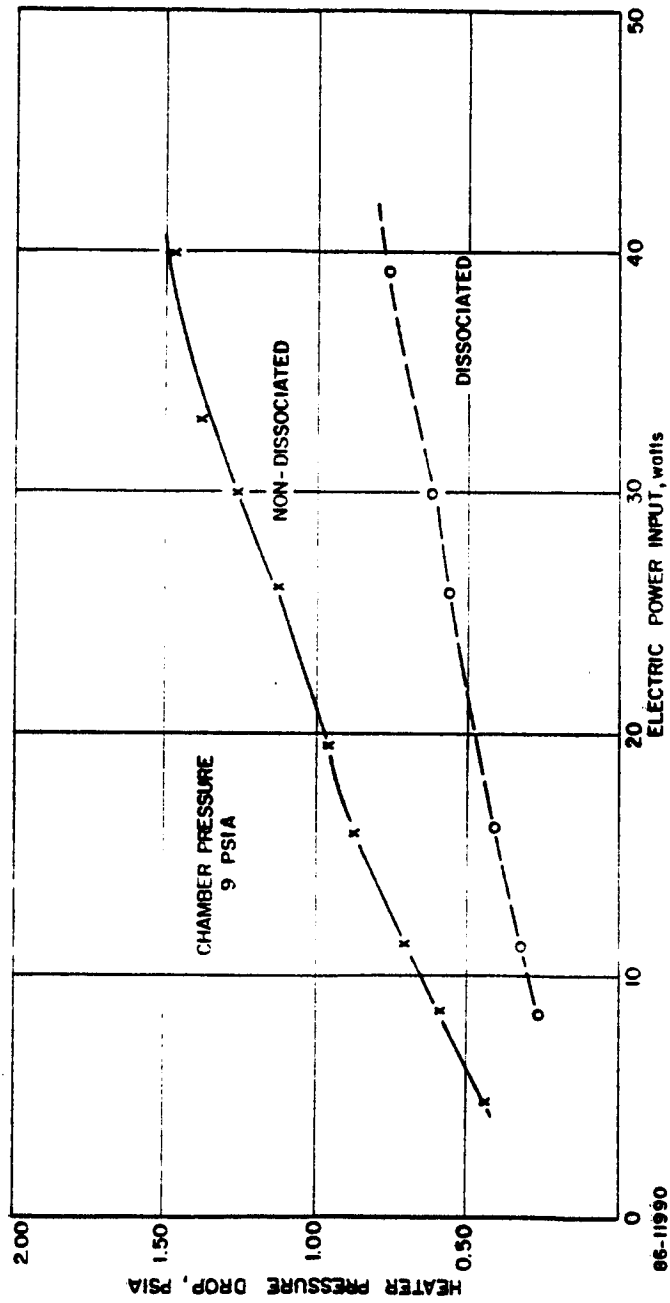
Figure 32 HEATER PRESSURE DROP VERSUS ELECTRIC POWER INPUT -- 9-PSIA
CHAMBER PRESSURE

86-11990

-60-
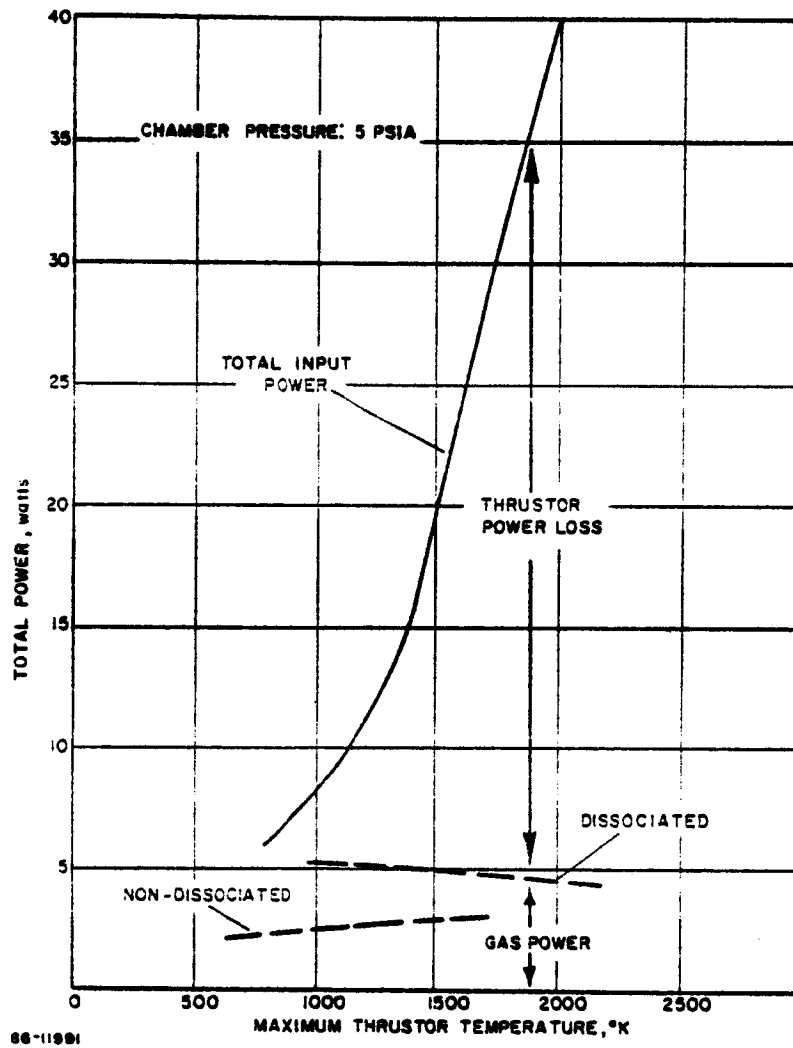
Figure 33 POWER DISTRIBUTION VERSUS MAXIMUM THRUSTOR TEMPERATURE --
5-PSIA CHAMBER PRESSURE
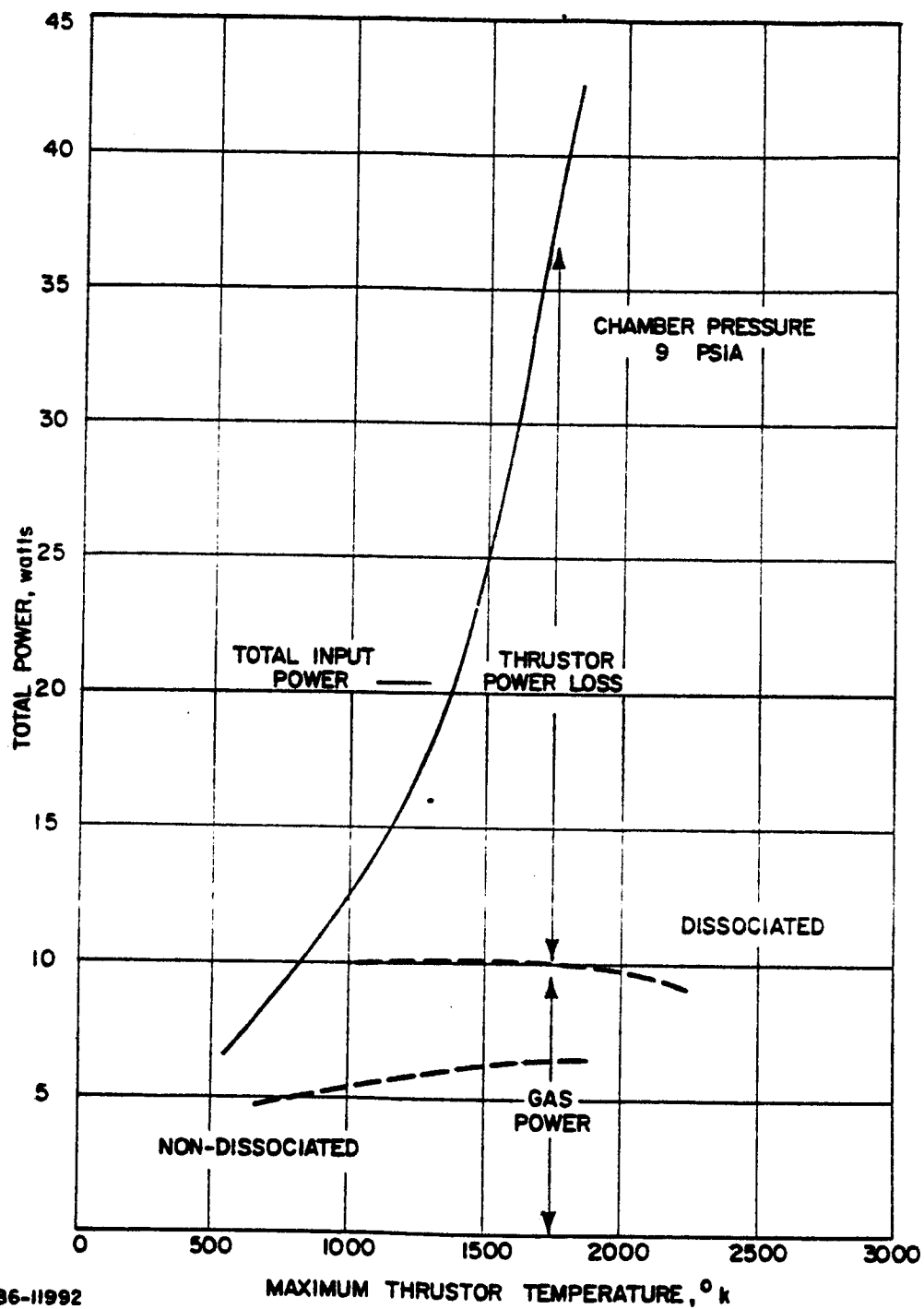
Figure 34 POWER DISTRIBUTIONS VERSUS MAXIMUM THRUSTOR TEMPERATURE--9-PSIA
CHAMBER PRESSURE

86-11992

-62-

of the inclusion of the dissociation energy. At 1750° K, as indicated pre-
viously it is likely that the ammonia is completely dissociated. In this
case the power transferred to the gas is about 5 watts for the 5-psia chamber
pressure and about 10 watts for the 9-psia chamber pressure. The thrustor
is 3/4 inch long; therefore, it has a heat transfer capability of at least 5
watts/cm. Referring to Figures 33 and 34,as the thrustor temperature is
increased an increasing portion of the input power goes into thrustor power
losses. At the higher temperatures the primary energy loss mechanism is,
of course, radiative energy transfer from the thrustor surface.

Figures 35 and 36 show the estimated thermal efficiency (based on total
input power) for the case of 5- and 9-psia inlet pressure. At 2000° K, the
thermal efficiency falls to about 10 percent for the 5-psia inlet pressure
and to about 20 percent for the 9-psia engine. The 3/4-inch-long engine
appears to be too long for the 5-psia inlet pressure. It is clear that the low
thermal efficiencies characteristic of the fast heat-up single pass heat ex-
changer can only be tolerated at relative low (order of watts) input power
levels.

4. Heater Electrical Characteristics

The electrical resistance of each unit length of the heater element is given
by an expression of the form

$$dR/dx = \rho/A \tag{18}$$

where ρ is the heater element material resistivity and A is the cross-section
area of the current path at heater station, x. Figure 37 shows a plot of the
resistivity of rhenium as a function of engine temperature. The local resis-
tance of the engine will, of course, increase as the engine temperature
increases. Estimates have been made of heater resistance by assuming a
linear temperature variation along the heater element from the initial tem-
perature to the maximum temperature. Figure 38 presents a comparison
of the estimated and observed heater resistances as a function of the
electric input power. The observed heater resistance is higher than the
predicted values. The discrepancy between the predicted and measured
heater resistance is probably due to a failure to properly take into account
the temperature variations along the heater element. The effective heater
temperature (and thus the resistance) are higher than the value determined
by assuming a simple linear temperature variation.
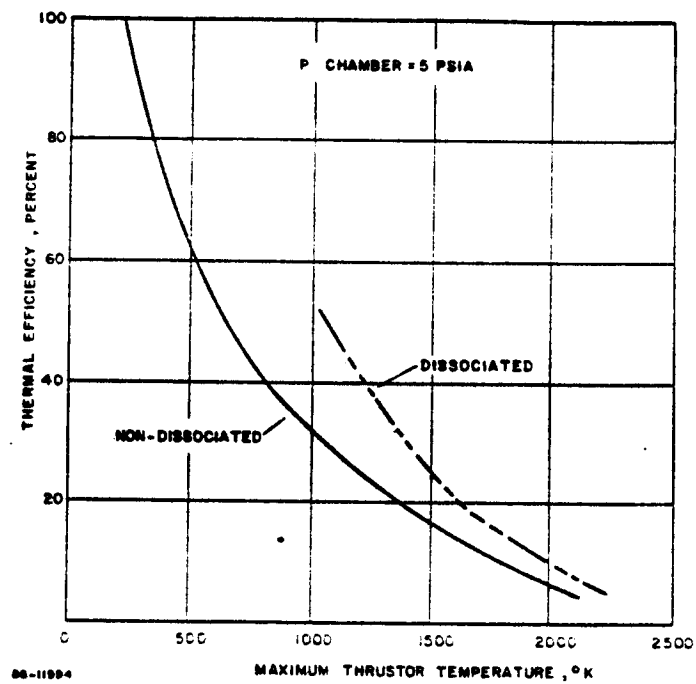
Figure 35 THERMAL EFFICIENCY VERSUS MAXIMUM THRUSTOR
TEMPERATURE — 5 PSIA
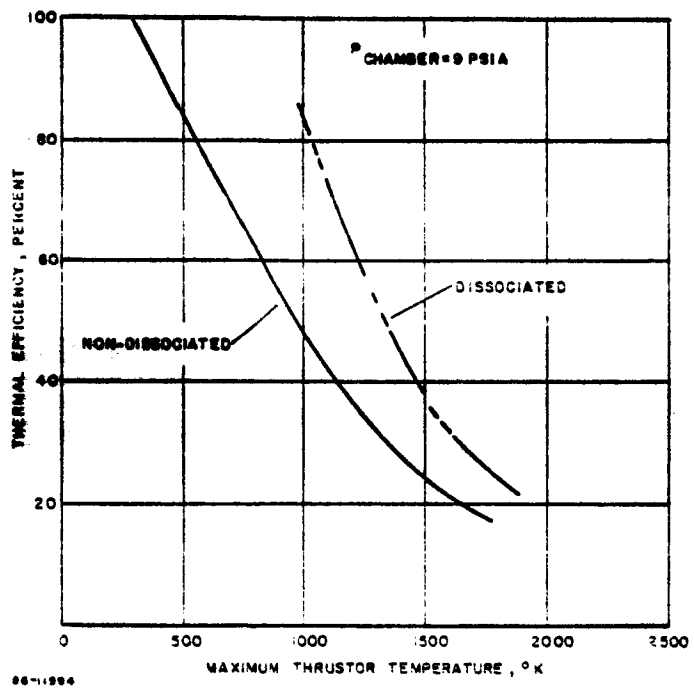
Figure 36 THERMAL EFFICIENCY VERSUS MAXIMUM THRUSTOR
TEMPERATURE — 9-PSIA
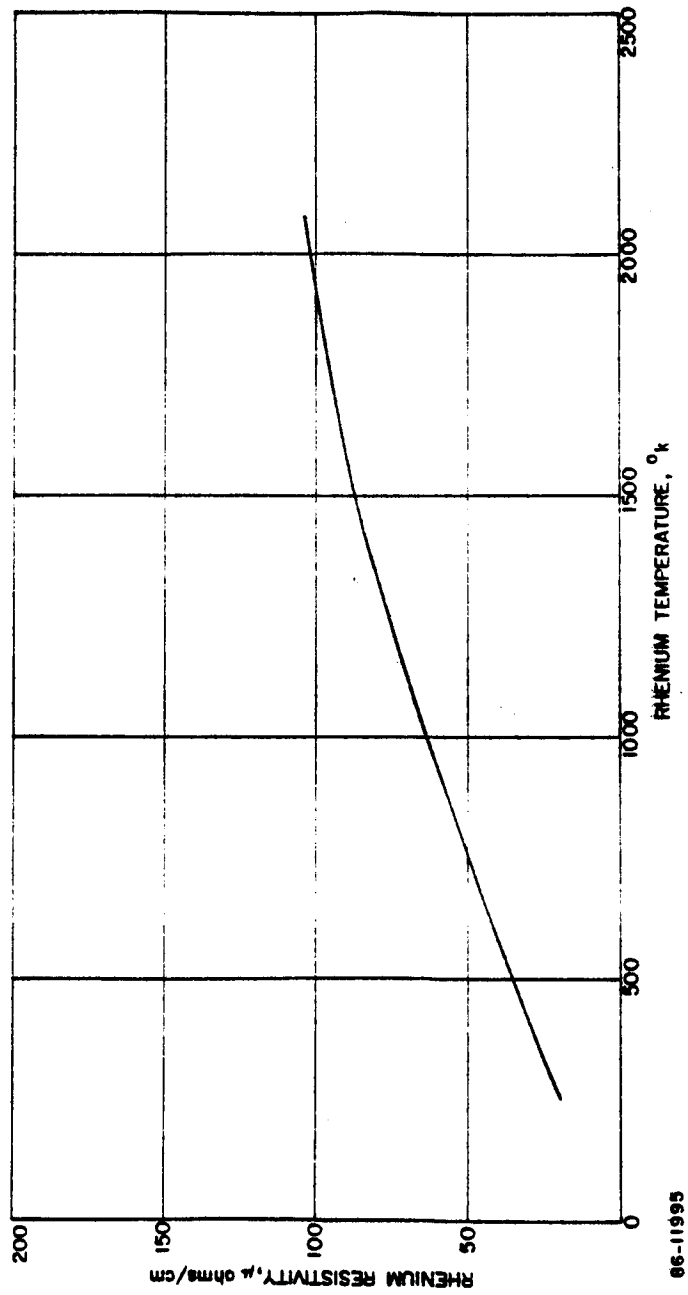
Figure 37 RHENIUM RESISTIVITY VERSUS TEMPERATURE

86-11995

-66-
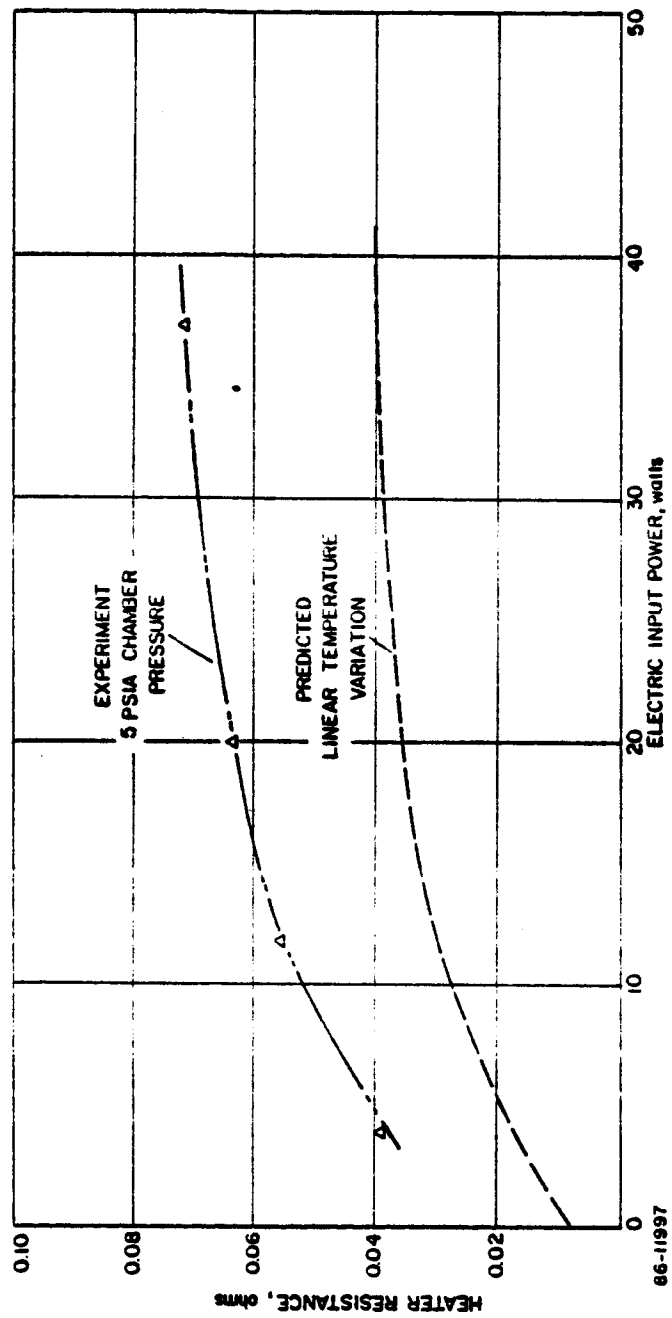
Figure 38 COMPARISON OF THE OBSERVED AND PREDICTED RHENIUM HEATER-
NOZZLE RESISTANCE

86-11997

-67-

5. Summary of Heat Transfer and Electrical Characteristics

The single-pass rhenium heater element has a heat transfer capability of at least 5 watts/cm, and a capability of bringing the ammonia to at least 2000° K (3140° F).

On the basis of mass flow and chamber pressure measurements it is estimated that ammonia dissociation is initiated at about 1250° K (1800° F) and is completed at about 1750° K (2700° F). The temperature values for the onset and completion of dissociation are only accurate to about ± 200° K.

The electric to gas power efficiency varies from about 75 percent at engine temperatures of about 750° K to about 20 percent at engine temperatures of about 2000° K.

E. PROPULSION PERFORMANCE OF THE FAST HEAT-UP THRUSTOR

1. Measurement of Engine Propulsion Performance

Two basic instruments have been developed for the measurement of engine propulsion performance. These are the wire-in-tension thrust stand and the single axis wire table. In the case of the wire-in-tension thrust stand the thrust produced by the engine deflects a wire and the deflection of the wire is recorded by means of a sensitive displacement transducer. The single axis wire table measures the impulse bit output of the thrust units when they are operated for a finite pulse length. The two basic thrust stands are described below.

a. Wire-In-Tension Thrust Stand

The basic wire-in-tension thrust stand is shown in Figure 39, and a photograph of the stand is shown in Figure 40.
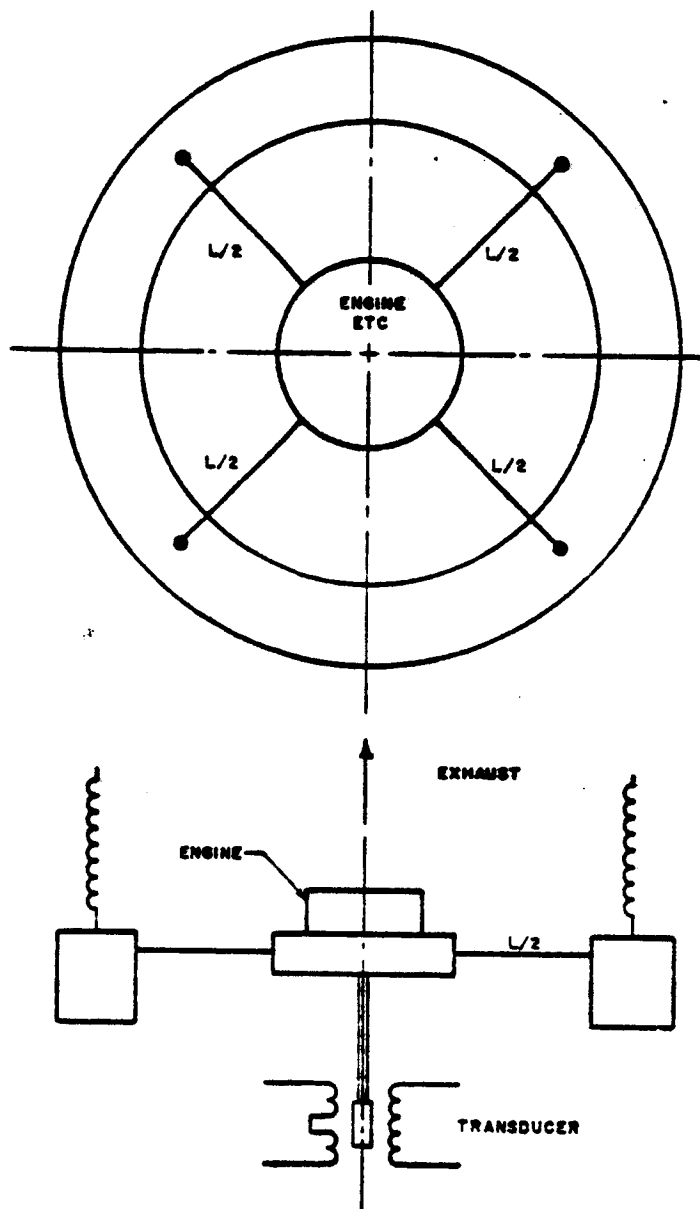
Figure 39 BASIC WIRE-IN-TENSION THRUST STAND

64-12244

REMOTELY CONTROLLED DEVICE FOR LIFTING WEIGHTS

DISPLACEMENT TRANSDUCER

OUTER RING

YOKE CONNECTED TO OUTER RING

WEIGHTS FOR CALIBRATION

YOKE CONNECTED TO INNER RING FOR CALIBRATION WITH WEIGHTS

WIRE CONNECTING INNER RING TO OUTER RING (ONE OF FOUR)

INNER RING TO WHICH RESISTOJET IS CONNECTED FOR THRUST MEASUREMENT
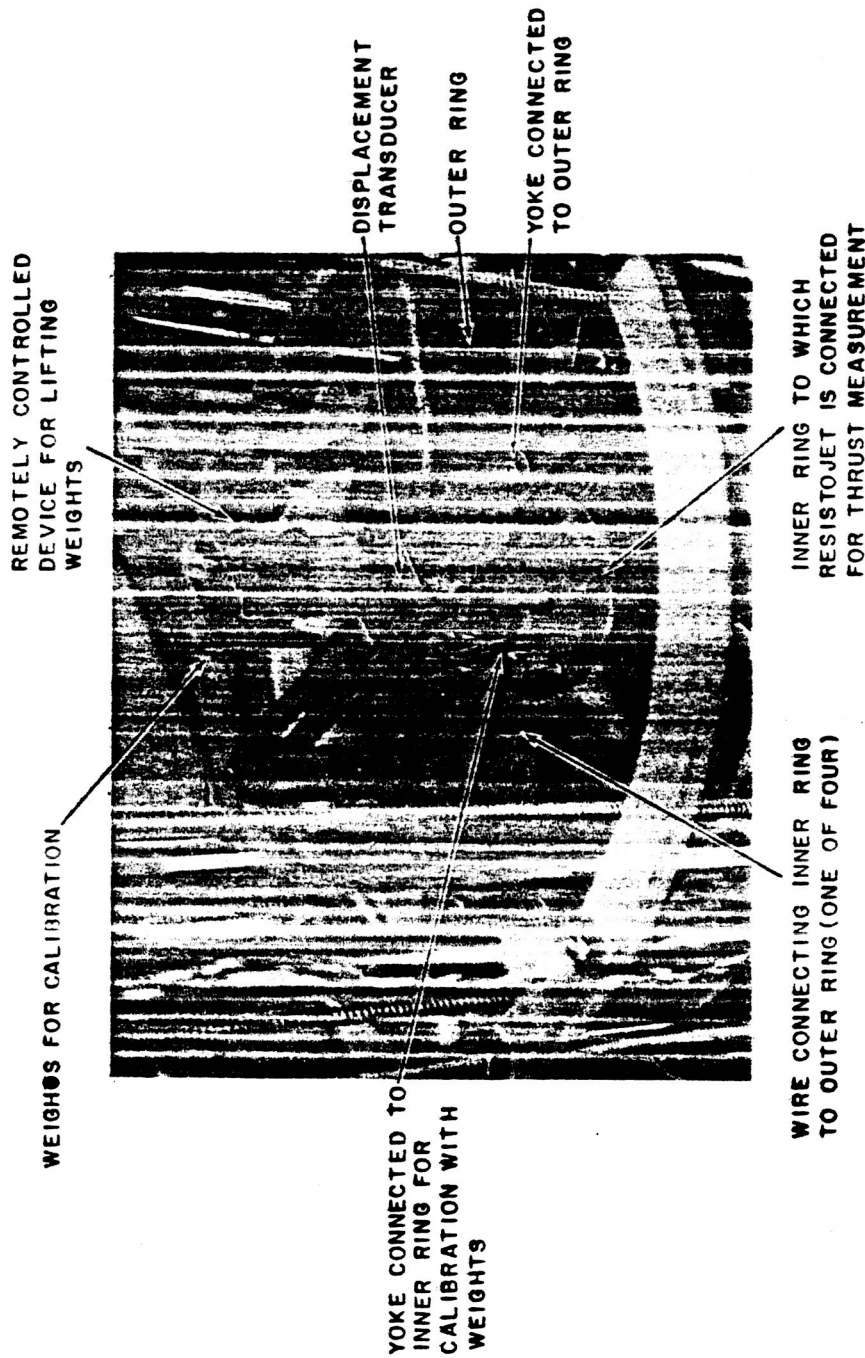
Figure 40 PHOTOGRAPH OF WIRE-IN-TENSION THRUST STAND

65-8162

-70-

The engine system horizontal mounting bracket is supported by four wires in tension. The wires are, in turn, connected to a surrounding aluminum ring which is shock mounted by means of springs. The thrust axis of the engine is vertical; the engine and its propellant tank are located on the mounting bracket. The entire assembly is located in a transparent bell jar, and the bell jar is evacuated to pressures of 10^{-4} torr and below by means of a 4-inch diffusion pump. Order of magnitude calculations have made it clear that conduction losses can be the predominant energy loss mechanisms (input power ~ 10 watts) for resistojets operated at a few torr pressure; thus, it is necessary to operate the low power resistojet in a relatively "hard" vacuum to prevent all the input energy from being conducted away to the surrounding environment. Further, as will be described subsequently, back pressure has a significant effect on engine propulsion performance.

A simplified analysis of the transient behavior of the thrust stand is based on the behavior of a string when loaded with a mass, M. For the simple analysis the ratio of string to mass weight is assumed to be small; and analysis for infinite values of string to mass weight is presented in Appendix A. The equation of motion for a string of length, L, in tension is given by

$$M \frac{d^2 y}{dt^2} = - Mg - F - 2T \sin \theta$$ (19)

$$= - Mg - F - 4T \frac{y}{L}$$

where, F is the applied force and y is the displacement.

The solution to this differential equation is

$$y = \frac{MgL}{4T} - \frac{FL}{4T} \left[1 - \cos 2 \sqrt{\frac{T}{ML}} t \right]$$ (20)

The inclusion of damping modifies Equation (19) to read

$$\frac{d^2 y}{dt^2} + \frac{f}{M} \frac{dy}{dt} + \frac{4T}{ML} y = - g - \frac{F}{m}$$ (21)

where $f/M \, dy/dt$ is the damping term.

The displacement is given by

$$y(t) = -\frac{MgL}{4T} - \frac{FL}{4T} \left[1 - \frac{2}{\omega} \sqrt{\frac{T}{ML}} \; e^{-\frac{fT}{2M}} \sin(\omega t + \phi) \right] \qquad (22)$$

where

$$\omega^2 = \frac{4T}{ML} - \frac{f^2}{4M^2}$$

and

$$\tan \phi = \frac{2\omega M}{f}$$

For times long compared with $\frac{2M}{f}$, this decays to the steady position given by

$$y = -\frac{MgL}{4T} - \frac{FL}{4T} \qquad (23)$$

as expected.

Figure 41 shows a plot of the two cases: (1) no damping, and (2) moderate damping. As can be seen from Figure 11, for moderate friction effects which damp the oscillations in just a few cycles, the frequency of oscillation is essentially the same for the damped as for the undamped situation. The actual period for the damped curve shown is

$$P_d = \frac{8}{\sqrt{63}} \; P_u = \frac{8}{\sqrt{63}} \; \pi \sqrt{\frac{ML}{T}} \; \text{sec} \qquad (24)$$

Thus, moderate damping of the thrust stand results in only minor changes in the period of the stand.

In the actual thrust stand shown in Figures 39 and 40 the central support bracket is essentially supported by two strings; the tension term in the above equations must thus be replaced by $2T$. The wire weight is about 0.01 pound, and the weight of the engine, propellant storage tank, etc., is about 2 pounds; the condition that wire weight to string weight is much less than unity is, therefore, satisfied.

The displacement of the engine support as a function of applied thrust is given by

-72-
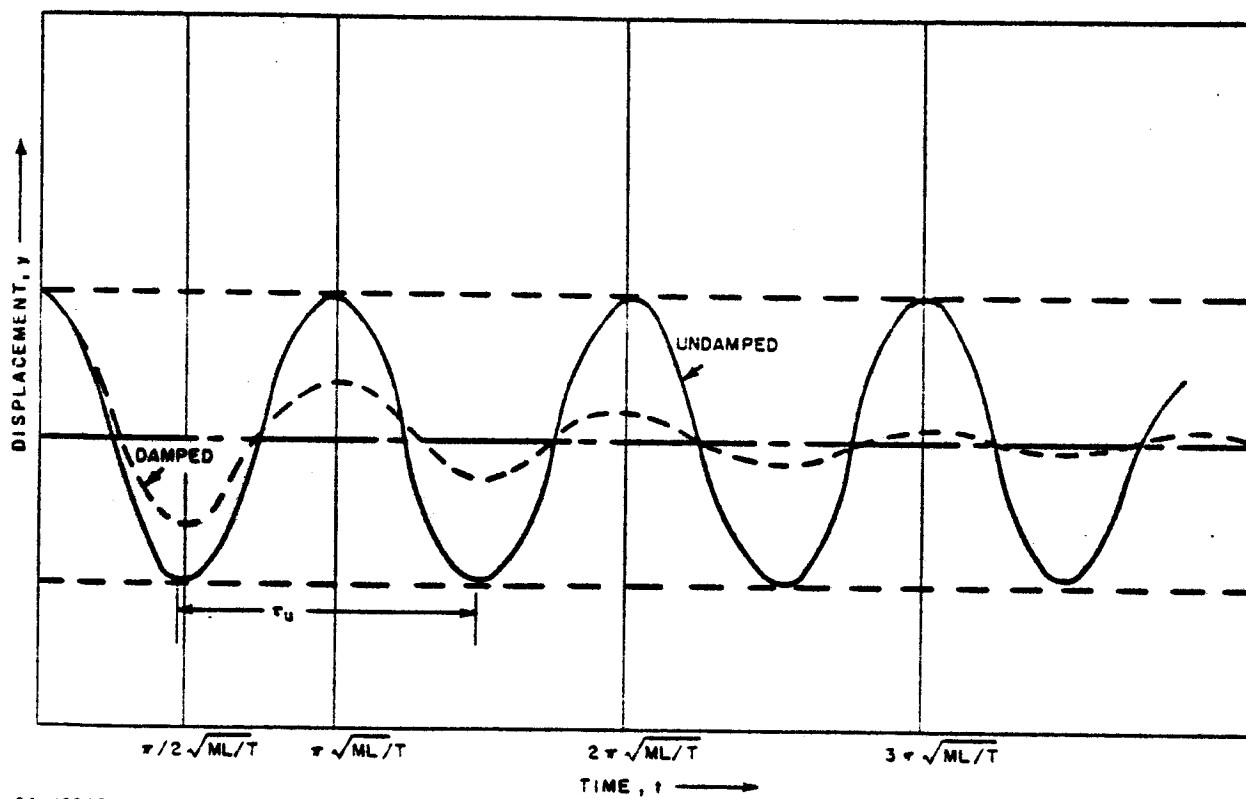
64-12245

Figure 41   DAMPED AND UNDAMPED THRUST STAND OSCILLATIONS

-73-

$$y = \frac{FL}{8T} \qquad (25)$$

or the engine thrust is given by

$$F = \frac{8T}{yL} \qquad (26)$$

For a fixed value of the string tension to length ratio the minimum detectable thrust level is inversely proportional to the displacement, y; similarly, for a fixed detectable displacement, y, the minimum detectable thrust varies directly as the string tension to length ratio. It is noted that the minimum measurable thrust is independent of the mass of the engine system, M. Figure 42 presents curves of minimum measurable displacements of 10^{-6}, 3×10^{-7}, and 10^{-7} inch. The minimum detectable thrust level can be decreased by reducing the T/L ratio, however, as will be shown below there is a corresponding decrease in the thrust stand response characteristics.

The natural frequency of oscillation of the thrust stand is given by

$$V = \frac{1}{\pi} \sqrt{\frac{2T}{ML}} \qquad (27)$$

and the natural time period is

$$P = \pi \sqrt{\frac{ML}{2T}} \qquad (28)$$

The natural frequency of the thrust stand, unlike the minimum detectable thrust level, is a function of the mass, M, of the engine system. Figure 43 presents a plot of natural frequency, ν, as a function of T/L ratio for an engine system weight of 2 pounds, which is comparable to the actual system weight. The natural frequency setting of the thrust stand for the measurements presented in this report was about 40 Hz corresponding to a tension to length ratio of about 40 lb/in. Assuming a minimum detectable displacement of 3×10^{-7} inch, this corresponds to a minimum detectable thrust level of 10^{-1} millipound. Estimated values of the natural frequency, time constant, and minimum detectable thrust, as a function of T/L ratio for an engine system weight of 2 pounds and a displacement transducer capable of detecting 3×10^{-7} inch is presented in Table VIII.
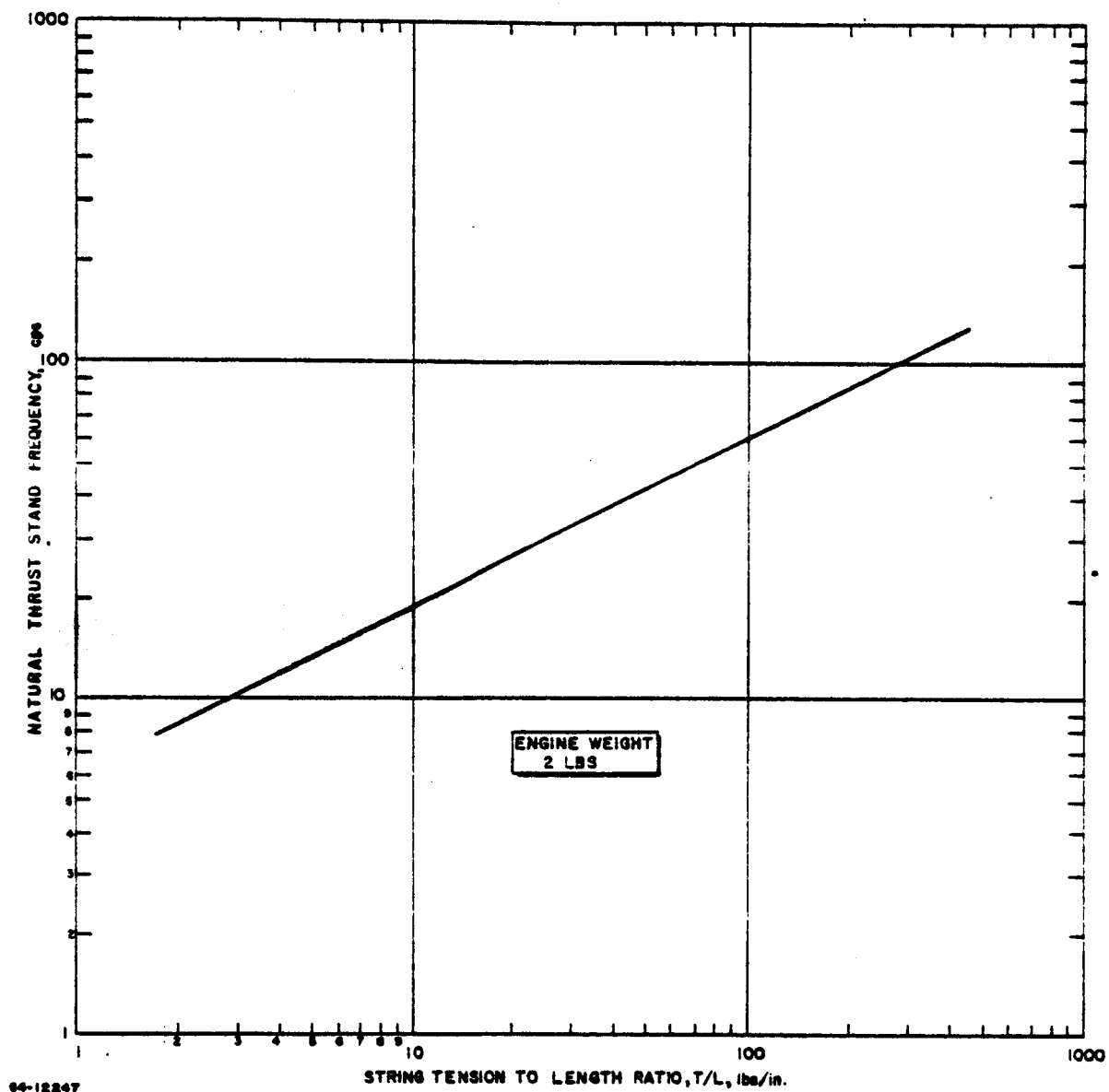
Figure 42 MINIMUM MEASUREABLE THRUST VERSUS STRING TENSION TO LENGTH RATIO
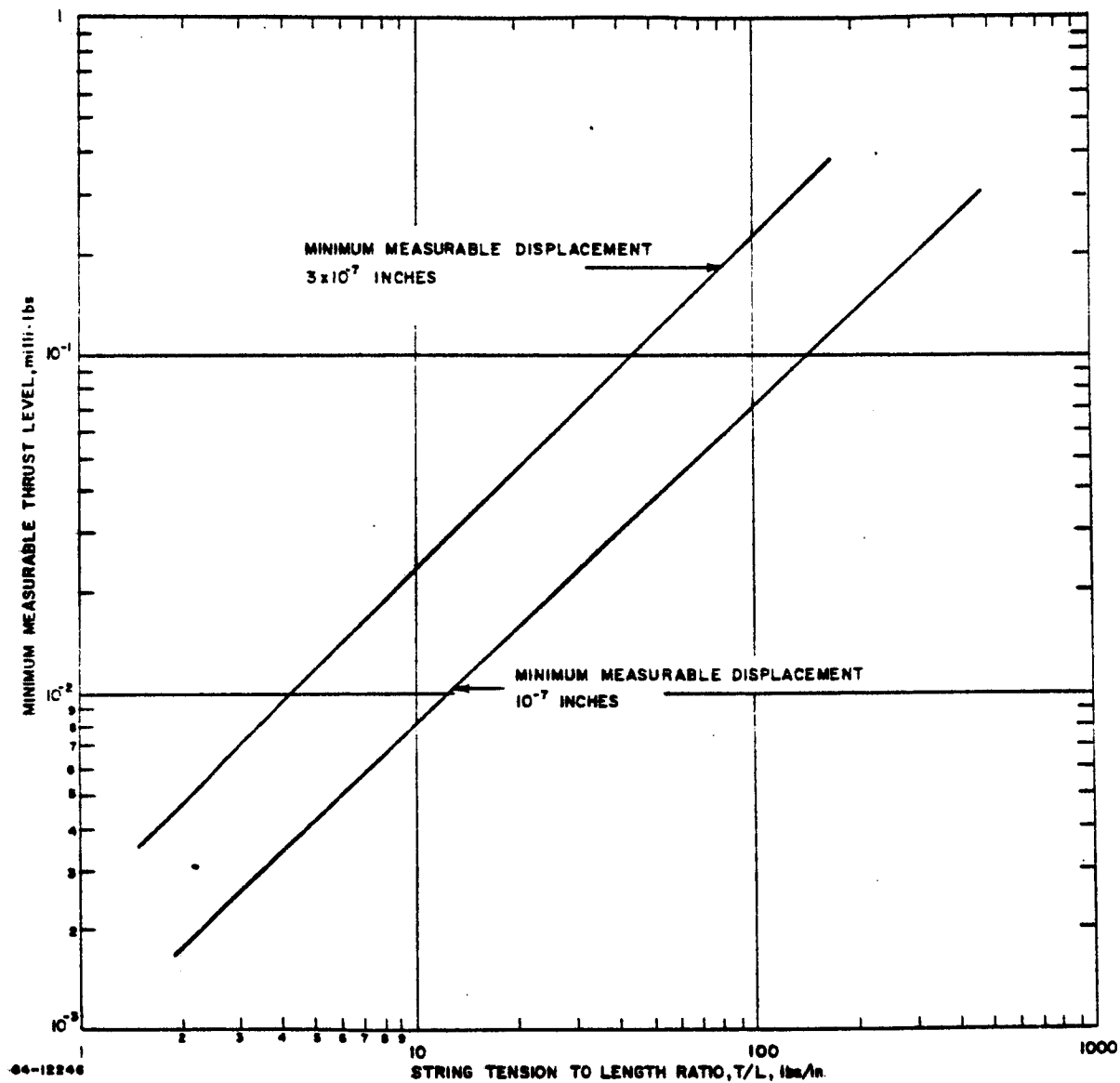
Figure 43 THRUST STAND NATURAL FREQUENCY VERSUS STRING TENSIONS TO LENGTH RATIO

-76-

TABLE VIII

FREQUENCY RESPONSE VERSUS MINIMUM DETECTABLE THRUST LEVEL AND STRING TENSION/LENGTH RATIO
(Engine Mass 2 pounds; Minimum Displacement 3×10^{-7} inch)

Tension/Length Ratio (lb/in)	Natural Frequency Response (Hz)	Time Constant (seconds)	Minimum Thrust Level (pounds)
2.5	10	100×10^{-3}	0.006×10^{-3}
10	20	50×10^{-3}	0.024×10^{-3}
40	40	25×10^{-3}	0.10×10^{-3}
160	80	12.5×10^{-3}	0.40×10^{-3}
640	160	6.25×10^{-3}	1.60×10^{-3}
2560	320	3.12×10^{-3}	6.40×10^{-3}
10240	640	6.24×10^{-3}	25.6×10^{-3}

Engine thrust is indicated by the measurement of the vertical displacement between the inner and outer rings. Since very small displacements are involved a highly sensitive linear differential transformer (Sanborn Model 595D-005BM) is used for the displacement measurement. One side of the displacement transducer is supported on a large yoke fastened to the outer ring; the other side is supported on a small yoke fastened to the inner ring. For calibration small weights are placed on a channel mounted on top of the inner ring. A motor-operated lifting device permits remote positioning of known weights on the inner ring; this permits the static determination of the displacement as a function of applied force. Figure 44 shows a typical displacement versus force curve showing that the displacement is linear with force.

The thrustor on the inner ring is connected to the ammonia propellant supply by a flexible tube. This tube introduces negligible error in the measurement since the calibration techniques include deflection of this tube and since the flexural force of the tube is orders of magnitude less than that of the four wires supporting the inner ring.

b.   Single Axis Wire Table

The single axis impulse table is shown in Figure 45. The unit basically consists of a horizontal table mounted on a vertical wire. Impulse bits (lb-sec) are given to the table by means of a thrustor and observations are made on the change of angular rate of the table. The angular

-77-
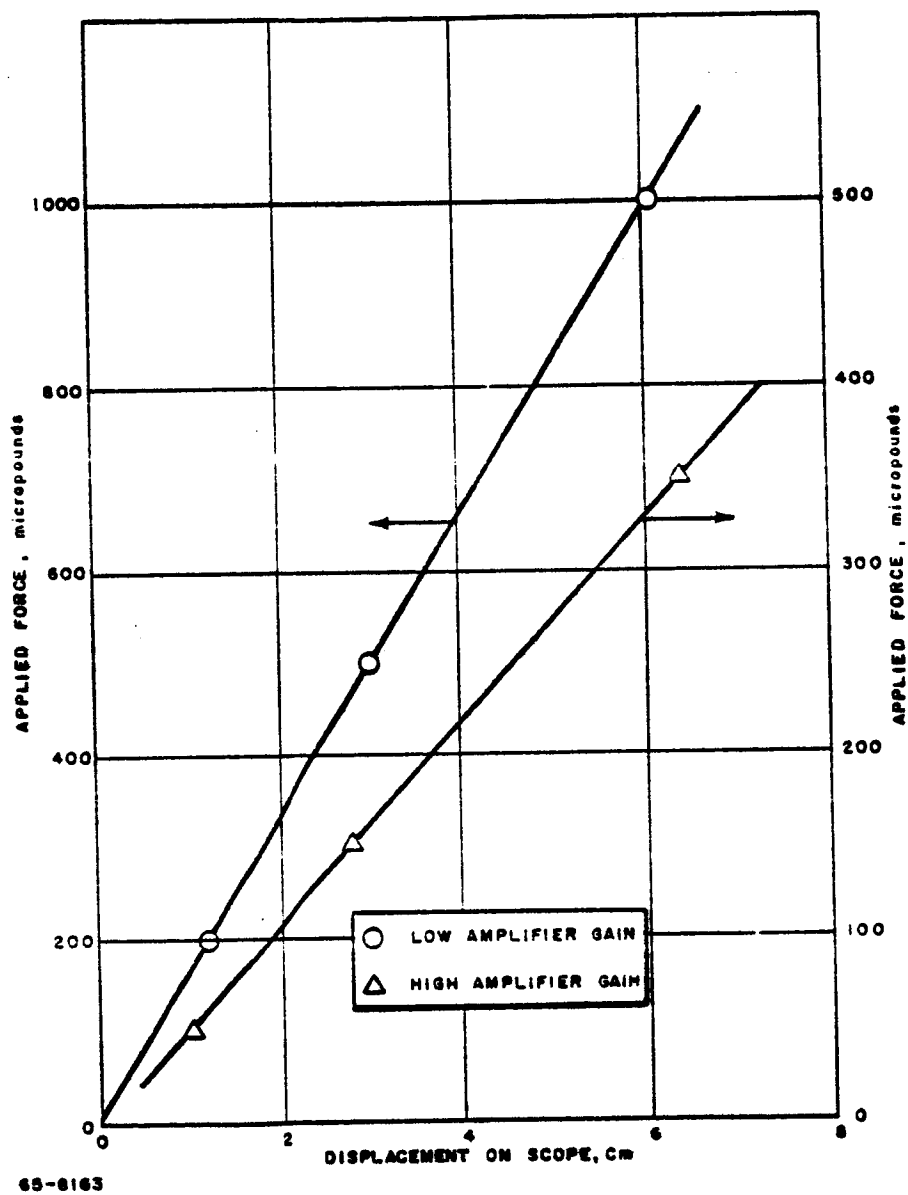
Figure 44 THRUST STAND DISPLACEMENT VERSUS APPLIED FORCE

65-8163

-78-

VACUUM-CHAMBER WALL

TORQUE MOTOR

CONTROL AND POWER CABLE

SERVO-FOLLOWER PLATFORM

LIGHT SENSOR

FLEX LEADS FOR RECORDER

SUSPENSION WIRE WITH PROTECTIVE COVER

MIRROR

TABLE WITHOUT EQUIPMENT
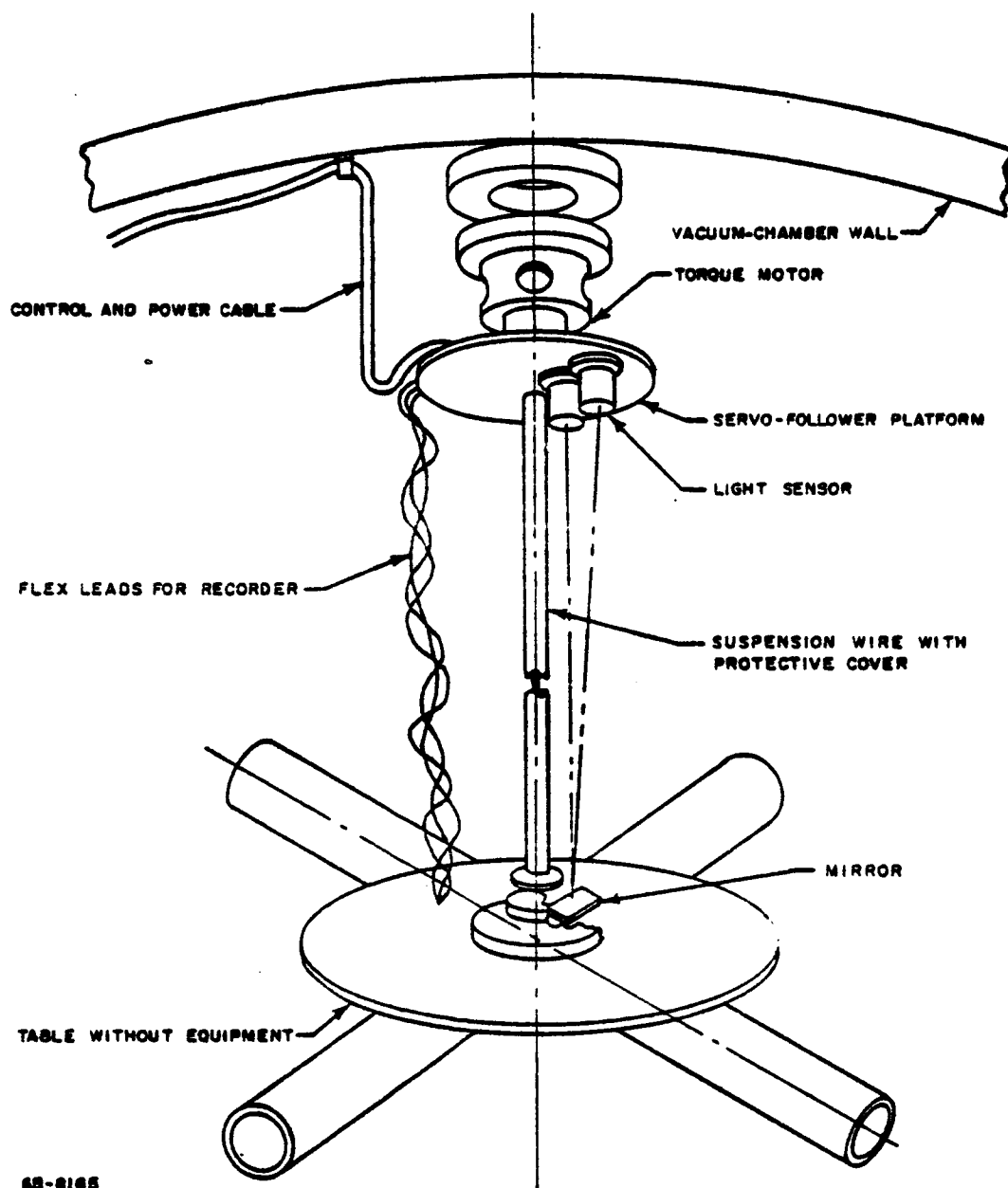
68-8165

Figure 45 SINGLE-AXIS IMPULSE TABLE

rate change of the table is measured with a rate gyroscope which has a sensitivity of 554 mv/deg/sec. The equation of motion of the table is given by

$$\Delta\dot{\theta} = \frac{\tau_R + \tau_D}{J}\,\tau_R \tag{29}$$

Where, $\Delta\dot{\theta}$ (radians/sec) is the measured change in angular rate, τ_R (lb-ft) = F (lbs) x l (ft) is the applied torque, τ_D (lb-ft) is the system disturbance torque, τ_R (sec) is the time the applied torque acts on the system and J (lb-ft-sec^2) is the table moment of inertia.

The major design goal in the development of the impulse table has been to hold the disturbance torque, τ_D, which primarily arises from wire tension to as low a value as possible. This has been accomplished by using a cable which has a spring constant of about 300 dyne-cm/deg, and by providing an optical driven servo system which can hold the table to less than 0.01 degree. Thus, the disturbance torque due to wire tension is less than 5 dyne-cm which corresponds to a thrust of less than 1 micropound, at a moment arm of 2 feet.

The impulse table is mounted in a test chamber which is 6 feet in diameter and 9 feet long. The chamber is connected to a 32-inch diameter diffusion pump which makes it possible to achieve a blank-off pressure of 3×10^{-6} torr and a pressure of less than 1×10^{-4} torr at ammonia flow rates of the order of 10×10^{-6} lb/sec. As will be discussed below it has been established that back pressure is a critical factor in the determination of the performance of low-thrust gas expulsion devices.

The table is calibrated in the following manner. The relationship between the applied torque and the resulting rotational velocity change is given by

$$FR = J\,\Delta\dot{\theta}/\Delta t \tag{30}$$

where, F is the applied thrust, R is the moment arm, J is the moment of inertia, $\Delta\dot{\theta}$ is the angular rate change, and Δt is the time period for which the force F is applied.

Referring to Figure 46, a known force is applied tangential to a radius of the table. A weight is suspended between the tank and the table by means of a fine (1/2-mil) tungsten wire; the weight W and thus a force $F = \cot \theta W$ are applied to the table at a radius, R, by a mechanical latch mechanism. Prior to the attachment of the sling the table is brought to a condition of constant velocity by adjusting the twist in the support table until the net torque on table is zero. This is evidenced by a constant level output from the rate gyroscope.

To illustrate the procedure the angular rate change is given by

$$\Delta \dot{\theta} = \Delta S / G \tag{31}$$

where ΔS is the signal change brought about by the change in rate. The table moment of inertia is then given by

$$J = FR\,G\,\Delta t / \Delta S \tag{32}$$

Typical calibration results are presented in Table IX.

TABLE IX

TYPICAL CALIBRATION RESULTS FOR THE SINGLE-AXIS TABLE

Calibration Force, T	499 micropounds
Torque Arm, R	1.50 feet
Gyro Sensitivity, G	554 mv/deg/sec
Signal Change, ΔS	80 millivolts
Time of Acceleration, Δt	23.6 seconds
Calculated Moment of Inertia, J	7.0 lb/ft/sec^2

From the preceding relations it immediately follows that the thrustor output is given by

$$T_1 = T_2 \; \frac{\Delta S_1}{\Delta S_2} \; \frac{R_2}{R_1} \; \frac{\Delta t_2}{\Delta t_1} \tag{33}$$

where the subscript 2 refers to calibration and the subscript 1 refers to the direct thrust measurement.

The lower impulse bit capability for the single-axis table is between 10^{-5} and 10^{-6} lb-sec.

SUPPORT WIRE

TABLE

θ

CALIBRATION WEIGHT

W

86-11997
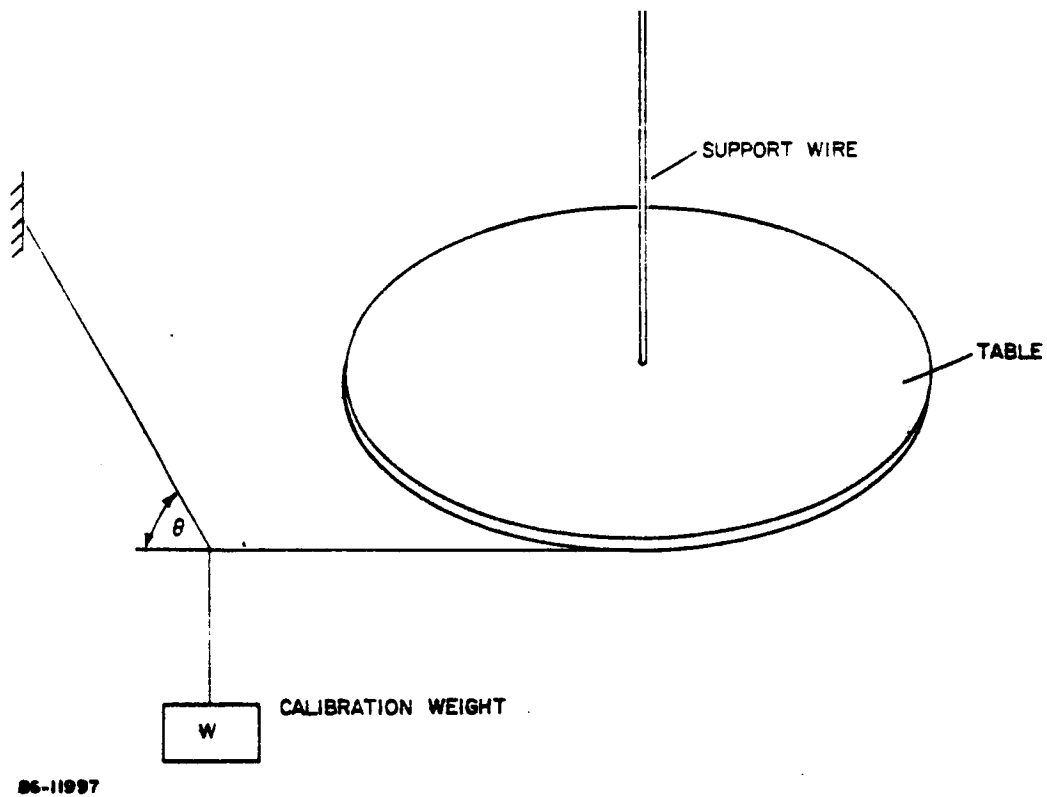
Figure 46 CALIBRATION TECHNIQUE FOR THE SINGLE-AXIS IMPULSE TABLE

-82-

2. Effect of Back Pressure on Thrustor Performance

During the course of the present study it has become apparent that test chamber pressure has a critical effect on the performance of thrustors operated in the thrust range below 1 millipound. Figure 47 shows a plot of measured engine thrust versus back pressure for the 11-mil orifice shown in Figure 47. The thrust shows a remarkable sensitivity to back pressure and only begins to level off at back pressures below the order of 10^{-4} torr. On the basis of these results, all the thrust data to be subsequently reported have been obtained at back pressures of less than 10^{-4} torr. The physical reasons for the strong variation of thrust level with back pressure are not at all understood and are outside the scope of the present investigation. It is suggested, however, that previous uncertainty with regard to the performance of micro-thrustors has been associated with this back pressure effect (refs. 5, 6, 7).

3. Comparison of Single-Axis Table and Wire-In Tension Thrust Stand Measurements

Figure 48 shows a comparison of thrust measurements on the 11-mil orifice made on the single-axis table and the wire-in tension thrust stand. The impulse bit lengths on the single-axis table were between 10 and 100. seconds. No significant difference can be observed in the two sets of data over the thrust range from 50 to 1200 micropounds. The lower thrust measurement capability of the wire-in tension thrust stand is about 50 micropounds. The thrust measurements are estimated to be accurate to about $\pm$ 5 percent.

4. Propulsion Performance of an 11-mil Orifice

The propulsion performance of a nozzle can be expressed in terms of a discharge coefficient, C_D, a thrust coefficient, C_F, and a specific impulse or exhaust velocity coefficient, C_v.

The discharge coefficient, as indicated previously, is defined as

$$C_D = \dot{m}_{actual} / \dot{m}_{ideal} \tag{34}$$

where, $\dot{m}_{actual}$ is the actual mass flow and $\dot{m}_{ideal}$ is the ideal mass flow passed by the nozzle under the same conditions. The discharge coefficient versus Reynolds number for the 11-mil orifice has been shown in Figure 24. As the throat Reynolds number decreases the discharge coefficient decreases due to the viscous flow effects.

The nozzle thrust coefficient is defined as the ratio of engine thrust to the product of throat area, A_t, and nozzle chamber pressure, P_c, or

-83-
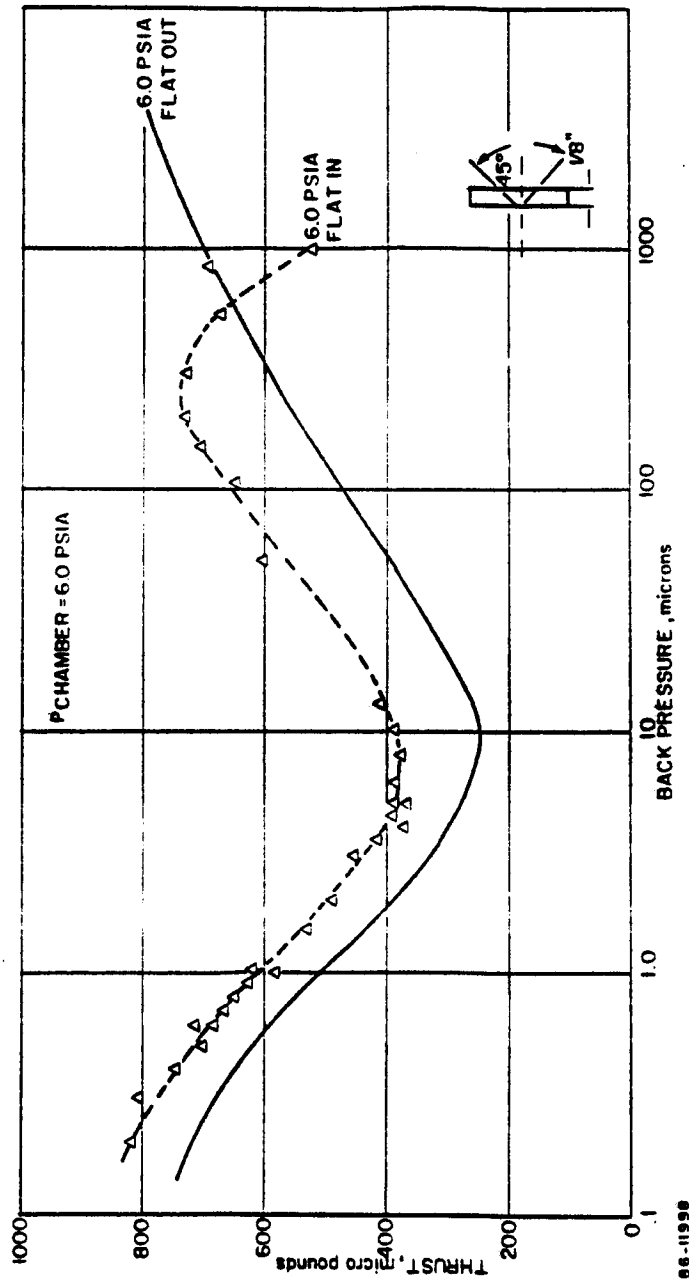
Figure 47 MEASURED ENGINE THRUST VERSUS BACK PRESSURE -- 11-MIL ORIFICE

86-11998

-84-
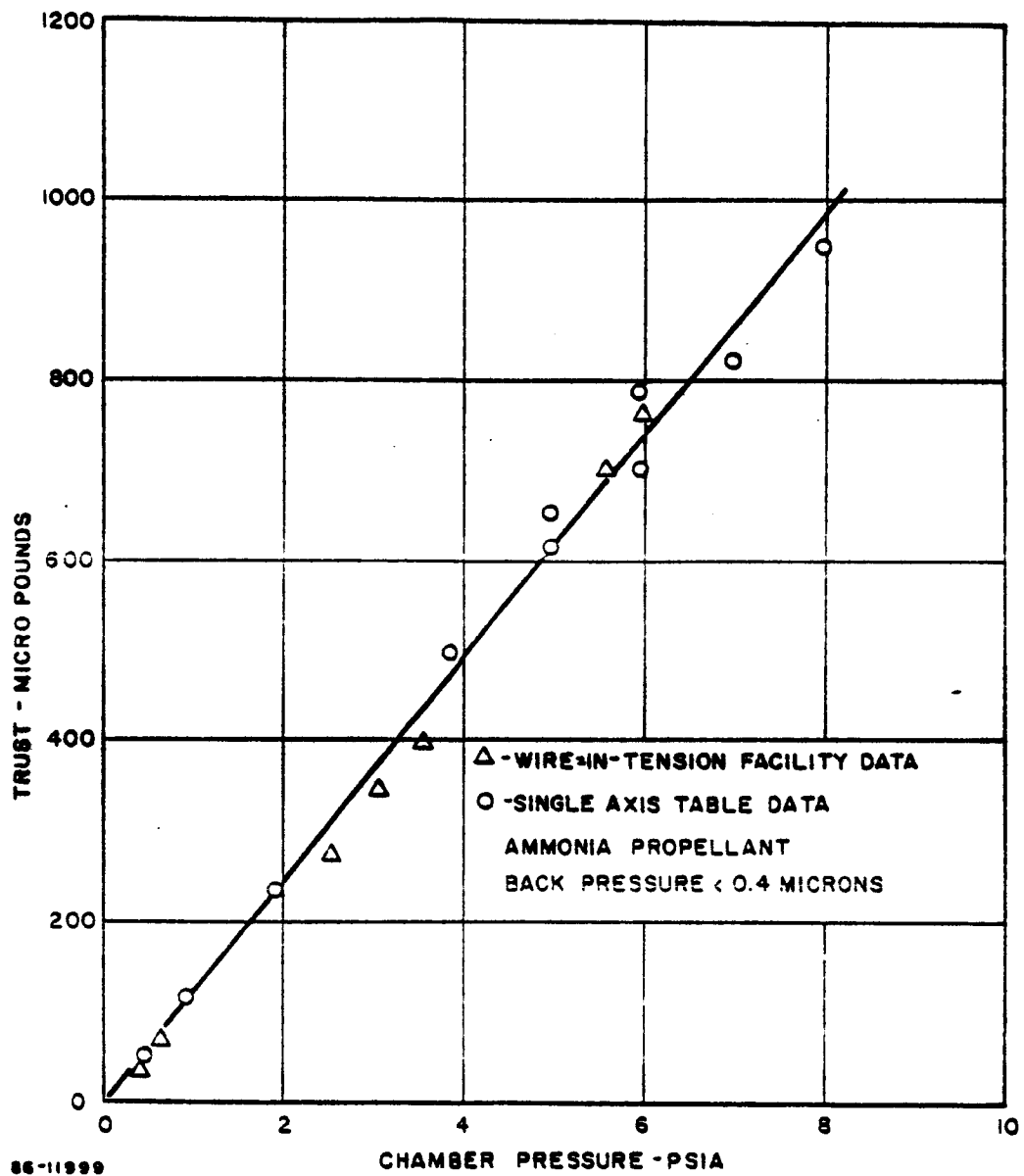
Figure 48 THRUST VERSUS CHAMBER PRESSURE — 11-MIL ORIFICE — COMPARISON OF WIRE-IN-TENSION
THRUST STAND AND SINGLE-AXIS TABLE

$$C_F = T/P_c A_t \tag{35}$$

It is proposed that the basic criteria for nozzle performance is the throat Reynolds number. The throat Reynolds number is given by

$$R_{e,t} = \frac{230 \quad T \text{ (micropounds)}}{I_{sp} \text{ (seconds) } D_t \text{ (inches) } \mu_t \text{ (μ-poises)}} \tag{36}$$

For example, for ammonia at 70° F and a thrust level of 10 micropounds, the measured I_{sp} is 95 seconds, the throat diameter is 10×10^{-3} inch, the viscosity is 100 micropoises and the Reynolds number is 24. At a fixed thrust level the Reynolds number will decrease with increase in engine temperature due to the increase in viscosity. A plot of the thrust coefficient as a function of Reynolds number for the 11-mil diameter orifice is shown in Figure 49.

As in the case of the orifice coefficient, the nozzle coefficient decreases markedly with decrease in throat Reynolds number.

From Equations (34) and (35) it follows that the specific impulse is given by

$$I_{sp} = \frac{T}{\dot{m}_{actual}} = \frac{C_F P_C A_t}{C_D \dot{m}_{ideal}} \tag{37}$$

or

$$I_{sp} \propto C_F / C_D \tag{38}$$

For a fixed nozzle inlet condition the specific impulse is thus proportional to the ratio of thrust coefficient, C_F, and orifice coefficient, C_D.

Since the advent of the technological need for microthrustors there has been considerable speculation as to the value of the throat Reynolds number at which nozzle viscous flow losses become predominant. Figure 50 presents a plot of the ratio of thrust to orifice coefficient as a function of throat Reynolds number. The thrust to orifice coefficient ratio and thus the specific impulse are remarkably insensitive to throat Reynolds number down to Reynolds numbers of about 5. The results imply that, (for the 11-mil orifice with a 45-degree half-angle) down to Reynolds numbers of the order of 5, the viscous flow effects primarily appear in the inlet region to the nozzle throat and do not significantly effect the nozzle downstream expansion process.
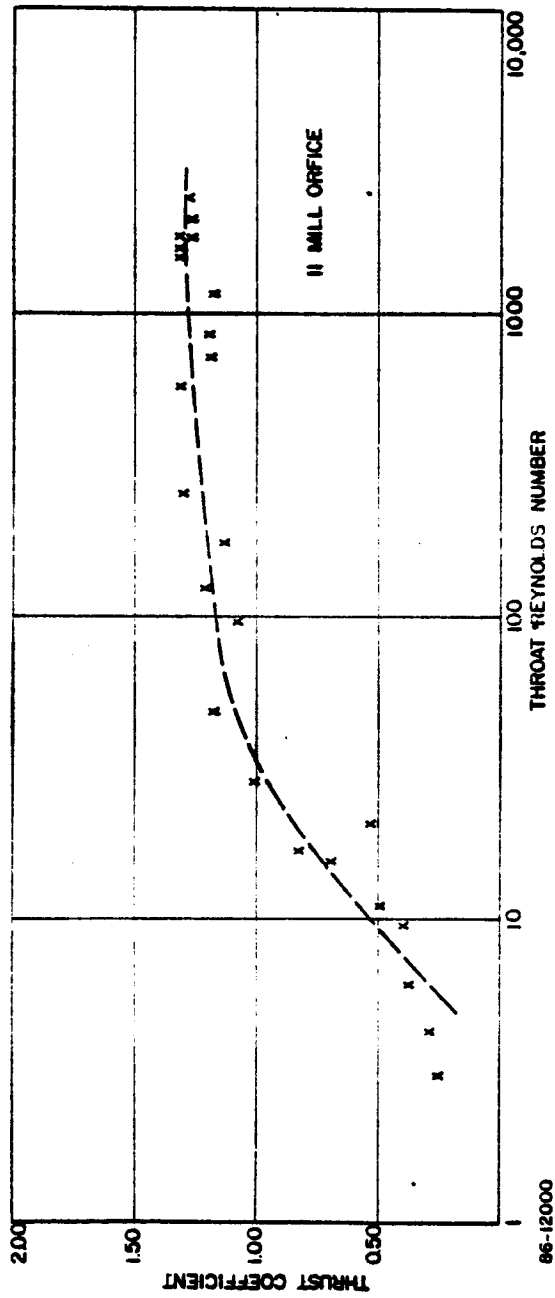
Figure 49 THRUST COEFFICIENT VERSUS THRUST REYNOLDS NUMBER --
11-MIL ORIFICE
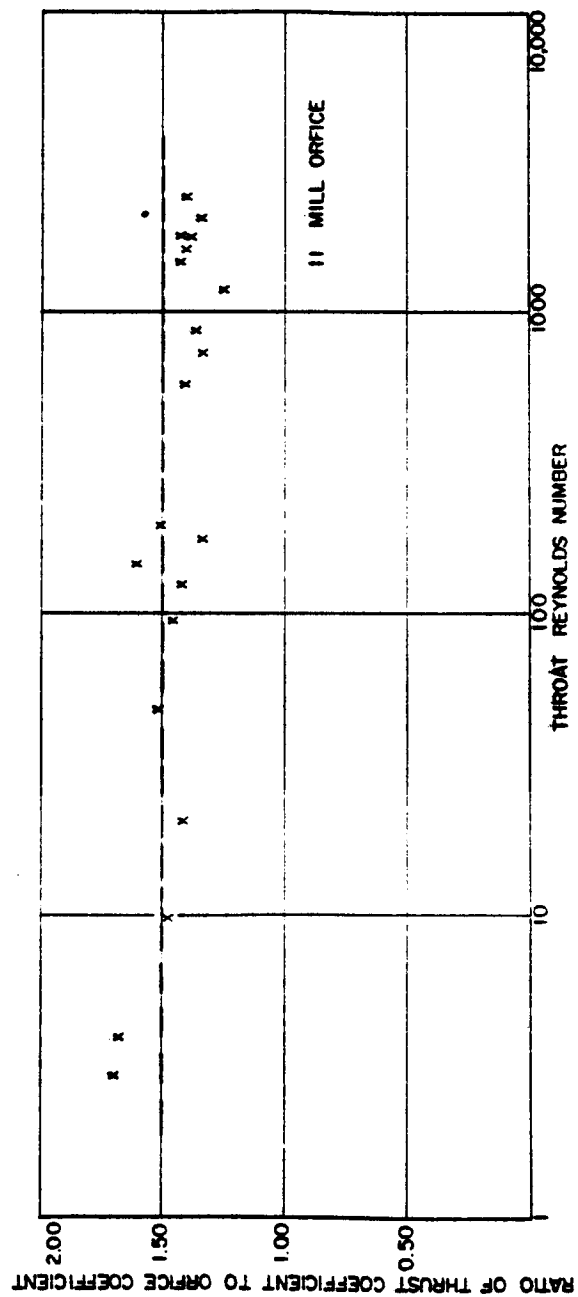
Figure 50 RATIO OF THRUST-TO-ORIFICE COEFFICIENT VERSUS THRUST REYNOLDS NUMBER -- 11-MIL ORIFICE

Figure 51 shows specific impulse versus thrust level for the 11-mil orifice. There is no significant falloff in specific impulse down to thrust levels as low as 2 or 3 micropounds.

The ideal specific impulse corresponding to the complete conversion of available energy to kinetic energy is given by

$$I_{sp, ideal} = 9.34 \sqrt{h} \tag{39}$$

where, h (cal/g) is the total energy in the gas. For cold ammonia at 70° F, the available energy is 159 cal/g and the corresponding maximum attainable specific impulse is 117 seconds.

In general, the nozzle will have a finite area ratio and will operate at a finite back pressure. The ideal isentropic specific impulse is given by

$$I_{sp, isen} = I_{sp, max} f(A_{exit}/A^*, P_{chamber}/P_{exit}, \gamma) \tag{40}$$

where,

$$f = \sqrt{1 - \left(\frac{P_{exit}}{P_{chamber}}\right)^{\frac{\gamma-1}{\gamma}} + \frac{A_{exit}}{A^*} \frac{1}{\gamma} \sqrt{\frac{\gamma-1}{2}} \left(\frac{2}{\gamma+1}\right)^{\frac{\gamma-1}{2(\gamma-1)}}}$$

$$\left(\frac{P_{exit}}{P_{chamber}} - \frac{P_{ambient}}{P_{chamber}}\right) \tag{41}$$

The ideal isentropic specific impulse for the 11-mil orifice 100-to-1 area ratio and pressure ratio of 10^4 to 1 is 104 seconds.

In order to correct for the non-axial component of the velocity a theoretical correction factor, λ, can be applied to the nozzle-exit momentum of an ideal rocket motor. This factor is the ratio between the momentum of the gases in a nozzle with a finite nozzle angle 2α and the ideal momentum of a nozzle with all gases flowing in an axial direction.

$$\lambda = 1/2 (1 + \cos \alpha) \tag{42}$$

For an ideal nozzle $\lambda = 1.0$. In the case of the 11-mil nozzle, which has a 45-degree half-angle, the nozzle correction factor is 0.86.

The isentropic specific impulse with nozzle correction for momentum losses is given by
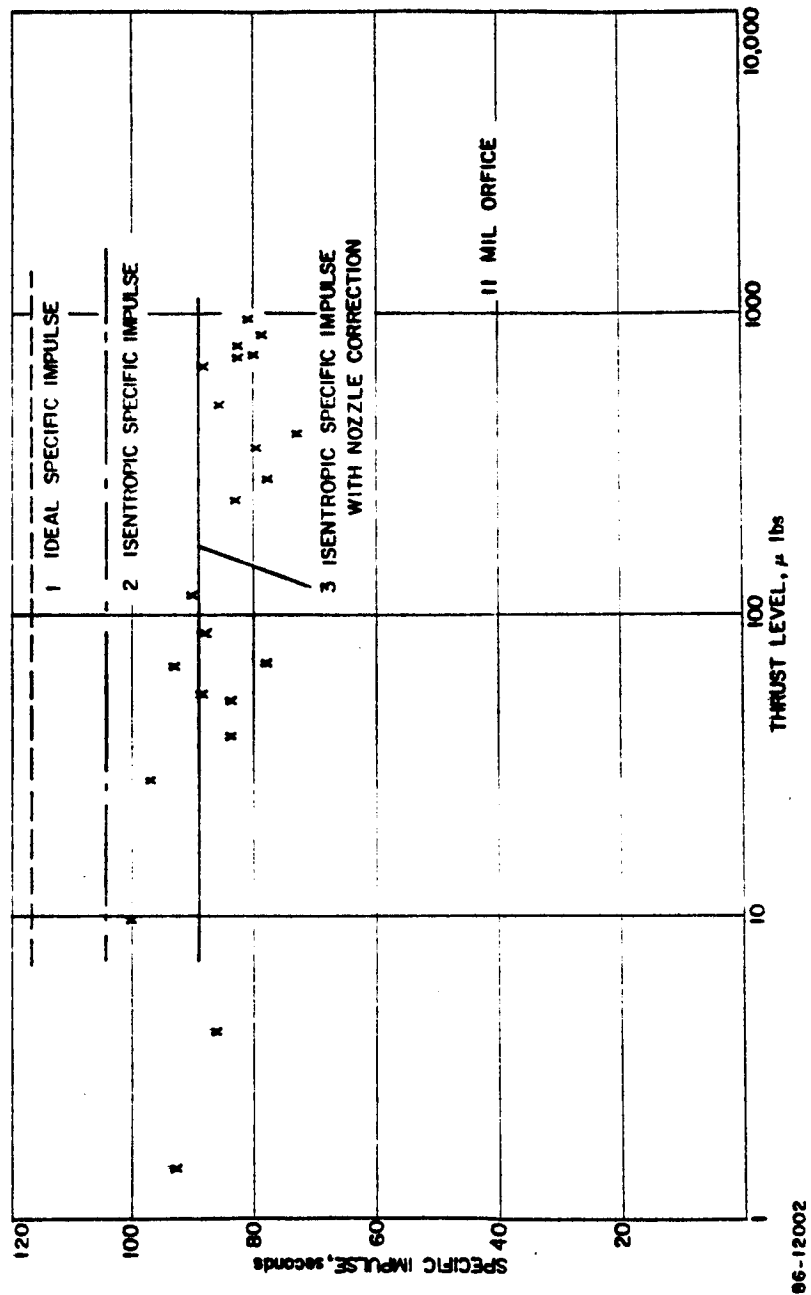
Figure 51 SPECIFIC IMPULSE VERSUS THRUST LEVEL -- 11-MIL ORIFICE

86-12002

$$I_{sp, isen, corr} = \lambda I_{sp, isen} \tag{43}$$

For the 11-mil orifice the isentropic specific impulse corrected for momentum losses is 87 seconds.

The ideal, isentropic, and isentropic with nozzle correction factor specific impulses for the 11-mil orifice are shown superimposed on the experimental data in Figure 51. The specific impulse of the 11-mil orifice is quite close to the ideal values predicted on the basis of isentropic flow and a nozzle correction factor. Thus, as concluded previously, there appears to be little significant effect of viscous flow losses on nozzle performance over the operating range of the present experiments..

5. Propulsion Performance of Fast Heat-Up Thrustors (300 to 1200 micropounds)

The thrust level versus electric input power for the rhenium thrustor operated at chamber pressures, respectively, of 5- and 9-psia is shown in Figures 52 and 53. The thrust level decreases with increase in the electric power input due to the pressure drop in the heater tube and viscous flow effects on the nozzle thrust coefficient. As discussed previously in Section II.D (see Figures 31 and 32), estimates have been made for the pressure drop in the heater tube on the basis of one-dimensional viscous flow and momentum considerations. Figure 54 shows the thrust coefficient, C_F, as a function of throat Reynolds number. The thrust coefficient, defined as $T/P_c A_t$, is based on the measured thrust and the estimated pressure at the nozzle inlet. As indicated estimates of the heater tube pressure drop were obtained both for the dissociated and nondissociated ammonia. Comparing Figures 50 and 54 the thrust coefficient for the rhenium engine both decrease with decrease in throat Reynolds number in about the same manner as the 11-mil orifice.

Figures 55 and 56 show specific impulse versus electric power input for the rhenium engine at chamber pressures, respectively, of 5- and 9-psia. At the same electric power input the specific impulse for the chamber pressure of 5-psia is slightly higher than for the chamber pressure of 9-psia. This apparent slight increase of specific impulse with decrease in chamber pressure probably corresponds to the fact that the gas and engine temperatures are more nearly equal for the lower mass-flow situation. Figure 57 shows a plot of the ratio of thrust-to-total-input power (cold gas plus electric input power) as a function of electric power input. The over-all efficiency is less than 20 percent at specific impulses greater than 200 seconds. The low-thrust efficiencies primarily result from the high radiative-power-loss characteristic of the high engine temperatures.
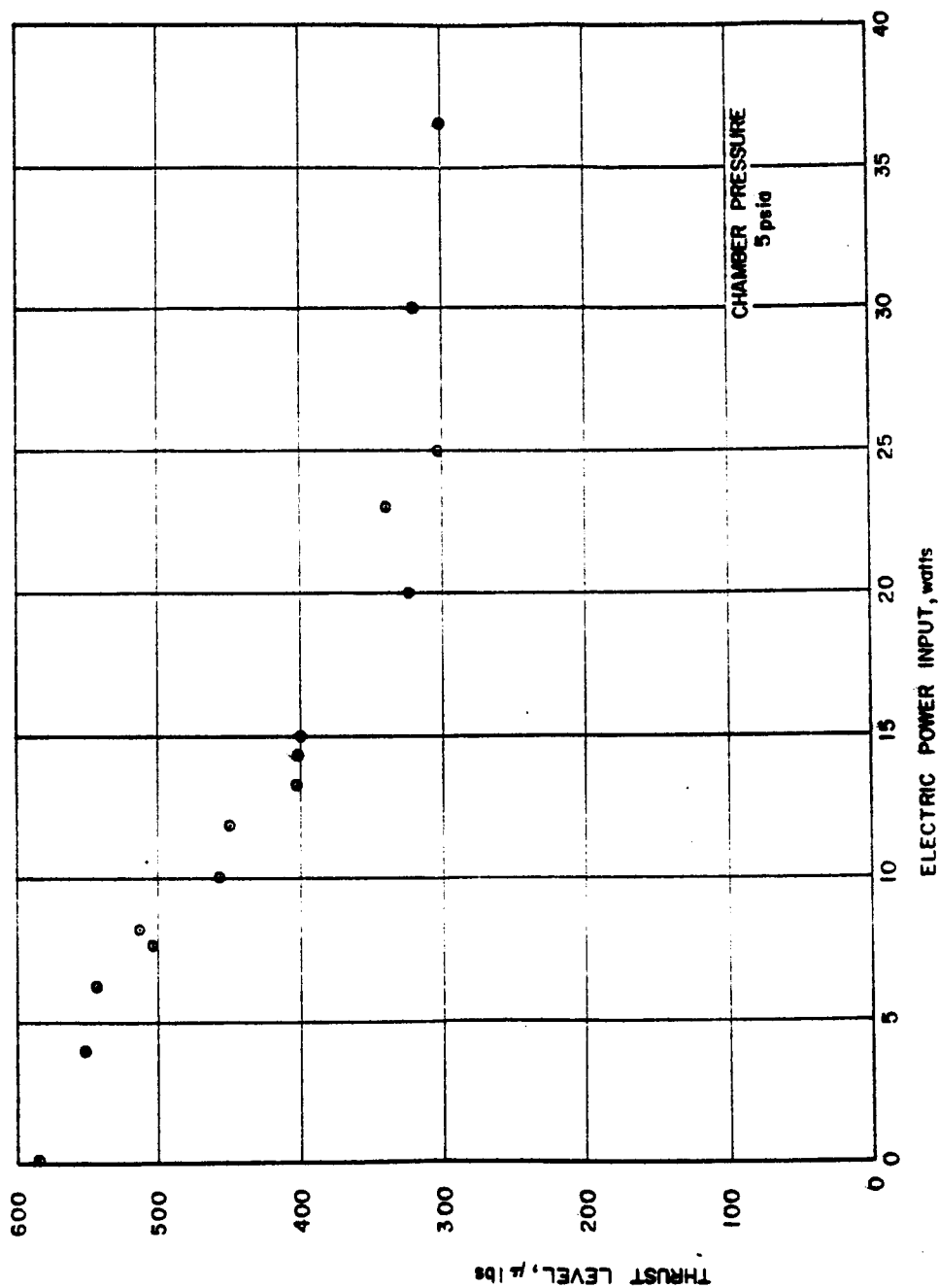
Figure 52 THRUST LEVEL VERSUS ELECTRIC INPUT POWER -- RHENIUM HEATER-NOZZLE --
5-PSIA CHAMBER PRESSURE

86-12003

-92-
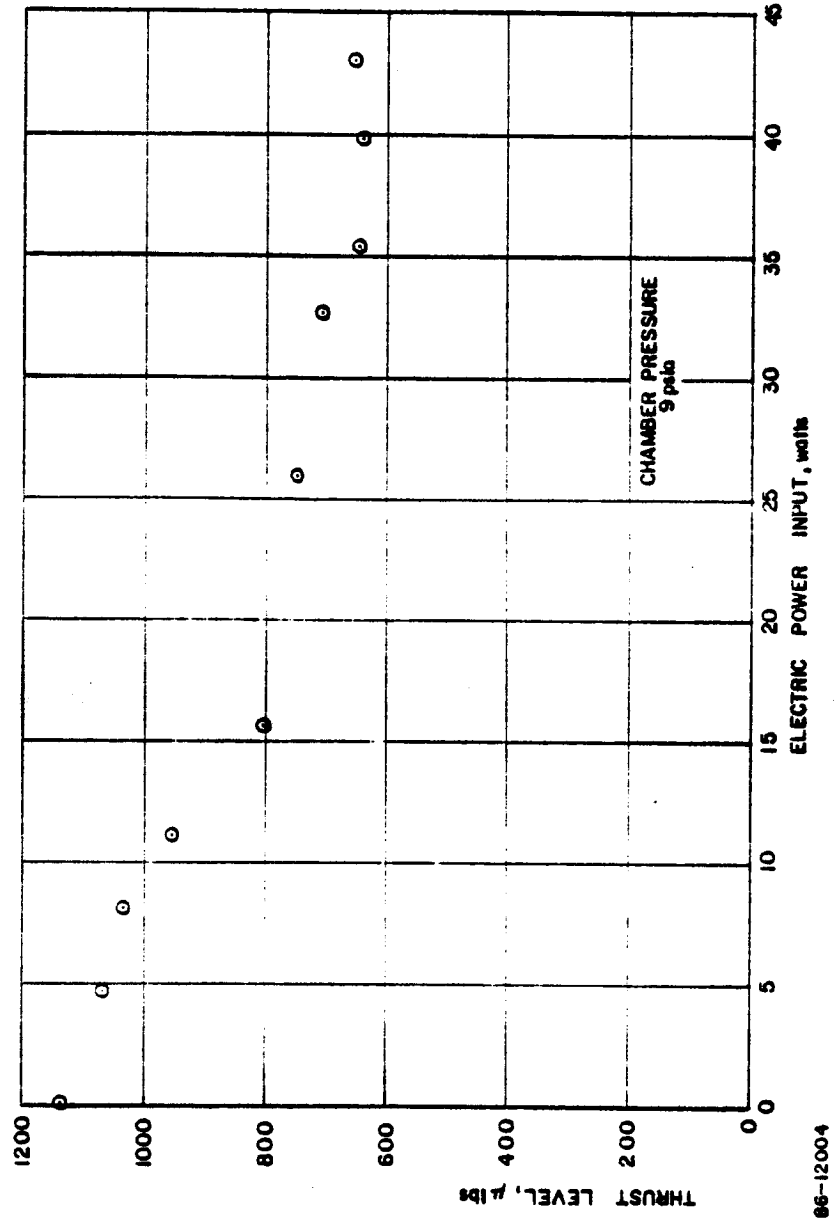
Figure 53 THRUST LEVEL VERSUS ELECTRIC INPUT POWER -- RHENIUM HEATER-
NOZZLE -- 9-PSIA CHAMBER PRESSURE

86-12004
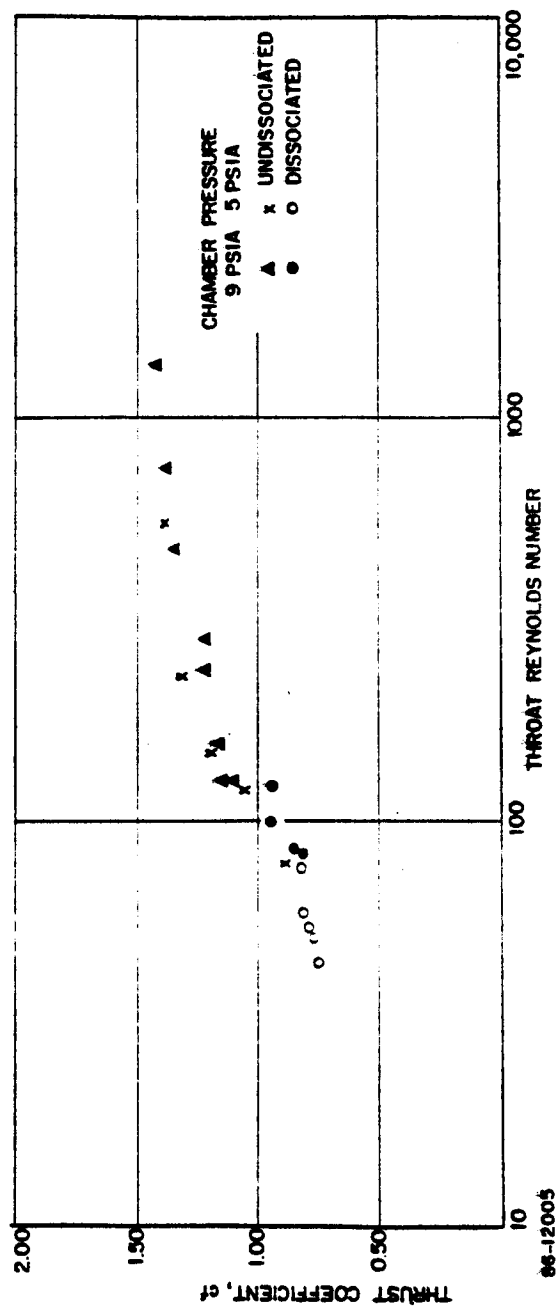
Figure 54 THRUST COEFFICIENT VERSUS THRUST REYNOLDS NUMBER

86-12005

-94-
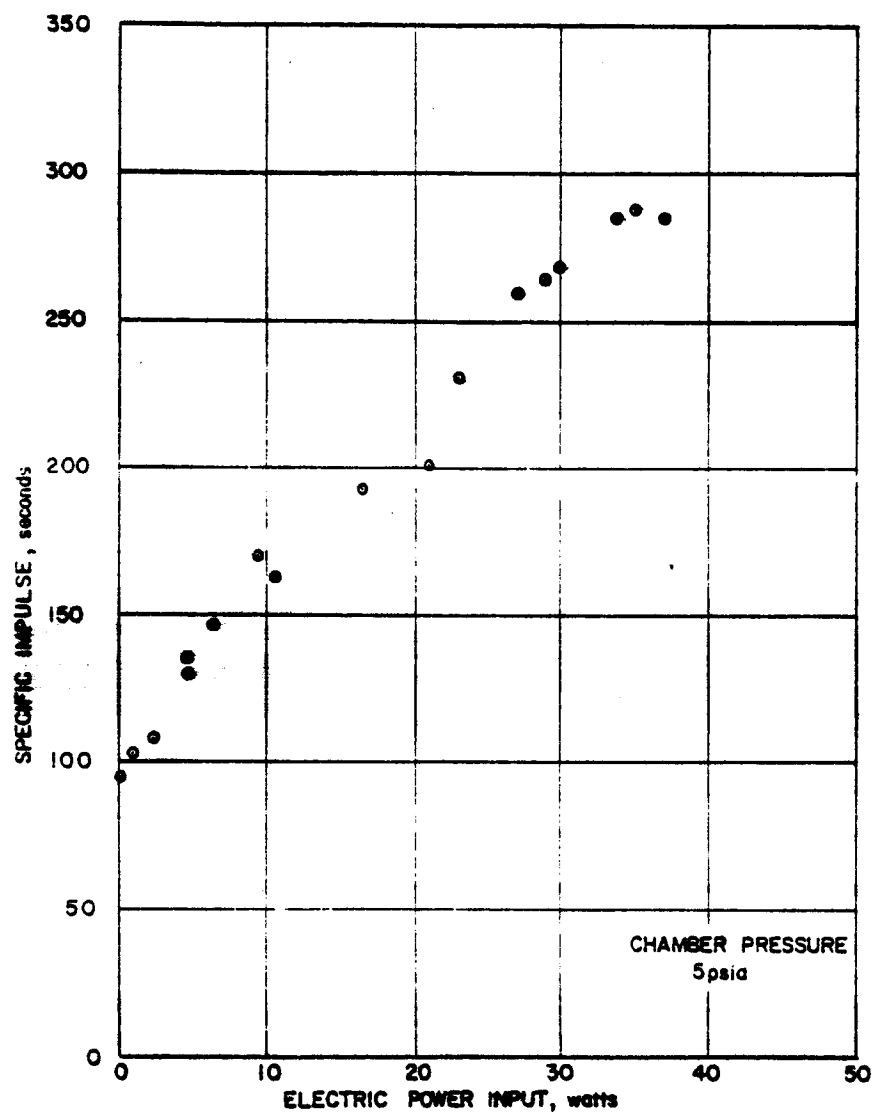
86-12006

Figure 55 SPECIFIC IMPULSE VERSUS ELECTRIC POWER INPUT — RHENIUM HEATER-
NOZZLE — 5-PSIA CHAMBER PRESSURE
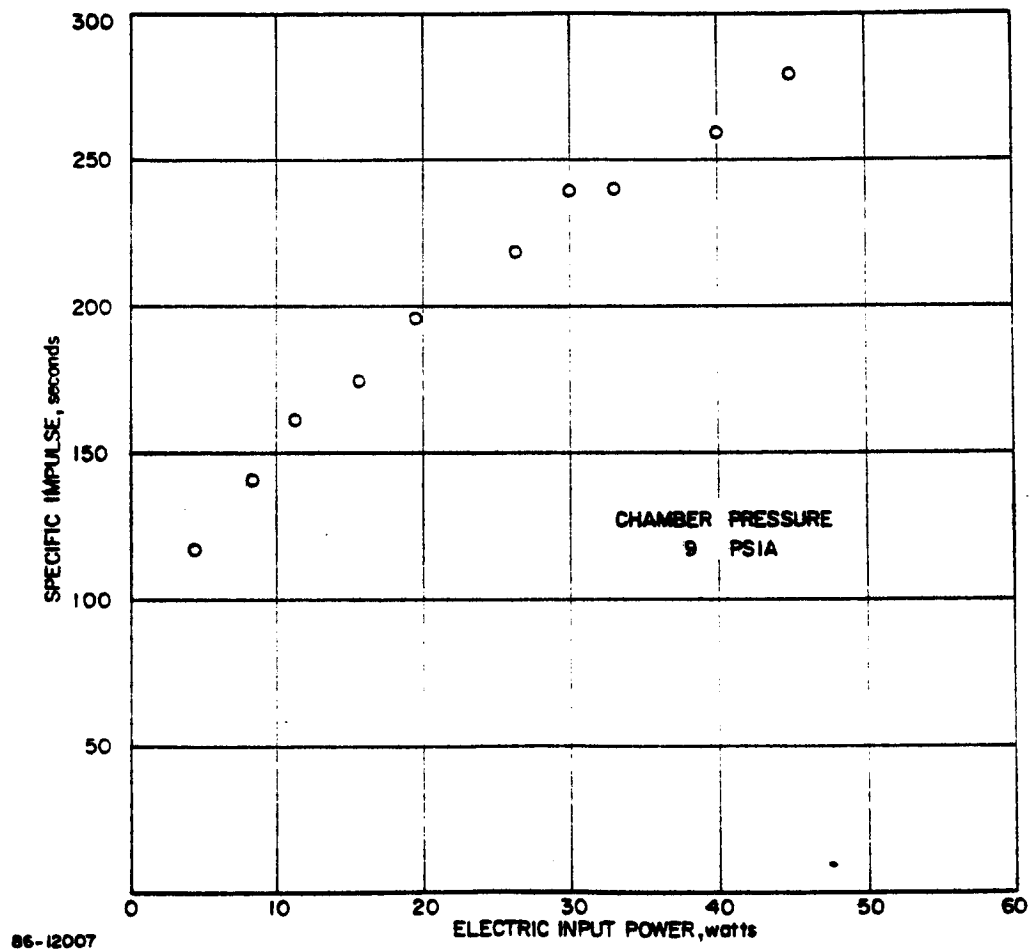
Figure 56 SPECIFIC IMPULSE VERSUS ELECTRIC POWER INPUT -- RHENIUM HEATER-
NOZZLE -- 9-PSIA CHAMBER PRESSURE
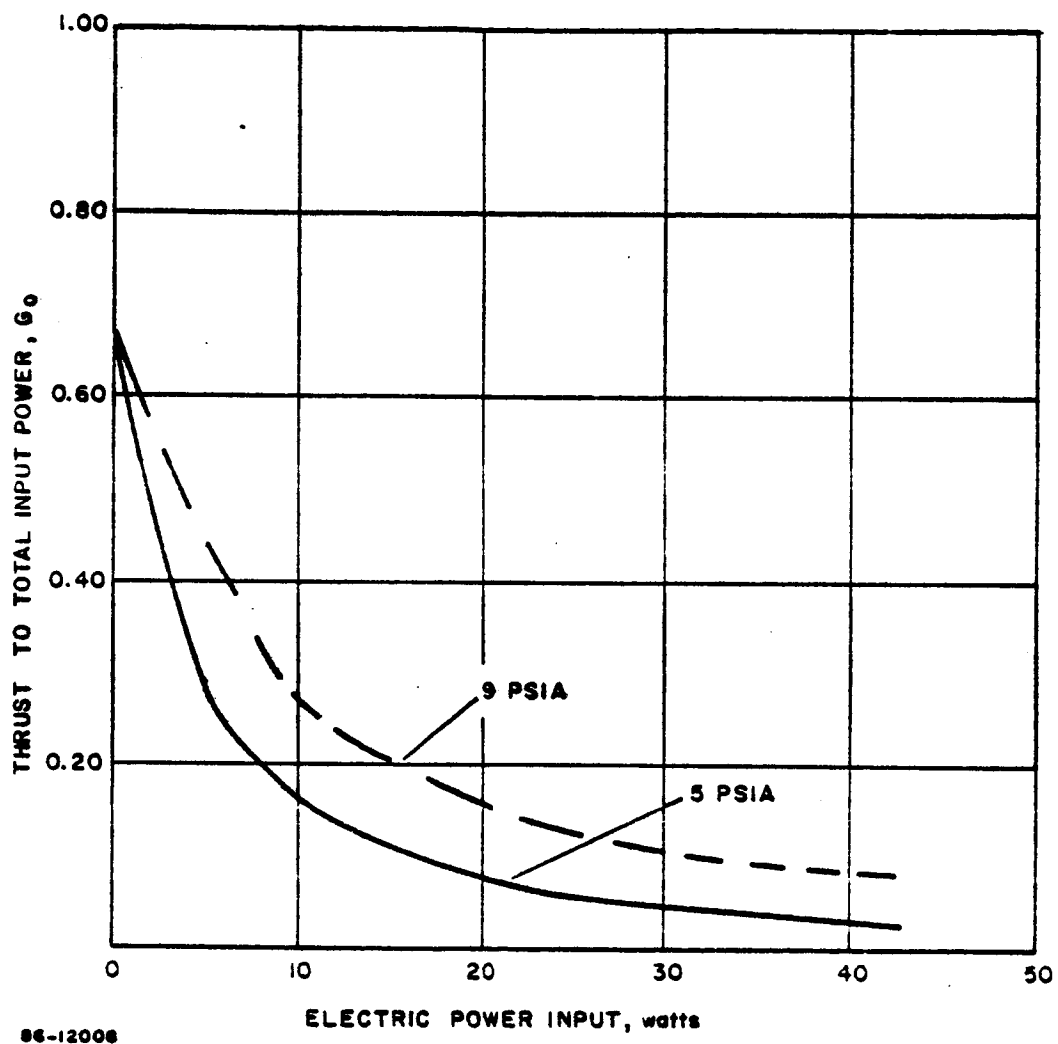
Figure 57 RATIO OF THRUST POWER TO TOTAL INPUT POWER VERSUS ELECTRIC INPUT POWER

86-12008

Figures 58 and 59 show the measured engine specific impulse as a function of engine temperature for chamber pressures of 5 and 9 psia, respectively. Superimposed on the experimental curves are plots of estimated specific impulse as a function of engine temperature for completely dissociated and nondissociated ammonia. It is assumed that the engine and gas temperature are equal. In estimating the engine specific impulse it has been assumed, on the basis of the cold flow data, that $I_{sp}/I_{sp, ideal} \approx 0.81$. The results suggest as in the case of the hot-flow, energy-transfer data that dissociation is initiated at temperatures of the order of 1250° K (2250° R).

6. Propulsion Performance of Fast Heat-Up Thrustors (1 to 300 micropounds)

During the course of the present program, data has been obtained on the performance of the rhenium thrustor operated at chamber pressures as low as 0.20 psia and thrust levels down to 1 micropound. Figures 60 and 61 indicate thrust level as a function of electric power input for chamber pressures over the range from 0.20 to 1.0 psia. As in the case of the previous runs at higher chamber pressure, the thrust level decreases with increase in input power and the corresponding increase in thrustor temperature. For example, in the case of the data obtained at 1-psia chamber pressure, the thrust level decreases from close to 70 down to 20 micropounds for an increase in power level from 0 to 12 watts.

Figure 62 shows measured specific impulse versus electric input power for the chamber pressures from 0.20 to 1.0 psia. The specific impulse at a given power level appears to be relatively insensitive to the chamber pressure. This is to be expected since the power transferred to the gas was in nearly all cases only a small fraction of the input power. In other words, at a fixed input power level the engine temperature was relatively insensitive to the gas-flow rate. At the lowest chamber pressure of 0.20 psia, there is some evidence that an increase in power input resulted in a decrease in specific impulse, probably due to viscous flow effects. In this case the throat Reynolds number was of the order of unity.

7. Summary of Fast Heat-Up Thrustor Performance Characteristics

The nozzle thrust coefficient, C_F, is a function of the nozzle throat Reynolds number. The thrust coefficient decreases with decrease in Reynolds number. Perhaps somewhat surprisingly the ratio of thrust coefficient to orifice coefficient as a function of Reynolds number is a constant down to Reynolds numbers of at least the order of 5. As a result, the ratio of actual-to-ideal specific impulse is relatively insensitive to Reynolds number down to Reynolds number of at least the order of 5.
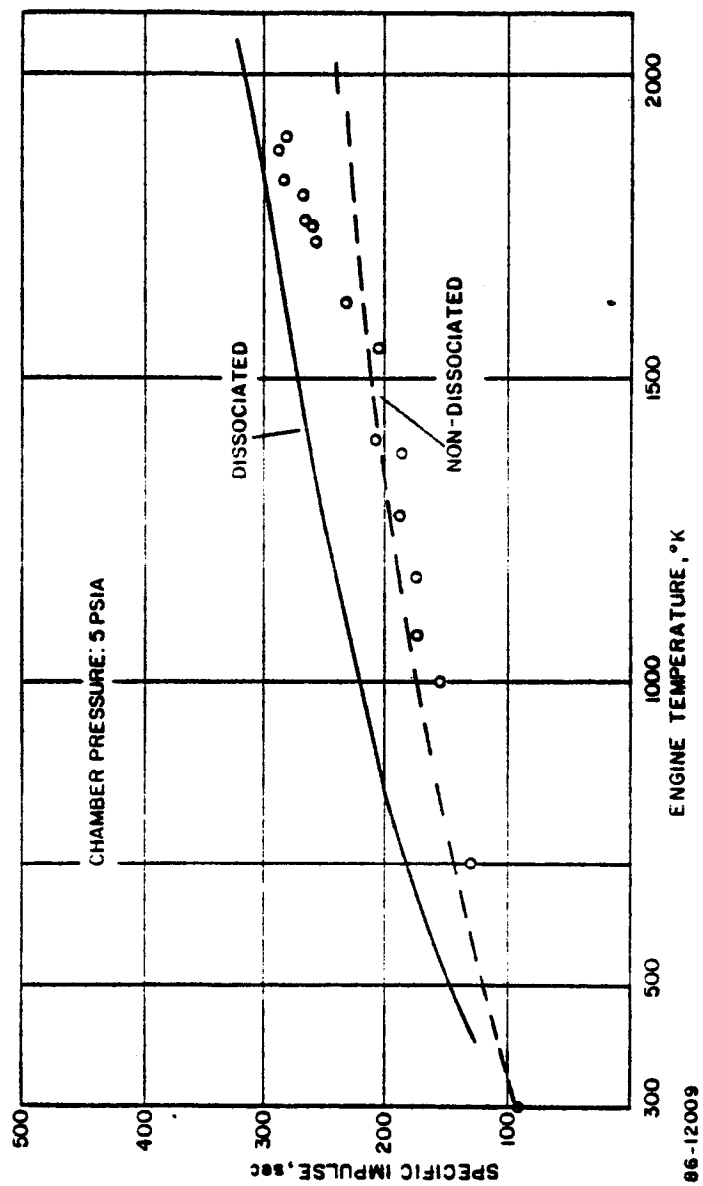
Figure 58 MEASURED ENGINE SPECIFIC IMPULSE VERSUS ENGINE TEMPERATURE --
RHENIUM HEATER-NOZZLE -- 5-PSIA CHAMBER PRESSURE

86-12009
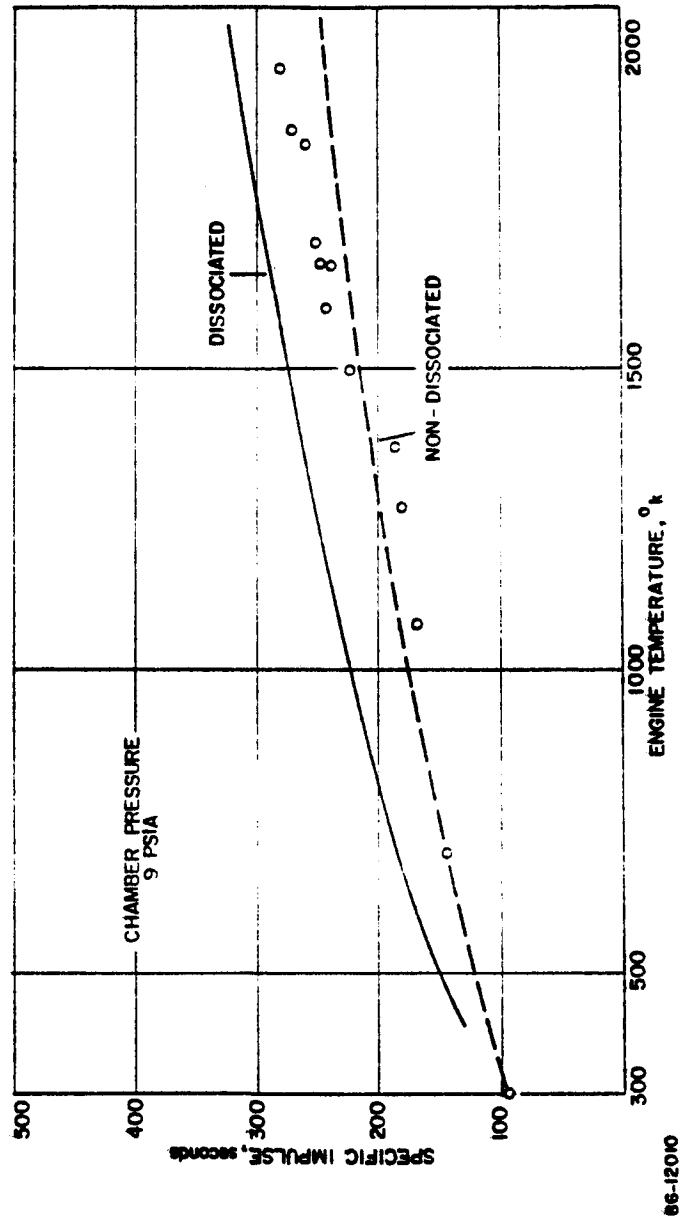
Figure 59 MEASURED ENGINE SPECIFIC VERSUS ENGINE TEMPERATURE --
RHENIUM HEATER-NOZZLE -- 9-PSIA CHAMBER PRESSURE

86-12010
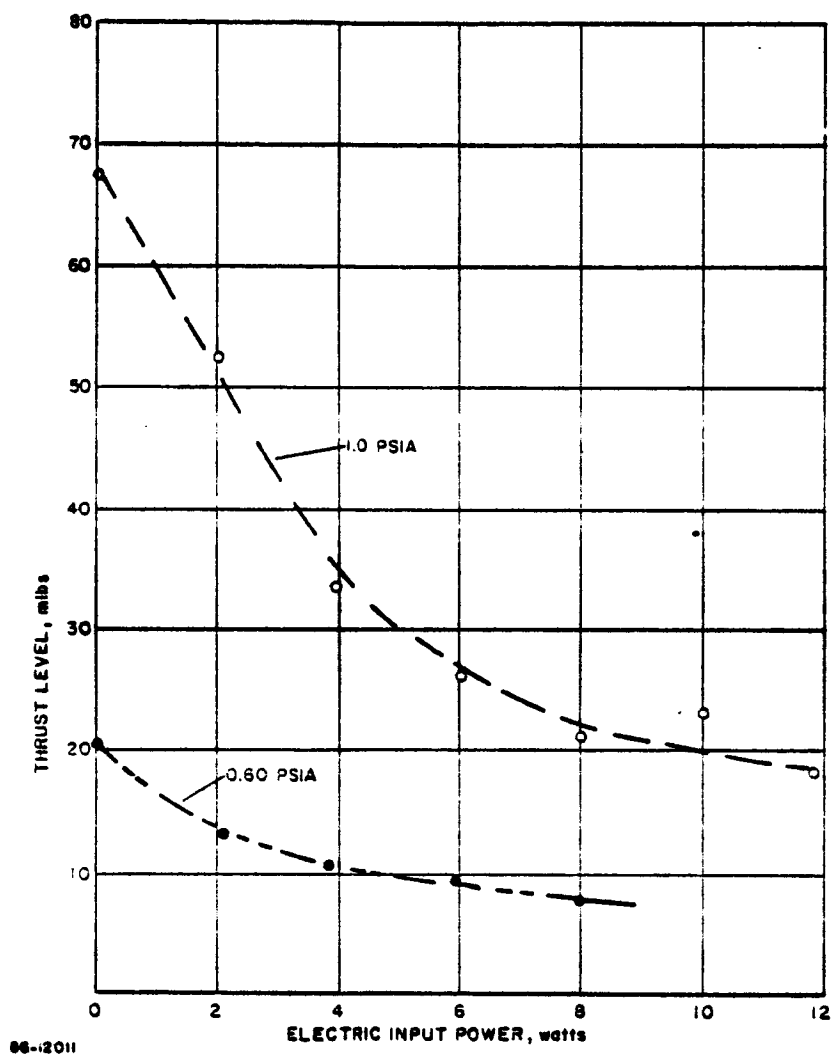
Figure 60 THRUST LEVEL VERSUS ELECTRIC INPUT POWER — RHENIUM HEATER-
NOZZLE — 0.60 AND 1.0-PSIA CHAMBER PRESSURE
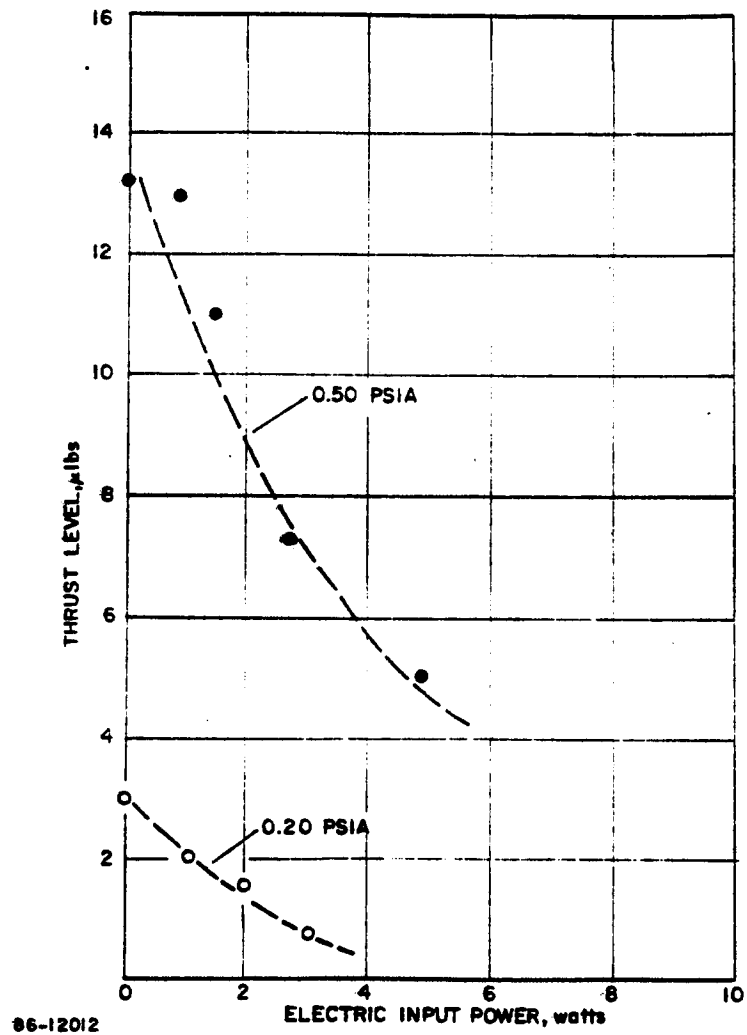
Figure 61 THRUST LEVEL VERSUS ELECTRIC INPUT POWER -- RHENIUM HEATER-
NOZZLE -- 0.20 AND 0.50-PSIA CHAMBER PRESSURE
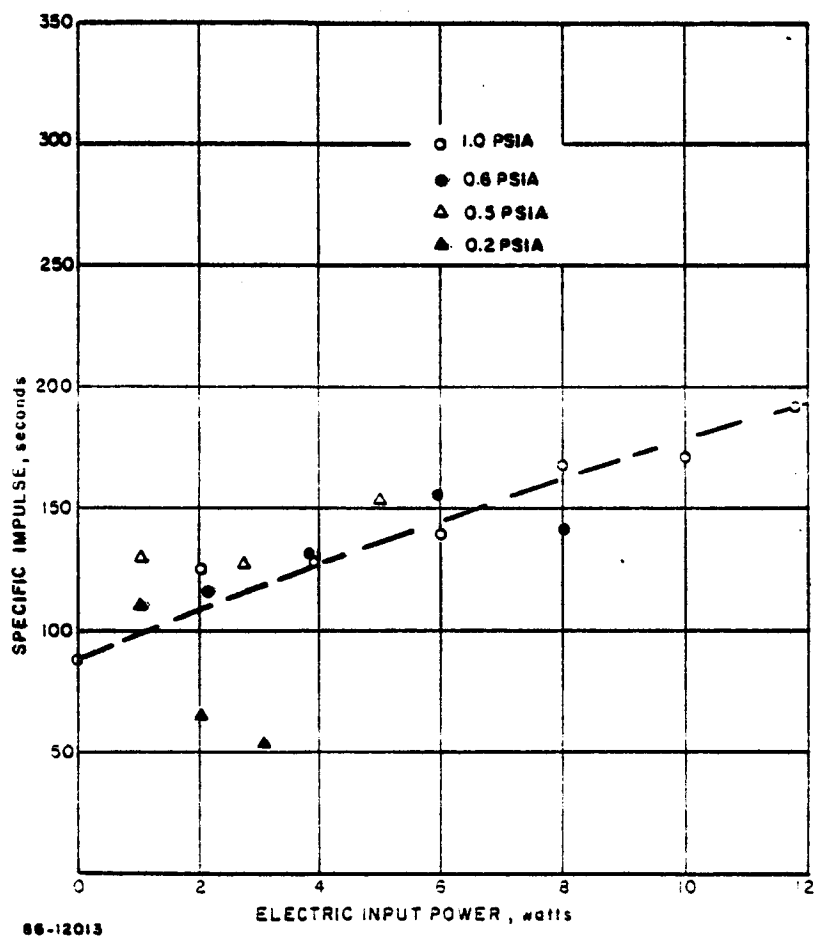
Figure 62 SPECIFIC IMPULSE VERSUS ELECTRIC INPUT POWER — RHENIUM
HEATER-NOZZLE -- 0.20 TO 1.0-PSIA CHAMBER PRESSURE

The rhenium fast heat-up thrustor has a maximum specific impulse capability of at least 300 seconds using ammonia as a working fluid. At these high specific impulse values the over-all electric-to-thrust-power efficiency for the engine is, however, less than 10 percent.

Performance data has been obtained on fast heat-up thrustor at thrust levels down to a few micropounds. The only evidence of a falloff in engine performance has occurred at Reynolds numbers of the order of unity or less. At a gas temperature of 300° K and an engine throat diameter of 10×10^{-3} inches, a Reynolds number of unity corresponds to a thrust of 0.30 micropound; on the other hand, at a gas temperature of 1500° K, a Reynolds number of unity corresponds to a thrust level of 3 micropounds.

The evidence from the thrust data, in agreement with previous information on the mass flow and pressure data suggests that ammonia dissociation is initiated at about 1250° K.

III. SINGLE AXIS LABORATORY ATTITUDE CONTROL SYSTEM

A. INTRODUCTION AND BACKGROUND

As part of the present program, a series of resistojet system tests have been carried out on an attitude control system test bed which has been recently installed at NASA Lewis. The attitude control system test bed is shown in Figure 63. The test bed is mounted on an air bearing in a vacuum chamber. During a typical attitude control system test, the test bed is completely isolated from the laboratory and is self-contained. Power is supplied from on-board batteries; propellant is suppled from an on-board propellant supply; and, finally, communication to and from the test bed is accomplished by means of telemetry. The test setup has been designed and developed by NASA Lewis to simulate an actual space control mission, as far as is possible, in the laboratory. The test bed and test setup are readily adaptable to the testing of a variety of attitude control systems based on gas and particle expulsion devices: these include both electrothermal plasma and ion electric propulsion engines, and cold-gas, subliming-solid, mono- and bipropellant rockets. The air-bearing test facility is thus ideally suited for comparing the over-all performance of different attitude control systems.

The primary purpose of the initial resistojet attitude control system tests on the NASA Lewis air bearing has been to demonstrate the feasibility of applying the resistojet concept to a complete satellite attitude control system, and to identify actual and potential interface problems. To simplify the control problem the initial air-bearing tests have been single rather than three-axis. It is stressed that in the design and development of the resistojet attitude control system for the single-axis, air-bearing test emphasis has been placed on demonstrating hardware feasibility, rather than demonstrating optimum resistojet attitude control system performance.

For the initial air-bearing resistojet attitude control system test, Avco RAD was responsible for the electrical and mechanical system components indicated in Table X.

TABLE X

RESISTOJET ACS SYSTEM COMPONENTS
SUPPLIED BY AVCO/SSD

Control Logic Package
Light Source and Sensor
Power Conditioning Package
Resistojet Engine System
Resistojet Engine
Propellant Storage and Regulation
Engine Instrumentation
Signal Conditioning Package
Checkout Console

COMMAND
RECEIVER

INVERTER

AMPLIFIER

SWITCH BOX

BATTERY

BATTERY

SIGNAL
CONDI-
TIONER

LOGIC

THRUSTOR

TEST PLATE

LIGHT SENSOR

THRUSTOR

BALLAST

AIR
BEARING

PROPELLANT
TANK
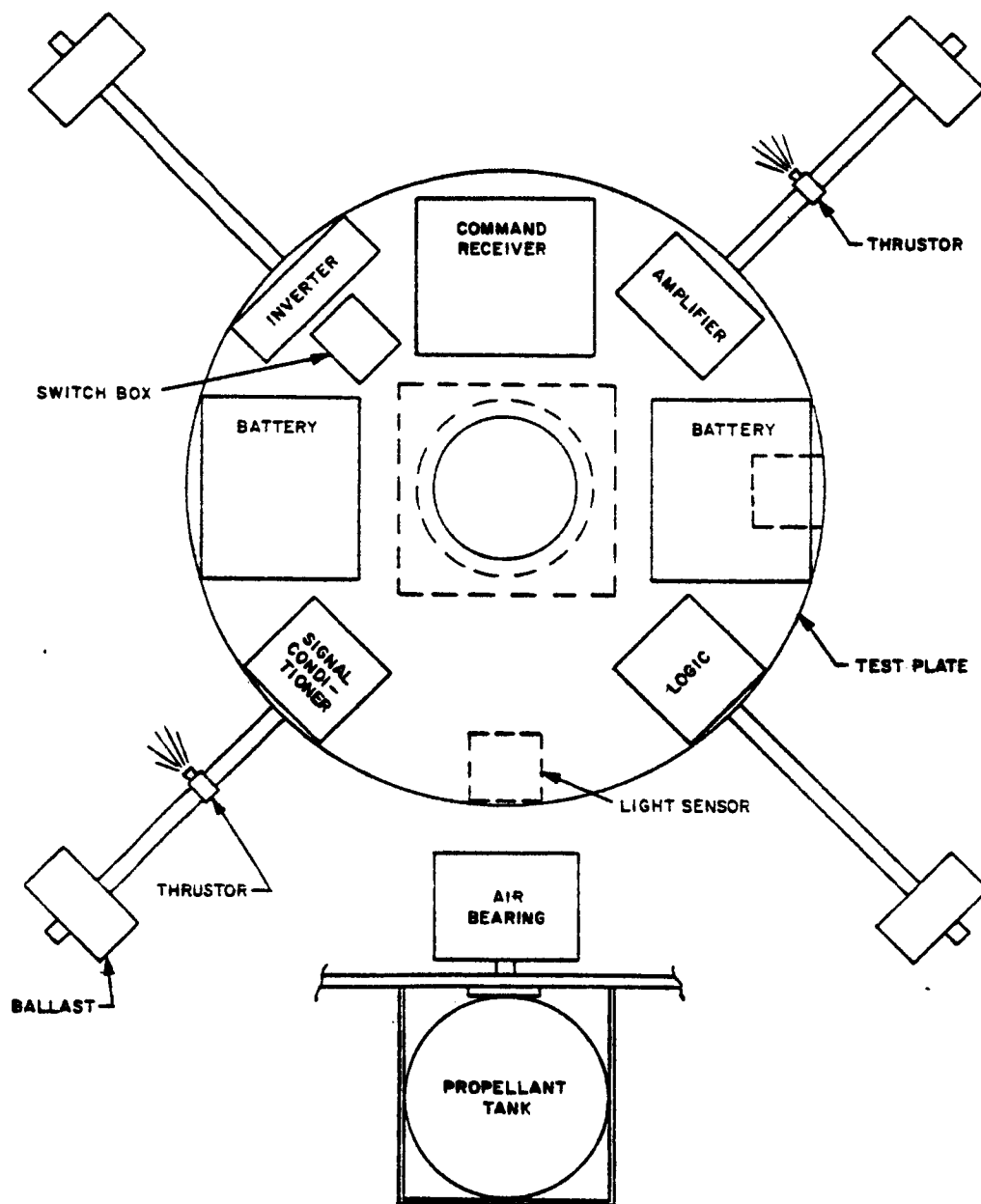
68-2857

Figure 63 NASA LEWIS SINGLE-AXIS AIR-BEARING ATTITUDE CONTROL SYSTEM
TEST BED

-106-

The control logic package includes a light source and sensor to establish test table position; basically, the control logic package signals the individual resistojet engines to turn off and on in response to signals from the light sensor located on the test table. The basic electrical system is shown in Figure 64.

The power conditioning package converts the regulated power obtained from the battery supply located on the test table into a form suitable for resistojet operation. It will be recalled from previous discussion that the power conditioner must be carefully matched to the resistojet engines because of their inherent low resistance.

The resistojet engine system includes three resistojet engines, two for attitude control and one for station keeping. The engine system also includes liquid and gaseous ammonia reservoirs. A block diagram of the system is shown in Figure 65. The propellant (ammonia) is stored as liquid in the ammonia reservoir. The liquid-ammonia tank is connected to the gaseous-ammonia reservoir by means of a solenoid valve operated by a pressure switch. The pressure switch opens the valve when the gas plenum pressure falls below a preset valve and closes the valve when the pressure rises to another preset valve. Referring to Figure 65, instrumentation is supplied to measure the resistojet chamber pressure, heater temperature, gas inlet temperature, and gas-flow rate.

The signal-conditioning package amplifies the signals produced by the pressure, temperature, and error sensors preparatory to transmission by the telemetry package.

The basic purpose of the initial resistojet attitude control system test was to hold the position of the test bed around a single axis to within ± 1/2 degree. The position of the test bed with respect to the light beam is established by means of a light sensor located on the test bed. If the angular displacement of the test bed is outside the prescribed limits, a signal is passed to the control logic package which, in turn, calls for power (from the power conditioner) and propellant (from the propellant gas reservoir) to be delivered to the proper thruster. The tests included both acquisition and limit-cycle operation.

In the following sections detailed descriptions are presented of the individual components of the total resistojet ACS. These include:

1. Control logic package,

2. Power conditioning package,

3. Resistojet engine system, and

4. Signal conditioning package.

A. ACS CONTROL SYSTEM

POWER PACK — POWER CONDITIONING — THRUSTOR

CONTROL LOGIC

PROPELLANT SOLENOID — PROPELLANT SUPPLY

LIGHT SENSOR

COMMAND CHANNELS

B. ACS DATA SYSTEM

POSITION SENSOR

PRESSURE

TEMPERATURE

SIGNAL CONDITIONING — TELEMETRY CHANNELS — RECEIVER

TAPE

METER

RECORDER
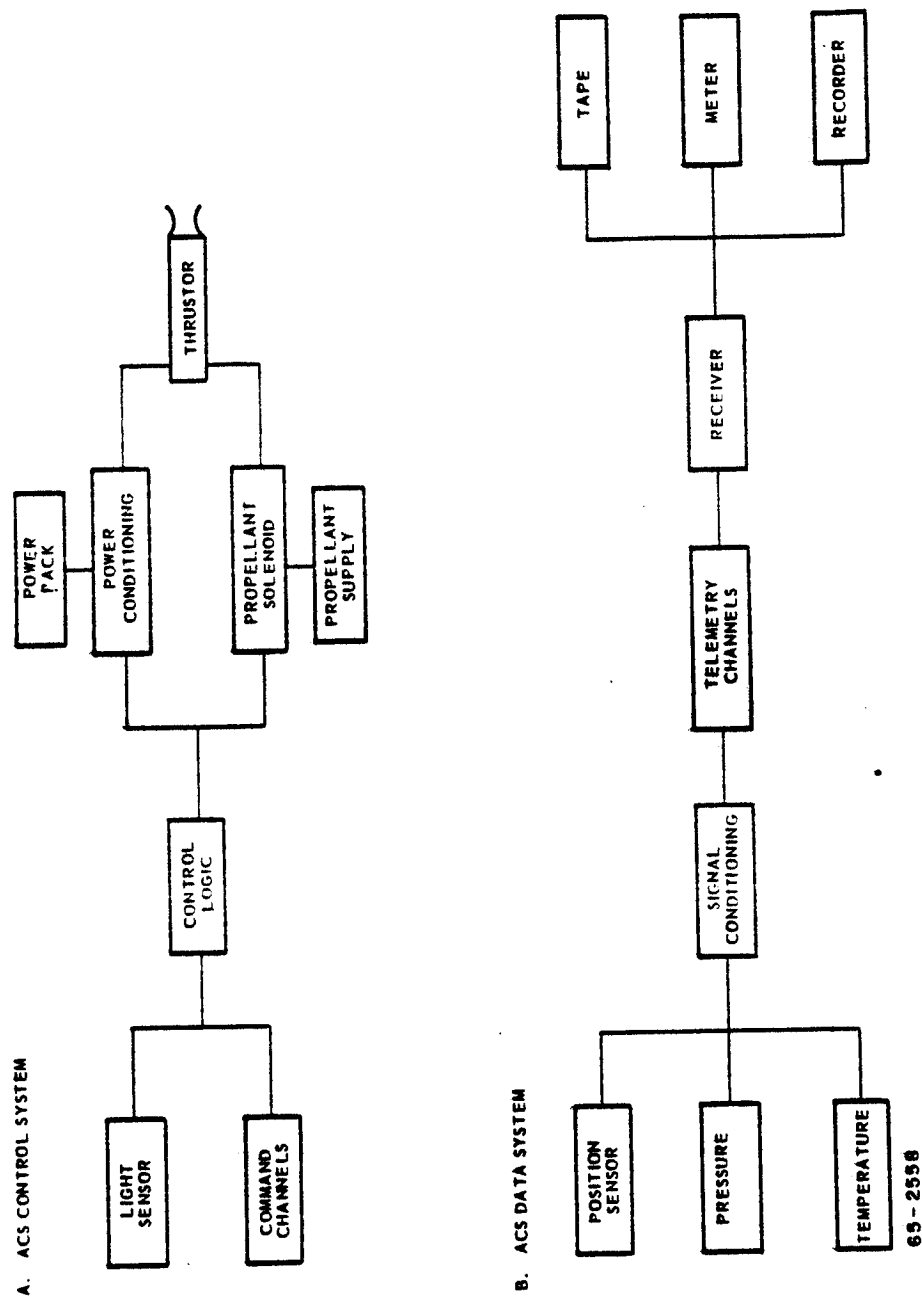
65 - 2558

Figure 64 BLOCK DIAGRAM FOR THE ATTITUDE CONTROL ELECTRICAL SYSTEM
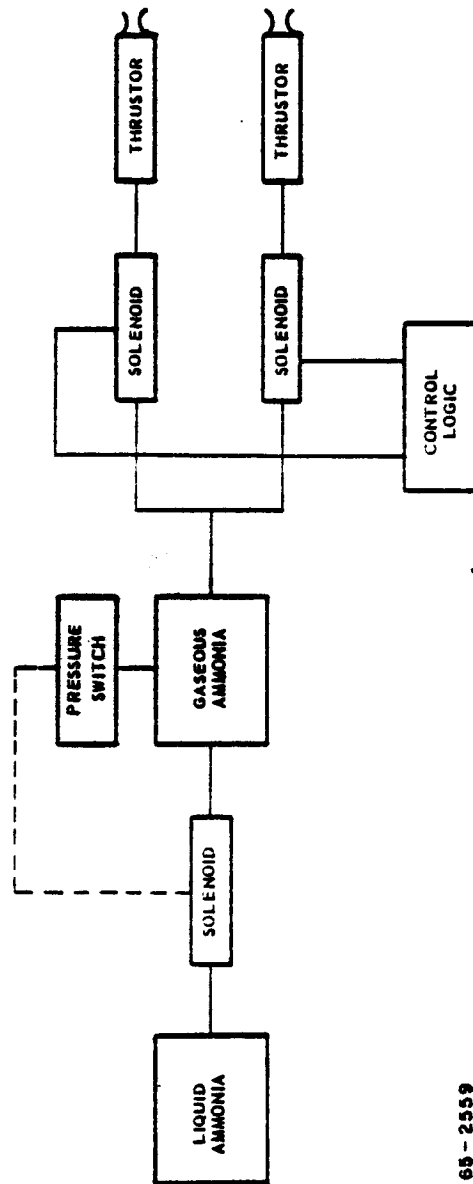
Figure 65 BLOCK DIAGRAM FOR THE PROPELLANT FEED SYSTEM

65 - 2559

B. CONTROL LOGIC PACKAGE

The discussion of the control logic package is subdivided into four parts: (1)
single axis control logic; (2) estimated performance of the single-axis control
logic system; (3) electronic circuitry for the control logic system; and (4)
description of the light sensor and light source.

1. Single-Axis Control Logic

A control system has been selected for control of the two resistojet attitude
control engines with the purpose of maintaining the attitude of the single
axis table within the desired angular limits with a minimum of fuel con-
sumption. The control method selected is based on the method proposed
by Vaeth (ref. 8). This method not only provides for effective damping
of initial conditions (that is, acquisition), but minimized fuel consumption
and the valve cycling frequency. The Vaeth technique accomplished the
same degree of limit-cycle optimization as obtained by the use of a num-
ber of different switching levels as originally proposed by Gaylord and
Keller (ref. 9), and, in addition, provides for the rapid damping of initial
conditions. Basically, the Vaeth method uses two sets of rate dependent
control commands. Both sets are controlled by a function of both the
angular divergence and the angular rate. Whenever the function exceeds
the smaller of two preset valves, the appropriate resistojet is pulsed on
for a preset time producing an impulse bit which, if the angular rate is
small enough, reverses the direction of rotation of the table. The system
thus oscillates between two preset limits resulting in limit-cycle control.
If the rate of rotation is too large, however, the impulse bit will not be
sufficiently large to reverse the rotation. With this condition, the func-
tion will reach and exceed the larger of the two preset values, above which
the resistojet is turned on and remains on continuously until the function
again drops below this preset valve. This set of commands is used for
acquisition and as a backup to the limit-cycle control lines.

The control logic can be explained in more detail by reference to Figure
66. The bottom sketch illustrates schematically the control system and
single-axis table. A well-collimated light source is placed inside the
vacuum tank containing the air-bearing table to serve as the reference for
orientation. On the table itself, a light sensor is placed which provides a
single proportional to the angular divergence, θ, of the table with the
null at $\theta = 0$. This light sensor covers a maximum range of ± 8 degrees.
The signal from the light sensor goes to the control logic system which,
in turn, controls the resistojet engine operation. The light source will be
described subsequently.

The top sketch of Figure 66 indicates the logic used in the control system.
Lines A and B represent the acquisition control lines, and also serve as
backup lines to the inner lines. Whenever the combination of θ and $d\theta/dt$
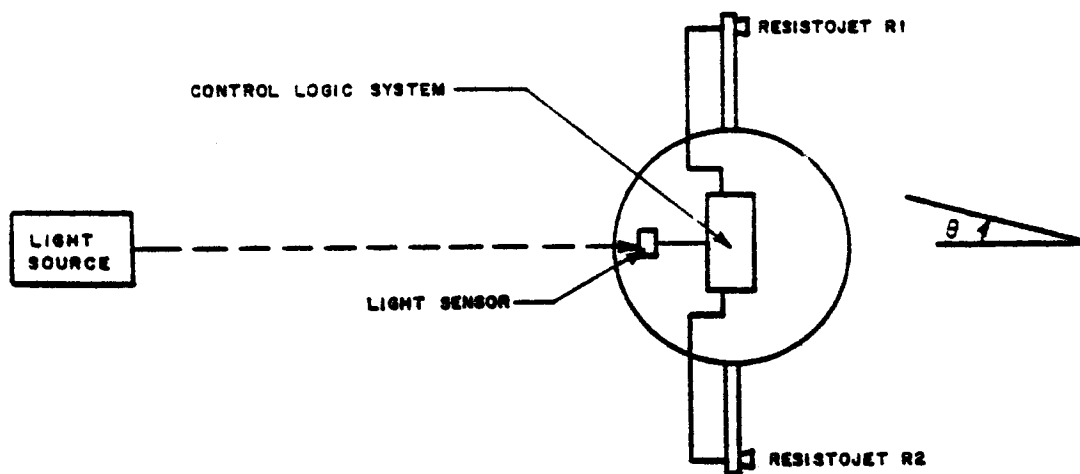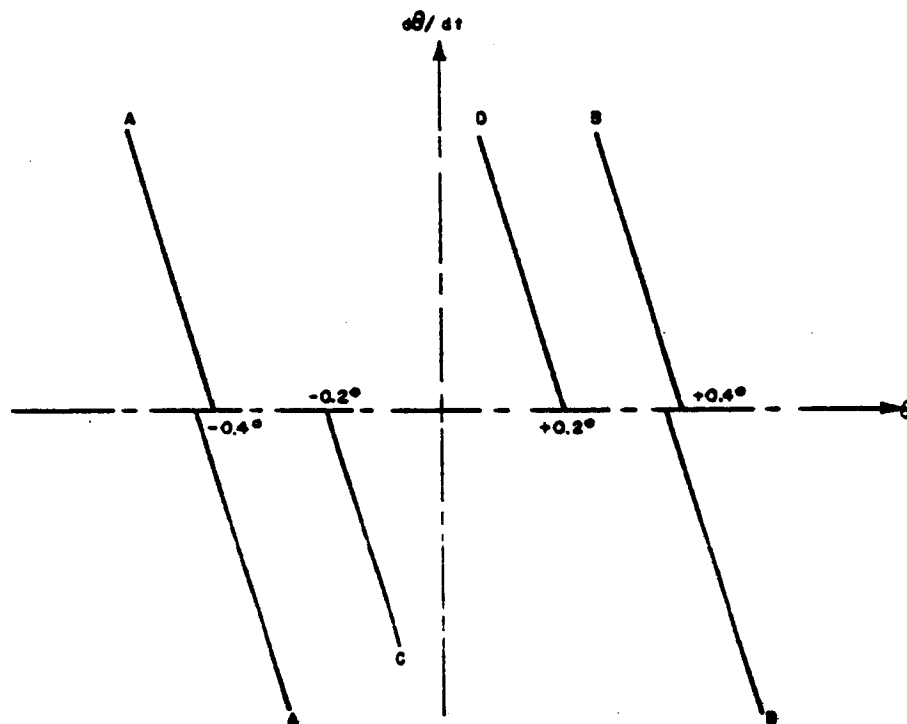
Figure 66 BASIC CONTROL LOGIC LINES FOR THE SINGLE-AXIS RESISTOJET ATTITUDE CONTROL SYSTEM

65-2560

lies outside of these lines, the appropriate resistoject engine (R1 for line B and R2 for line A) is operated continuously until the table is rotated to a state within these lines. These lines are set at $\pm$ 0.4 degree with $d\theta/dt$ = 0. Lines C and D represent the limit-cycle control lines for control after acquisition. Whenever θ and $d\theta/dt$ change such that line D is crossed, resistojet R1 is pulsed on for a preset short time period to provide an impulse bit. Whenever line C is crossed, resistojet R2 is pulsed on to provide an impulse bit in the opposite direction. Lines C and D are set at $\pm$ 0.2 degree with $d\theta/dt$ = 0. It should be noticed that both sets of lines have a slope to the left, and thus the operation of the resistojet control is not only dependent on the angular error, θ, but also on the rotation rate, $d\theta/dt$.

The operation of the logic in acquisition can now be explained by reference to Figure 67, which is a plot of the acquisition lines only extending out to the limit of the optical sensor, $\pm$ 8 degrees. Consider the case of the table initially at a large positive angle with zero rate of rotation. A telemetry command signal for counter-clockwise rotation is given from the "ground" station and resistojet engine R1 turned on.

The resistojet operates continuously until line B is reached following the dotted line 1 to 2 in Figure 67. This resistojet is then turned off and the system drifts from B to A. When line A is crossed, resistojet R2 is turned on automatically and operates continuously driving the table along the parabolic path 3 to 4 where line A is again intersected and resistojet R2 turned off; the table then drifts at constant rate between lines A and B where resistojet R1 is turned on automatically. The system again follows a parabolic path along the dotted line from 5 to 6 where resistojet R1 is turned off automatically as line B is crossed. It is seen that due to the slope of the control lines, a spiral-like path is followed which tends to reduce both θ and $d\theta/dt$. Continuation of this cycling thus reduces both θ and $d\theta/dt$ to very small values so that the inner control lines can take over the control. The dynamics of the control system and table have been simulated on an analogue computer (see Appendix E). In Figure 68, a typical plot from the computer is presented illustrating acquisition from an angle of +60 degrees with an initially zero rate of rotation. For this particular case, the acquisition time for the table was 2090 seconds with a thrust torque of 10^{-3} ft-lb and table moment of inertia of 27 slug-ft^2.

Attention will now be turned to limit-cycle operation between lines C and D of Figure 66. During the acquisition phase, control lines C and D are active, and the resistojets are actually pulsed on when these lines are crossed. The rate of rotation is high enough, however, so that lines A or B, respectively, are reached before the pulse period is over and the resistojets remain on. As the rate decreases, a value is eventually reached where the rate is small enough for the pulse from lines C or D to change
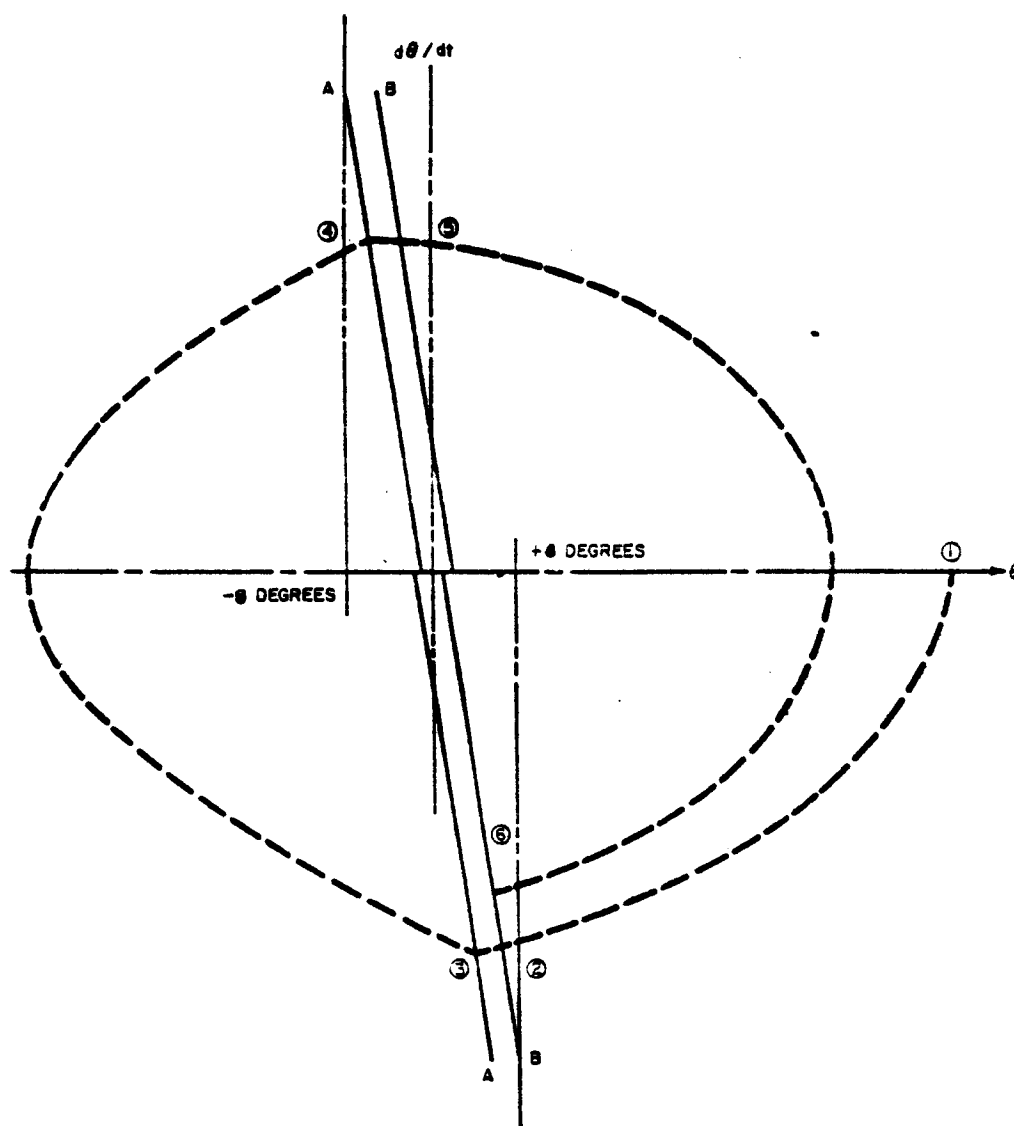
Figure 67 ILLUSTRATION OF LARGE ANGLE ACQUISITION
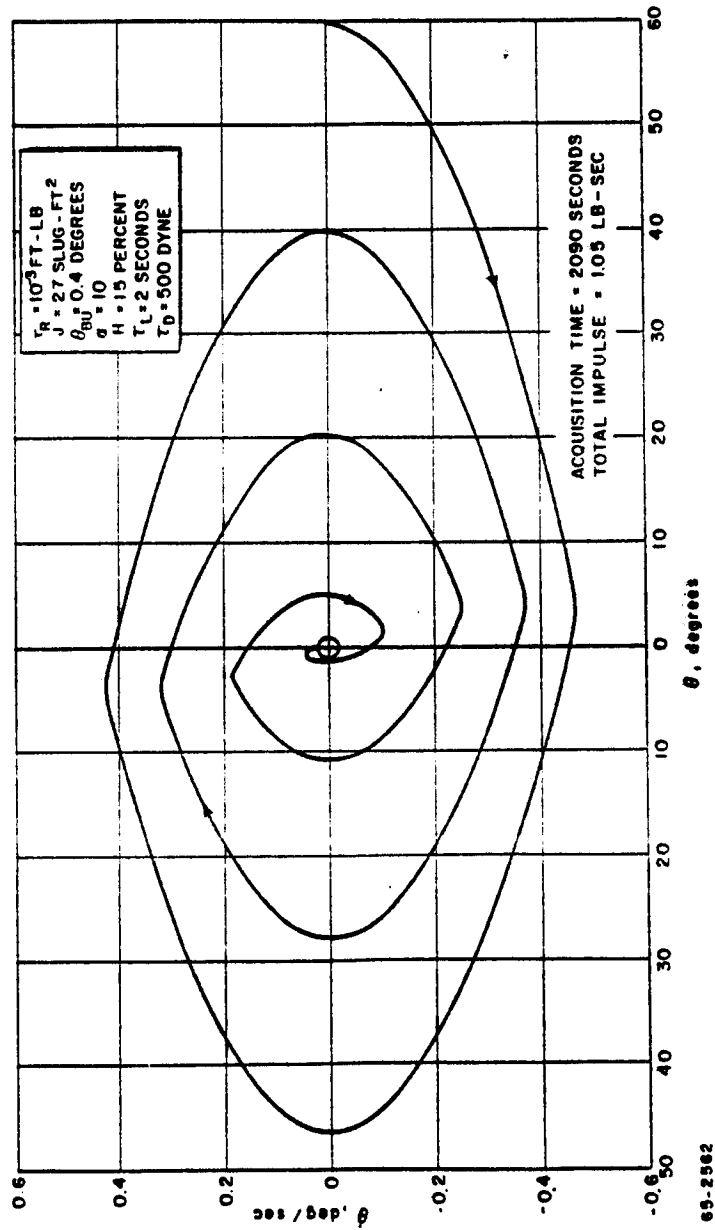
Figure 68 ANALOG COMPUTER SOLUTION FOR LARGE ANGLE ACQUISITION OF THE SINGLE-AXIS LIST TABLE

65-2562

-114-

the direction of rotation and to prevent lines A or B from being crossed. When this condition occurs, the system drops out of the acquisition phase into limit-cycle control between lines C and D, with lines A and B serving now as a backup in case the system should leave the limit-control cycle due to some unusual disturbance.

The effect of disturbance torque on limit-cycle operation is very strong. Operation can be either in a "hard" limit cycle or a "soft" limit cycle, depending on the relative magnitude of the disturbance and control torques. The difference between these modes of operation can be explained by reference to Figure 69. In this figure, it is assumed that the rate of rotation is small enough so that no change in θ occurs during the resistojet pulse, that is, the resistojet produces a step change in $d\theta/dt$. In the soft limit cycle, as illustrated in the top sketch, the resistojet impulse produced by crossing line D is insufficient to drive the system to an intersection with line C; instead, the disturbance torque changes the $d\theta/dt$, θ state along the dotted parabolic curve during the drift phase until line D is again crossed and the resistojet pulsed. Thus, the resistojet is pulsed only once per cycle and the impulse from the disturbance torque is exactly balanced by the impulse from the resistojet. This mode of operation thus represents a minimum in fuel consumption and, for a given disturbance torque, the fuel consumption is independent of the thrust parameters (thrust, pulse length, moment arm length) so long as these parameters are such that operation in a soft limit cycle is maintained.

It should be noted here that a soft limit cycle need not be symmetrical as illustrated in Figure 69A. In figure 69B a nonsymmetrical soft limit cycle is illustrated; as is evident from this sketch, this type of cycle is nonrepeating. The type of cycle encountered in any particular case depends on the acquisition or point of entry into the soft limit cycle. It should be emphasized again, however, that the fuel consumption and number of resistojet pulses are independent of the thrust parameters or the acquisition phase so long as soft cycle operation is maintained.

The dotted lines 1 and 2 on the symmetrical soft limit-cycle sketch of Figure 69 represent two different levels of disturbance torque for constant thrust parameters, line 1 representing the smaller disturbance torque. It is obvious that below some disturbance torque limit the sytem will be over-driven, and will cross control line C so that the resistojet in the opposite direction will be pulsed on. Thus, instead of exactly balancing the disturbance torque and having only one pulse per cycle, there will be two pulses per cycle, and the two resistojets will be partially counterbalancing each other. This type of operation is called "hard" limit-cycle operation and results in a significant increase in the fuel consumption relative to the soft limit cycle. If the disturbance torque is zero, it is apparent that the limit cycle must necessarily be "hard", and the operation will be as illustrated
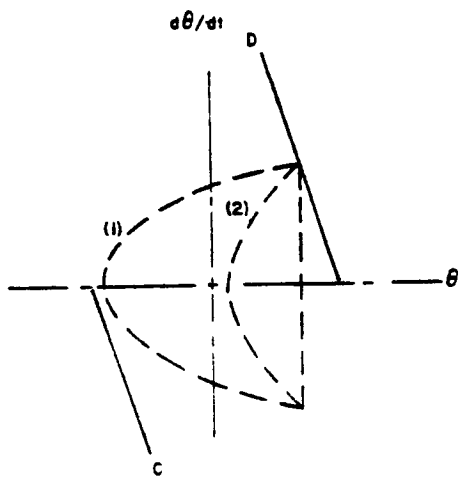
(a) SYMMETRICAL SOFT LIMIT CYCLE
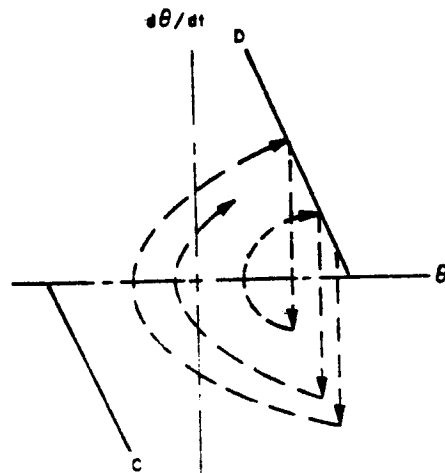
(b) NON-SYMMETRICAL SOFT LIMIT CYCLE
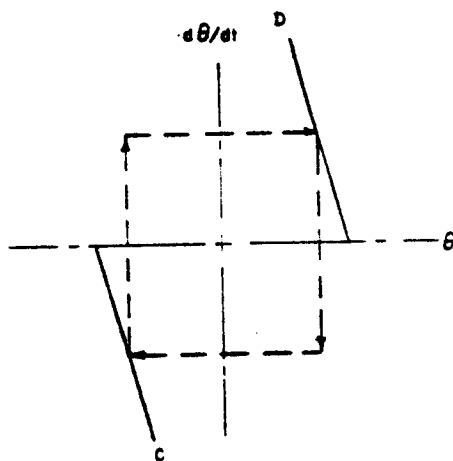
(c) SYMMETRICAL HARD LIMIT CYCLE —
NO DISTURBANCE TORQUE
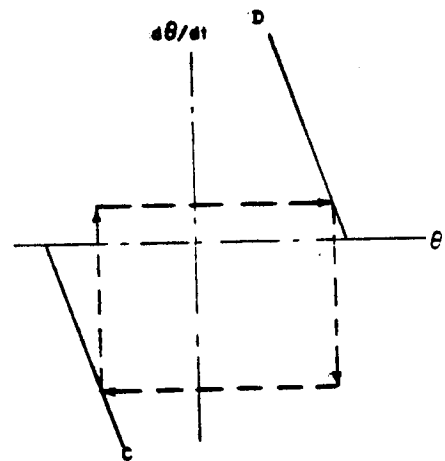
(d) NON-SYMMETRICAL HARD LIMIT CYCLE-
NO DISTURBANCE TORQUE

63-2863

Figure 69 ILLUSTRATION OF HARD AND SOFT LIMIT CYCLE OPERATION

-116-

in parts C and D of Figure 69. The drift phase here takes place at constant $d\theta/dt$, and the resistojet pulsing serves to reverse the rotation, thus keeping the orientation within the desired limits. The path of the cycle repeats itself regardless of whether the cycle is symmetrical or nonsymmetrical.

It should be noted that the slope (or rate dependence) of the control lines is necessary to provide stability to the control cycle. This is illustrated in Figure 70, where the hard limit cycle with no disturbance torque is presented for the practical situation where the two resistojet pulses do not exactly balance each other. In these sketches, the pulse controlled by line C is assumed to be one and one-half times as large as that controlled by line D. In the top sketch, with rate-dependent control lines, the path starting from point 1 returns to that point after two cycles and the control system is basically stable. In the bottom sketch, with control lines dependent only on θ, the imbalance in impulse from the two opposing resistojets results in the system "jumping out" of the limit-cycle control as shown; this system is thus basically unstable and requires backup lines.

The case of a hard limit cycle with a disturbance torque is illustrated in Figure 71. In the coast phase, the rate of rotation, $d\theta/dt$, changes due to the disturbance torque. The exact path followed by the hard limit-cycle operation with a disturbance torque is strongly dependent on the state of entry into the cycle; that is, on the acquisition phase. A nonrepeating type of cycle can be obtained, as illustrated in Figure 71. Under certain conditions of entry into the cycle, a combination soft and hard limit cycle can be produced, as illustrated in the three-pulse-repeating cycle of Figure 71. The soft limit cycle results when the control torque changes the rate to a small negative valve so that the disturbance torque can change $d\theta/dt$ to a positive valve before the opposite control line is reached. The occurrence of these soft limit cycles will increase in frequency as the disturbance torque is increased for constant thrust parameters. At zero disturbance torque, no soft limit cycles will occur; as the disturbance torque is increased, more and more soft limit cycles will occur until the disturbance reaches or exceeds a limiting valve where the operation will be completely in the soft limit cycle.

2. Estimated Performance of the Single Axis Control Logic System

The basic goals in optimizing the attitude control system performance for a mission are: (1) to minimize fuel consumption, and (2) to minimize the pulsing frequency for reliability reasons.

The tests to be performed on the NASA Lewis air-bearing table will eventually permit study and comparison of various control systems, as well as a test of the resistojet itself and the associated mechanical equipment. The first tests have primarily been a test of the control logic and total system.
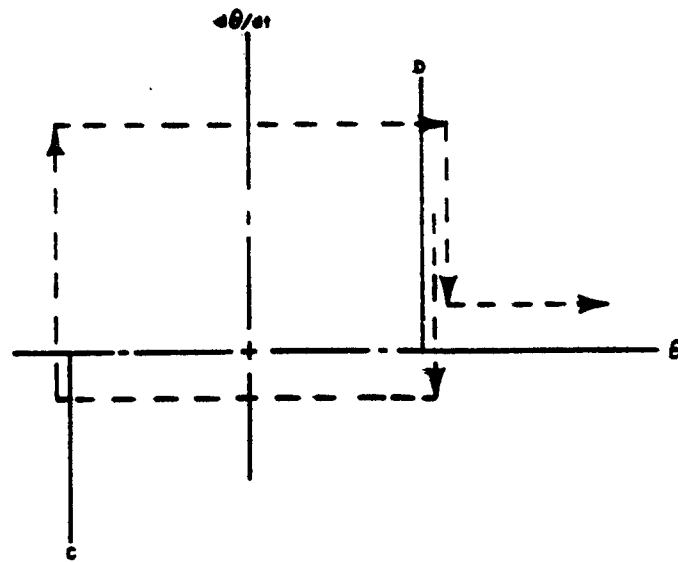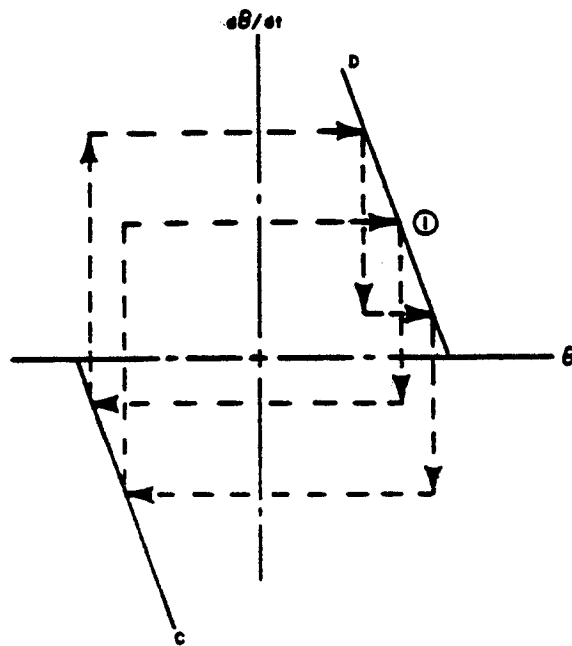
Figure 70 ILLUSTRATION OF CONTROL LOGIC STABILITY DUE TO RATE DEPENDENCE OF CONTROL LINES

-118-
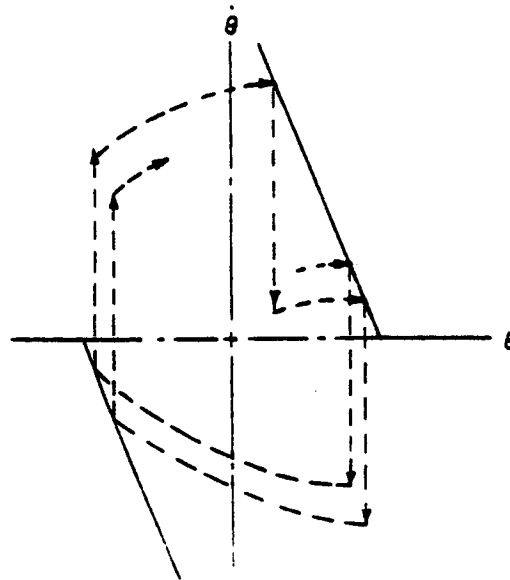
a) HARD LIMIT CYCLE WITH DISTURBANCE TORQUE
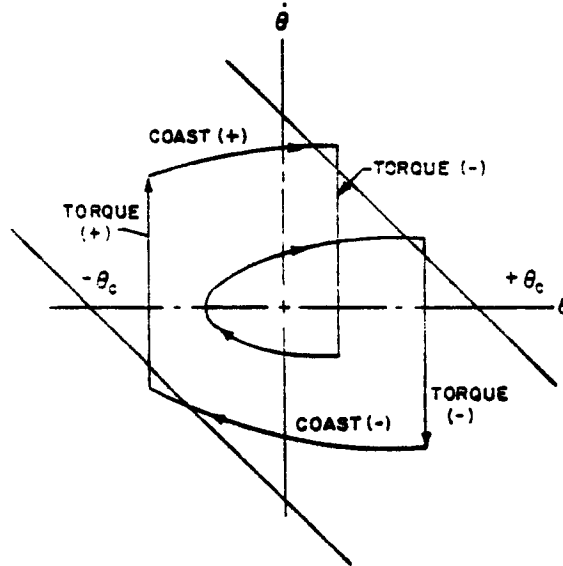
b) THREE PULSE COMBINATION HARD-SOFT LIMIT CYCLE

68-2668

Figure 71 ILLUSTRATIONS OF HARD LIMIT CYCLE WITH DISTURBANCE TORQUE

-119

This section presents the calculated performance of the system as a function of the air-bearing disturbance torque level. At this time, the disturbance torque level characteristic of the NASA Lewis air bearing has not been completely established; however, it is in the range from 100 to 1000 dyne-cm. The nominal characteristics of the first resistojet single-axis attitude control system, which will be referred to as Avco Resistojet Attitude Control System-Model 1, are presented in Table XI.

TABLE XI

AVCO SINGLE AXIS RESISTOJET ATTITUDE CONTROL SYSTEM - MODEL 1
NOMINAL PERFORMANCE CHARACTERISTICS

Engine Thrust Level	5×10^{-4} pounds
Engine Specific Impulse	120 seconds
Power Level	5 to 10 watts
Engine Chamber Pressure	30 psia
Ammonia Flow Rate	4.2×10^{-6} lbs/sec
Heat-up Period (No Propellant Flow)	1 second
Fixed Pulse Length (Inner Lines)	4 seconds
One-Half Deadband (Inner Lines)	0.2 degree
One-Half Deadband (Outer Lines)	0.4 degree
Table Moment of Inertia	27 slug-ft^2
Initial Attitude	2.25 degrees

a. Soft Limit-Cycle Operation

The fuel consumption, as mentioned previously, is a minimum for soft limit-cycle operation and, for a given disturbance torque, should be independent of the thrustor characteristics as long as their magnitude is in the range to maintain soft limit-cycle operation. The fuel consumption for operation in this mode can be written as:

$$m_s = \frac{\tau_D \, T}{980 \, I_{sp} \, L} \tag{44}$$

where

m_s = total mass of propellant required for soft limit cycle operation, gmm

τ_D = disturbance torque, dyne-cm

T = total time period of control, seconds

I_{sp} = specific impulse of propellant, $\frac{gmf \ sec}{gmm}$

The number of resistojet pulses or of soft limit cycles can be written as:

$$N = \frac{\tau_D \, T}{980 \, F \, L \, t_R} \tag{45}$$

where

N = number of required resistojet pulses

F = thrust force from resistojet, gmf

t_R = thrust time per pulse, sec

The duty cycle or ratio of time of thrust on to total time is given by

$$\eta = \frac{\tau_D}{980 \, F \, L} = \frac{\tau_D}{\tau_R} \tag{46}$$

where τ_R is the torque generated by the resistojet in dyne cm. Thus, very simple relations suffice to describe the performance of a system controlling in a "soft" limit cycle with a constant disturbance torque. The quantities m_s, N, and η are presented in Figure 72 as a function of disturbance torque for the conditions expected in the NASA, Lewis tests. As indicated in the following discussion, the limiting disturbance torque above which soft limit cycle operation is positively obtained is 575 dyne cm for the nominal operating condition.

b. Maximum Thrust Force for Soft Limit-Cycle Operation

The question now arises as to when the limiting value of disturbance torque is reached for soft cycle operation. This occurs when the control impulse bit is just sufficient to rotate the table to the opposite control line, as discussed in the preceding section. A quantitative relation will now be derived for this limit. Consider the following sketch.

-121-
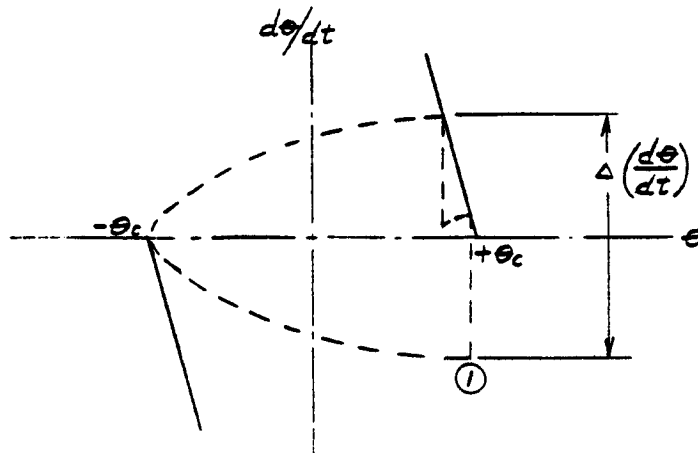
It is desired to determine the magnitude of the thrust force below which soft limit-cycle operation will definitely occur. The worst possible case must be considered and is illustrated in the above sketch. This worst case occurs when the limit cycle is entered so that the control pulse decreases the rate very close to zero. When this occurs, the same control line is again crossed producing a second pulse in the cycle. Thus, the control pulse in this case is two pulses from the resistojet instead of one. In the following discussion, the small change in orientation between the two pulses will be assumed to be negligible.

The relation describing the table motion in the absence of the control torque is:

$$\frac{d^2\theta}{dt^2} = \frac{T_D}{J} \tag{47}$$

where J is the table moment of inertia. Let condition (1) represent $t = 0$, where $\theta = \theta_o$, and $\frac{d\theta}{dt} = \left(\frac{d\theta}{dt}\right)_o$

Integration thus gives with these initial conditions:

$$\left(\frac{d\theta}{dt}\right)^2 - \left(\frac{d\theta}{dt}\right)_o^2 = 2\frac{T_D}{J}(\theta - \theta_o) \tag{48}$$

Assuming that the control pulse width is short relative to the total cycle time, the two control pulses produce a step change in $d\theta/dt$. Thus,

$$\Delta\left(\frac{d\theta}{dt}\right) = 2 t_R \frac{T_R}{J} \tag{49}$$

-122-
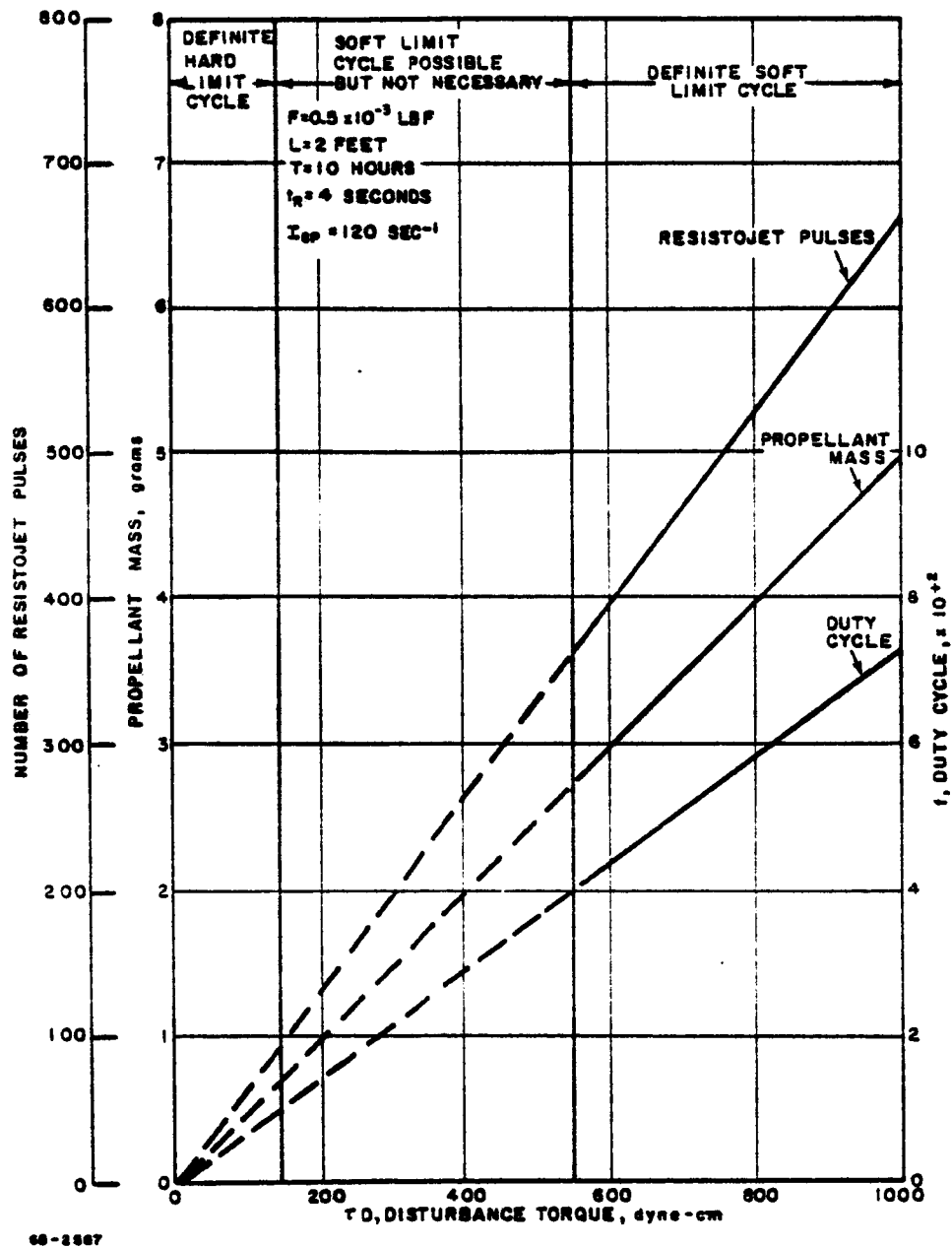
Figure 72 ESTIMATED TOTAL PROPELLANT CONSUMPTION -- TOTAL NUMBER OF
RESISTOJET PULSES AND RESISTOJET DUTY CYCLE VERSUS
DISTURBANCE TORQUE FOR SOFT LIMIT CYCLE
OPERATION IN THE NASA LEWIS TEST BED

where t_R is the pulse time of the resistojet. Also, at position (1), $(d\theta/dt)_o = -1/2 \Delta\left(\dfrac{d\theta}{dt}\right)$. Now, assuming that the slope of the control, line is small and can be neglected, $\theta_o = \theta_c$. Substitution of these quantities gives

$$\left(\frac{d\theta}{dt}\right)^2 = \left(\frac{t_R \, \tau_R}{J}\right)^2 + 2\,\frac{\tau_D}{J}\,(\theta - \theta_c) \tag{50}$$

The limit for soft cycle operation occurs, where $d\theta/dt = .0$ at $\theta = -\theta_c$ or

$$t_R \, \tau_R = \sqrt{2\,\tau_D \,\theta_c \, J} \tag{51}$$

Letting $\tau_R = F_1 L$, where F_1 is the limiting thrust force and L the moment arm, gives

$$F_1 = \frac{2}{L t_R}\,\sqrt{\tau_D\,\theta_c\,J} \tag{52}$$

Thus, for a given disturbance torque and pulse time, any force greater than F_1 may or may not result in hard limit-cycle operation depending on the entry point into the cycle; any force smaller than F_1 will always result in soft limit-cycle operation, however.

Another limiting case can be derived which gives the maximum thrust force, F_2, with which soft limit-cycle operation can be obtained. Soft limit-cycle operation cannot be guaranteed in the region $F_1 < F \leq F_2$, however, and the mode of operation will depend on the entry point into the cycle. Whenever the thrust force is greater than F_2, the limit cycle will always be hard, although soft limit branches may occur in the cycle. The limiting force, F_2, is given by the cycle with only one pulse rather than two as was the case for determining F_1. In this case

$$\Delta\left(\frac{d\theta}{dt}\right) = t_R\,\frac{\tau_R}{J} \tag{53}$$

and

$$F_2 = \frac{4}{L t_R}\,\sqrt{\tau_D\,\theta_c\,J} \tag{54}$$

Thus,

$$F_2 = 2F_1\,. \tag{55}$$

In Figure 73, a plot of F_1 and F_2 as a function of disturbance torque is given, and the areas of definite soft limit cycle, possible but not necessary soft limit cycle, and definite hard limit-cycle operation are indicated for the nominal conditions of the NASA Lewis test. It is seen that at a thrust level of 0.5×10^{-3} lbf, a disturbance torque greater than 575 dyne-cm will definitely insure soft limit-cycle operation, while one less than 144 dyne-cm will definitely insure hard limit-cycle operation. For disturbance torques between these two values, the operation may be in either a soft or hard limit cycle, depending on the entry point into the cycle. The type of control operation to be experienced in the NASA Lewis tests will thus depend on the disturbance torque of the table.

c. Hard Limit-Cycle Operation

The performance of the system when operating in a hard limit cycle is difficult to determine analytically, and reliance must be placed primarily on the analogue computer calculations. The situation is further complicated by the fact that the cycle of operation, and hence the fuel consumption, is strongly dependent on the entry point into the cycle and also on the disturbance torque. The only case which permits limited study analytically is the zero disturbance torque case. Consider the following nonsymmetrical hard limit cycle with zero disturbance torque.
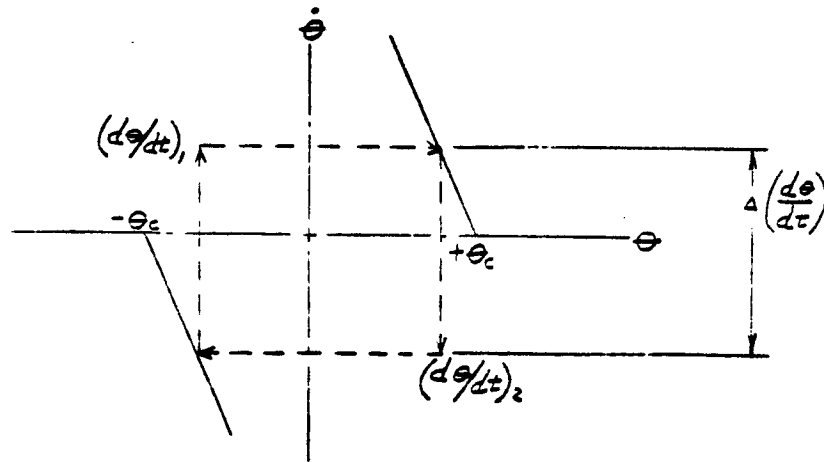
The effect of the slope in the control lines will be neglected and it will be assumed that the pulse duration relative to the total cycle duration is negligible. Then, the time per cycle is
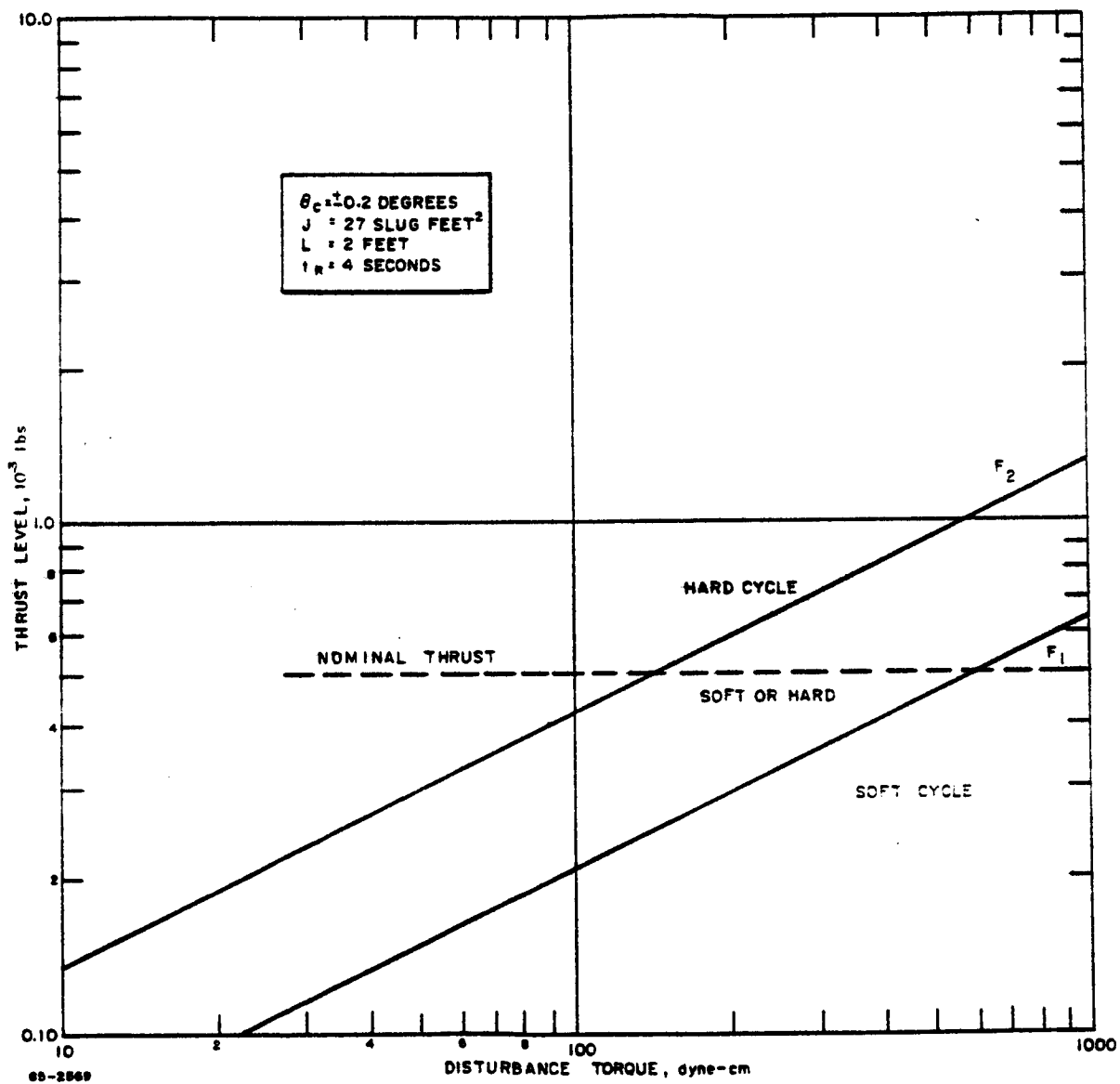
Figure 73 THRUST FORCE LIMITS FOR SOFT CYCLE OPERATION VERSUS APPLIED DISTURBANCE TORQUE

-126-

$$t_c = \frac{2\theta_c}{(d\theta/dt)_1} - \frac{2\theta_c}{(d\theta/dt)_2} = 2\theta_c \left[\frac{1}{\dot{\theta}_1} - \frac{1}{\dot{\theta}_2}\right] \tag{56}$$

Now, $\dot{\theta}_2 = \dot{\theta}_1 - \Delta\dot{\theta}$

Substitution gives

$$t_c = 2\theta_c \frac{\Delta\dot{\theta}}{\dot{\theta}_1(\Delta\dot{\theta} - \dot{\theta}_1)} \tag{57}$$

The cycle time thus depends not only on the $\Delta\dot{\theta}$ value, but also on whether the control cycle is symmetrical or unsymmetrical and how unsymmetrical.

The values of $\dot{\theta}_1$ which gives a miximum and a minimum in t_c are:

    Minimum t_c: $\dot{\theta}_1 = \dfrac{\Delta\dot{\theta}}{2}$, that is, a symmetrical cycle.

    Maximum t_c: $\dot{\theta}_1 = \Delta\dot{\theta}$, that is, one leg of the cycle falls on the zero rate line giving an infinite cycle time.

For a symmetrical cycle which gives the maximum fuel consumption, substitution of $\dot{\theta}_1 = \dfrac{\Delta\theta}{2}$ gives:

$$t_c = 8 \frac{\theta_c}{\Delta\dot{\theta}} \tag{58}$$

Now,

$$\Delta\dot{\theta} = \frac{{}^r R \, {}^t R}{J} \tag{59}$$

Substitution gives

$$(t_c)_{min} = 8 \frac{\theta_c J}{{}^r R \, {}^t R} \tag{60}$$

There are two pulses per cycle; the duty cycle can thus be written as:

$$f = \frac{2 \, {}^t R}{t_c} = 1/4 \frac{{}^r R \, {}^t R^2}{\theta_c J} \tag{61}$$

The fuel consumption can be written as

$$m_s = f \frac{F}{I_{sp}} T = 1/4 \frac{(F t_R)^2 L T}{\theta_c J I_{sp}} \tag{62}$$

For the nominal parameters of the NASA, Lewis test, the calculated values are (for the zero disturbance torque case):

$(m_s)_{max} = 2.90$ grams

$(t_c)_{min} = 314$ sec

$(f)_{max} = 2.55 \times 10^{-2}$

The above analysis represents the limit of simple analysis of the hard limit-cycle case. Analogue simulation of the system has been performed, however, and the results are presented in Figure 74 in terms of duty cycle versus disturbance torque. The plots are for pulse times, t_R, of 2, 3, and 4 seconds. In addition, the curve is given for the case of control between the outer backup lines only (pulse time, t_R, = 0) moved into θ_c = 0.2 degree. These curves are for acquisition from an attitude of 2.25 degrees. For the t_R = 3 seconds and t_R = 4 seconds cases, the duty cycle (or fuel consumption) first rises rapidly with increasing disturbance torque reaching a maximum in both cases at 100 dyne-cm. The duty cycle then decreases rapidly with increasing disturbance torque and approaches soft limit-cycle operation as represented by the solid line. For the t_R = 4 seconds case, soft limit cycle occurs for disturbance torques above 300 dyne-cm and for the t_R = 3 seconds case, above about 200 dyne-cm. For the t_R = 2 seconds case, the duty cycle is very close to the soft limit-cycle case above a disturbance torque of 50 dyne-cm. It is apparent from this plot that for this particular acquisition angle, a pulse length of 2 seconds would be the most desirable operating condition. It is also apparent that control without the inner control lines is better than operation with the control lines and pulse lengths of three or four seconds.

In Figure 75, a plot is given of the limit-cycle period as a function of the duty cycle with pulse duration and disturbance torque as parameters. This plot is based on the results of analogue computer calculations, including those presented in Figure 74, to determine the soft limit-cycle boundary. This boundary as given is thus applicable only for an acquisition angle of 2.25 degrees. As discussed earlier, the fuel consumption for soft limit-cycle operation is dependent only on the disturbance torque and the constant disturbance torque lines are thus vertical lines on this plot (constant duty cycle).
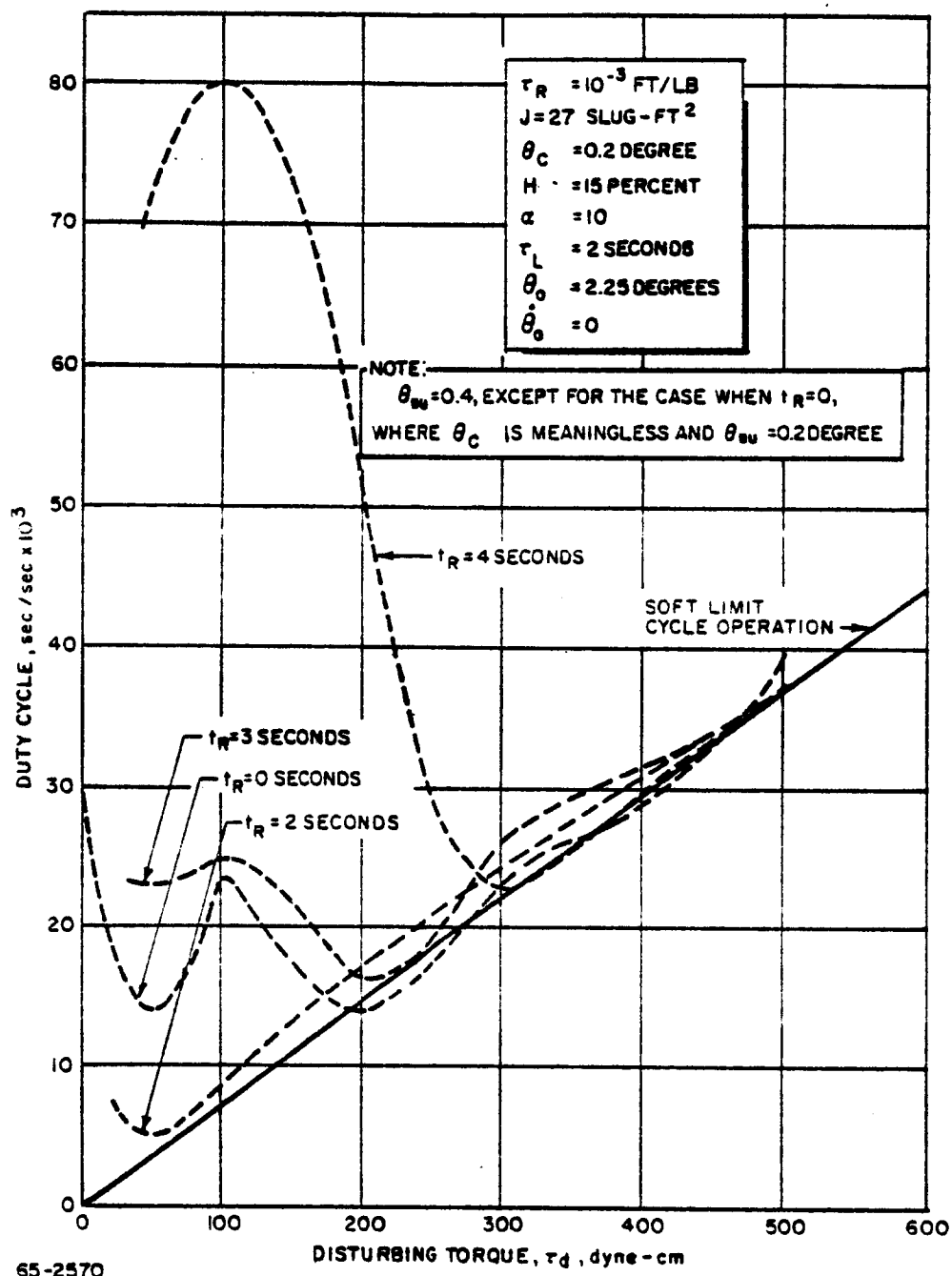
Figure 74 DUTY CYCLE VERSUS DISTURBANCE TORQUE FOR DIFFERENT INNER LINE
FIXED PULSE WIDTHS

65-2570
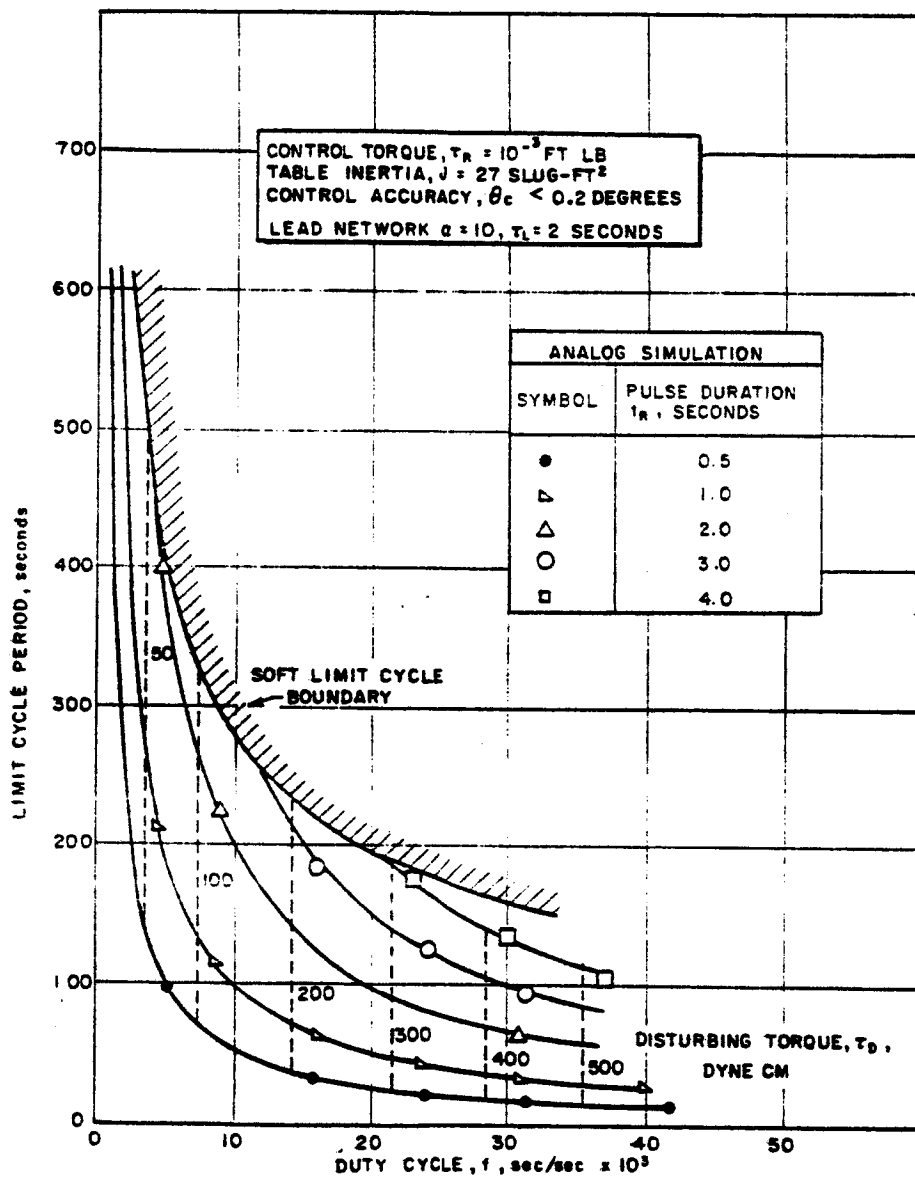
Figure 75 LIMIT CYCLE PERIOD VERSUS DUTY CYCLE FOR DIFFERENT INNER LINE
FIXED PULSE

65-2871

d. Acquisition Performance

The acquisition performance of the system has been determined using results from the analogue simulation. In Figure 76, the acquisition performance is given in terms of the time and impulse required for acquisition as a function of the initial acquisition angle. Additional analogue computor solutions are printed in Appendix E.

3. Electronic Circuitry for the Control Logic System

a. Control Logic Circuitry

A functional diagram of the control logic system is shown in Figure 77. The control function, $Z(t)$ is generated by the lead network. The lead network takes the sensor signal, $\theta(t)$, and generates a control function, $Z(t)$, which is proportional to the sum of the vehicle position, $\theta(t)$, and rate, $\dot{\theta}(t)$. The lead network is described in Appendix D. The control function, $Z(t)$, is then fed into a switching network which controls the operation of the appropriate engine.

The control method, which governs the design of both the lead and switching networks, is based on a method proposed by Vaeth. (ref. 8) The Vaeth method uses two sets of engine control commands. Whenever, the control function, $Z(t)$ exceeds the smaller; i.e., θ_{inner}, of two preset values, the appropriate engine is pulsed for a preset time producing an impulse bit, Fdt, which if the angular rate is small enough, reverses the direction of rotation of the table. The system thus oscillates between the preset limits resulting in limit-cycle control. If the rate of rotation is too large, however, the impulse bit will not be sufficiently large to reverse the rotation. With this condition, the control function will reach and exceed the larger of the two preset values, and the engine will be turned on and remains on continuously until the control function again drops below the larger preset value. This set of commands is used for acquisition and as a backup to the limit-cycle control lines. For the resistojet ACS the switching network also provides a finite heat-up time before the gas flow is pulsed.

A schematic of the switching network is presented in Figure 78. A reset circuit (shown in dashed lines) has been placed in to the switching network to prevent two valves from going on simultaneously due to noisy signals from the polarity detector.
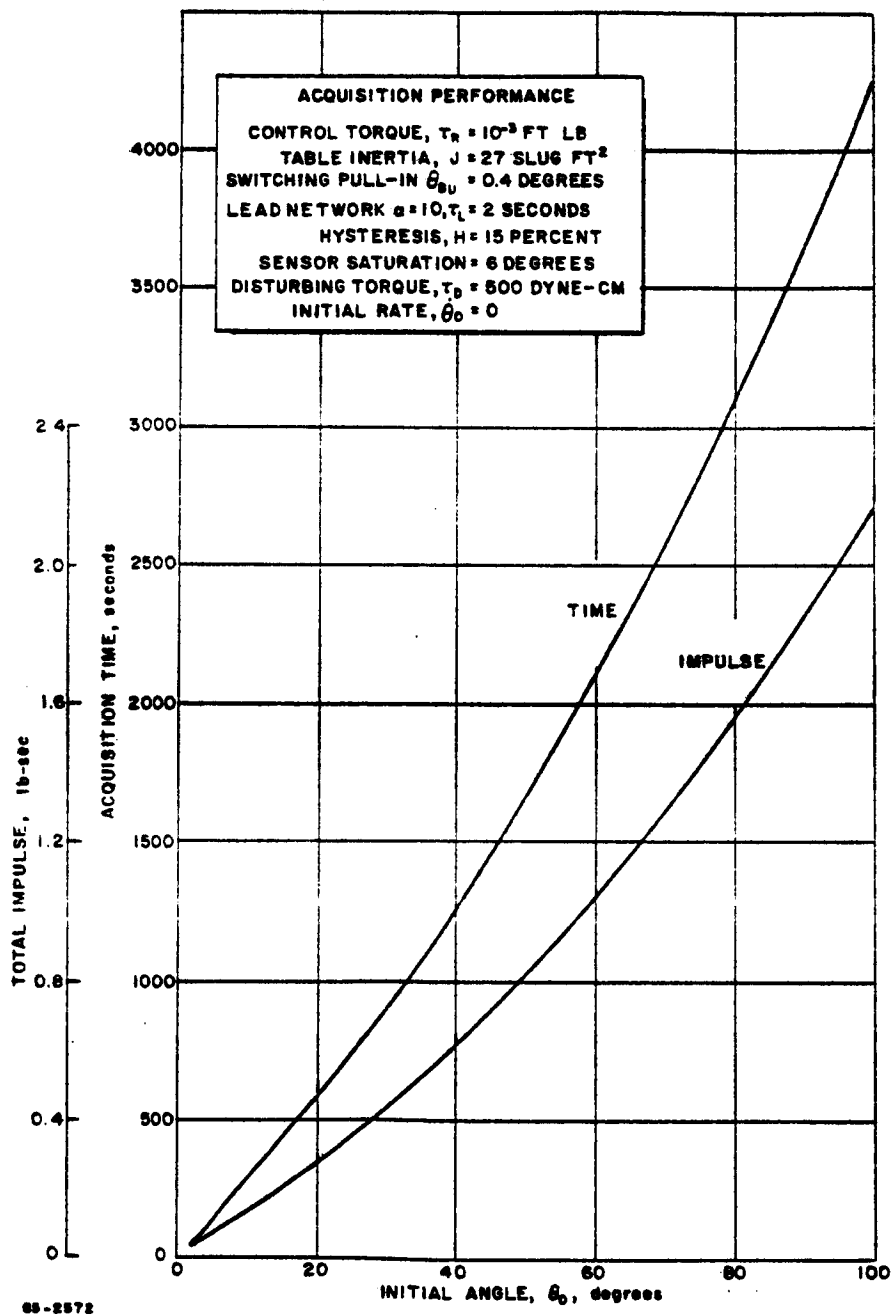
Figure 76 ACQUISITION TIME AND TOTAL ACQUISITION IMPULSE VERSUS
ACQUISITION ANGLE

POSITION SENSOR

$\theta(t)$

PREAMP

GAIN = K

$K\theta(t)$

LEAD NETWORK

$G(s) = \dfrac{1+\alpha T_L s}{1+T_L s}$

$Z(t)$

SWITCHING NETWORKS CONTROLLING RESISTOJETS
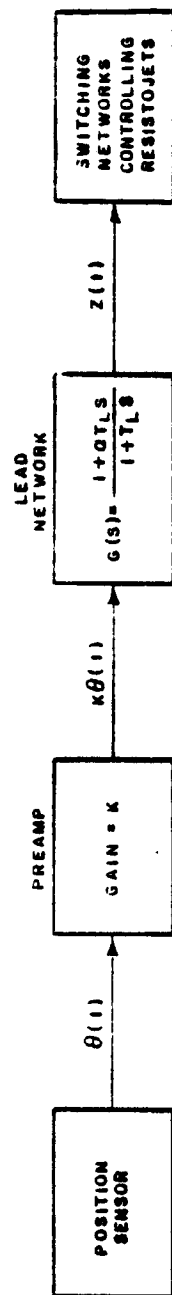
Figure 77 FUNCTIONAL DIAGRAMS OF THE CONTROL LOGIC SYSTEM
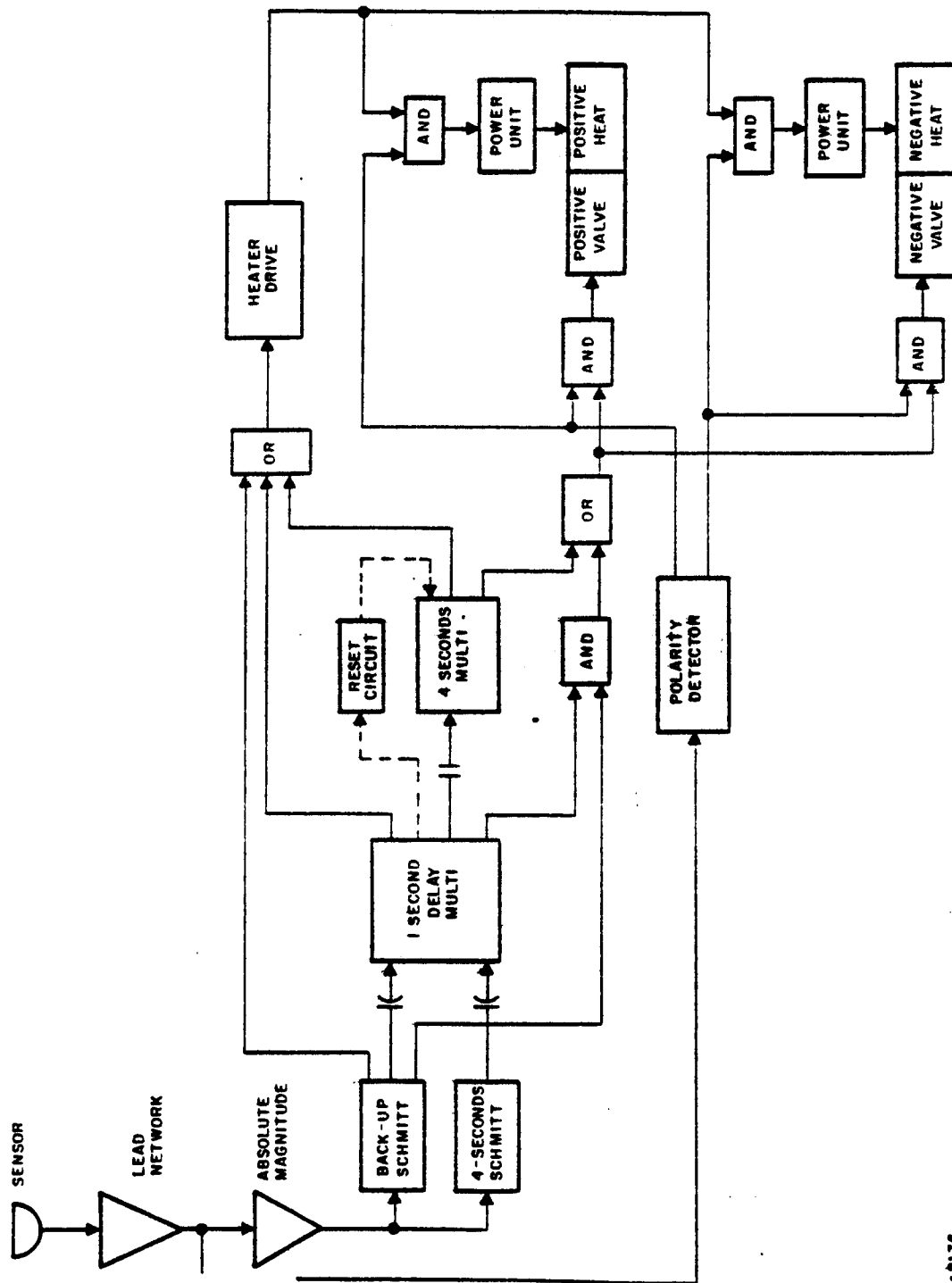
65-0176

Figure 78 FUNCTIONAL DIAGRAMS OF THE CONTROL LOGIC SWITCHING NETWORK

66-8176

-134-

Referring back to the signal output from the lead network of Figure 78 now, this output goes to two Schmitt trigger circuits. The two Schmitt triggers are set to trigger at different signal levels, and the sequence of events resulting in the operation of a resistojet is different, depending upon which Schmitt is triggered. For the lower signal level Schmitt, which is triggered when the error angle of the light sensor is 0.2 degree (inner control lines), the sequence is as follows:

The error signal energizes the Schmitt trigger which in turn energizes the first monostable multivibrator. Trigger of the multivibrator turns on the power supply for the resistojet heaters; the polarity detector determines which resistojet heater is turned on by means of an "and" circuit requiring two simultaneous signals (from heater power supply and polarity detector) before power is passed. The multivibrator operates for a preset time to provide time for the resistojet to be heated to the operating temperature without propellant flow. For the initial tests the heat-up time has been set at 1 second. At the end of the one second heat-up period, the monostable multivibrator returns to its stable state and triggers the second monostable multivibrator. The second multivibrator triggers the heater power supply, thus maintaining power to the resistojet heater and, at the same time, supplies a signal to the valve "and" circuits. The "and" circuit receiving a signal from both the polarity detector and second multivibrator, then passes the signal to the valve solenoid, allowing propellant to flow through the heated resistojet providing thrust. The heater and valve remain energized through the delay period of the second monostable multivibrator and become deenergized when the multivibrator returns to its stable state. For the initial tests (Resistojet Single-Axis Attitude Control System-Model 1) the propellant pulse length was preset at 4 seconds.

The above sequence is used for the low level signals to give a "fixed duration pulse". The second Schmitt trigger is used for higher level signals and overrides the effect of the first Schmitt trigger. The sequence for the second Schmitt, which is triggered at an error angle of 0.4 degree (backup or acquisition control lines) is as follows:

The error signal triggers the Schmitt, which turns on the heater supply and the first monostable multivibrator; the resistojet heater receives a signal from the polarity detector, as well as the one turned on. At the end of the 1-second heating period, the multivibrator returns to its stable state and supplies a signal to an "and" circuit. If the Schmitt trigger is supplying a signal to the "and" circuit also, a signal is passed to the "and" circuits controlling the valves. The "and" circuit also receives the polarity detector signal, then passes a signal to the proper valve solenoid opening that valve. The valve and heater remain energized continuously until the error signal drops to the level at which the Schmitt trigger returns to its untriggered state.

The polarity detector is necessary since the output of the absolute magnitude amplifier is always positive regardless of whether the signal polarity is positive or negative. The polarity detector detects the polarity of the error signal and provides outputs to the "and" circuits controlling the resistojet heaters and valve solenoids so that the proper heater and valve are energized. The polarity detector also serves the purpose of eliminating separate positive and negative channels, thereby reducing the number of components in the system.

The control electronics as described above have been fabricated and tested. Results of the breadboard testing have shown that the system operates as desired. The physical system will now be described.

b. Control Logic Circuit Hardware

The control logic circuit test package for installation on the single-axis air bearing contains the control logic circuitry for both the attitude control and station keeping resistojet thrustors, and the power-conditioning equipment for the attitude control resistojet thrustors. A circuit diagram for the control logic circuit is presented in Figure 79.

A sectional view of the control logic test package is shown in Figure 80. The package is approximately 6-1/2 inches long, 5 inches wide, and 4-1/4 inches high. The package is subdivided into three shelves. The bottom shelf, which is shown in Figure 81, contains the resistojet attitude control engine power-conditioning equipment; the middle and top shelves, shown in Figures 82 and 83, contain the control logic circuitry for the resistojet attitude control and station keeping engines. A photograph of the control logic test package is presented in Figure 84.

The station keeping resistojet heater and control valve are operated by telemetered commands. The logic circuit for this purpose is illustrated schematically in Figure 85. The circuit consists of a monostable multivibrator, diode logic, and a power stage. This circuitry is also contained in the logic package.

4. Light Source and Sensor

The basic input to the control system lead network is the table position $\theta(t)$, which comes from the sensor.

The single-axis resistojet attitude control optical system consists of an angle sensor and a collimated light source. The collimated light source was structurally attached to the vacuum chamber in which the single-axis tests were made and projected a collimated light beam toward the axis of the air-bearing test table. The sensor was mounted on the test table

-136-

Figure 79 DIAGRAMS FOR THE ATTITUDE CONTROL THRUSTORS CONTROL
LOGIC CIRCUIT

-137-
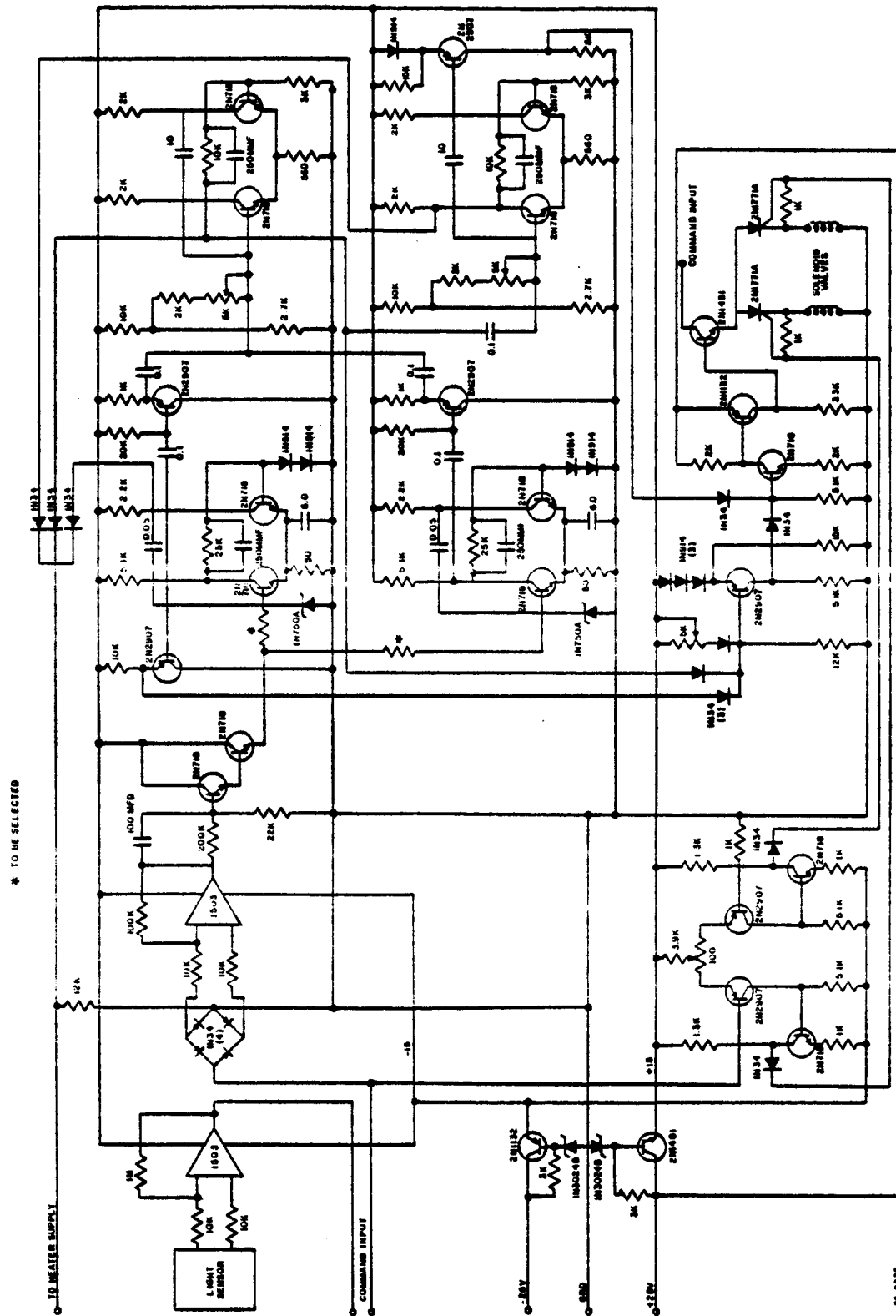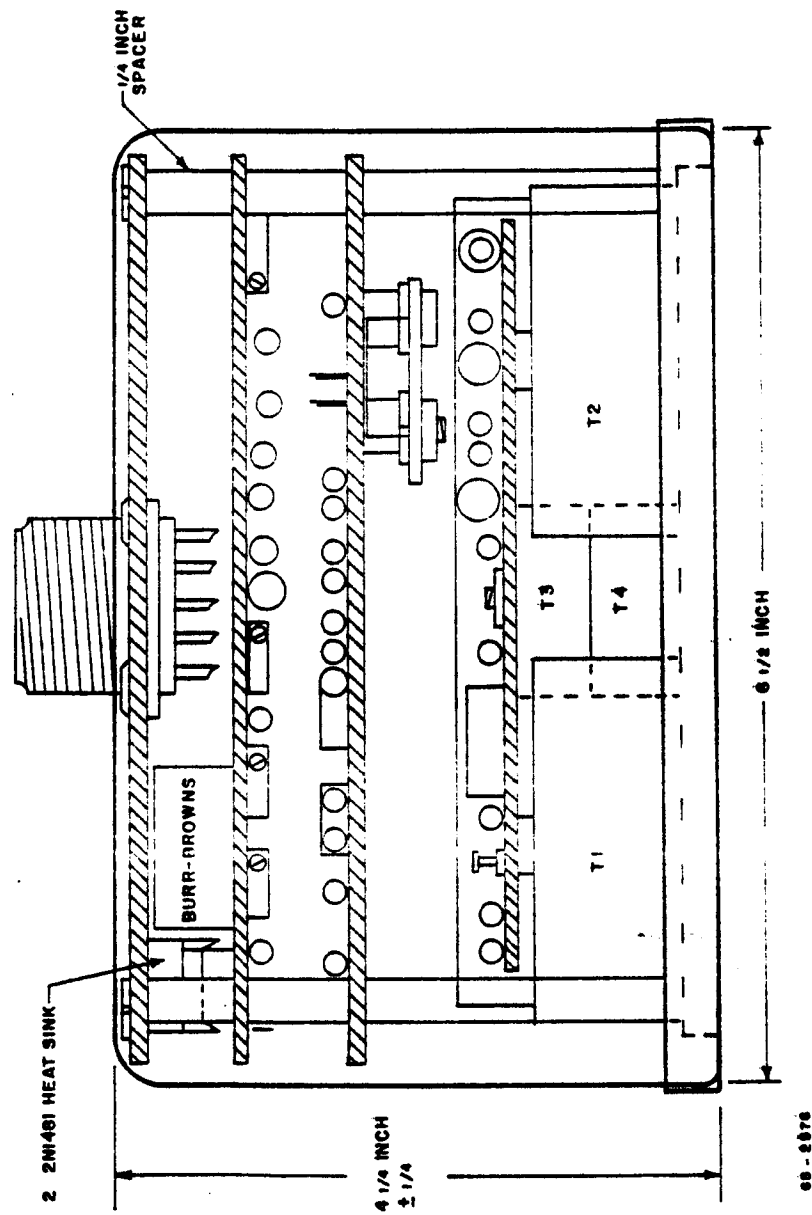
Figure 80 SECTIONED VIEW OF THE CONTROL LOGIC TEST PACKAGE
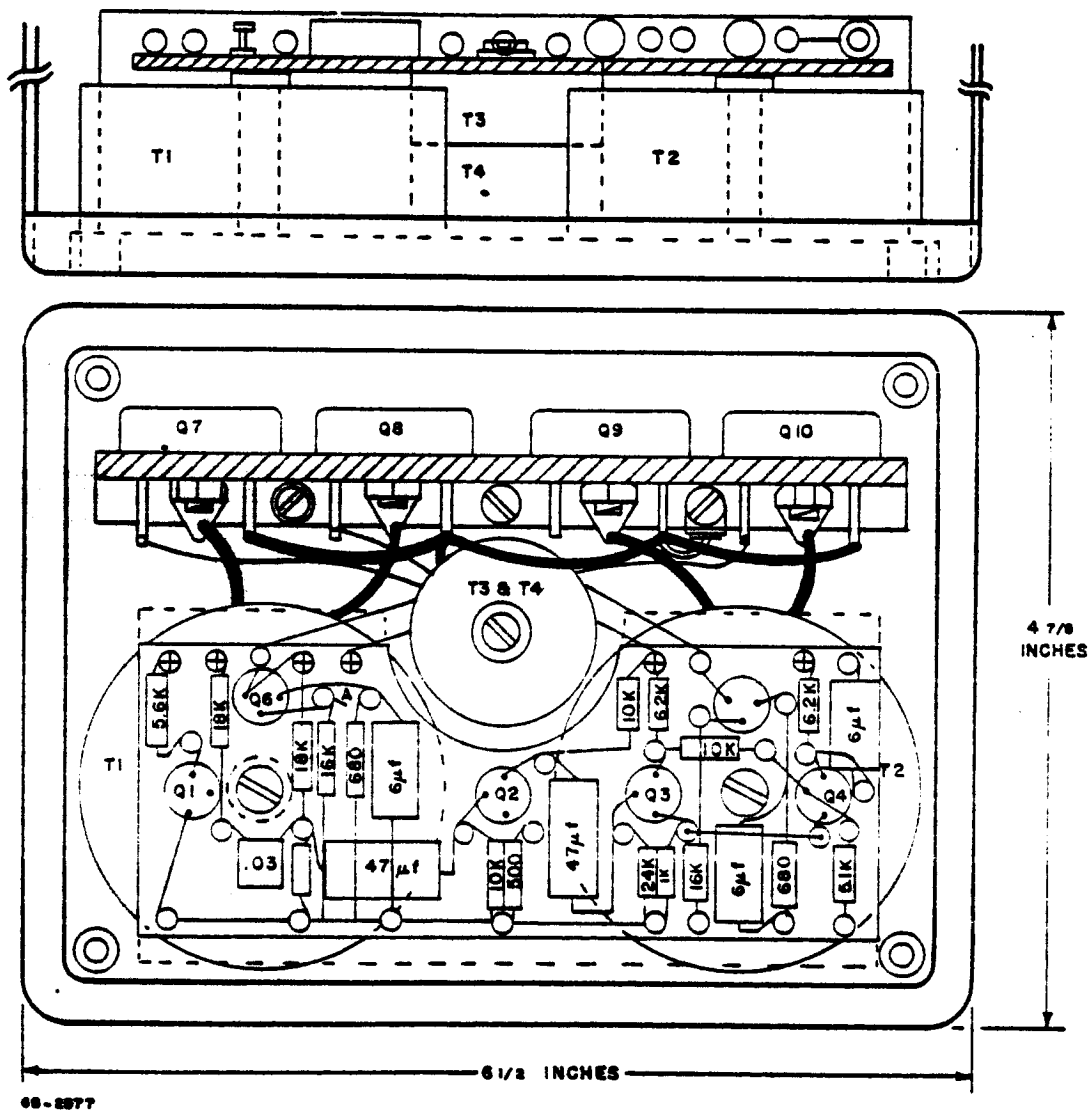
Figure 81 SECTIONED VIEW OF THE BOTTOM SHELF OF THE CONTROL LOGIC
TEST PACKAGE

Figure 82 SECTIONED VIEW OF THE MIDDLE SHELF OF THE CONTROL LOGIC TEST PACKAGE

-140-
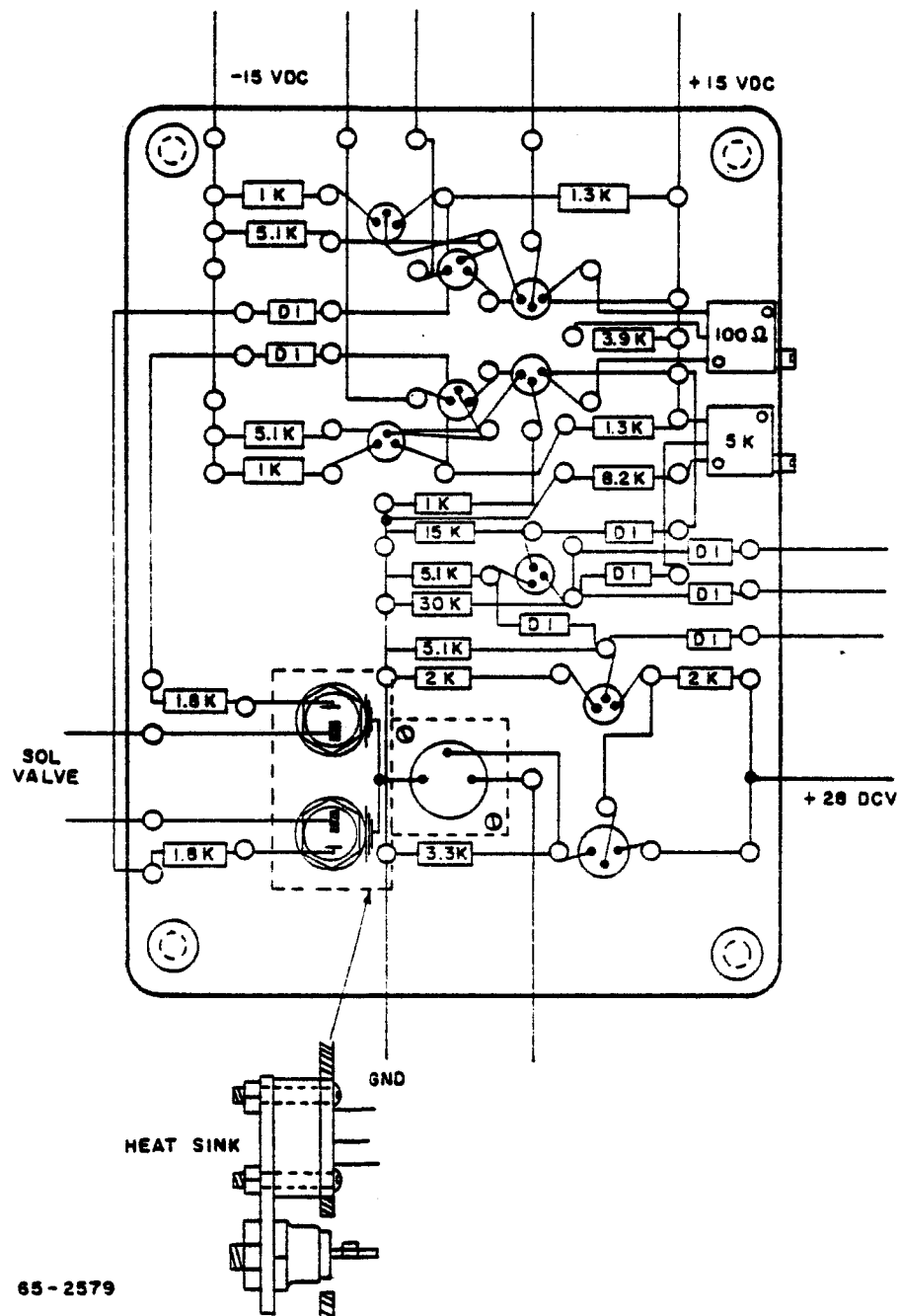
Figure 83 SECTIONED VIEW OF THE MIDDLE SHELF OF THE CONTROL LOGIC TEST PACKAGE

CONTROL LOGIC
CIRCUITS

POWER SUPPLY FOR
RESISTOJET (ONE OF TWO)

CABLES SUPPLYING POWER TO
ATTITUDE CONTROL RESISTOJETS

65-2580
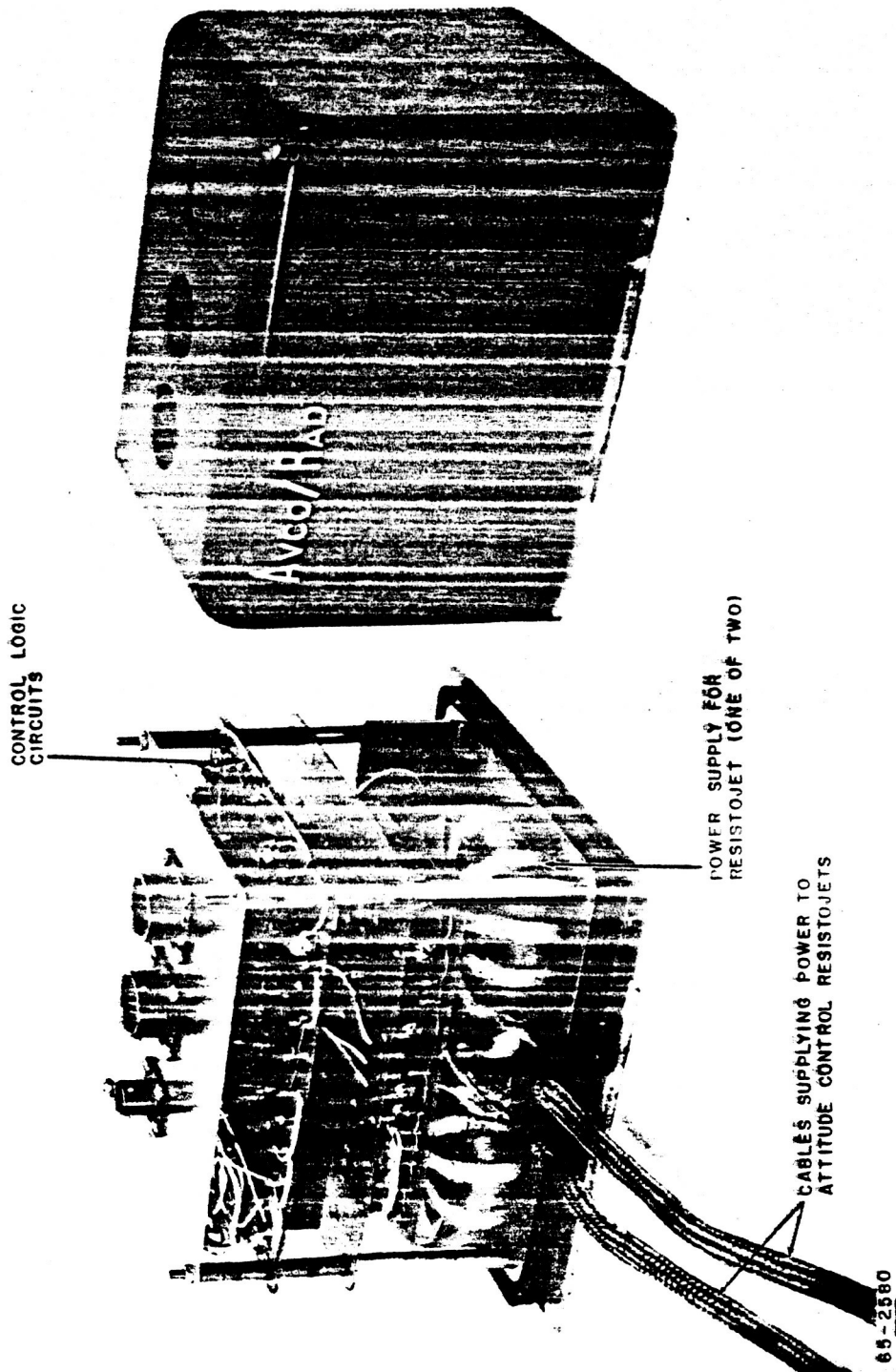
Figure 84 PHOTOGRAPH OF THE CONTROL LOGIC TEST PACKAGE

-142-
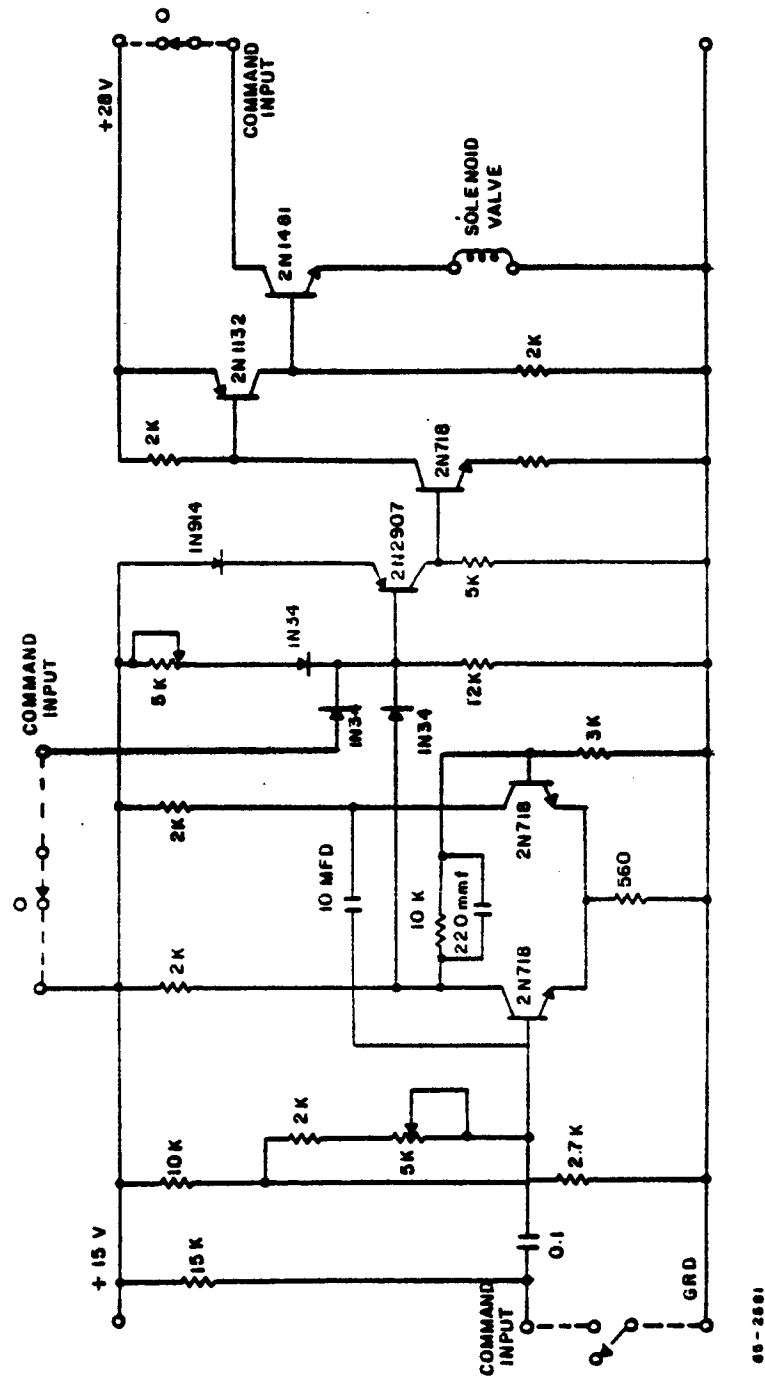
Figure 85 DIAGRAMS FOR THE STATION KEEPING THRUSTOR AND CONTROL
LOGIC CIRCUIT

-143-

and used the light source as an angular reference detecting angular error of the air-bearing table position. The electrical error signal generated by the sensor was used as an input to the air-bearing table control system commanding resistojet thrustor operation to reduce table position error to zero.

a. Light Source

The light source used a straight-line filament incandescent lamp. The filament is spring-loaded so that straightness is constantly assured. This lamp filament is located at the focal point of an Aero Elector Lens, having a focal length of 7 inches and an aperture of F:2.5.

The light source projected a collimated beam of light onto the angle sensor. Due to the collimated characteristic of the light beam, distance between the sensor and the light source was not critical. The lens diameter of the light source has been made larger than that of the sensor permitting small lateral displacements between the two units with full illumination of the sensor.

b. Angle Sensor

The optical angle sensor originally consisted of a silicon photo voltaic semiconductor sensing element and a small lens system used to focus the light source reference on the sensing element. Operation of the original sensor can be explained if we consider the sensing element to be made up of a pair of triangular shaped silicon photo voltaic cells as shown below.

A CELL $\longrightarrow$ $\longleftarrow$ B CELL

Project (optically) an image of a straight-line filament on to this pair of cells as shown below.

A   B

X   H   X'
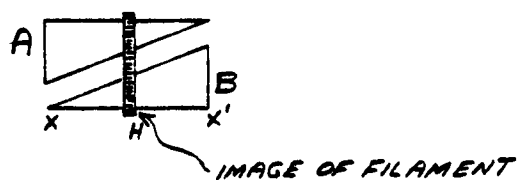
IMAGE OF FILAMENT

When the filament is centered between X and X', the cells will receive equal amounts of illumination and therefore the voltage output of each cell will be identical. A displacement of the image in the X-X' axis will cause the illumination on one cell to increase with a corresponding decrease on the other. The summation of the two cells will then produce a direct-current signal with magnitude and sign determined by the location of the image. Sensor null will occur when the image is centered on the cells.

During the early testing of the Resistojet Attitude Control System a control problem arose and was traced to the the optical angle sensor. As previously described, the angle sensor should theoretically be sensitive only about rotations in the desired plane. Lateral displacements or rotations about other planes should, because of symmetry, cause no change in the output. Investigations revealed that this optical angle sensor was also quite sensitive to rotations about an axis normal to the desired one. This effect was traced to the fact that the temperature of the filament was not uniform, being hotter in the middle and cooler at the ends. The result of this condition was that as the image of the filament was displaced vertically due to cross axis motions, either cell A or cell B received more energy thus producing a differential output. The net effect of this condition was that the angle sensor was sensitive to swinging motions of the wire suspended table and as a result, triggering of the electronics at unwanted times produced spurious impulses affecting the limit cycle of the system.

The design of the target was changed as shown in Figure 86.

From this geometry, it can be seen that for cross axis motions, resulting in an up and down motion of the image on the target, the output will not change even though the temperature of the filament is not constant. For displacements to the right or left, corresponding to angular displacements in the wanted plane, it can be seen that more energy will fall on either cell A or cell B thus producing a differential output. The edges of the cells were cut to a particular shape so as to linearize the output voltage by compensating for the non-uniformity of the filament radiation.

Tests with this new optical angle detector confirmed the fact that the cross axis sensitivity was so low as to eliminate problems due to swinging motions of the table. The closed loop attitude control systems tests were thus successfully completed on the wire suspended test table.

The performance characteristics of the position sensor are summarized in Table XII.
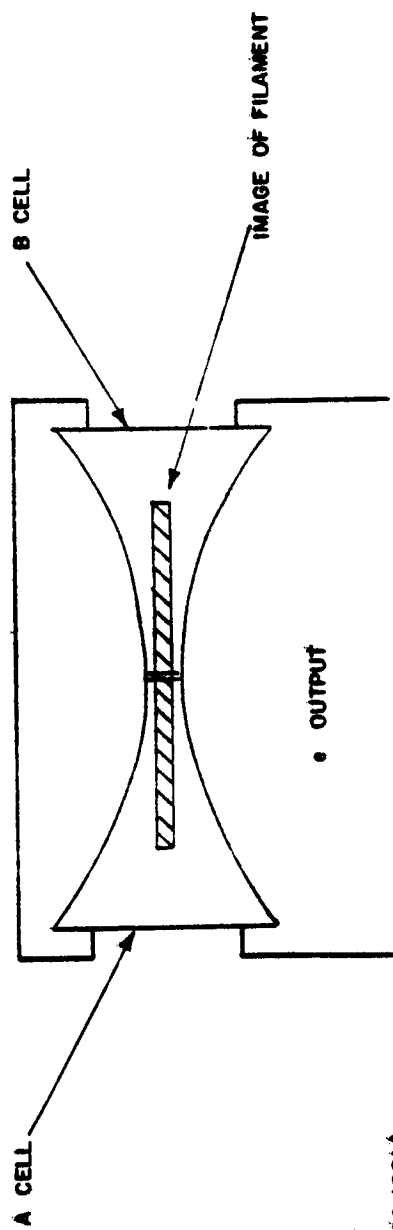
Figure 86 PHOTOGRAPH OF THE LIGHT SOURCE AND LIGHT SENSOR

86-12014

-146-

TABLE XII

PERFORMANCE OF POSITION SENSOR

Scale Factor	30 mv/deg
Linear Range ± 2 percent	± 3 degrees
Maximum Output	± 8 degrees

C. POWER CONDITIONING PACKAGE

The basic power supply system was furnished by NASA Lewis. The system consisted of a battery bank capable of supplying 60 amp-hr at 24 vdc. The battery bank was connected to three voltage regulators, two of which supplied a regulated voltage of + 28 vdc at a maximum rating of 2.13 amperes; the other supplied a regulated voltage of -28 vdc at a maximum rating of 1.0 ampere. In Table XIII the estimated power requirements for the 10-hour test are given for each regulated supply, indicating that the power supply was ample for this test. The basic ± 28-vdc supply is conditioned by Avco/SSD equipment to the desired levels required for the test; the power conditioning equipment will now be described.

Power is required for the resistojet heaters, for the solenoid-operated valves, and for the transducers and signal conditioning equipment. The solenoid valves all operate on 28 vdc and can be connected directly to the NASA power supply through the appropriate control system.

1.   Power Supply for Attitude Control Resistojet Heaters

The resistojet engine has a resistance of approximately 0.1 ohm at operating temperature. For the desired power of about 10 watts for the test of the Resistojet Attitude Control System, Model 1, a voltage of 1 volt and current of 10 amperes is required for heating the resistojet. To convert the 28-vdc supply to this level with a reasonable overall efficiency, the inverter circuit illustrated in Figure 87 was used. The direct-current supply was converted to 10-kHz alternating current with a square wave shape. This alternating-current signal was then transformed to the desired voltage level. The high frequency resulted in a high efficiency and reduced output transformer size. In Table XIV the measured characteristics of the resistojet power supply used for the initial test are presented. The power output as well as the overall efficiency from the system is seen to be a strong function of load resistance.

TABLE XIII

POWER AND TOTAL ENERGY REQUIREMENTS FOR A TEN HOUR
SINGLE AXIS TEST OF THE RESISTOJET ATTITUDE CONTROL SYSTEM

A. Peak Current Drain from Regulated Power Supplies			
Power Supply Number	Power Supplied to	Maximum Current Drawn (amperes)	Power Required
1 +28vdc, 2.7 amps	Attitude Control Resistojets Station Keeping Resistojet Total	0.8 0.8 1.6	Intermittent
2 +28vdc, 2.7 amps	Control Logic Package Signal Condition Package Pressure Regulating Valve Total	0.16 0.11 0.30 0.57	Continuous Continuous Intermittent
3 -28vdc, 1.0 amps	Sensor Excitation Control Logic Package Signal Condition Package Total	0.580 0.050 0.110 0.740	Continuous Continuous Continuous

B. Battery Drain for 10-Hour Test Period

1 Continuous Operation

Supply No. 2   0.270
Supply No. 3   0.740

Total   1.010

Power = (28) (1.01) = 28.28 (watts)
Energy = 282.8 (watt-hours)

2 Intermittent Operation

Acquisition - It is assumed that 0.5 hours is required for acquisition.

Resistojet Operation

     Power = (0.8) (28) = 22.4 (watts)
     Energy = (22.4) (0.5) = 11.2 (watt-hours)

Control Valve Operation

     Power = (0.300) (28) = 8.4 (watts)
     Energy = $(8.4)(\frac{1}{60})$ (0.5) = 0.07 (watt-hours)

         Total Energy = 11.3 watt-hours

Limit Cycle Control - It is assumed that limit-cycle control occurs
for 9.5 hours with a duty cycle of 5 percent.

Resistojet Operation

     Energy = (22.4) (9.5) (0.05) = 10.6 (watt-hours)

Control Valve Operation

     Energy = (8.4) $(\frac{1}{60})$(9.5) (0.05) = 0.07 (watt-hours)

         Total Energy = 10.7 watt-hours

3 Total Battery Drain = 316 watt-hours

Figure 87 INVERTER CIRCUIT FOR THE ATTITUDE CONTROL RESISTOJET HEATERS

TABLE XIV

OUTPUT CHARACTERISTICS OF THE HEATER
POWER SUPPLY FOR RESISTOJET ATTITUDE
CONTROL SYSTEM – MODEL 1

Lead Resistance Ohms	RMS Voltage	Power (watts)		Efficiency
		Input	Output	
0.052	0.40	12.60	3.08	24.4
0.104	0.76	11.48	5.55	48.4
0.215	1.27	8.40	7.50	8º.3

The power supply described above for the two attitude control resistojet thrustors is physically located in the Control Logic Test Package described previously.

2. Power Supply for the Station-Keeping Resistojet Thrustor

The circuit schematic of the station-keeping resistojet heater power supply is shown in Figure 88. Operation of the power supply is identical to that used with the attitude control resistojet heaters except that the operating signal is derived from "ground" command through telemetry rather than from the attitude control logic system. The station-keeping power supply is physically located in the Signal Conditioning Test Package.

3. Signal Conditioning Power Supply Circuitry

The signal conditioning power supply provides regulated voltages necessary for the signal conditioning circuits for the various transducers and for the transducers themselves. This system converts + 28 VDC to regulated + 15 VDC and - 28 VDC to - 15 VDC. The - 15 VDC if further attenuated by resistive divider networks to the - 7 VDC, - 5 VDC, and - 4 VDC levels necessary to power the transducers. This power supply is located in the Signal Conditioning Test Package.

D. RESISTOJET ENGINE SYSTEM

A flow diagram of the resistojet engine system is given in Figure 89; also shown in Table XV are the manufacture and model number of the major components. As indicated previously, three identical resistojets will be used for the test, two for attitude control (clockwise and counterclockwise rotation of the table in the horizontal plane) and one for station keeping.

Figure 88 INVERTER CIRCUIT FOR THE STATION KEEPING RESISTOJET HEATERS

65-2565

-151-
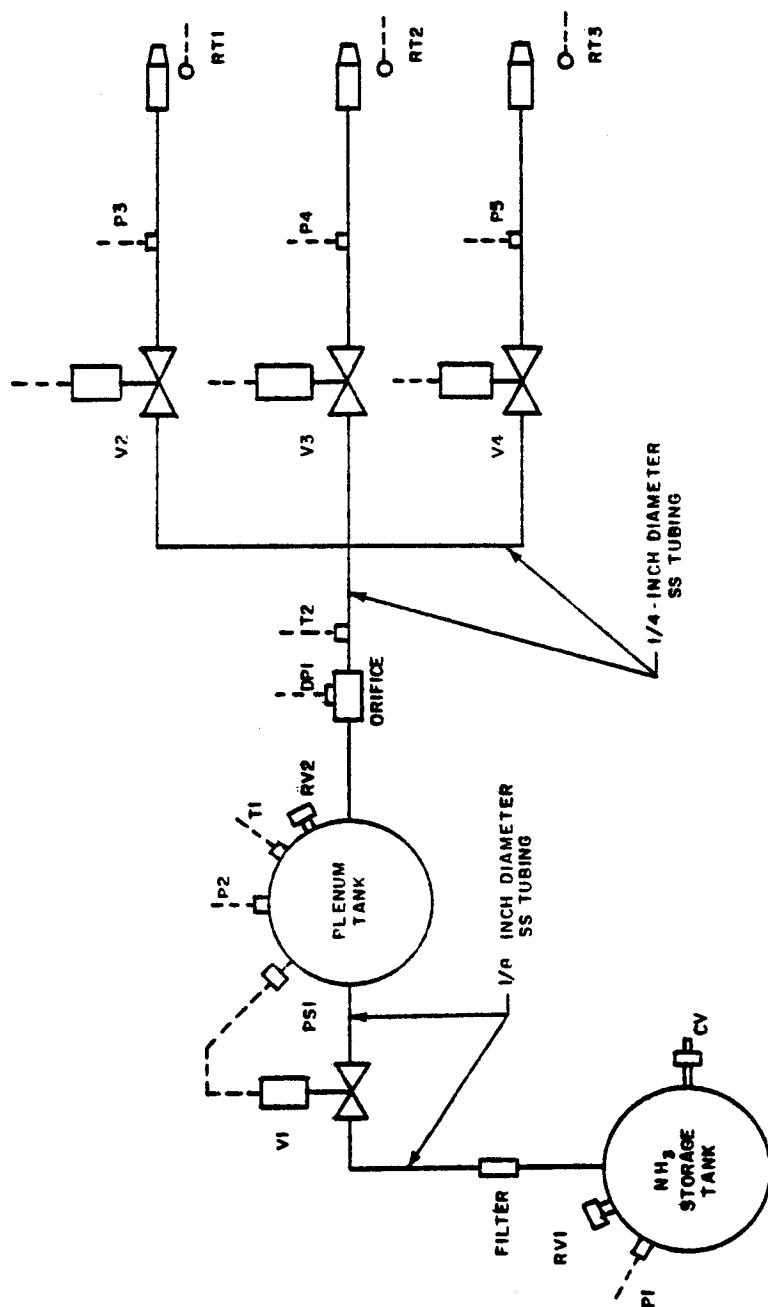
Figure 89 SCHEMATIC DIAGRAM OF THE RESISTOJET AMMONIA FLOW SYSTEM

TABLE XV

MANUFACTURE AND MODEL NUMBER OF MAJOR PURCHASED COMPONENTS

Symbol	Description	Source
P1	Pressure Transducer, PA208TC, Range 0-250 psia	Statham Instr. Inc. Los Angeles 64, Cal.
P2	Pressure Transducer, PA208TC, Range 0-50 psia	Statham Instr. Inc. Los Angeles 64, Cal.
P3, P4, P5	Pressure Transducer, PA222TC, Range 0-50 psia	Statham Instr. Inc. Los Angeles 64, Cal.
V1	Pressure Regulating Valve, No. B2DA9175 Two-way Solenoid Valve	Skinner Electric Valve Div. New Britain, Conn.
V2, V3, V4	Solenoid Operated Valve, No. AF70C-37 Norm. Closed Type "E" Ends	Eckel Valve Co. San Fernando, Cal.
T1, T2, T3, T4	4K ISO Curve Bead Thermistor Assy.	Fenwal Electronics, Inc. Framingham, Mass.
DP1, DP2, DP3	Differential Pressure Transducer, PL283TC, Range 0-1 psia	Statham Instr. Inc. Los Angeles 64, Cal.
PC2, PC3, RT1, RT2, RT3	Type 1N2175 N-P-N Diffused Silicon Photo-Duo-Diode	Texas Instr. Inc. Dallas 22, Texas

1. Resistojet Assembly

Referring to Figure 89 each of the three resistojet assemblies consists of a control valve for pulsing the ammonia flow, a pressure transducer, a resistojet heater element and exit nozzle, and a photocell for resistojet temperature measurement.

A resistojet assembly drawing is presented in Figure 10 and a photograph of the resistojet engine is shown in Figure 11.

Referring to Figure 10, the volume between the propellant control valve and the heater element has been held to a minimum to increase the transient response of the resistojet. The propellant valve, pressure transducer, and heater tube are all connected to the main thrustor body. The heater element is surrounded by a concentric heater support. The heater support serves to provide a stable surface to which the resistojet leads at the end of the nozzle can be connected, and also serves the protect the relatively fragile heater tube against misalignment. The support tube is electrically insulated from the main thrustor body by a ceramic insulator. One electrical connection can thus be made to the heater support tube and the other to the main thrustor body.

The Eckel solenoid valve weighs only 0.017 pound and requires only 1.92 watts (0.08 ampere at 24 vdc) input power. The leakage rate of the valves as received is being measured using a helium leak detector. The leakage rate of the two valves which have been delivered is quite low with a typical value being 2.0×10^{-5} cm^3/hr for a 35-psi pressure differential across the valve. For comparison, a leakage of 1 gram of ammonia over a three year period is equivalent to 1.75×10^{-4} cm^3/hr.

A photo-diode is used to monitor the resistojet heater element temperature. Figure 90 shows a plot of detector response at a fixed bias voltage as a function of distance from the thrustor. The heater element is observed by the photo-diode through a 3/16-inch hole located in the heater support.

2. Ammonia Supply System

The ammonia supply system is illustrated in Figure 91; a photograph of the complete assembly is shown in Figure 92. The supply system which was mounted beneath the NASA Lewis test bed, consists of a liquid ammonia tank and a gas reservoir is controlled by means of a pressure switch and solenoid operated valve.

The ammonia liquid storage tank, which has a volume of 775 ml, has an ammonia capacity of about 1 pound of liquid ammonia at 70° F. Continuous operation of a resistojet engine for 10 hours at a nominal flow rate of 5×10^{-6} lb/sec consumes only 0.18 pound of fuel so that the storage tank

-154-
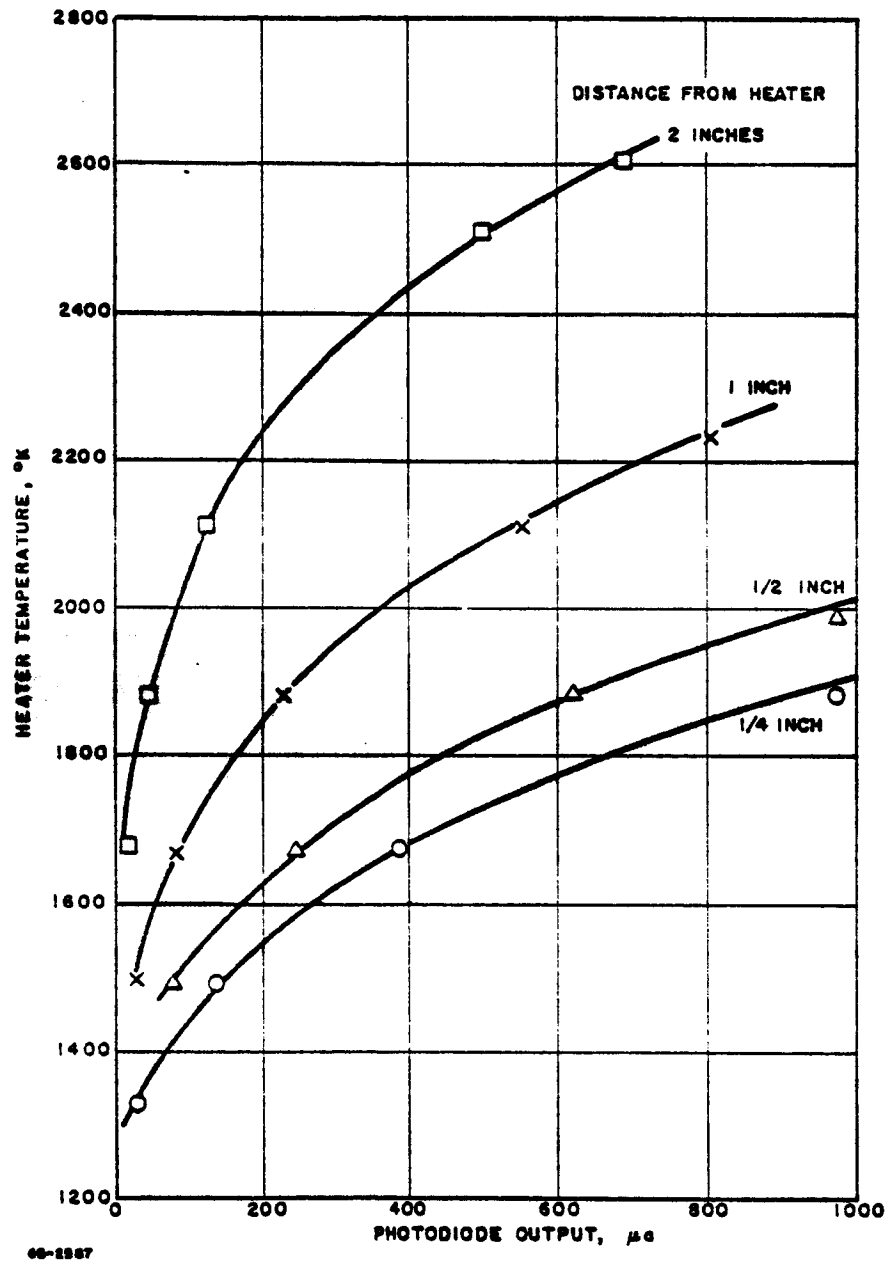
Figure 90 PHOTODIODE RESPONSE VERSUS RESISTOJET HEATER TEMPERATURE
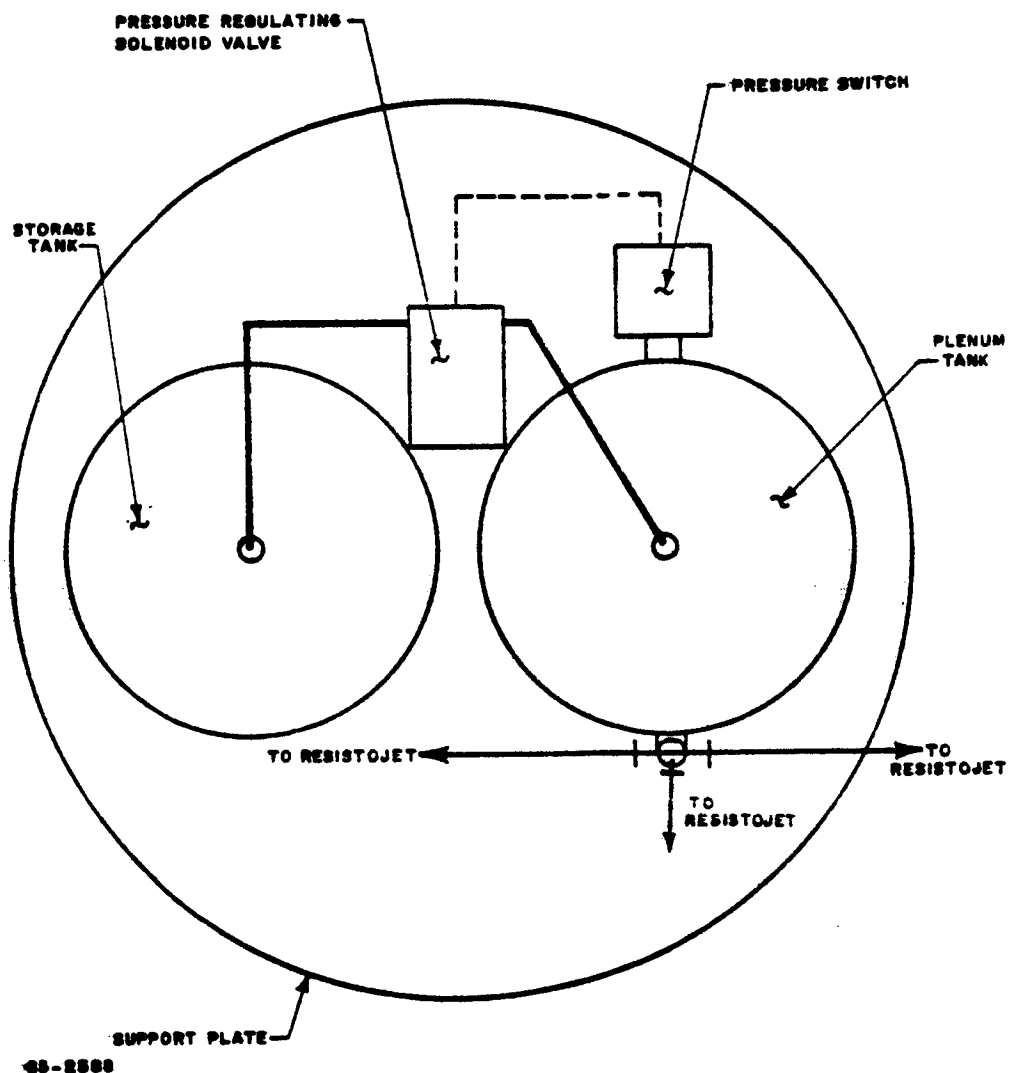
Figure 91 AMMONIA SUPPLY SYSTEM ASSEMBLY
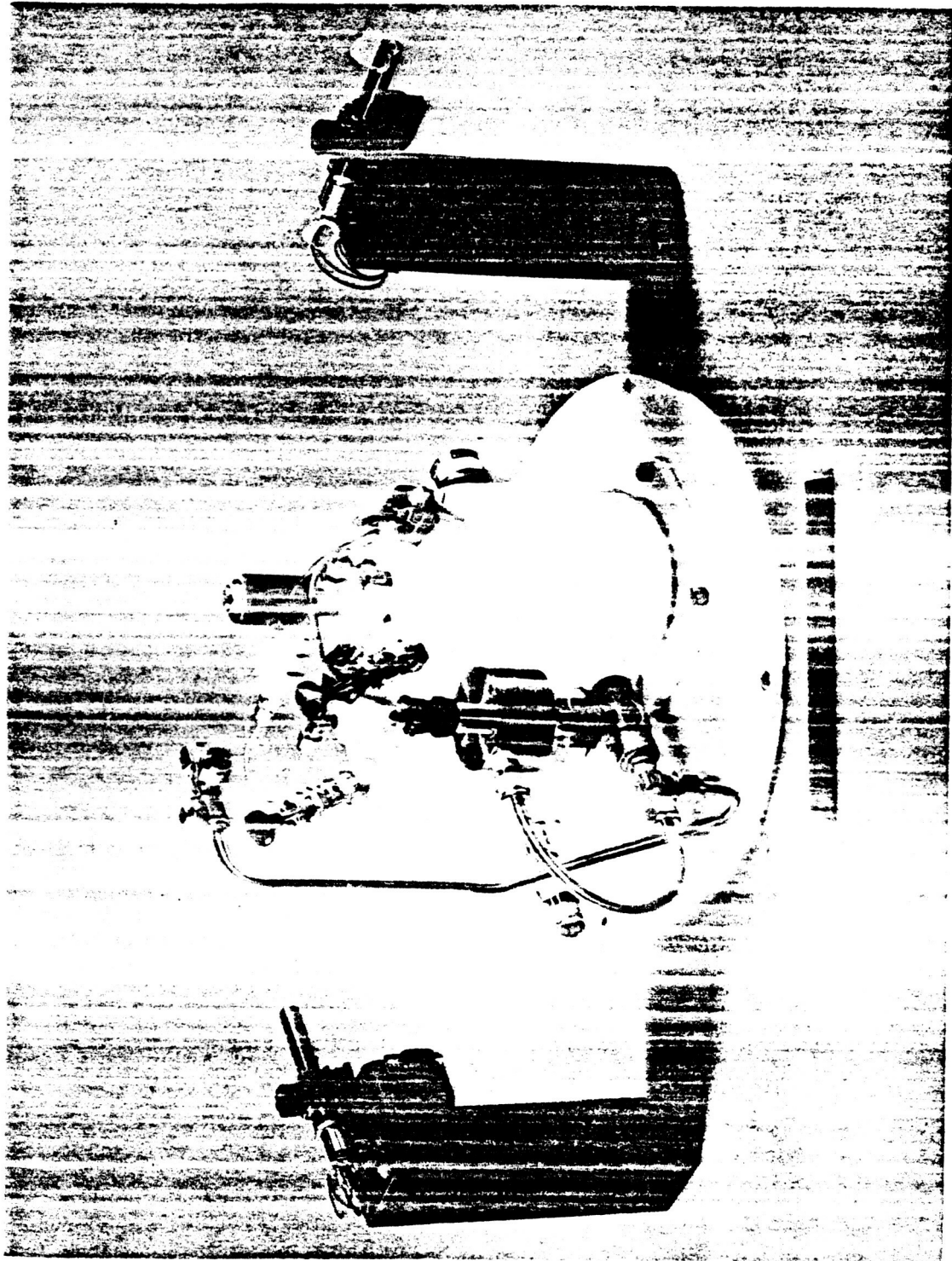
Figure 92 PHOTOGRAPH OF AMMONIA-FUELED SYSTEM

provides a more than ample fuel reserve for the single axis test. The gas
reservoir volume of 775 ml minimizes the number of cycles of operation
required of the pressure switch and solenoid valve. For example, assuming
the pressure switch operates between 24 and 26 psia, the resistojet engine
can be pulsed about 15 times (4-second pulse) before the pressure drops
from 26 to 24 psia, and the pressure regulating switch and valve operate.

Both the liquid and gas storage tanks have a combination pressure relief
and venting valve; the liquid ammonia storage tank has a check valve for
ease in tank charging. The stainless-steel tubing between the ammonia gas
reservoir and the filter flowmeter assembly is 1/8 inch in diameter.

The filter-flowmeter assembly is illustrated in Figure 93. The filter, a
sintered stainless-steel plug, is located upstream of the flowmeter to pre-
vent plugging of the system downstream of this point. The filter will stop
any particulates with a size larger than about 10 microns.

The flowmeter consists of a 10-mil diameter, sharp-edged orifice located
immediately downstream of the filter. The pressure drop is measured
with a differential pressure transducer. The orifice size has been selected
so that the pressure drop across the orifice is small; e.g., 0 to 1 psia,
relative to the plenum pressure, and so that the ammonia flow is choked
across the exit nozzle rather than across the orifice. A thermistor is
located immediately upstream of the flow orifice in order to measure the
ammonia inlet temperature.

E. SIGNAL CONDITIONING PACKAGE

The signal conditioner test package is connected to the NASA telemetry package.
Both the signal conditioner test package and the NASA telemetry package are
located on the air bearing test bed. The NASA telemetry package, which is
located on the test bed, receives command signals from a transmitter and
transmits data signals from test bed to a receiver. Both the command trans-
mitter and signal receiver are located away from the proximity of the test
tank. In this manner, actual space-flight test conditions are thus simulated
as closely as possible in the laboratory.

For convenience the power conditioning unit for the station-keeping resisto-
jet thruster has been included in the signal conditioning test package.

BRAZE

ORIFICE.
AVCO DWG R6-2724

SWAGELOCK 400-3-4T FT-316
CRAWFORD FITTING CO.

FILTER 603-3 WITH ELEMENT
90347.3 HOKE INC.
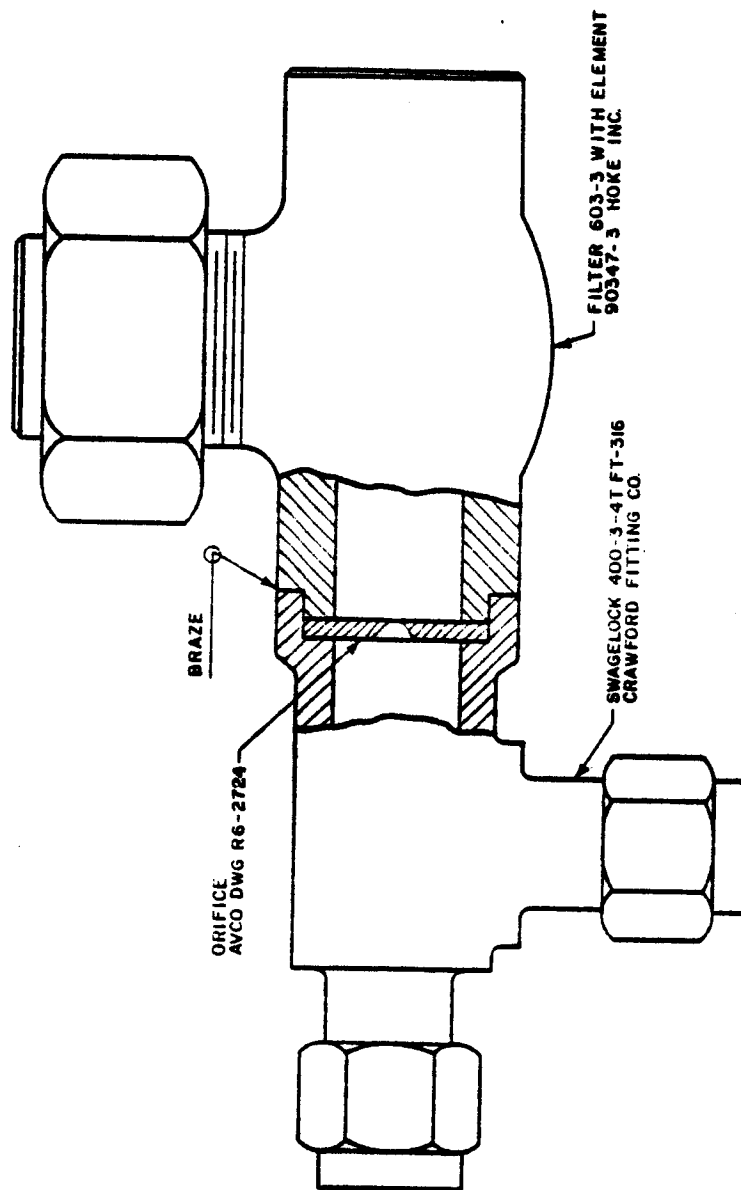
Figure 93 SCHEMATIC DIAGRAM OF FILTER FLOW-METER ASSEMBLY

65—6890

-159-

1. Telemetry Command Channels

Eight telemetry command on-off channels will be used for the signal axis resistojet attitude control system test. When a command channel on-off switch is turned on at the telemetry transmitter console (located outside the tank) a signal is transmitted to the test bed telemetry receiver. The test bed receiver passes this signal to the signal conditioner test package to which it is connected. The test bed receiver delivers 24-volt on-off command signals to the signal test package.

The functions of the eight individual on-off command channels are indicated in Table XVI.

TABLE XVI

COMMAND CONTROL CHANNELS FOR THE RESISTOJET SINGLE AXIS TEST

Command Channel 1	(4)*	Table Power On
Command Channel 2	(5)	Table Power Off
Command Channel 3	(1)	Table Clockwise Slew
Command Channel 4	(2)	Table Counterclockwise Slew
Command Channel 5	(7)	Station Keeping Thrustor On
Command Channel 6	(8)	Station Keeping Thrustor Off
Command Channel 7	(6)	Close Three Propellant Valves
Command Channel 8	(3)	Table on Automatic Control

*Actual pin numbers in plug number 206
J-1DD50S are indicated in parentheses.

The clockwise slew (channel 3), counterclockwise slew (channel 4), the close three propellant valves (channel 7) and table on automatic control (channel 8) are interconnected and operate in the following fashion:

-160-

The clockwise (channel 3) and counterclockwise (channel 4) slew commands remove the optical sensor and preamp from the control logic circuit and replace the preamplifier output with a 1.5-volt or a -1.5-volt signal depending on the desired direction of rotation.

The automatic control command (channel 8) connects the optical sensor and preamp to the logic circuitry and applies power to the valve solenoid and resistojet heater control portion of the control logic circuit. The table power on-off commands (channels 1 and 2) operate a latching relay which controls all table power.

The station keeping thrustor on-off commands (channels 5 and 6) operate a latching relay which provides a voltage sufficient to start the stop the thrustor operation.

2. Telemetry Data Transmission Channels

The on-board telemetry transmitter provides nine continuous telemetry channels. The input to one of the continuous channels is a 43-channel commutator manufactured by Fifth Dimension, Inc. and supplied by NASA Lewis. The commutator sends a signal from each of its 43 input channels every 1/2 second; thus, the commutator permits sampling of each of the input signals at 1/2-second intervals.

During the initial resistojet single-axis attitude control system, test use was made of seven continuous channels and 13 intermittent on commutated channels. The signals passing into the commutated channels, as indicated above, will be sampled every 1/2 second.

A basic instrumentation diagram has been shown in Figure 89, and a list of the telemetry data transmission channels is presented in Table XVI.

As indicated in Table XVII, all the signals received at the laboratory telemetry receiver are recorded on tape (T). Some of the signals can also be immediately read out on a panel meter (M), or on a pen recorder (R) for possible diagnostics during a test.

The seven continuous (C) channels are used to measure the following quantities: 1 - the sensor preamplifier output indicating the test bed position (fine control); 2 - the control logic output indicating the test bed total error; 3, 4 - the valve actuation signals for the attitude control engines; 5, 6 - the nozzle box pressure for the attitude control engines.

TABLE XVII

TELEMETRY DATA CHANNEL LIST FOR MODEL I RESISTOJET ACS

Channel No.	Commutated Channel No.	Channel Identification	Description	Channel	Range	Telemetry Output	Instrumentation
1		V_1	Sensor Preamplifier Output (Fine)	C	$\pm 0.5°$	-2.5V-+2.5V	T, R
2		V_3	Total Error Signal	C	0-.05/sec	0-5V	T, R
3		V_4	Valve Actuation Signal (Clockwise Rotation)	C	28 VDC	.	T
4		V_5	Valve Actuation Signal (C-Clockwise Rotation)	C	28 VDC	0-5V	T
5		P_3	Nozzle Box Pressure (Clockwise Rotation)	C	0-50 psi	0-5V	T, R
6		P_4	Nozzle Box Pressure (C-Clockwise Rotation)	C	0-50 psi	0-5V	T, R
7		DP_1	ACS Differential Pressure (Flow)	C	0-1 psi	0-5V	T, M
9	38	P_1	Ammonia Tank Pressure	I	0-250 psi	0-5V	T, M
10	39	P_2	Plenum Pressure	I	0-50 psi	0-5V	T, M
11	33	T_1	Plenum Temperature	I	0-100° F	0-5V	T, M
13	34	T_2	Ammonia Line Temperature at DP_1	I	0-100° F	0-5V	T, R
16	40	P_5	Nozzle Box Pressure (Station Keeping)	I	0-50 psi	0-5V	T, M
17	41	RT_1	Resistojet Temperature (Clockwise Rotation)	I	1000-1700K	0-5V	T, M
18	42	RT_2	Resistojet Temperature (C-Clockwise Rotation)	I	1000-1700K	0-5V	T, M
19	31	RT_3	Resistojet Temperature (Station Keeping)	I	1000-1700K	0-5V	T
20	4	V_2	Sensor Preamplifier Output (Coarse)	I	$\pm 5°$	-2.5V to +2.5V	T, R
21	8	V_6	Valve Actuation Signal (Station Keeping)	I	28 VDC	0-5V	T
22	7	V_7	Resistojet Heater Voltage CW	I	2 VDC	0-5V	T, M
23	6	V_8	Resistojet Heater Voltage CCW	I	2 VDC	0-5V	T, M
24	5	V_9	Resistojet Heater Voltage Station Keeping	I	2 VDC	0-5V	T

The 13 intermittent channels are used to measure the following quantities:
9 - ammonia liquid reservoir pressure; 10, 11 - ammonia gas plenum
pressure and temperature; ammonia line temperature 16 - nozzle box
pressure for the station keeping thrustor; 17, 18, 19 - heater temperature
for the resistojet engines; 20 - the sensor preamplifier output indicating
the test bed position (coarse control); 21 - valve actuation signal for the
station keeping thrustor; 22, 23, 24 - heater voltages for the three resisto-
jet engines.

Signal conditioning circuitry is provided to convert the transducer, position
sensor and rate sensor signals into voltage signals in the 0- to 5-volt range
suitable for transmission by the test bed telemetry package. Five voltage
dividers are used to provide the 0- to 5-volt actuation signals from the
three solenoid valves and the coarse (1) and the fine (1) position sensors.
Three alternating-current amplifiers are provided to amplify the heater
voltage signals, and finally 12 direct-current amplifiers are provided to
amplify the engine pressure transducer signals (3), the engine temperature
sensor signals (3), the engine line temperature sensor signals (1), the
engine flow rate sensor signals (1), the ammonia liquid storage pressure
sensor (1), the ammonia gas pressure and temperature sensors (2), and
the total table error signal (1).

A photograph of the signal conditioner test package is shown in Figure 94.

3. Checkout Console

A check-out console has been designed and built to provide a means for
determining whether or not the control logic and instrumentation electronic
circuitry is functioning properly before the attitude control system is placed
on the air bearing in the test tank.

F. EVALUATION OF THE MODEL I SINGLE-AXIS RESISTOJET ACS

1. Chronological Summary of System Tests

The Resistojet System - Model I was delivered to NASA Lewis on 4 March
1965. The system electrical checkouts were carried out on 17 and 18
March 1965. A summary of the four single-axis resistojet ACS tests
completed during March and April 1965 is shown in Table XVIII. In all of
the tests described in Table XVIII the resistojet ACS held the position
of the test bed to ± 0.5 degree for extended periods of time, and with
reasonable propellant consumption.

CABLE SUPPLYING POWER TO
STATION KEEPING RESISTOJET

TRANSDUCER SIGNAL
CONDITIONING CIRCUITS

AMPLIFIERS FOR
TRANSDUCER OUTPUTS

Avco/Rad
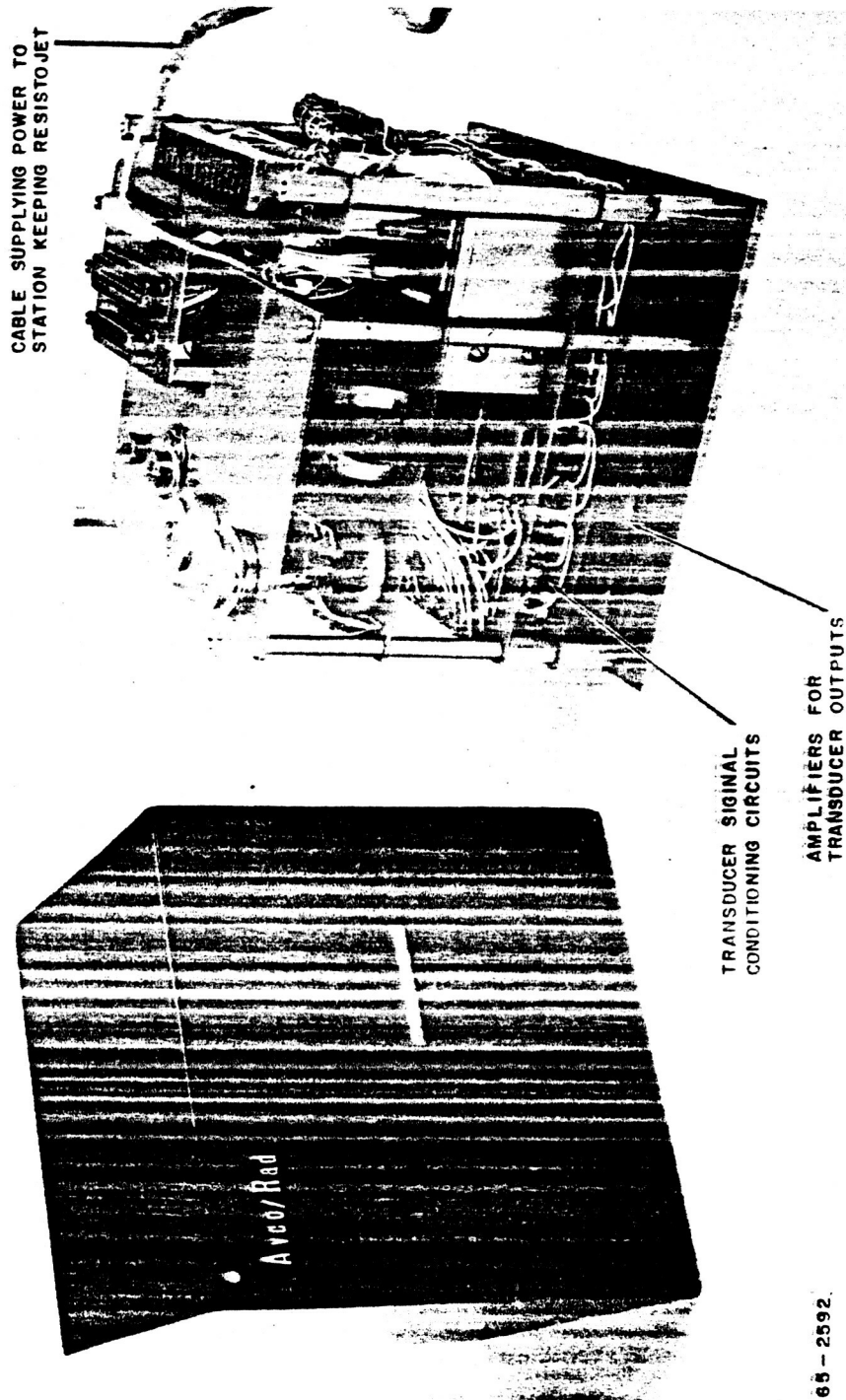
65-2592.

Figure 94 PHOTOGRAPH OF THE SIGNAL CONDITIONED TEST PACKAGE

TABLE XVIII

SUMMARY OF SINGLE-AXIS RESISTOJET ACS
TESTS AT NASA, LEWIS (MARCH-APRIL, 1965)

Run No.	Date	Comment
1	March 25-26	(i) System Controlled (ii) RF Interference (iii) Valve Chatter
2	April 1-2	(i) System Controlled (ii) Valve Chatter (Inner and Outer Lines)
3	April 12-13	(i) System Controlled (ii) Valve Chatter (Inner and Outer Lines)
4	April 22	(i) System Controlled (ii) Valve Chatter (Outer Lines)

2. Sensor Calibration

Figures 95 through 98 present the sensor calibration curves. Figure 95 shows vehicle position, θ, versus output signal voltage; Figures 96 and 97 show nozzle box pressure versus output signal voltage for, respectively, the clockwise and counterclockwise thrustors; finally, Figure 98 shows pressure-normalized orifice mass flow rate versus output signal voltage.

Typical outputs from the continuous telemetry channels are shown in Figures 99 through 102. Results are presented illustrating the acquisition mode (Figure 99) and both hard (Figure 100) and soft (Figure 101 and Figure 102) cycle operation. Data are presented for seven continuous telemetry channels. Channel 1 presents vehicle position $\theta(t)$, and Channel 2 shows vehicle total error, $z(t) = \theta(t) + (\dot\theta(t) + \ddot\theta(t))$. Channels 3 and 5 show nozzle box pressure, respectively, for the counterclockwise (CCW) and clockwise (CW) thrustors, while Channels 4 and 6 show the nozzle valve actuation signals. Finally, Channel 7 is the pressure drop across the differential orifice.

3. Thrustor Performance Characteristics

The thrustor design has been shown in Figure 10; the heater element-nozzle combination is removable and can be replaced by other heaters.
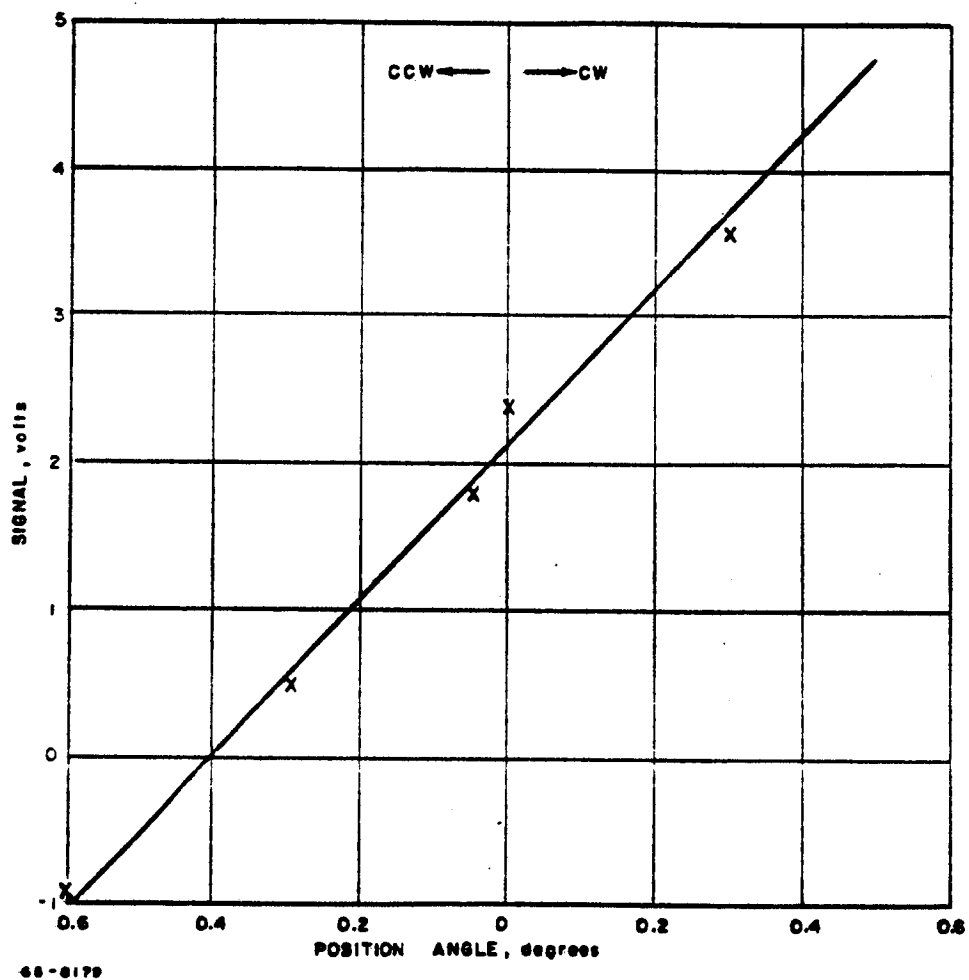
Figure 95 VEHICLE POSITION VERSUS OUTPUT SIGNAL VOLTAGE
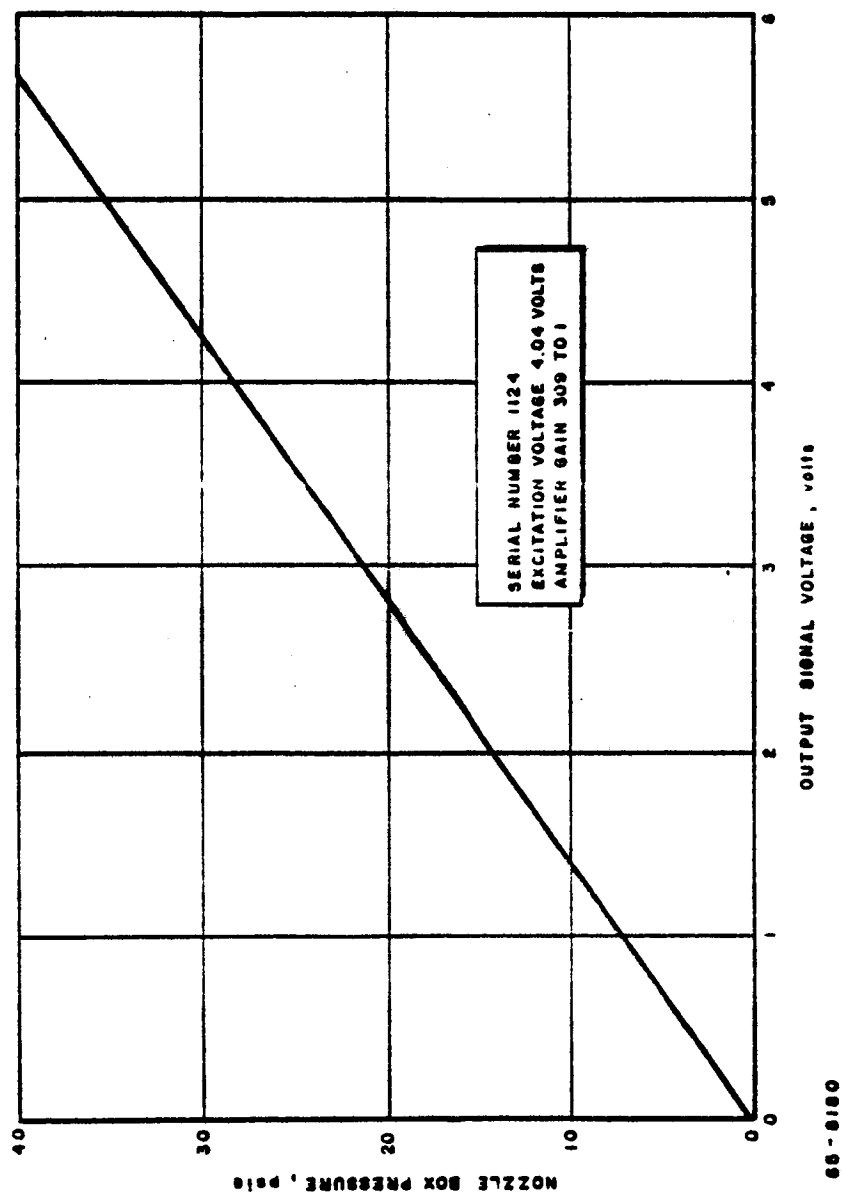
Figure 96 NOZZLE BOX PRESSURE (CLOCKWISE) VERSUS OUTPUT SIGNAL VOLTAGE

SERIAL NUMBER 1125
EXCITATION VOLTAGE 4.04 VOLTS
AMPLIFIER GAIN 309 TO 1

68-8181
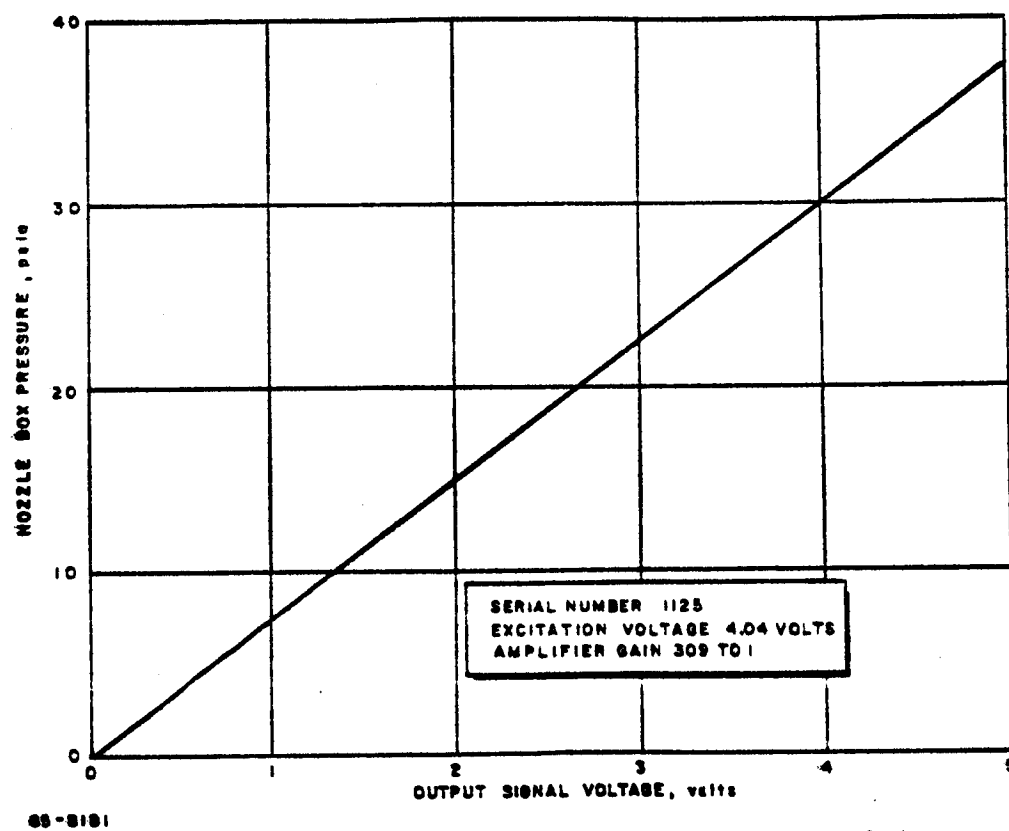
Figure 97 NOZZLE BOX PRESSURE (COUNTERCLOCKWISE) VERSUS OUTPUT SIGNAL VOLTAGE
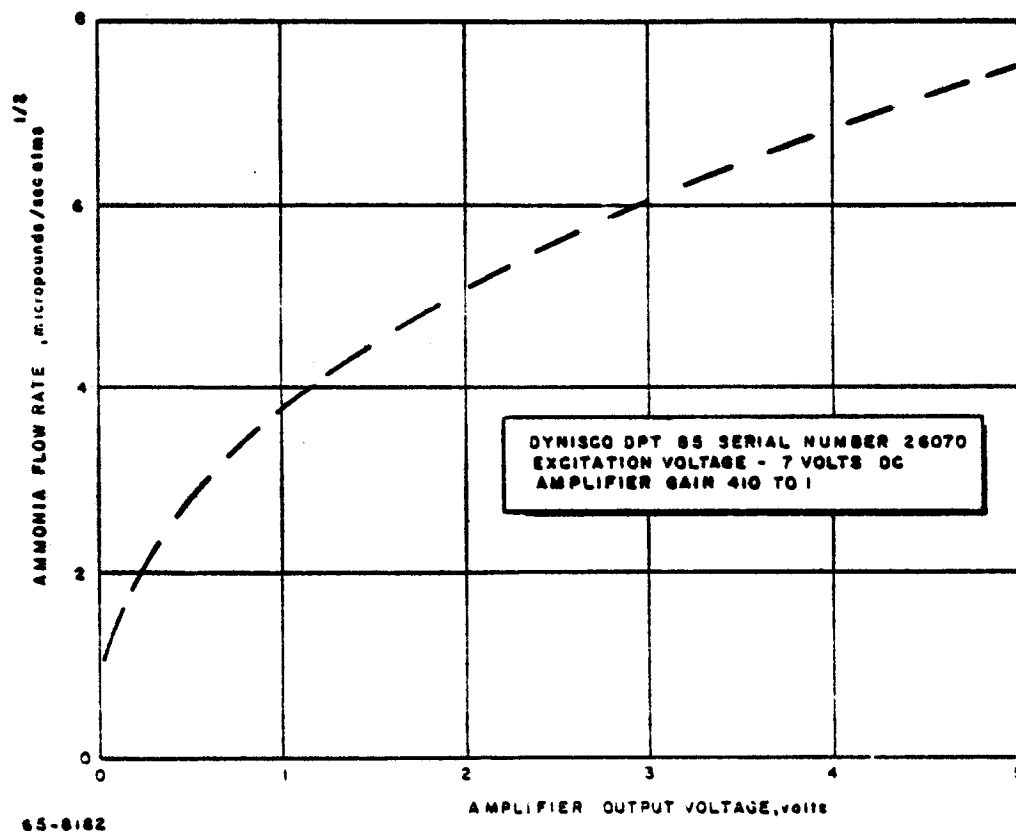
Figure 98 PRESSURE NORMALIZED ORIFICE MASS FLOW RATE VERSUS OUTPUT SIGNAL VOLTAGE
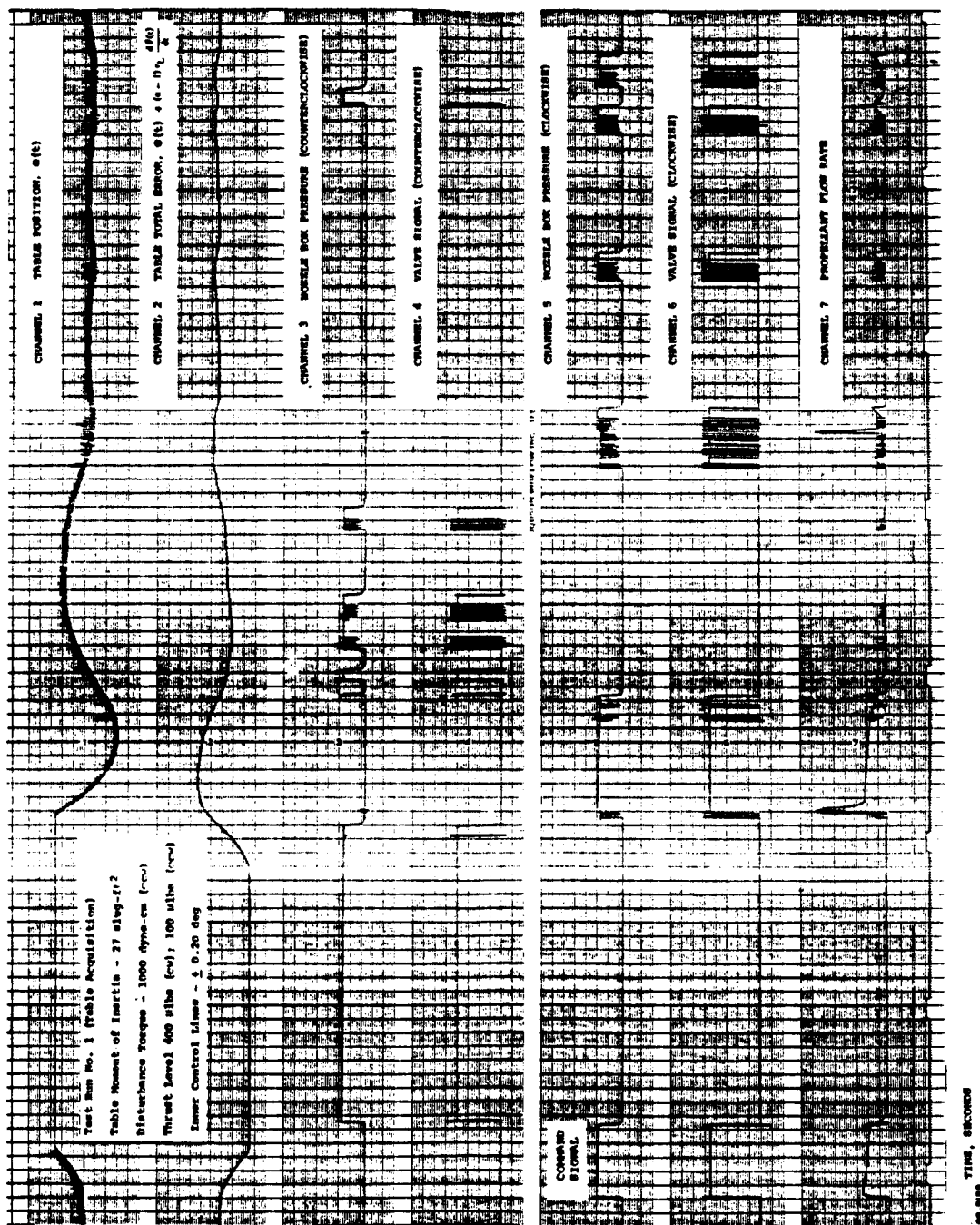
Figure 99 OPERATION OF THE SINGLE-AXIS RESISTOJET ACS IN THE ACQUISITION MODE
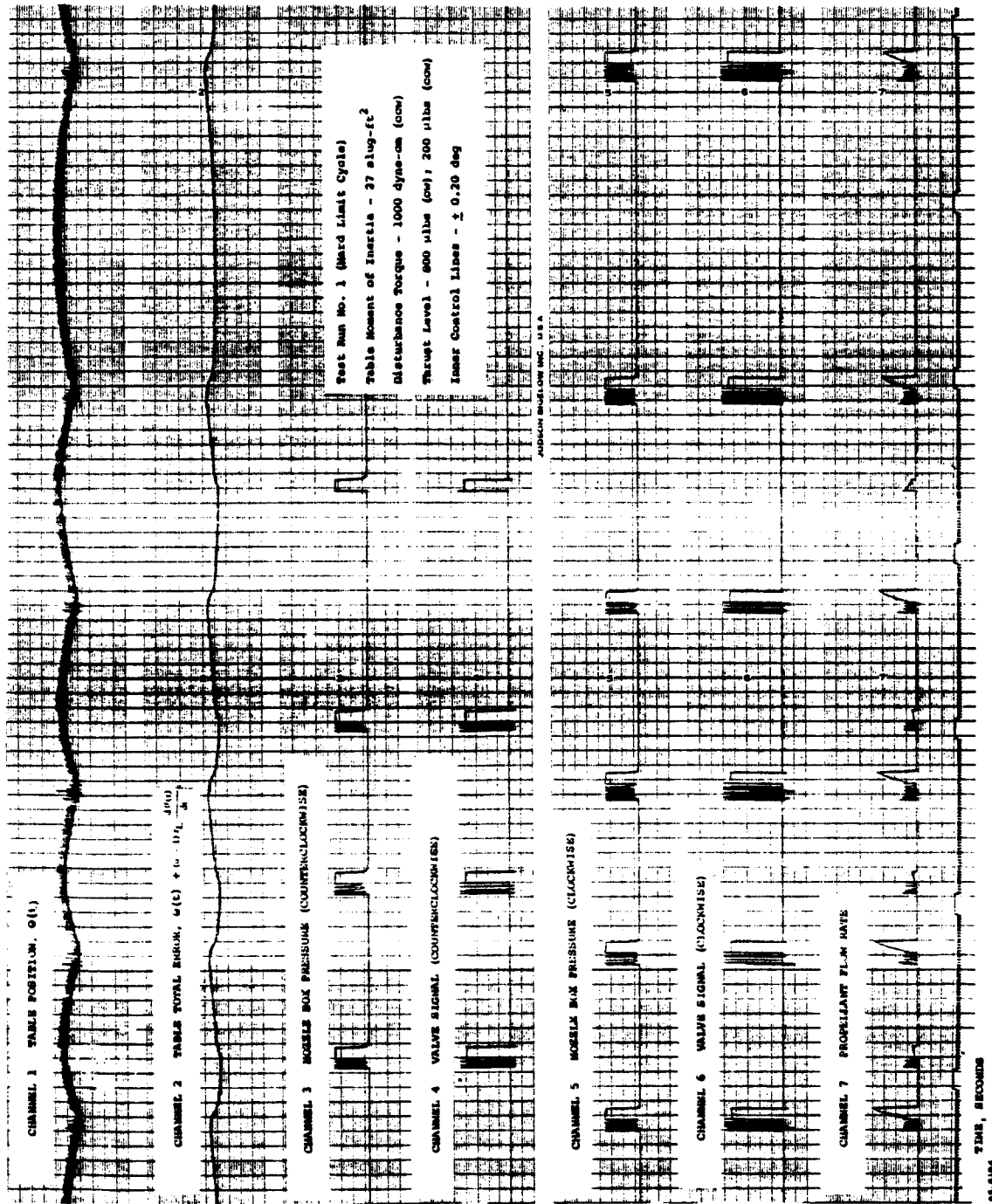
Figure 100 OPERATION OF THE SINGLE-AXIS RESISTOJET ACS IN A HARD LIMIT CYCLE
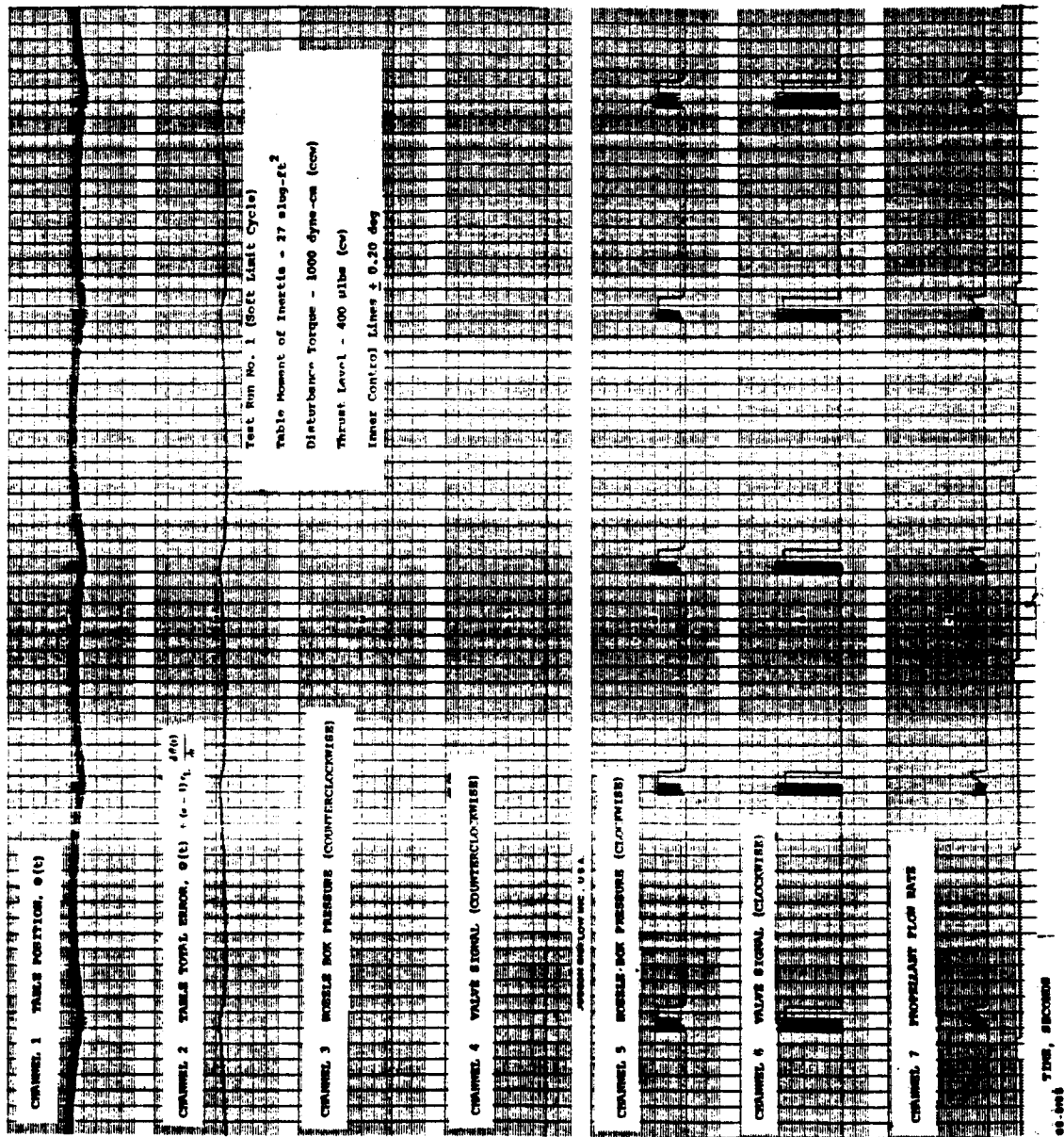
Figure 101 OPERATION OF THE SINGLE-AXIS RESISTOJET ACS IN A SOFT
LIMIT CYCLE, T_D 1000 DYNE-CM (CCW)

-172-
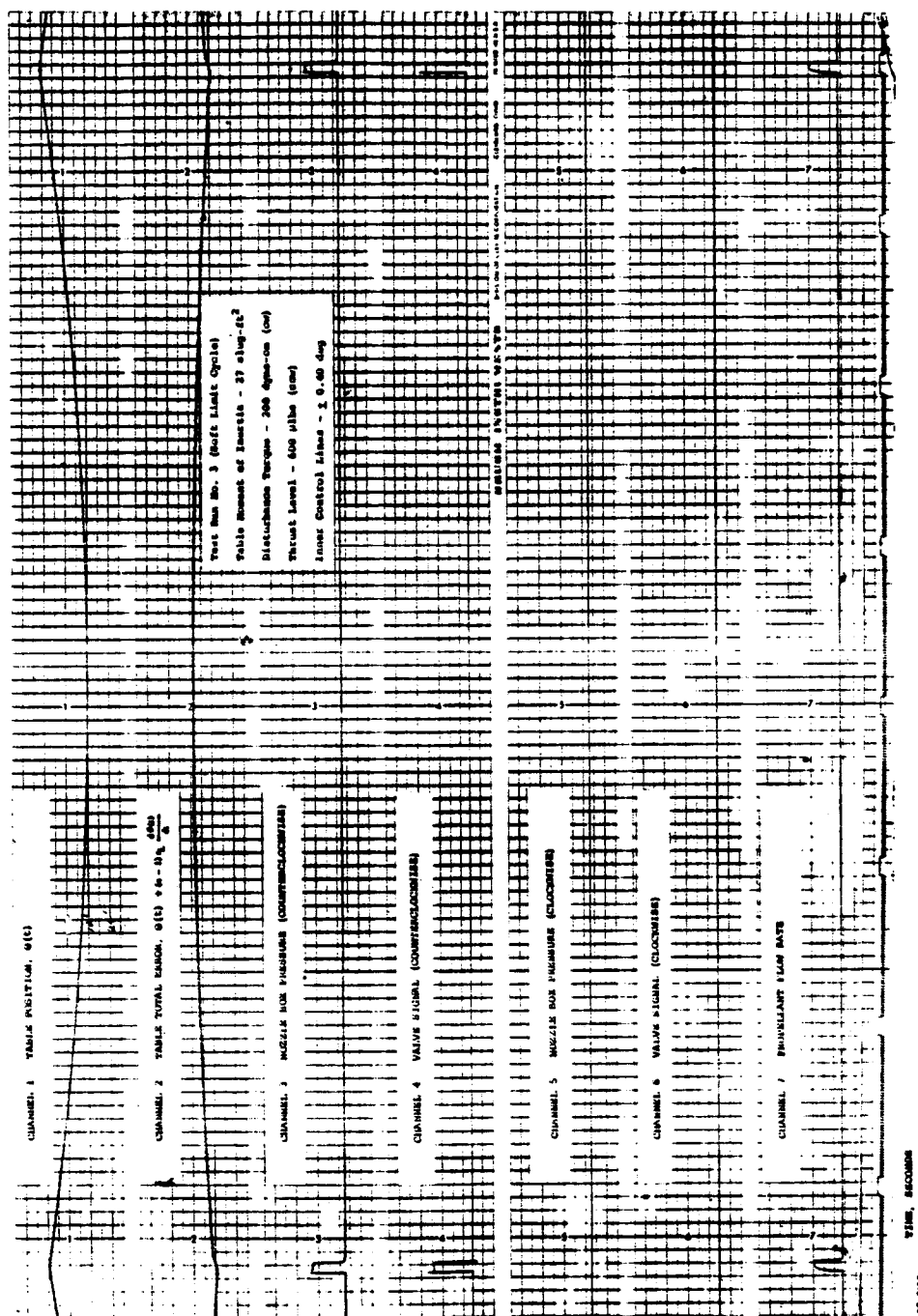
Figure 102 OPERATION OF THE SINGLE-AXIS RESISTOJET ACS IN A SOFT
LIMIT CYCLE, T_D 200 DYNE-CM (CW)

Table XIX shows the nominal characteristics of the heater element-nozzle combinations used in the NASA Lewis tests. It is stressed that it is a simple matter to interchange the heater-nozzle elements.

TABLE XIX

SUMMARY OF PERFORMANCE CHARACTERISTICS OF HEATER-NOZZLE ELEMENTS USED IN INITIAL RESISTOJET ACS TESTS AT NASA-LEWIS

Engine Description		
Designation	6-A	7-A
Table Motion	Clockwise	Counter-Clockwise
Heater Element Length, inches	1.25	1.25
Heater Element, OD inches	0.022	0.024
Heater Element, ID inches	0.013	0.013
Nozzle Throat Diameter, inches	0.006	0.006
Heater Material	Molybdenum	Molybdenum
Heater Resistance (Cold), ohms	0.036	0.028
Nominal Performance		
Chamber Pressure, psia	14	14
Thrust Level, μ lbs	360	300
Cold Flow, μ lbs/sec	4.3	3.6
Power Input, watts	10	10
Heater Resistance (Hot), ohms	0.11	0.12
Heater Current, amperes	9.5	9.1
Heater Voltage, volts	1.05	1.1
Hot Flow Rate, μ lbs/sec	2.4	2.0
Cold Specific Impulse, sec	84	84
Hot Specific Impulse, sec	150	150

4. Calibration of the Air Bearing

The disturbance torque, τ_D', on the air bearing can be varied both in magnitude and direction by changing the bearing pressure and bearing angular position. The input disturbance torque, τ_D', can be estimated from observations on changes in the table angular rate, $\Delta\dot{\theta}_D$, during a fixed time period, Δt_D when no other disturbances are acting on the table. The disturbance torque is given by

$$\tau_D' = J\, \Delta\dot{\theta}_D / \Delta t_D \tag{63}$$

-174-

where , τ_D (lb-ft or 1 lb-ft = 1.36 x 10^7 dyne-cm), is the disturbance torque, J (lb-ft-sec^2) is the table moment of inertia, $\Delta\dot{\theta}_D$ (rad/sec) is the change in vehicle angular rate over the time period, Δt_D (seconds).

Referring to Figure 101 the change in vehicle rate, $\Delta\dot{\theta}$, between pulses is about 1.8 x 10^{-4} rad/sec, the time, Δt_D, over which the rate change occurs is about 65 sec, and the table inertia is 27 lb-ft/sec^2, the disturbance torque for this test condition, i.e., air bearing pressure of 45 psia, is thus about 75 x 10^{-6} lb-ft or about 1000 dyne-cm.

The control torque is given by

$$\tau_c = J \; \Delta\dot{\theta}_c / \Delta t_c \tag{64}$$

where τ_c (lb-ft) is the control torque, and $\Delta\dot{\theta}_c$ is the change in vehicle angular rate over the period, Δt_c, that the control torque is applied.

The control thrust is given by

$$T_c = \tau_c / l \tag{65}$$

where l (ft) is the thrustor moment arm.

For soft cycle operation the control torque is given by

$$\tau_c / \tau_D = \Delta t_D / \Delta t_c \tag{66}$$

or

$$\tau_c = \tau_D \; \Delta t_D / \Delta t_c \tag{67}$$

5. <u>Criteria for Soft and Hard Limit-Cycle Operation</u>

For a fixed disturbance torque soft cycle operation is always obtained if the control impulse bit is less than a value given by

$$T_c \Delta t_c)_{soft} \leq 2 \sqrt{\tau_D \, \theta_c \; J / l} \tag{68}$$

where, θ_c (radians) is the control angle and the other quantities have been described previously. For example, at an input disturbance torque, τ_D, of 1000 dyne-cm, a vehicle moment of inertia, J, of 27-lb-ft-sec^2, a moment arm, l, of 2 feet, and a control angle, θ_c, of 0.20 degree (or 3.5 x 10^{-3} radian), the control impulse bit, $T_c \Delta t_c)_{soft}$, must be less than 2.64 x 10^{-3} lb-sec; for a 4 second pulse, (Δt_c = 4 seconds), the thrust level for soft cycle operation must be less than 0.66 x 10^{-3} lb (660 micropounds).

For a fixed disturbance torque hard cycle operation is always obtained if the control impulse bit is greater than a value given by

$$T_c \Delta t_c)_{hard} \geq 4 \sqrt{\tau_D \theta_c J/l}$$ (69)

For the conditions cited in the previous example of the control impulse bit must be greater than 5.28×10^{-3} lb-sec for hard cycle operation, and for a 4-second pulse the thrust level for hard cycle operation must be greater than 1.32×10^{-3} lb.

It follows from equation (69) that for a fixed impulse bit, $T_c \Delta t_c$, soft cycle operation is obtained for disturbance torques greater than a value given by

$$\tau_D)_{soft} \geq T_c \Delta t_c)^2 \ l^2/4\theta_c J$$ (70)

Hard cycle operation is obtained for disturbance torques less than a value given by

$$\tau_D)_{hard} \leq T_c \Delta t_c)^2 \ l^2/16\theta_c J$$ (71)

To illustrate, for a thrust level, T_c, of 300 micropounds, an impulse bit length, Δt_c, of 4 seconds, a vehicle moment of inertia of 27 lb-sec^{2}ft, moment arm, l, of 2 feet, and a control angle of 0.2 degree, soft cycle operation will occur at disturbance torques greater than 200 dyne-cm; and hard cycle operation at disturbance torques less than 50 dyne-cm. Either soft, hard, or a combination of soft and hard limit cycles can occur between these two limiting torque values. Analog computer solutions for this situation are presented in Appendix E.

6. Table Acquisition

Figure 99 shows a portion of the sensor traces obtained during Test Run No. 1*.

An external 25-second clockwise slew command, indicated by the voltage signals on channels 5, 6, and 7 was transmitted to the table. The clockwise thrustor was operating at a nozzle box pressure (channel 5) of about 15.5 psia, and a nominal thrust level of about 400 micropounds. Following the clockwise slew command the table was put on automatic control.

---

*The noise on the position trace, i.e., channel 1, was associated with an rf interference problem and was eliminated in later runs. The valve chatter problem, after considerable investigation, has been clearly identified with test tank vibration, which, in turn results in light source vibration. Some success, e.g., Figure 101 has been obtained in reducing valve chatter by strengthening the light source mount and decreasing control circuit sensitivity; however, the problem is not yet completely resolved.

As indicated in the trace of table position (channel 1) the table initially moved in the clockwise direction until it saturated the position sensor. The sensor saturates at about ± 1.5 degrees; however, the system will still acquire out to about ± 8 degrees. After the table control system was placed on "automatic control" the counterclockwise thrustor was activated and the table was decelerated in the counterclockwise direction.*

Following activation of both the clockwise and counterclockwise thrustors the system passed into a soft limit cycle. In this soft cycle the counterclockwise disturbance torque of about 1000 dyne-cm (or 0.735×10^{-4} lb-ft) was counterbalanced by the control torque of 8×10^{-4} lb-ft (400 micropounds thrust at a 2-foot moment arm). The control impulse bit time, Δt_c, was 4 seconds, compared to the cycle time, Δt_D of about 50 seconds. The estimated duty cycle, i.e., τ_D/τ_c, is equal to about 0.09 compared to a measured duty cycle, i.e., $\Delta t_c/\Delta t_D$, equal to about 0.08.

7. Hard Limit-Cycle Operation

Figure 100 shows a typical series of sensor traces obtained during Test Run No. 1 and is illustrative of hard limit cycle operation. The nozzle box pressure was 32.5 psia and the corresponding thrust level was 800 micropounds. The table counterclockwise disturbance torque, τ_D, was estimated to be about 1000 dyne-cm. The engine thrust level was thus sufficient to result in hard limit-cycle operation.

At the beginning of the control cycle the table was moving in a counterclockwise direction. As the table traveled passed the 0.20-degree inner control line the clockwise thrustor was activated and the direction of the table was reversed. The clockwise thrustor moved the table to the opposite control line, the counterclockwise thrustor was activated and the cycle was repeated.

As indicated previously the counterclockwise thrustor for Test Run No. 1 was clogged and in this case at a chamber pressure of 32.5 psia the thrust level was reduced to about 200 micropounds from its nominal value of 800 micropounds (at 32.5 psia). Nevertheless, as shown in Figure 100, the system still controlled.

8. Soft Limit-Cycle Operation

Figure 101 shows typical soft limit-cycle obtained during Test Run No. 1. The nozzle box pressure has been reduced to about 15 psia and the resulting engine thrust is about 400 micropounds. At the 1000-dyne-cm

---

*Due to line blockage the counterclockwise thrustor produced only about 100 micropounds or about 25 percent of its full thrust capability. As a result the clockwise thrust time, Δt_c, necessary to reacquire the table was considerably longer than the original command disturbance pulse.

counterclockwise disturbance torque level characteristic of Test Run No.
1 this thrust level is low enough to assure soft limit-cycle operation.
Referring to Figure 102 the clockwise control thrust is just sufficient to
overcome the counterclockwise disturbance torque.

Figure 102 shows a typical soft limit cycle obtained during Test Run No.
3. To eliminate valve chatter the sensitivity of the control logic system
was decreased by moving the control lines out to ± 0.4 degree and the
outer lines were moved out to ± 0.6 degree; further, the light source vibra-
tions were reduced by strengthening the optical source mount. As indi-
cated in Figure 102, these changes reduced the valve chatter problem.
During this portion of the test run the bearing pressure was at about 34
psia and the disturbance torque level was about 200 dyne-cm in the clock-
wise direction. It is noted that the disturbance torque level is quite sensi-
tive to bearing pressure. During Test Run No. 1, the bearing pressure
was about 45 psia and the disturbance torque level was about 1000 dyne-
cm in the counterclockwise direction.

Other examples of hard and soft limit-cycle operation for the single-
axis resistojet ACS, obtained on the Impulse Table are presented in
Appendix F.

G. MODEL II SINGLE-AXIS RESISTOJET ACS

As indicated, the primary objective underlying the initial single-axis resisto-
jet attitude control system test has been to demonstrate the feasibility of apply-
ing the resistojet concept to the attitude control and station keeping of satel-
lites. During the course of development, construction, and operation of the
Model I ACS a number of modifications which would make the Model I more
suitable for test purposes apparent. The changes which have been incorporated
into the Model II Resistojet ACS are indicated below:

1. The heater power supply has been modified to permit variation of the
    input power to the individual ACS engines over the range from 5 to 35
    watts. The engine input power in the Model I ACS was uniquely fixed by
    the lead resistance and for a hot engine resistance of about 0.10 ohm was
    about 5 watts. (See Reference 1, Table IX). The power supply has been
    further modified to permit one power level during the warmup period, and
    another during actual gas ejection. The heater warmup and operational
    power levels are varied by two separate potentiometers with screwdriver
    adjustment slots.

2. The control logic circuit has been adjusted so that the heater warmup
    time defined as the time period between power-on time and propellant on-
    time) can be varied from 1 to 10 seconds in 1-second increments. The
    heatup time pulse is adjusted by a 10-position selector switch.

3. The control logic circuit has been further adjusted so that the fixed inner pulse width can be varied from 1 to 10 seconds in 1-second increments. The inner pulse width is adjusted by means of a 10-position selector switch. The length of the heatup time and the inner pulse width can be varied independently of each other and offer 100 different combinations of heatup time and inner pulse width.

4. The hysteresis of the Schmitt triggers will be preset at 40 percent.

5. A manually adjustable pressure regulator will be placed on the gas reservoir tank so that the engine pressure can be varied over the range from 1 to 30 psia. This will make it possible to obtain over an order of magnitude range in resistojet thrust level.

6. Provision has been made to measure the time rms voltage and rms current across the clockwise and counterclockwise thrustors. This will permit a direct estimate of the "true" power into the individual engines; this measurement is not possible with the Model I system. To review briefly, the power conditioning equipment inverts the battery supply dc power into 10,000 Hz alternating current; the high frequency results in a high efficiency and reduced output transformer size. Since the engine is supplied with high frequency ac power it is necessary to measure the rms voltage and current. The dc voltage and direct current into the power conditioner will also be measured which will permit determination of the overall efficiency of the power conditioner.

7. The light sensor electronics will be modified to permit acquisition and a linear sensor output for angles up to ± 8 degrees.

8. The commutator channel assignments have been changed and are summarized in Table XX. All unused channels have been made available through an additional connector mounted on top of the signal-conditioning package. The outputs from the signal-conditioning amplifiers have been wired to test points mounted on the top of the unit.

The Model II resistojet ACS provides a flexible tool for characterizing the performance of low-power resistojet systems over a wide range of operating conditions.

TABLE XX

TELEMETRY DATA CHANNEL LIST (COMMUTATOR CHANNELS) FOR
MODEL II RESISTOJET ACS

Channel Number	Model I	Model II
1	Calibrated Voltage	Calibrated Voltage
2	Calibrated Voltage	Calibrated Voltage
3	Calibrated Voltage	Calibrated Voltage
4	Position Sensor Coarse	Position Sensor Coarse
5	Station Heater Monitor	Station Heater Monitor
6	CCW Heater Monitor	CCW Heater RMS Voltage
7	CW Heater Monitor	CW Heater RMS Voltage
8	Station Valve Voltage	Station Valve Voltage
9	Not Used	CCW Heater RMS Current
10	Not Used	CW Heater RMS Current
11	Not Used	Spare Connector No. 1
12	Not Used	Spare Connector No. 2
13	Not Used	Spare Connector No. 3
14	Not Used	Spare Connector No. 4
15	Not Used	Spare Connector No. 5
16	NASA Telemetry Channels	NASA Telemetry Channels
17	NASA Telemetry Channels	NASA Telemetry Channels
18	NASA Telemetry Channels	NASA Telemetry Channels

TABLE XX (Cont'd)

Channel Number	Model I	Model II
19	NASA Telemetry Channels	NASA Telemetry Channels
20	NASA Telemetry Channels	NASA Telemetry Channels
21	NASA Telemetry Channels	NASA Telemetry Channels
22	NASA Telemetry Channels	NASA Telemetry Channels
23	NASA Telemetry Channels	NASA Telemetry Channels
24	NASA Telemetry Channels	NASA Telemetry Channels
25	NASA Telemetry Channels	NASA Telemetry Channels
26	NASA Telemetry Channels	NASA Telemetry Channels
27	NASA Telemetry Channels	NASA Telemetry Channels
28	NASA Telemetry Channels	NASA Telemetry Channels
29	Not Used	Spare Connector No. 6
30	Not Used	Spare Connector No. 7
31	Station Jet Temperature	Station Jet Temperature
32	Not Used	Spare Connector No. 8
33	Plenum Tank Temperature	Plenum Tank Temperature
34	Station Line Temperature	Station Line Temperature
35	Not Used	Spare Connector No. 9
36	Not Used	Spare Connector No. 10
37	Not Used	Spare Connector No. 11
38	Ammonia Tank Pressure	Ammonia Tank Pressure
39	Plenum Tank Pressure	Plenum Tank Pressure

TABLE XX (Concl'd)

Channel Number	Model I	Model II
40	Station Nozzle Pressure	Station Nozzle Pressure
41	CW Jet Temperature	CW Jet Temperature
42	CCW Jet Temperature	CCW Jet Temperature
43	Not Used	Spare Connector No. 12

H. OVERALL OBJECTIVES AND FUTURE DIRECTION OF THE SINGLE-AXIS ATTITUDE CONTROL SYSTEM EVALUATION TESTS

The objectives of the single-axis attitude control system tests include:

1. Verification of the compatibility of all the ACS components including the propulsion subsystem, power conditioner, control logic package, sensors, signal conditioner, and telemetry system.

2. Demonstration of the performance of the ACS in the acquisition control mode, and in soft and hard limit control cycles. (The three-axis air bearing and the single-axis impulse table make it possible to observe ACS operation as a function of disturbance torque, r_D , acquisition angle, θ_i , and initial rate of angular acquisition, $\dot{\theta}_i$.)

3. Confirmation of the validity of the analog computer solutions pertinent to the performance of the ACS control logic system. (See Appendix E.)

4. Comparison of the performance, i.e., total impulse, fuel consumption and reliability, of different types of attitude control systems as a function of disturbance torque, acquisition angle, and angular acquisition rate.

5. Establishment of a technological base for the development of three-axis attitude control systems.

The future direction for the single axis tests includes the following:

a. Performance data, including total impulse requirements, and fuel consumption, will be obtained for the single axis resistojet attitude control system as a function of heater input power from 0 to 35 watts, and for different propellants. In this manner it will be possible to make a quantitative tradeoff between propellant weight and heater power supply weight.

b.   Performance data will be obtained as a function of the resistojet attitude control logic parameters including inner θ_c, and outer θ_c, the slope of the control logic lines, the Schmitt trigger hysteresis, H, and the disturbance torque, τ_D . This data will be compared to similar data obtained from the analog computer. (See Appendix E.) Assuming that the air-bearing test data correlate with the analog computer results, the analog computer can then be used to obtain system performance data over a much wider range of input variables than would be feasibile (due to time and cost considerations) on the single-axis air bearing.

c.   Exploratory studies will be carried out on the feasibility of charging the on-board battery power supply with solar voltaic cells. This would make it possible to perform extended system lifetests, and, further, to checkout the compatibility of the solar cell power supply and battery charging system with the other subsystem components.

IV. THREE-AXIS ATTITUDE CONTROL AND STATION KEEPING SYSTEM

As part of the present program, a study has been carried out on the application of 5- to 50-watt resistojets to the attitude control and station keeping of satellites in the 500- to 1000-pound class. A preliminary development program and system weight breakdown have been prepared and are presented below.

A. PRELIMINARY PROGRAM PLAN FOR THE DEVELOPMENT OF A FLYABLE THREE-AXIS RESISTOJET ACS AND STATION-KEEPING SYSTEM

The six basic subsystems for a flyable three-axis resistojet attitude control and station-keeping system are indicated in Table XXI. The subsystems are, of course, the same as those for the laboratory single-axis systems described in the previous section; however, in this case, the hardware must all eventually be flight-qualified.

TABLE XXI

BASIC SUBSYSTEMS FOR A FLYABLE 3-AXIS ATTITUDE CONTROL AND STATION-KEEPING SYSTEM

Propulsion
Control Logic
Power Supply and Power Conditioning
Sensors
Signal Conditioning
Telemetry

1. The propulsion subsystem consists of the thrusters and propellant storage and feed system. The propulsion performance, i.e., thrust level, specific impulse, and overall electric to thrust power efficiency, of the individual thrustors will be measured on the wire-in-tension thrust stand and the impulse table at pressure levels of less than 10^{-3} torr. Ammonia is a prime contender as a possible resistojet working fluid because of its low storage pressure and resulting low tank weight. Potential

problems of 0-g feed for liquid ammonia systems, the determination of reliable space-qualified techniques for regulation of the ammonia storage pressure (order of 100 psia) to the operating nozzle box pressure (order of 10 psia) and the establishment of valve reliability are under study.

2.   The control logic system will be developed using an existing analog computer. Results obtained from the analog computer for a single-axis system have been presented in Appendix E. Due to uncertainties in the level of applied disturbance torque characteristic of the space environment, adaptive control system will be used to minimize fuel consumption and the total number of valve cycles. Briefly, the adaptive control system will vary the length of the impulse bit to assure soft limit cycle operation independent of the applied disturbance torque. Preliminary studies of a possible adaptive control system suitable for a low thrust ACS are presented in Appendix G.

3.   Referring to Figure 103, the power supply and power conditioning subsystem will consist of a solar cell array, battery charging equipment, battery pack, power conditioning for the: (a) propulsion system (including the resistojet heaters); (b) control logic package; (c) signal conditioner package; (d) sensors; and (e) telemetry package. The low-power, fast heat-up resistojet presents a power-conditioning problem because of the low resistance (~ 0.10 ohm) and voltage requirement (~ 1 volt) of the heater elements. In the present single-axis tests, the battery voltage was inverted to 1 kilocycle alternating current and stepped down from 24 volts to 1 volt using a torroidal transformer. The power supply and power conditioning subsystem will be initially bench-tested before being integrated with the other subsystem components.

4.   Sensors for the three-axis system will be selected either by or in conjunction with NASA Lewis. The sensors will be representative of the present state of the art.

5.   As in the case of the present single-axis system the signal conditioning package will be compatible with NASA Lewis supplied telemetry equipment.

6.   Again, as in the case of the present single-axis tests, the telemetry package will be supplied by NASA Lewis.

7.   All the subsystems will be individually bench-tested. Total system performance will be evaluated on the three-axis air bearing at NASA Lewis. These tests will permit a compatibility checkout of the individual resistojet ACS subsystems. The three-axis system compatibility checkout will be analogous to the work currently being carried out on the single-axis tests, which has been described in the previous section. Further, as indicated previously for the single-axis tests, it may also be possible to include an on-board solar array for battery charging, and thus permit extended life tests.

65-8187
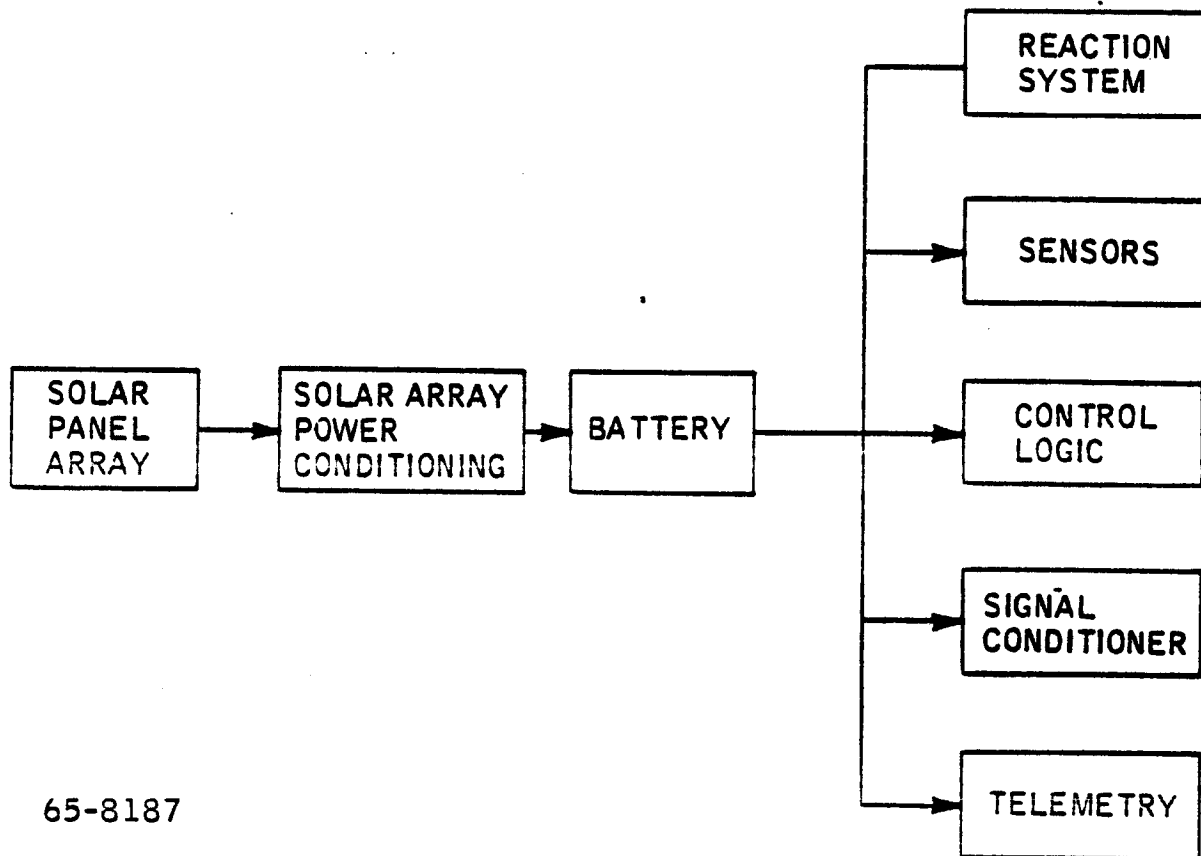
Figure 103 POWER SUPPLY AND POWER CONDITIONING SUBSYSTEM

8. Some subsystems compatibility testing of the type described in Appendix F can also be carried out on the Impulse Table. Finally, Appendix H presents a brief description of the Avco/SSD Astrolab, which is presently being installed, and is designed for evaluation of ACS subsystem compatibility, with particular emphasis on sensor performance.

B. WEIGHT ESTIMATES FOR A FLYABLE ORBIT AND ATTITUDE CONTROL SYSTEM

Preliminary weight estimates of the attitude control and station keeping system for a 500-pound satellite similar to that described in the first quarterly report are presented below.

These estimates are being continually revised and performed for a variety of missions. The present calculations are for a synchronous satellite.

1. Weight of Resistojet Power-Conditioning Equipment

A schematic of the power-conditioning circuit is presented in Figure 104. The electric input power which can originate either from a battery pack or directly from solar panels is inverted from direct current to 1000 Hz alternating current by means of an oscillator and amplifier. The amplifier is, in turn, connected to the primary winding of a transformer, which steps down the amplifier output voltage (order of 1 volt). To avoid line I^2R losses a separate voltage stepdown transformer will be located at each resistojet. The resistojet heater element can thus be directly coupled to the secondary of the transformer with negligible line losses. Table XXII presents estimated values of the weight of 24-volt to 1-volt stepdown transformers for operation at 1000 Hz. These figures are not to be taken as definitive and work is proceeding in this area.

TABLE XXII

ESTIMATED WEIGHTS FOR
THE RESISTOJET VOLTAGE
STEP-DOWN TRANSFORMER

Power Input (watts)	Transformer Weight (pounds)
5	0.20
25	0.50
100	1.00
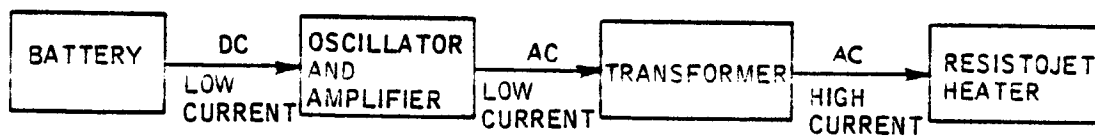
65-8188

Figure 104 SCHEMATIC DIAGRAM OF THE RESISTOJET POWER CONDITIONING CIRCUIT

It is probable that a single amplifier and oscillator can be used for the entire system, although this point must be examined further. Estimated values of the oscillator-amplifier combination are shown in Table XXIII as a function of power level. The weight of the oscillator is, of course, negligible compared with the amplifier. The specific power values (lb/watt) tend to be smaller at the higher power inputs. Again the values presented in Table XXIII are preliminary and still being examined.

TABLE XXIII

ESTIMATED WEIGHT FOR THE
OSCILLATOR AMPLIFIER
PACKAGE

Power Input (watts)	Oscillator-Amplifier Package (pounds)
5	0.40
25	1.25
100	3.00

2. Weight of Resistojet Engine

The weight of the resistojet engine heater, structure, and solenoid valve is 0.04 lbs.

3. Resistojet Engine Performance

For the present exercise the performance of the resistojet will be assumed to be 400-micropound thrust, at 15 watts input power, and 175 seconds specific impulse. The valves require 2 watts of power to operate. The overall efficiency of the power conditioning system, defined as the ratio of transformer power output to amplifier power input will be assumed to be equal to 70 percent. The required power input is then about 25 watts to operate both the engine heater and the valve.

4. Mission Assumptions

The basic mission assumptions are shown in Table XXIV.

TABLE XXIV

BASIC ASSUMPTIONS FOR THE SYNCHRONOUS SATELLITE MISSION

Disturbance Torque	500 dyne-cm
Limit Cycle	Soft
Mission Time	3 years
Attitude Control Impulse Requirements	5265 lb-sec
Station Keeping Impulse Requirements	7920 lb-sec
Total Impulse Requirements	13, 185 lb-sec

5. System Weight Comparison

Assuming that 400-micropound thrust is the maximum which can be tolerated by the spacecraft, Table XXV presents a weight comparison between a cold ammonia system operated at a specific impulse of 65 seconds and a hot system operated at a specific impulse of 175 seconds. The ammonia propellant feed and storage system is assumed to be equal to 0.10 percent of the propellant weight. Each system is assumed to have 12 engines. The specific weight of the solar power supply is assumed to be 0.25 lb/watt.

TABLE XXV

WEIGHT COMPARISON BETWEEN A COLD AND HOT AMMONIA ATTITUDE CONTROL AND STATION-KEEPING SYSTEM, SYNCHRONOUS SATELLITE

Item	Cold	Hot
Engine - Valves (12)	0. 5 lbs	0. 50 lbs
Ammonia Propellant	200. 0	75. 0
Tankage	20. 0	7. 5
Solar Power Supply	0. 8	6. 3
Oscillator-Amplifier	---	1. 3
Step-Down Transformer (12)	---	5. 0
Control Logic Package	1. 5	1. 5
Total System	222. 8	97. 1

Referring to Table XXV, it is noted that the hot engine system offers
nearly a 130-pound weight advantage over the cold system.

V. DIRECTIONS FOR FUTURE RESEARCH AND DEVELOPMENT

A. RESISTOJET THRUSTOR DEVELOPMENT

1. Systematic experimental studies should be continued on the effort of the length and diameter of fast heat-up heaters on the mean heat-transfer coefficient and the efficiency of energy conversion from electric input power to gas power. The experimental study should include measurement of the heat-up time and heater resistance as a function of temperature and geometry.

2. Exploratory and comparative studies should be carried out on other resistojet concepts and on the use of propellants other than ammonia for application to a variety of ACS thrust and duty cycle regimes.

B. SINGLE-AXIS ACS

1. Evaluation of the resistojet ACS Model I and ACS Model II should be continued on either an air-bearing or single-axis table. Performance of the systems should be studied as a function of acquisition angle, $\theta_{initial}$, acquisition rate, $\dot{\theta}_{initial}$, disturbance torque, τ_D, and control system time constants. Direct measurements should be made of the fuel requirements for acquisition and hard and soft limit-cycle operation.

2. Comparison should be made between the control system performance obtained experimentally and the results obtained on an analog computer.

C. DESIGN AND DEVELOPMENT OF A FLYABLE THREE-AXIS PROTOTYPE ACS AND SK SYSTEM

1. Studies should be initiated on the development of flight prototype hardware for the fast heat-up resistojet ACS. Particular emphasis should be be placed on the determination of the current status of control valves and regulators for low pressure (order of 1 atmosphere), low flow rate (order of micropounds per second),ammonia propellant storage and feed systems.

VI. REFERENCES

1. Boucher, R. A., J. Spacecraft and Rockets, 1, 164 (1964).

2. Molitor, J. H., and M. H. Kaplan, J. Spacecraft and Rockets, 1, 557 (1964).

3. Molitor, J. H., J. Spacecraft and Rockets, 1, 170 (1964).

4. Milligan, M. W., AIAA Journal, Vol. 2, No. 6, pg. 1088, (June 1964).

5. Tinling, B. E., Measurement of Steady-State Performance of Water Vapor Jets for Use in Space Vehicle Attitude Control Systems, NASA TN D-1302, NASA Ames, (May, 1962).

6. Tinling, B. E., Personal Communication, NASA Ames, (February 1965).

7. Jonath, A. D., Gasdynamic Problems in Low Pressure Microthrust Engines, AIAA Propulsion Joint Specialist Conference, Colorado Springs, Colo., (14-18 June 1965).

8. Vaeth, James E., "Vapor Jet Control of Space Vehicles," IRE Transactions on Automatic Control, (1962).

9. Gaylord, R. S., and W. H. Keller, "Attitude Control System Using Logically Controlled Pulses." ARS Preprint No. 1921-61.

APPENDIXES

APPENDIX A

THRUST STAND SYSTEM

In order to measure performance of thrustors operating in the millipound thrust range in the pulsed mode, the thrust measurement system depicted in figure 9 has been employed. Basically, the thrust stand consists of a central horizontal ring suspended by four wires in tension from a massive concentric ring. The thrustor and propellant supply are mounted on the central ring, aligned so that the thrust direction is vertical. Application of thrust causes the central ring to move until the vertical component of the wire tension exactly balances the applied thrust. The response time of the thrust stand is related to the natural frequency of vibration of the light central ring, which is in turn controlable through adjustment of the tension in the supporting wires. The displacement of the central ring, which is proportional to the applied thrust, is measured by a linear differential transformer. The massive support ring is suspended on long, fairly soft springs to provide seismic isolation.

To solve the equation of motion for the thrust stand; the thrust stand is simplified to the case of a string of mass per unit length, ρ, under a tension T, stretched between two fixed supports separated by a distance L, and loaded at its center with a mass M. (See figure A1.) A force (thrust) F is instantaneously applied at the center $X = \xi = \frac{L}{2}$ and the ensuing motion, for constant force, is governed by the differential equation:

$$[\rho + M\delta(x - \xi)] \frac{\partial^2 y}{\partial t^2} + f \frac{\partial y}{\partial t} = T \frac{\partial^2 y}{\partial x^2} - \rho g - (Mg + F)\delta(x - \xi) \tag{A1}$$

where the thrust is assumed to be directed in the negative direction (down). The displacement of each point on the string, $y(x, t)$, is fully determined by the boundary and initial conditions, viz:

$$y(0, t) = 0 \qquad\qquad y(L, t) = 0 \tag{A2}$$

$$\frac{\partial y(x, 0)}{\partial t} = 0 \qquad\qquad y(x, 0) = v(x) \tag{A3}$$

M >> ρL

M = ρL

M << ρL
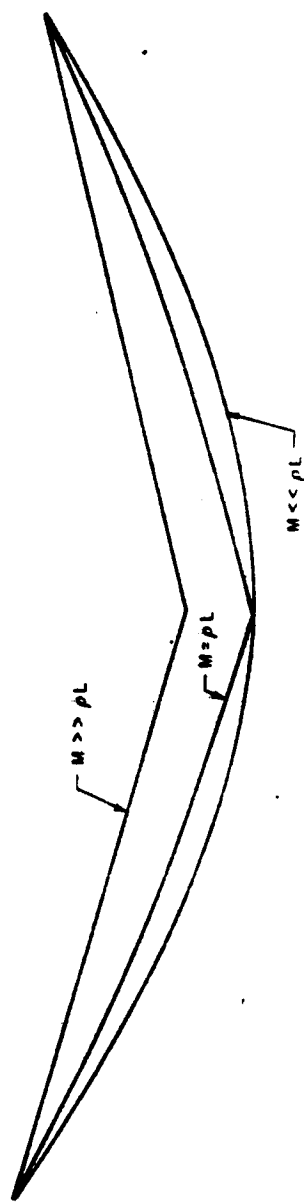
84-12261

Figure A1 SIMPLIFIED SCHEMATIC OF WIRE-IN TENSION THRUST STAND

-A2-

The conditions (A2) fix the end points of the string, the first of the conditions (A3) is the stipulation that the string is at rest when the thrust is applied, and the last condition states that before the thrust is applied the string's shape is given by some function $v(x)$.

Before the application of the thrust, the steady state shape of the string is given by the solution of equation (A1), with F set equal to zero, and with the time dependence removed, i.e.,

$$T \frac{\partial^2 v}{\partial x^2} = \rho g + Mg \, \delta(x - \xi) ; \quad v(0) = v(L) = 0 . \tag{A4}$$

After the thrust has been applied, the string will come to rest in a new position, and its steady state orientation is given by the solution of (A1) with the time dependence removed, viz:

$$T \frac{\partial^2 \omega}{\partial x^2} = \rho g + (Mg + F) \delta(x - \xi) ; \quad \omega(0) = \omega(L) = 0 . \tag{A5}$$

It is clear from the above, that the steady state position of the string at a time long after the thrust has been applied is given by the solution for the position found for the time immediately before the thrust has been applied, with the addition of the thrust force to the gravitational force, i. e., $Mg \to Mg + F$.

The solution of equation (A4) is given by

$$v(x) = -\frac{\rho g}{2T} \, x(L - x) \; - \; \frac{Mg}{2T} \left\{ \begin{array}{ll} x & x < \dfrac{L}{2} \\[2em] (L - x) & x > \dfrac{L}{2} \end{array} \right. \tag{A6}$$

This is plotted in figure A2 for the three cases where the fixed central weight is respectively much greater than, equal to, and much less than the total weight of the string. It is readily seen that the shape is that of a parabola, and that for the practical cases ($Mg \gg \rho g L$) the shape approaches that of a triangle.
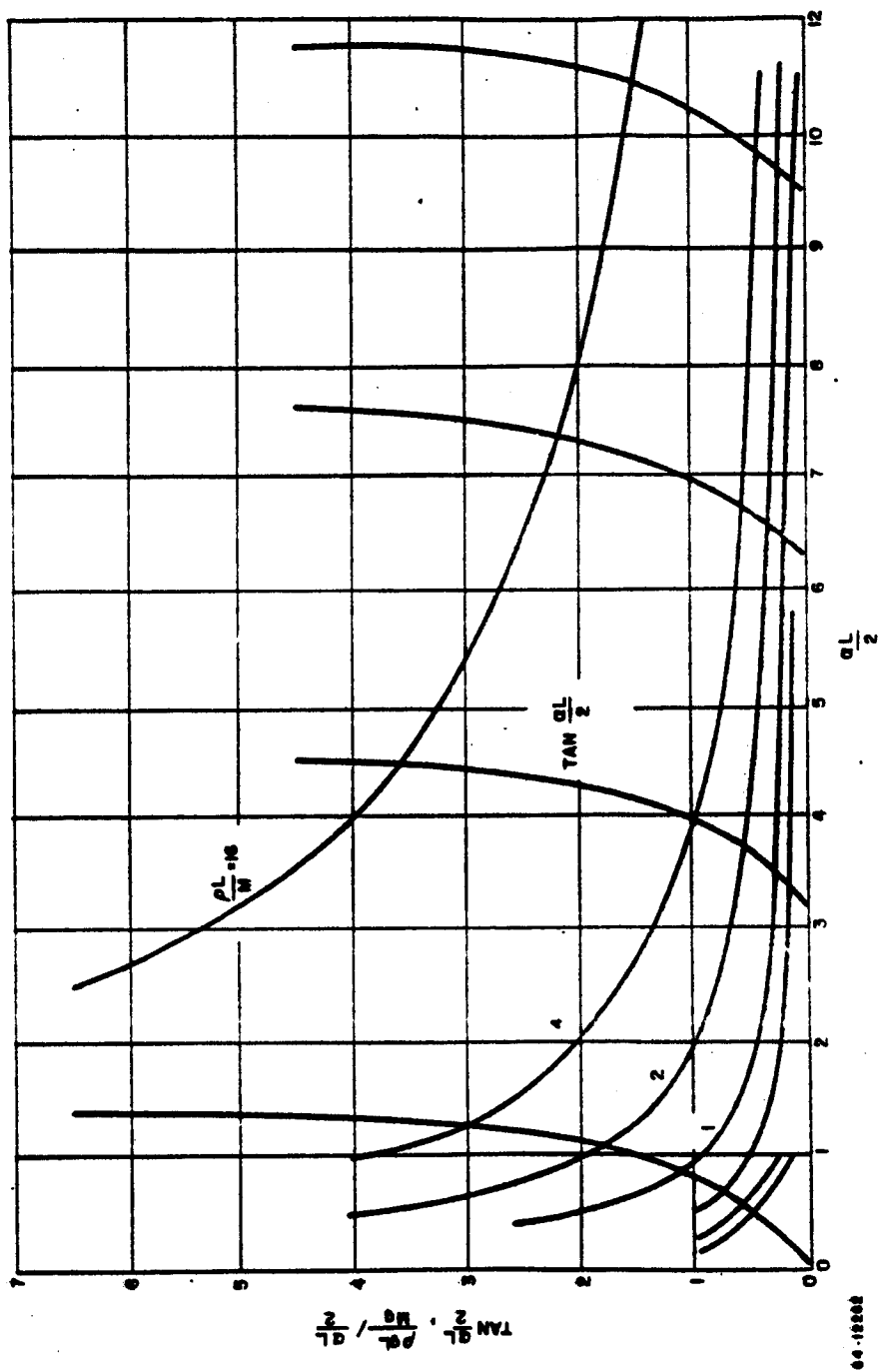
Figure A2 STRING CONTOUR FOR VARIOUS RATIOS OF ENGINE WEIGHT TO STRING WEIGHT

-A4-

The steady state solution of equation (A5) is simply

$$\omega(x) = -\frac{\rho g}{2T} \; x(L-x) \; - \; \frac{Mg+F}{2T} \left\{ \begin{array}{ll} x & x < \dfrac{L}{2} \\ \\ \\ (L-x) & x > \dfrac{L}{2} \end{array} \right. \tag{A7}$$

and is obtained from the solution of equation (A4) by the replacement of Mg by the sum of the "external" forces, $Mg + F$.

Of greatest interest is the position of the string midpoint. Before the application of the thrust, this is simply

$$v\left(\frac{L}{2}\right) = -\frac{L}{4T} \; \left\{ Mg + \frac{\rho g L}{2} \right\} \tag{A8}$$

a long time after the application of a step thrust it becomes

$$\omega\left(\frac{L}{2}\right) = -\frac{L}{4T} \; \left\{ Mg + \frac{\rho g L}{2} + F \right\} \tag{A9}$$

Hence, the new position of the string center is just lower by an amount $\dfrac{FL}{4T}$; this is linearly dependent upon the magnitude of the thrust level and the string length, and inversely proportional to the tension. It is independent of both the string weight per unit length <u>and</u> the weight of the central mass. This is important since for the measurement of the thrust levels without regard to response time of the system, no limitation on engine weight is required.

In order to consider the transient response of the thrust stand, it is convenient to first solve the problem with the assumption of no damping forces, i.e., f in equation (A1) is zero. The displacement of any point on the string is then given by

$$y(x, t) = \omega(x) + \phi(x, t) \tag{A10}$$

where $\omega(x)$ is given above (equation A7) and $\phi(x, t)$ is given by

$$\phi(x, t) = \frac{F\rho^2 L^3}{4MT} \sum C^2_m \left(\frac{2}{q_n L}\right)^3 \cos\left(\frac{q_n L}{2}\right) \cos\left(\sqrt{\rho/T} \, q_n t\right) \sin q_n x \tag{A11}$$

for points on the string to the left of center, and

$$\phi(x, t) = \frac{F \rho^2 L^3}{4MT} \sum C_n^2 \left(\frac{2}{\alpha_n L}\right)^3 \cos\left(\frac{\alpha_n L}{2}\right) \cos\left(\sqrt{\rho/T}\, \alpha_n t\right) \sin \alpha_n (L - x)$$
(A12)

for points to the right of center. C_n and α_n are defined by the relations

$$C_n = \left(\frac{\rho L}{2} + \frac{2 M \rho^2}{\alpha_n^2 M^2 + 4 \rho^2}\right)^{-1/2}$$
(A13)

and

$$\left(\frac{\alpha_n L}{2}\right) \tan\left(\frac{\alpha_n L}{2}\right) = \frac{\rho L}{M}$$
(A14)

In particular, the position of the center of the string is given by

$$y\left(\frac{L}{2}, t\right) = -\frac{L}{4T}\left[Mg + \frac{\rho g L}{2} + F\right] +$$
(A15)

$$+ \frac{F \rho L^2}{4T} \sum_{n=0}^{\infty} C_n^2 \left(\frac{2}{\alpha_n L}\right)^2 \sin^2\left(\frac{\alpha_n L}{2}\right) \cos \sqrt{\rho/T}\, \alpha_n t$$

Figure A3 shows plots of $\frac{\rho g L}{Mg} / \frac{\alpha L}{2}$ and $\tan \frac{\alpha L}{2}$, both against $\frac{\alpha L}{2}$, and with the ratio $\frac{\rho g L}{Mg}$ as a parameter. The intersections of the tangent curves with the hyperbolas are the values of $\frac{\alpha_n L}{2}$ which satisfy equation (45b) for the parameter values of the ratio of string weight to mass weight to mass weight, $\frac{\rho g L}{Mg}$.

For limitingly small relative weight of the central mass, $Mg \ll \rho g L$, the values of $\frac{\alpha_n L}{2}$ approach the values $\frac{2n + 1}{2} \pi$. The series of equation (A15) may then be summed analytically and yields

$$y\left(\frac{L}{2}, t\right)_{M \to 0} = -\frac{\rho g L^2}{8T} - \frac{F L}{2T} g (t)$$
(A16)

where $q(t)$ is shown plotted in figure A4. The curve of figure A5 then represents the position of the center of the string as a function of time. It is seen to be periodic with a period given by

$$\tau = 2L \sqrt{\rho/T} .$$
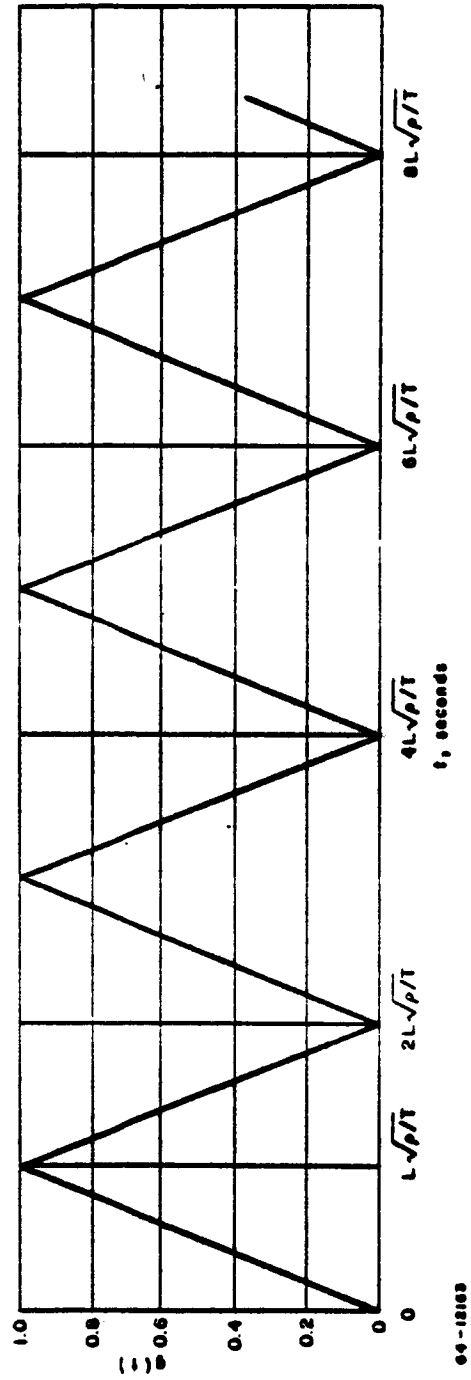
Figure A3 STRING VIBRATIONAL MODE CHARACTERISTICS
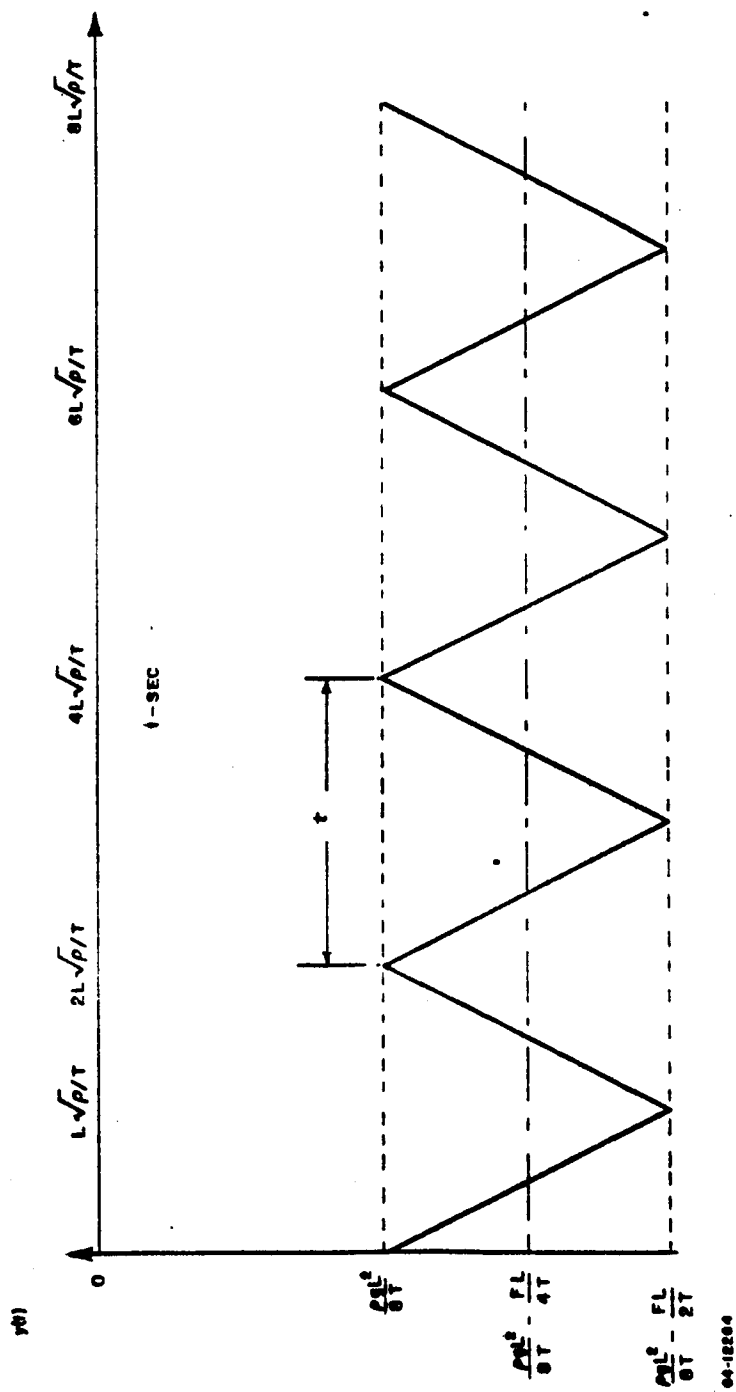
Figure A4 FUNCTION TO DETERMINE STRING VIBRATIONAL AMPLITUDE
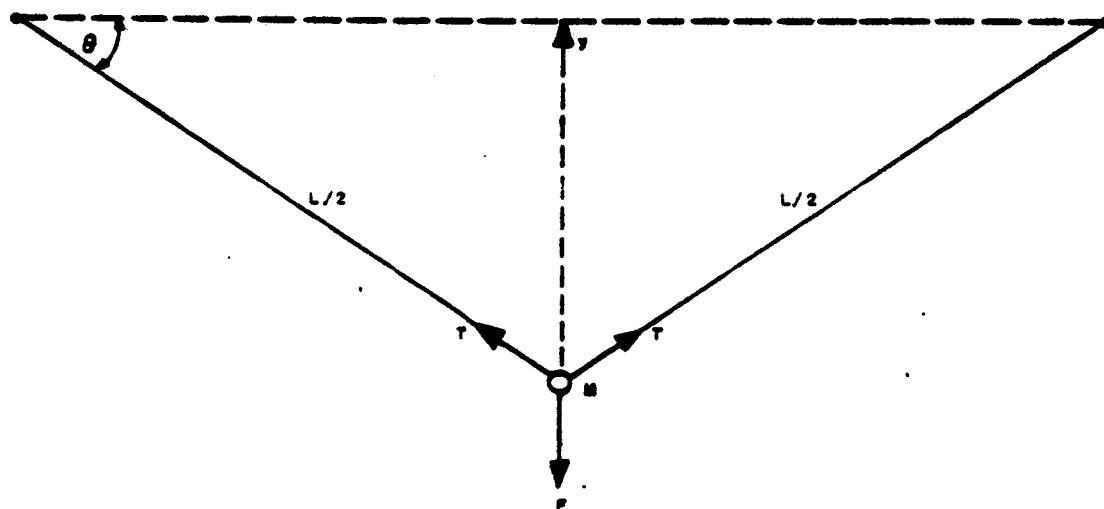
Figure A5 STRING CENTER POSITION VERSUS TIME

The average position is given by

$$\bar{y}\left(\frac{L}{2}, t\right)_{M \to 0} = -\frac{\rho g L^2}{8T} - \frac{FL}{4T} . \qquad (A17)$$

This is indeed the value of the steady state position in the limit of small M, as seen from equation (A9). The effect of damping upon the system should be to reduce the magnitude of the oscillation as time goes on and the steady state position should then be just the average value of the position as shown in equation (A9).

In the more practical case, it is the string's weight which is small compared with the weight of the engine and engine mounting, i.e., $Mg \gg \rho g L$.

For this case, the introduction of the substitutions

$$R = \frac{L}{M} \rho$$

and

$$X_n = \frac{a_n L}{2}$$

reduces equation (11) to

$$y\left(\frac{L}{2}, t\right)_{\rho L \to 0} = -\frac{(Mg + F)L}{4T}$$

$$\qquad (A18)$$

$$+ \frac{FL}{2T} \frac{R^2}{X_1^2 (R^2 + R + X_1^2)} \left[\cos \frac{2}{L} \sqrt{T/\rho}\, X_1 t + \sum_{n=2}^{\infty} \left(\frac{X_1}{X_n}\right)^2 \left(\frac{R^2 + R + X_1^2}{R^2 + R + X_n^2}\right) \cos \frac{2}{L} \sqrt{T/\rho}\, X_n t \right].$$

It is seen from figure A3 that

$$X_n \approx X_{n-1} + \pi .$$

Moreover, for $\frac{\rho L}{M} \ll 1$,

$$\tan X_1 \approx X_1 \quad \text{and} \quad X_1 \approx \sqrt{R} .$$

These approximations lead to the final results for the position of the center of a string of negligible weight,

$$y\left(\frac{L}{2}, t\right)_{\rho \to 0} = -\frac{MgL}{4T} - \frac{FL}{4T} \left[1 - \cos \sqrt{\frac{4T}{ML}}\, t \right] . \qquad (A19)$$

To test the limits of validity of the above for larger values of the ratio $R = \dfrac{\rho L}{M}$, substitution of $R = 1$ yields:

$$y\left(\frac{L}{2}, t\right)_{\rho L = M} = -\frac{MgL}{4T} - \frac{FL}{4T}\left[1 - 1.02 \cos\left(0.85 \sqrt{\frac{4T}{ML}}\ t\right)\right]. \tag{A20}$$

It is thus clear that for a practical thrust stand, the relation (A19) is valid to very high order of precision.

APPENDIX B

HEATUP TIME FOR FAST HEATUP THRUSTOR

In order to determine more exactly the transient heating characteristic of the heatup thrustor, an existing digital computer program has been utilized. The program solves for temperature as a function of time and position given the geometry, power input, material properties as a function of temperature, and boundary conditions. Conductive and radiative heat transfer are accounted for.

The idealized thrustor for which the transient heating calculations were made is drawn in figure B1. It consists of a heater tube made of tungsten with the dimensions 1.9 cm length (0.75 inch), 0.28 mm inner diameter (0.011 inch), and 0.38 mm outer diameter (0.015 inch). At one end, this tube is attached to a stainless steel tube with the dimensions 2.54 cm length (1.0 inch), 1.52 mm inner diameter (0.060 inch), and 3.13 mm outer diameter (0.125 inch). The other end of the tungsten tube terminates in a flat tungsten power lead, with the dimensions 3.8 mm length (0.15 inch), 2.54 mm width (0.10 inch), and 0.128 mm thickness (0.005 inch).

Power is supplied to this thrustor at a constant rate, which can be adjusted to various levels to perform parametric studies. The boundary conditions employed are that: (1) the base of the large stainless steel tube (the end furthest removed from the thrustor) is maintained at 300° K, as is the end of the flat power lead, (2) each exposed surface radiates an amount of power consistent with its temperature and emissivity.

Results of this analysis are given in figures B2, 33, and B4. Figure B2 shows, as a function of input power, the final steady state temperature distribution over the chosen geometry. At each power level the thrustor assembly temperature reaches a peak near the center of the thin-walled tungsten tube and falls off at each end. Neither the stainless steel mounting cylinder nor the power lead are themselves appreciably heated. A power input of 20 watts brings the thrustor to a temperature of the order of 2500° K in steady state, with no gas flow.

Figure B3 shows the transient temperature rise at the center of the tungsten tube. Even with a power input of only 10 watts the warmup time is below 1 second, while 20 watts it is of the order of one-half second, and one-quarter second at 40 watts of input power.

Finally, for a power level of 40 watts, figure B4 shows the temperature distribution as a function of time. From figure B4 it can be seen that the general shape of the temperature distribution varies little with time.

It can be concluded from this analysis, that, with an input power of 20 watts, with losses both by conduction and radiation, the thrustor will reach operating temperature in less than one second. Since the dominating loss mechanism at the higher temperatures is radiation, and since a thrustor twice as long will radiate twice as much, essentially, the conclusions can be simply scaled within a limited range of thrustor sizes. Hence, it appears reasonable to assume that a thrustor x centimeters long will require a power 10 x watts to reach steady state temperature in about one-half second, and that the steady state temperature will be approximately 2500°K, for values of x which do not depart too much from 2 cm.

0.125 IN O.D. x 0.060 IN I.D.

0.10 IN

0.015 IN O.D. x 0.011 IN I.D. TUBE

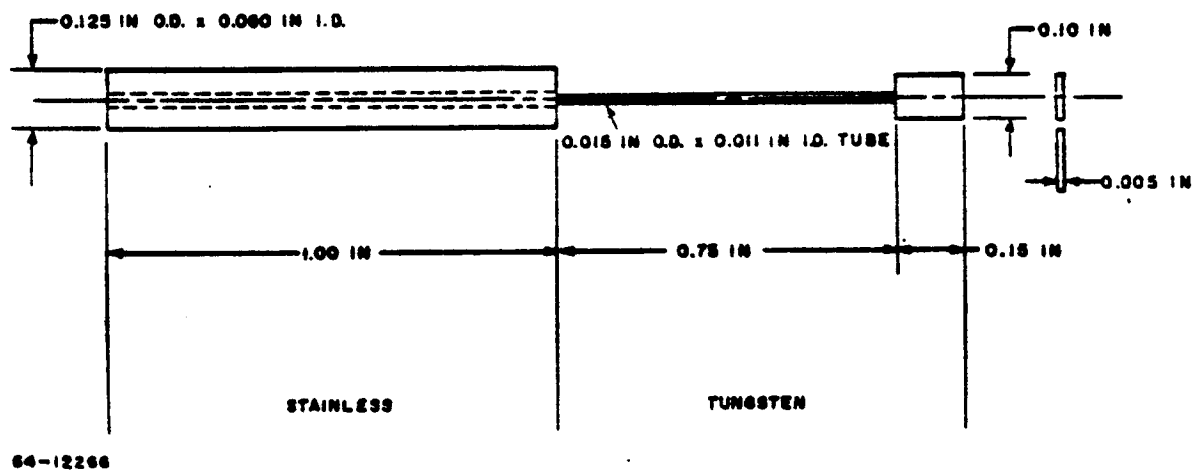0.005 IN

1.00 IN

0.75 IN

0.15 IN

STAINLESS

TUNGSTEN

64-12266
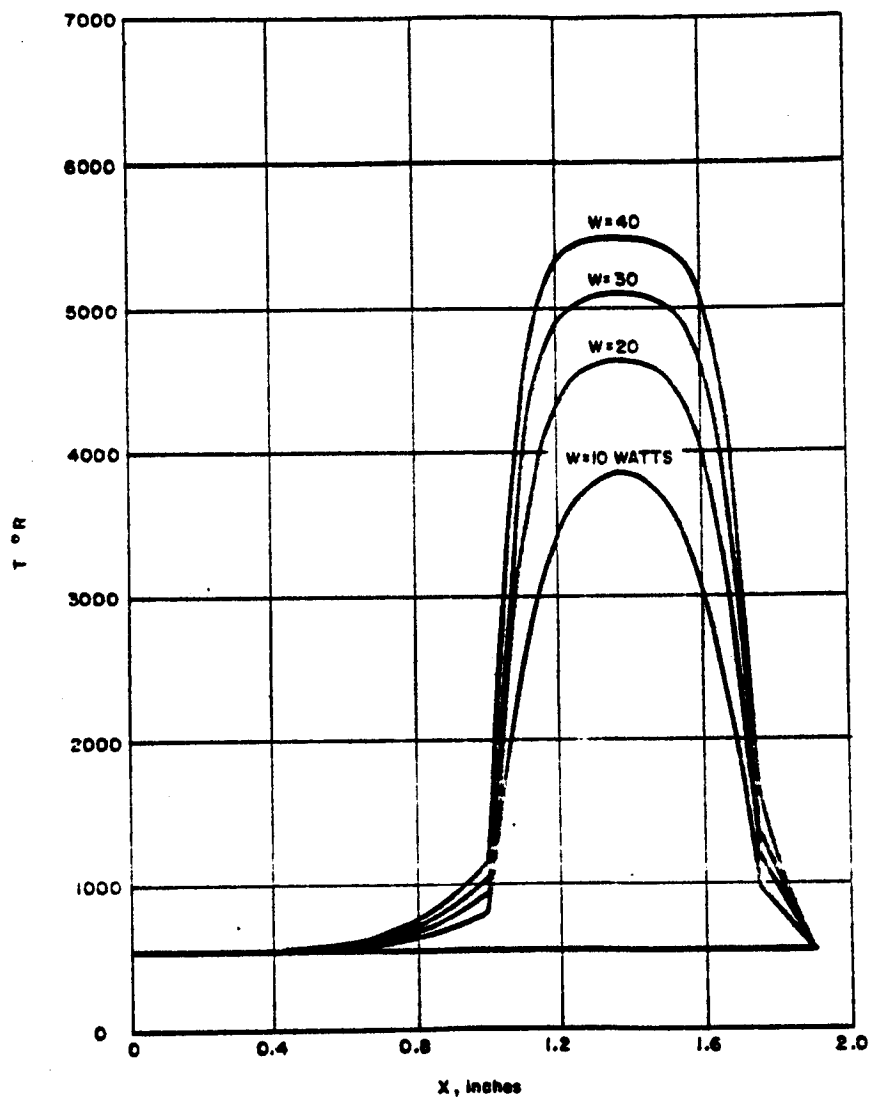
Figure B1 MODEL FOR HEAT TRANSFER ANALYSIS

Figure B2 TEMPERATURE DISTRIBUTION AFTER 5 SECONDS
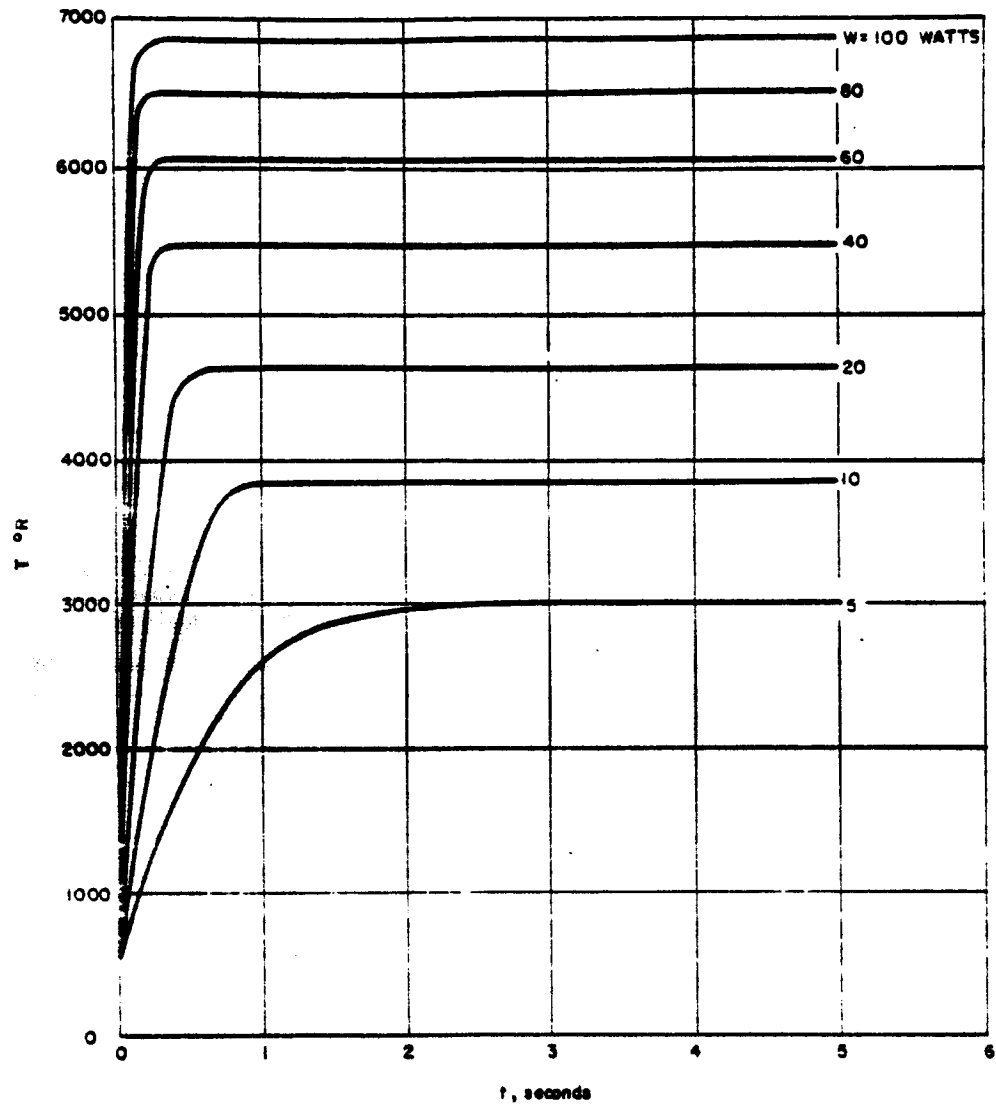
Figure B3 MAXIMUM THRUSTOR TEMPERATURE VERSUS TIME FOR DIFFERENT POWER INPUT LEVELS

64-12266
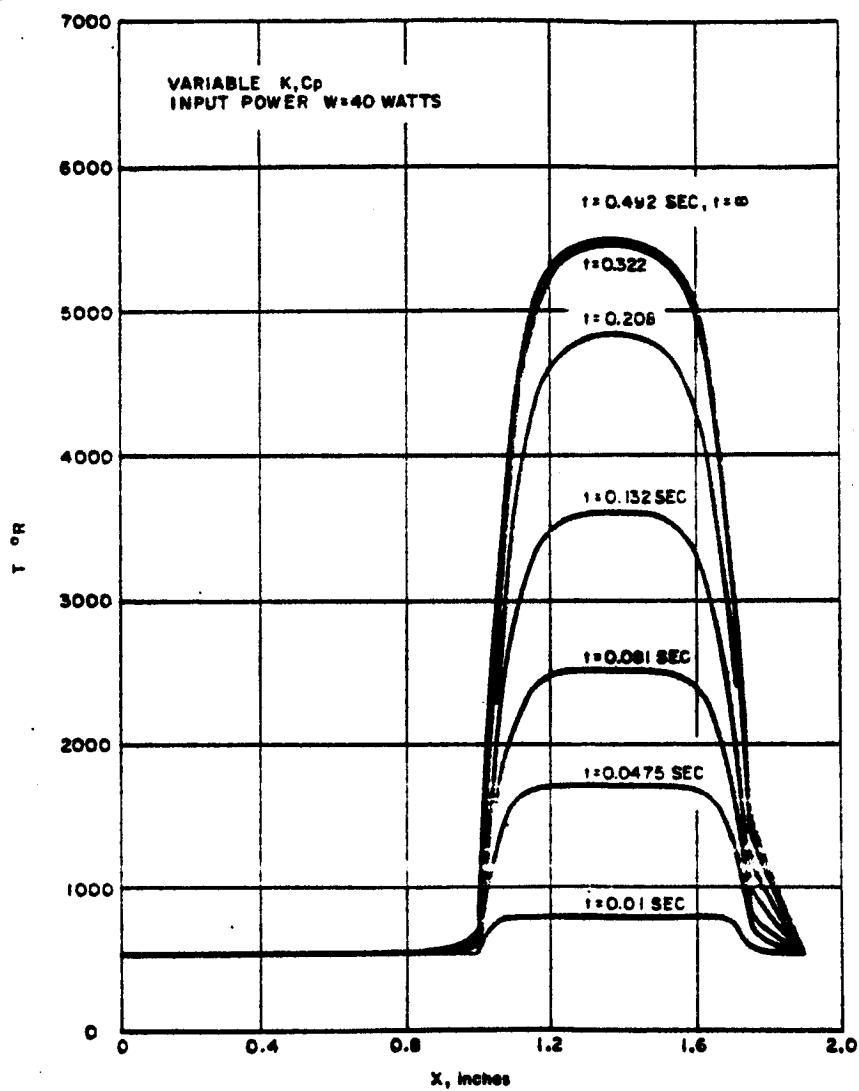
Figure B4 THRUSTOR TEMPERATURE DISTRIBUTION VERSUS TIME AT INPUT POWER OF 40 WATTS

APPENDIX C

HEAT LOSS FROM A THERMAL STORAGE THRUSTOR

Estimates have been made of the standby power loss associated with a thermal storage thrustor. The thermal storage thrustor is defined as one which is continuously supplied with electrical power. In the steady state, with no gas flow, the input power level equals exactly the power loss. Reduction of losses therefore directly reduces the required input power. It is assumed that the thrustor heat capacity greatly exceeds the heat capacity of the total propellant mass heated by the thrustor during a thrust pulse, and that the average over a long time of the power absorbed by the propellant is small compared to the input power level. Under these conditions the power requirements for the thrustor are determined by the standby conditions, and the propellant flow can actually be treated as a small perturbation on these standby conditions.

There are two principal loss modes associated with the thermal storage thrustor; these are radiation and conduction along the input power leads and propellant supply tube. These are treated separately below.

Radiation Loss

For a body surrounded by a radiation shield, it is shown in reference 1 that the heat lost by radiation from the body is given by

$$Q = \frac{A_o \sigma}{\frac{1}{\epsilon_o} + \frac{A_o}{A_1}\left(\frac{1}{\epsilon_1} - 1\right)} (T_o^4 - T_1^4) \tag{C1}$$

where Q is the heat loss in watts/cm^2-$^oK^4$, A_o is the body surface area, σ is 5.67×10^{-12}, A_1 is the shield surface area, ϵ_o and ϵ_1 are the body and shield emissivities, respectively, and T_o and T_1 are the body and shield temperatures, respectively. For the thrustor of figure 23 it is a useful approximation to neglect end effects, and to evaluate the power radiated per unit length of the cylindrical thrustor body. Equation (C1) can be written

$$Q^1 = \frac{Q}{L} = \frac{2\pi r_o \sigma}{\frac{1}{\epsilon_o} + \frac{r_o}{r_1}\left(\frac{1}{\epsilon_1} - 1\right)} (T_o^4 - T_1^4) \tag{C2}$$

[1] Eckert, E. R. G., and R. M. Drake, Jr., Heat and Mass Transfer, p. 405, McGraw-Hill, New York (1959).

where r_o and r_1 are, respectively, the radii of the thrustor and the shield. In the event that the emissivities of the body and the shield are equal, equation (C2) can be further simplified:

$$Q' = \frac{2\pi\epsilon\sigma}{\dfrac{1}{r_o} + (1-\epsilon)\dfrac{1}{r_1}} (T_o^4 - T_1^4) \, . \tag{C3}$$

If now there are N such concentric shields, and if Q' and the geometry are fixed, there are N + 1 unknown temperatures T_i for a given heat flux. Equation (C3) can be used to relate the temperature of the thrustor to that of the first shield, the temperature of the first shield to that of the second, etc., yielding N equations. The N + 1st comes from the radiation between the Nth shield and the surrounding space.. This system of equations can then be solved for T_o in terms of the heat flux, the geometry, and the emissivity. The solution is

$$T_c^4 = \frac{Q'}{2\pi\epsilon\sigma}\left[\frac{1}{r_o} + (2-\epsilon)\sum_{n=1}^{N}\frac{1}{r_n}\right] \, . \tag{C4}$$

Solutions to equation (C4) have been obtained using a digital computer, and the results are presented below. Some physical insight can be gained, however, by considering a special case. If the shields are equally spaced by distance δ , and if the number of shields is large so that the sum can be replaced by an integra, equation (C4) becomes:

$$T_o^4 = \frac{Q'}{2\pi\epsilon\sigma}\left[\frac{1}{r_o} + \frac{2-\epsilon}{\delta}\, \ln\frac{r_o + N\delta}{r_o + \delta}\right] \tag{C5}$$

It is clear from equation (C5) that, for a given T_o, Q' is reduced as ϵ , r_o, and/or δ are reduced; Q' is also reduced as N increases, but only logarithmically. Therefore, the number of shields which can be usefully employed is subject to diminishing returns.

Figure C1 shows the radiation per unit length in watts/cm as a function of number of radiation shields. The assumptions of this calculation are that the thrustor outer wall temperature is 2000°K, the thrustor radius is 0.5 cm, and the emissivity is 0.3. The shield separation, δ , is taken as a parameter and curves are plotted in figure 26 for values of δ of 0.01, 0.05, and 0.1 cm. The shield thickness is assumed small compared to δ.

If the radiation loss is to be kept below about 2 watts/cm, which is imperative if the thrustor overall standby heat loss is to be kept of the order of 10 watts, then the number of shields required is seen to exceed 30 even with the rather optimistic value of 0.01 cm for δ. If the shield separation is as much as milli-

84-12270
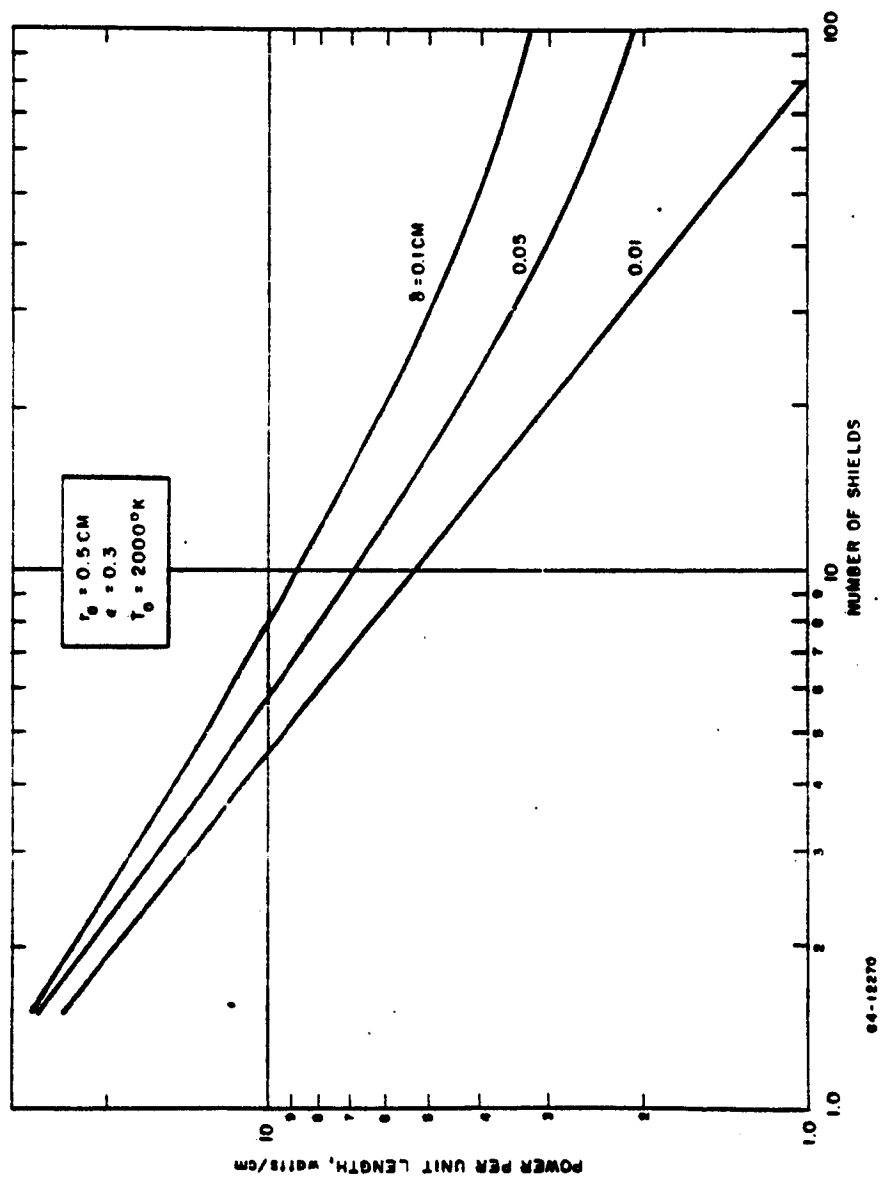
Figure C1 HEAT RADIATED PER UNIT LENGTH VERSUS NUMBER OF SHIELDS, ϵ = 0.3

meter, even 100 shields are not sufficient to keep Q' below 2 watts/cm.

If the emissivity is decreased to 0.1, the situation is greatly improved. Figure C2 indicates that only 15 shields would be required at the quite reasonable spacing of 1 mm, if this emissivity can be obtained, to limit the loss per unit length by radiation to 2 watts/cm.

The effects of emissivity and shield separation are shown again in figure C3, drawn for a total of 20 shields with a thrustor temperature of 2000°K and radius of 0.5 cm. The indication of this figure is that the emissivity must not exceed ~0.2 if Q' is to be kept below 2 watts/cm with shield separation distances of the order of one-half millimeter. Figure C4 shows the effect of heater diameter on the required number of shields.

This analysis has not accounted for radiation from the ends of the thrustor; however, it is thought that proper design can keep this loss smaller than the loss through the sides for a thrustor with a length-to-diameter ratio greater than 2; if the thrustor can be made with a length to diameter ratio of the order of 8 or 10, this loss can be made very small.

2. Conduction Loss

The conduction loss has been estimated from the results of the computer program reported in appendix B. Briefly, the steady state temperature distribution obtained from the computer was used to estimate the temperature gradient at the end of the thrustor section, and this was in turn used with the thermal conductivity and the known cross sectional area to evaluate the heat loss. For a 10-watt input power level, which corresponds to a central temperature of 2000°K, the calculated conduction loss was 2.9 watts into the stainless steel holder and 2.7 watts into the tungsten power lead, for a total of 5.6 watts. It is anticipated that the larger thermal storage thrustor would have a larger lead loss than the very small fast heatup unit, so that these estimates may serve as lower limit values.
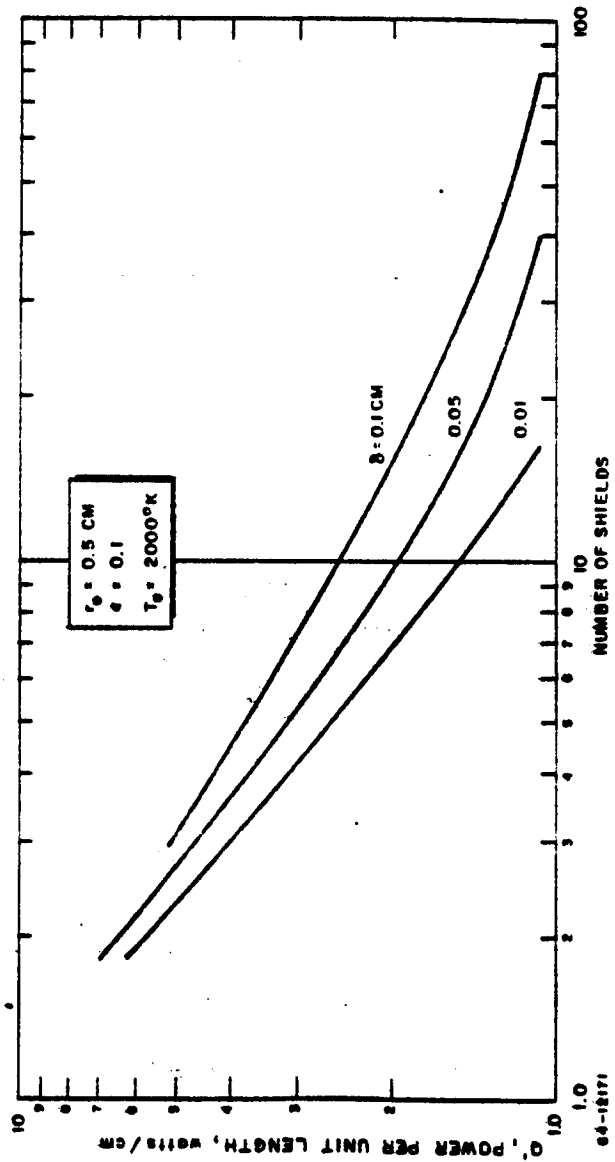
Figure C2 HEAT RADIATED PER UNIT LENGTH VERSUS NUMBER OF SHIELDS, ϵ = 0.1
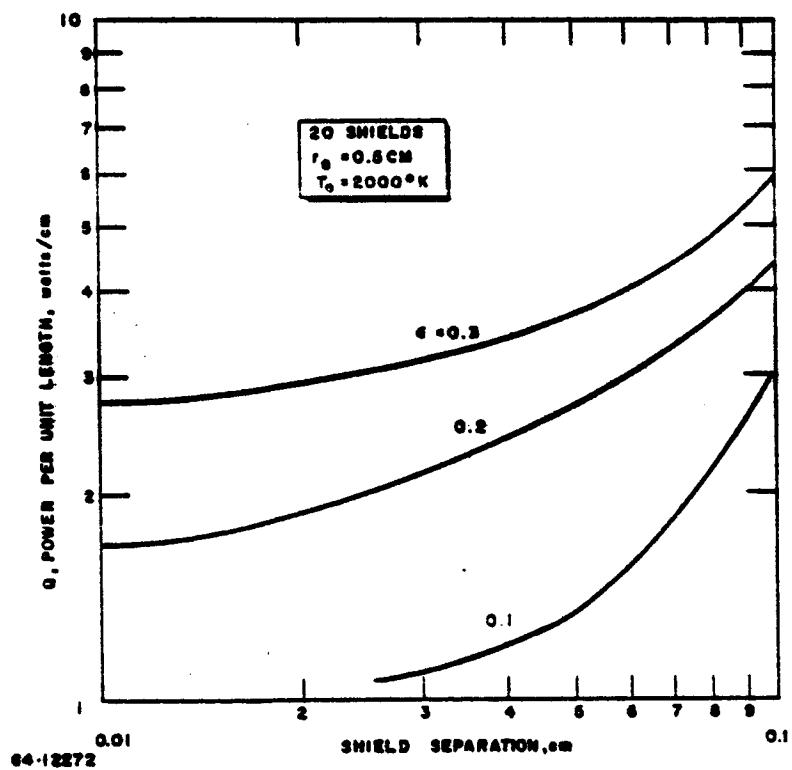
-C3-

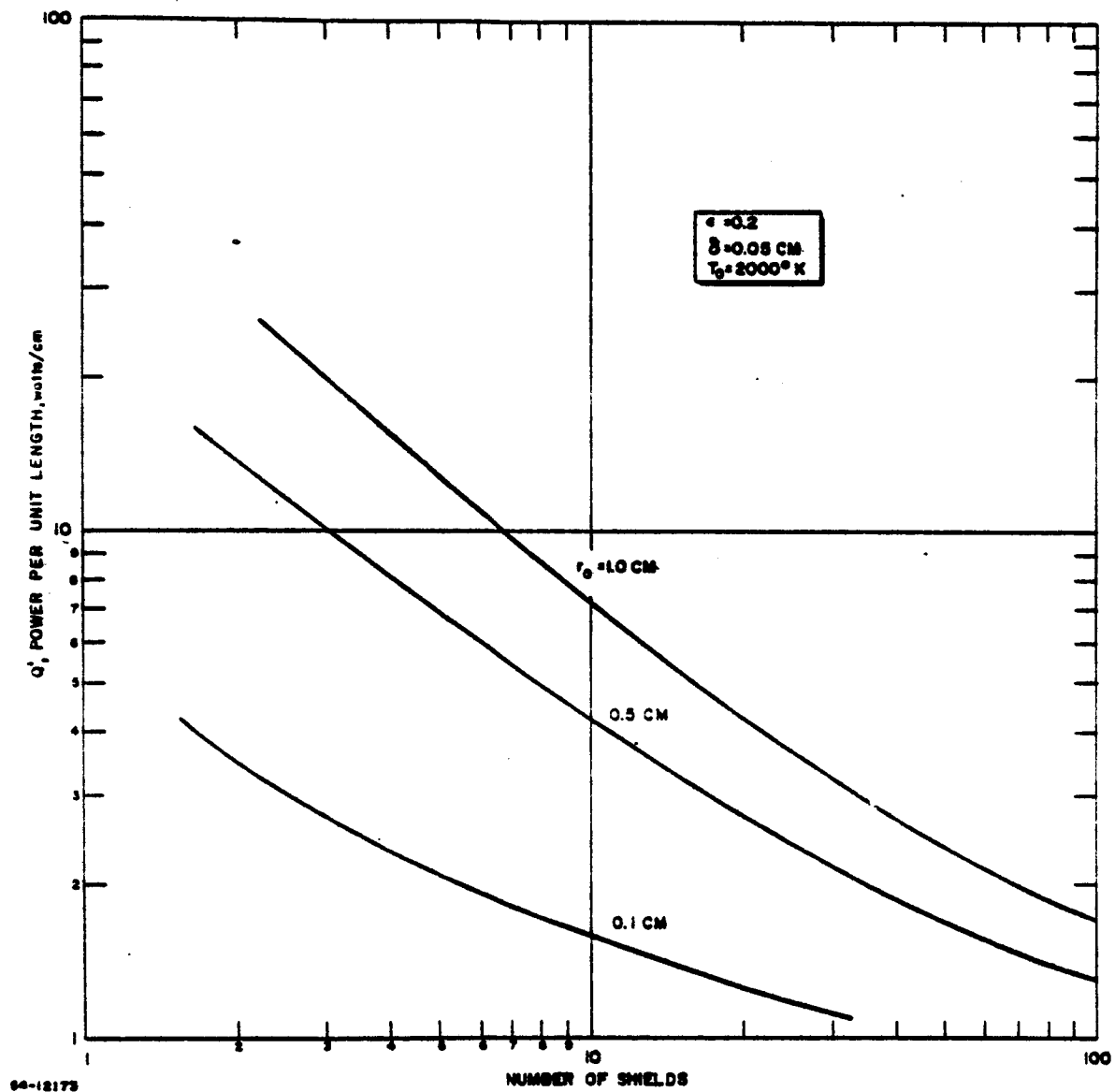Figure C3 HEAT RADIATED PER UNIT LENGTH VERSUS SHIELD SEPARATION

Figure C4 HEAT RADIATED PER UNIT LENGTH VERSUS NUMBER OF SHIELDS AND THRUSTOR
RADIUS

APPENDIX D

LEAD NETWORK CHARACTERISTICS FOR
THE RESISTOJET SINGLE AXIS
ATTITUDE CONTROL SYSTEM

1. INTRODUCTION

A block diagram of the basic control logic for the Model I and II resistojet
attitude control systems is given in figure D1.   The position sensor provides
a voltage signal, $\theta(t)$, which is directly proportional to the angular error at
a time t . The response of the position sensor is illustrated in figure D2.
This sensor has a linear response ($\pm$ 2 percent) over a range of $\pm$ 1 degree of
angular error with a null at zero-degree angular error. For positive angular
errors, the voltage output is negative as shown. Outside the linear range,
a nonlinear response occurs out to an angle which represents the maximum
sensor output; from figure D2 this angle is about $\pm$ 2.5 degrees and repre-
sents the maximum useful range of the sensor. For angular errors larger
than 2.5 degrees, the signal output gradually decreases approaching a value
of zero at an angle of $\pm$ 10 degrees. In the linear range of the sensor, the
sensitivity is about 180 millivolts per degree of angle.

The voltage signal from the position sensor is amplified by a preamp with a
gain K to give an output signal $K\theta(t)$. This signal is in exact phase with the
input signal to the preamp, $\theta(t)$.

The preamp output represents the input signal to the lead network which is the
basic control element of the resistojet control logic system. The lead network
provides an output signal $Z(t)$, to the switching networks which then control
the pulsing of the appropriate resistojets. If the output signal, $Z(t)$, equals
and exceeds the lower of two preset values, the switching network provides
a resistojet pulse of preset duration in the proper direction. If $Z(t)$ equals
and exceeds the larger of the two preset values, the appropriate resistojet is
turned on and remains on continuously until $Z(t)$ is reduced below this larger
value. (Hysteresis will make the dropout voltage of the switch slightly less
than the pullin voltage.) The operation of the resistojet pulsing to provide
attitude control of the satellite is thus directly related to the output signal $Z(t)$
of the lead network. It is the purpose of the remaining discussion to investi-
gate the relationship between the input signal, $K\theta(t)$, and the output signal
$Z(t)$, for the lead network being used in the control logic of the Models I and
II resistojet control systems.

POSITION SENSOR — $\theta(t)$ — PREAMP GAIN = K — $K\theta(t)$ — LEAD NETWORK $\theta(s) = \dfrac{1 + \alpha T_L s}{1 + T_L s}$ — $z(t)$ — SWITCHING NETWORK CONTROLLING RESISTOJETS
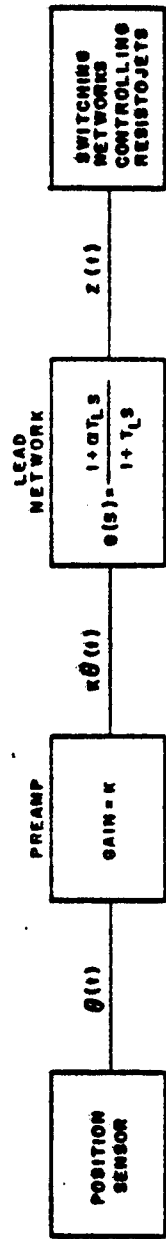
Figure D1 BASIC CONTROL LOGIC DIAGRAM FOR RESISTOJET ATTITUDE CONTROL SYSTEM

65-8156
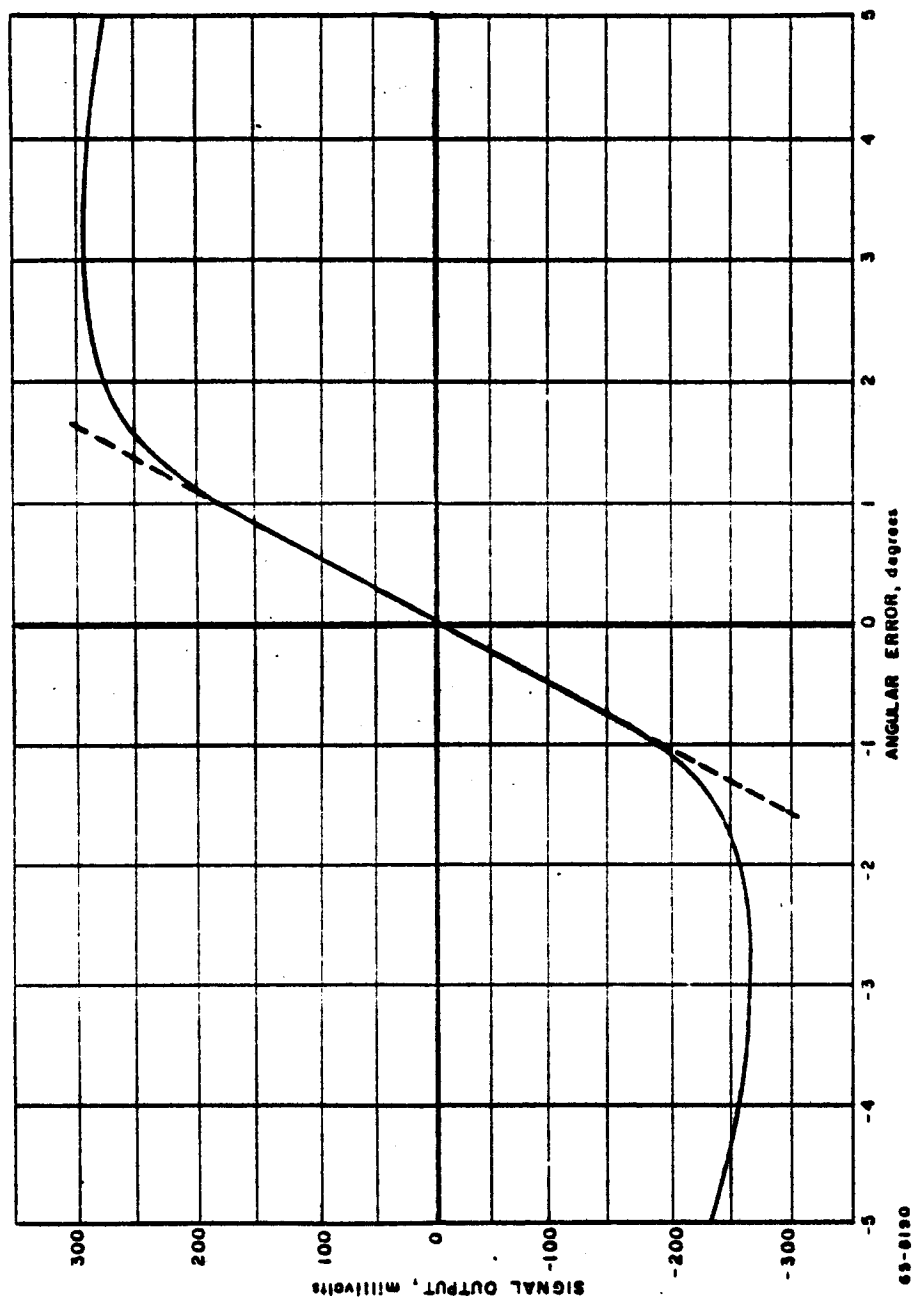
Figure D2 SIGNAL OUTPUT FROM POSITION SENSOR AS FUNCTION OF ANGULAR ERROR

65-0190

-D3-

2. LEAD NETWORK CHARACTERISTICS

The characteristics of operation of the lead network are contained in the transfer function, G(s):

$$G(s) = \frac{1 + a\,\tau_L\,s}{1 + \tau_L\,s} \tag{D1}$$

where

a = constant of lead network, dimensionless

τ_L = constant of lead network, seconds

s = complex frequency variable

The transfer function is the ratio of the Laplace transform of the output signal to the Laplace transform of the input signal. The type of control represented by this transfer function is widely used in process control systems and is frequently referred to as "proportional plus derivative of error" control; in other words, the control element output depends not only on the absolute angluar error, $\theta(t)$, but also on the rate with which the angular error is changing, $d\theta(t)/dt$.

From the definition of the transfer function, equation (D1) can be rewritten as:

$$\frac{Z(s)}{K\,\theta(s)} = \frac{1 + a\,\tau_L\,s}{1 + \tau_L\,s} \tag{D2}$$

where

$Z(s)$ = Laplace transform of $Z(t)$

$\theta(s)$ = Laplace transform of $\theta(t)$

-D4-

Or as:

$$Z(s) = \frac{K}{\tau_L} \frac{1}{s + (1/\tau_L)} \theta(s) + aK \frac{s}{s + (1/\tau_L)} \theta(s) \qquad (D3)$$

The output signal $Z(t)$ which is the inverse of $Z(s)$ thus depends on the function $\theta(s)$ which in turn depends on the variation of $\theta(t)$ with time. The solution for $Z(t)$ will be derived for two special cases to illustrate this dependence, the first in which $\theta(t)$ varies as a step increase followed by a linear increase with time and the second in which $\theta(t)$ varies sinusoidally with time.

a. <u>Step Increase in Angle Followed by a Linear Change of Angle with Time (Constant Rate of Rotation)</u>

In a hard limit cycle with zero disturbance torque, the drift phase of the limit cycle takes place with a constant rate of rotation. The angle at anytime with an initial step increase can thus be written as:

$$\theta(t) = 0 \qquad t < 0$$

$$\qquad\qquad\qquad\qquad\qquad\qquad\qquad (D4)$$

$$\theta(t) = \theta_0 + \psi t \qquad t \geq 0$$

where

$$\theta_0 = \text{step increase in angle at } t = \text{zero}$$

$$\psi = \frac{d\theta}{dt} = \text{rate of rotation}$$

The case of constant ψ corresponds to the drift phase of the limit cycle with zero disturbance torque.

The Laplace transform of (D4) is:

$$\theta(s) = \frac{\theta_0}{s} + \frac{\psi}{s^2} \qquad (D5)$$

Substitution of this relation into (D3) gives:

$$Z(s) = \frac{1}{s + (1/\tau_L)} aK\theta_0 + \frac{1}{s[s + (1/\tau_L)]} \left[\frac{K\theta_0}{\tau_L} + aK\psi \right] + \frac{1}{s^2[s + (1/L)]} \frac{K\psi}{\tau_L}$$

$$\qquad\qquad\qquad\qquad\qquad\qquad\qquad\qquad\qquad\qquad (A.6)$$

Taking the inverse of this relation and algebraic simplification results in:

$$Z(t) = K \left\{ (a-1)(\theta_0 - \tau_L \psi) e^{-t/\tau_L} + \psi t + [\theta_0 + \tau_L \psi (a-1)] \right\} \qquad (D7)$$

For $t \gg \tau_L$ this relation simplifies to:

$$Z(t) = K \{ (\theta_0 + \psi t) + (a-1)\tau_L \psi \}$$

$$= K \left\{ \theta(t) + (a-1)\tau_L \frac{d\theta(t)}{dt} \right\} \qquad (D8)$$

This expression, which is the same as that given in the second quarterly report illustrates the dependence of $Z(t)$ on both $\theta(t)$ and $d\theta(t)/dt$ and justifies the description of this type of control as "proportional plus derivative of error control".

Rewriting equation (D8):

$$\frac{d\theta(t)}{dt} = \frac{Z(t)/K}{(a-1)\tau_L} - \frac{1}{(a-1)\tau_L} \theta(t) \qquad (D9)$$

Switching occurs when $Z(t) = Z_{sw}$ so that the control line is represented by:

$$\left(\frac{d\theta}{dt} \right)_c = \frac{Z_{sw}/K}{(a-1)\tau_L} - \frac{1}{(a-1)\tau_L} \theta_c$$

$$\left(\frac{d\theta}{dt} \right)_c = \frac{\theta_{co}}{(a-1)\tau_L} - \frac{1}{(a-1)\tau_L} \theta_c \qquad (D10)$$

Equation (D7) can be used to obtain the response for a step change in $\theta(t)$ alone and for a linear increase of $\theta(t)$ alone starting from $\theta(t) = 0$. For the step change, ψ in equation (D7) is set equal to zero giving:

$$Z(t) = K \theta_0 \left[(a-1) e^{-t/\tau_L} + 1 \right] \qquad (D11)$$

At $t = 0$, $Z(t) = K\theta_0 a$

For $t \gg \tau_L$, $Z(t) = K\theta_0$

For the linear increase alone, set θ_0 of equation (D7) equal to zero giving:

$$Z(t) = K\psi \left\{ (a-1)\tau_L \left[1 - e^{-t/\tau_L} \right] + t \right\} \tag{D12}$$

At $t = 0$, $Z(t) = 0$

For $t \gg \tau_L$, $Z(t) = K\psi [(a-1)\tau_L + t] = K[\theta(t) + (a-1)\tau_L \psi]$

b. Sinusoidal Variation of Angle with Time

The usual way of expressing the response of a control element is to present the response to a sinusoidal variation in the input to the control element. The response is generally given in the form of the ratio of peak output magnitude to peak input magnitude versus frequency and the phase angle versus frequency. The response of the lead network to a sinusoidal input can be considered, to a first approximation, as the response to a symmetrical hard limit cycle with zero disturbance torque. This is illustrated in the sketch of figure D3.

The response to a sinusoidal input can be obtained directly from the transfer function by substituting $j\omega$ for s in the transfer function where $j = \sqrt{-1}$.

Thus:

$$G(j\omega) = \frac{1 + (a\tau_L \omega)j}{1 + (\tau_L \omega) j}$$

$$= \frac{1 + a(\tau_L \omega)^2}{1 + (\tau_L \omega)^2} + j \frac{a\tau_L \omega - \tau_L \omega}{1 + (\tau_L \omega)^2} \tag{D13}$$

The magnitude of this relation is given by:

$$G = \sqrt{ \left[\frac{1 + a(\tau_L \omega)^2}{1 + (\tau_L \omega)^2} \right]^2 + \left[\frac{a\tau_L \omega - \tau_L \omega}{1 + (\tau_L \omega)^2} \right] }$$

$$= \sqrt{ \frac{1 + (a\tau_L \omega)^2}{1 + (\tau_L \omega)^2} } \tag{D14}$$

The phase angle is obtained from:
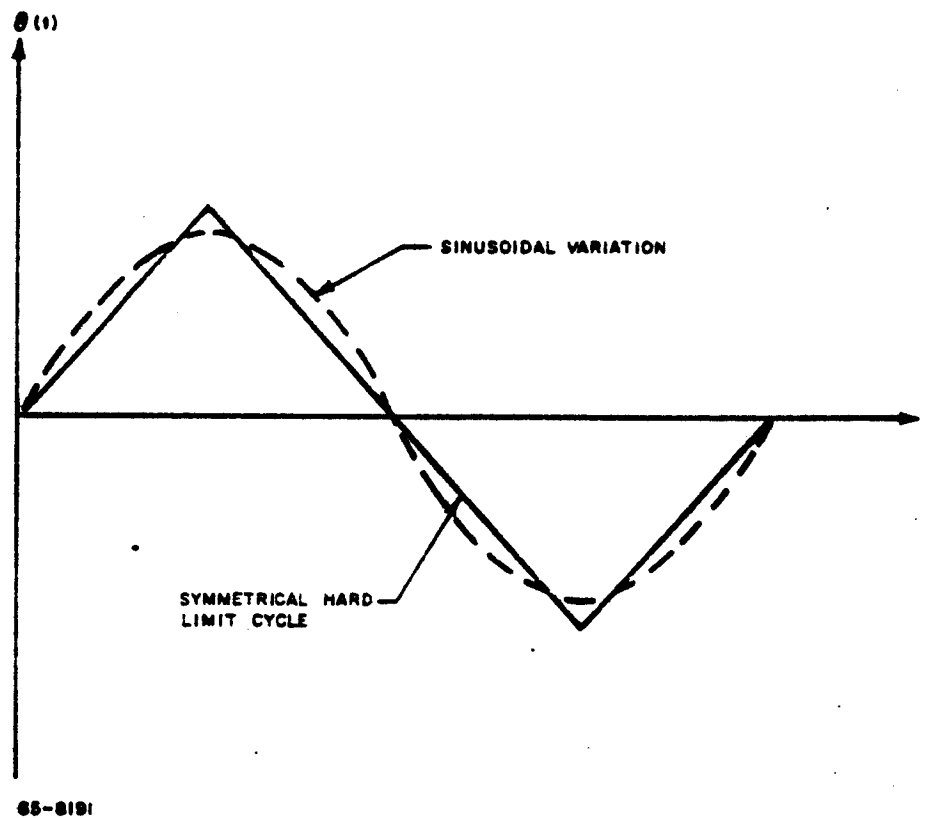
Figure D3 COMPARISON OF HARD LIMIT-CYCLE OPERATION
WITH SINUSOIDAL VARIATION OF ANGLE WITH TIME

$$\tan \phi = \left[\frac{a\tau_L \omega - \tau_L \omega}{1 + (\tau_L \omega)^2}\right] \Bigg/ \left[\frac{1 + a(\tau_L \omega)^2}{1 + (\tau_L \omega)^2}\right]$$

$$= \frac{\tau_L \omega (a - 1)}{1 + a(\tau_L \omega)^2} \tag{D15}$$

The phase angle is defined as $\phi = (\omega t)_1 - (\omega t)_2$ as illustrated in figure D4.
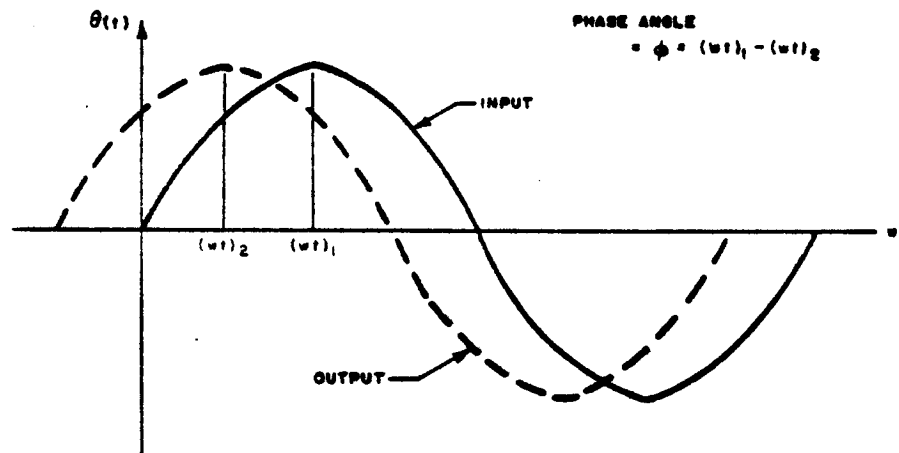
65-6192

Figure D4 ILLUSTRATION OF PHASE ANGLE DEFINITION

The sketch of this figure is for a positive phase angle; from equation (D15), it is apparent that the phase angle is positive for the Model I and II resis-tojet control systems. A positive phase angle means the response "leads" the input as illustrated in figure D4; hence, the expression "lead network".

The lead network response has been calculated and plotted for several values of a and τ_L. In figures D5 and D6, the ratio of output peak mag-nitude to input peak magnitude and the phase angle respectively are pre-sented as a function of the dimensionless frequency, $\tau_L \omega$, for a's of 10, 20, and 30. The amplitude ratio at large frequencies is seen to be equal to a and drops to one at low frequencies. The point at which the peak amplitude ratio is approached occurs for a constant $\tau_L \omega$ of about 2π for all a's or when:

Figure D5 RATIO OF PEAK OUTPUT MAGNITUDE TO PEAK INPUT MAGNITUDE
VERSUS DIMENSIONLESS FREQUENCY

DIMENSIONLESS FREQUENCY, $T_L w$ (w = 2π FREQUENCY)

$$G = \frac{\text{PEAK MAGNITUDE OF OUTPUT SIGNAL}}{\text{PEAK MAGNITUDE OF INPUT SIGNAL}}$$

65-8193

α = 30
α = 20
α = 10
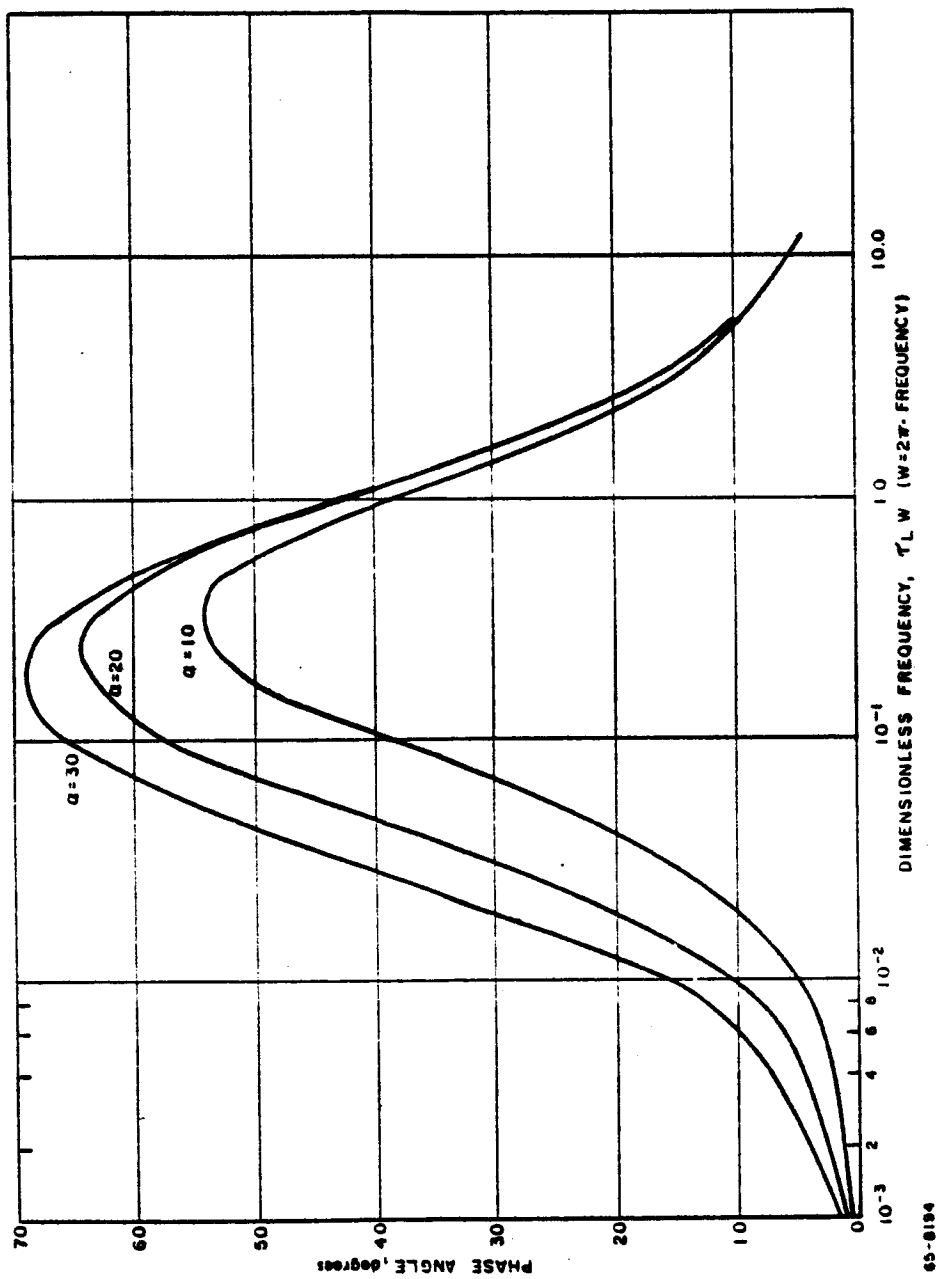
Figure D6 PHASE ANGLE VERSUS DIMENSIONLESS FREQUENCY

65-8194

$$f(G \to a) \;=\; \frac{\omega}{2\pi} \;=\; \frac{1}{\tau_L} \tag{D16}$$

At the low frequencies, the point at which the amplitude ratio approaches one is dependent on a as well as τ_L and can be obtained by expanding equation (A.14) and throwing away higher order terms:

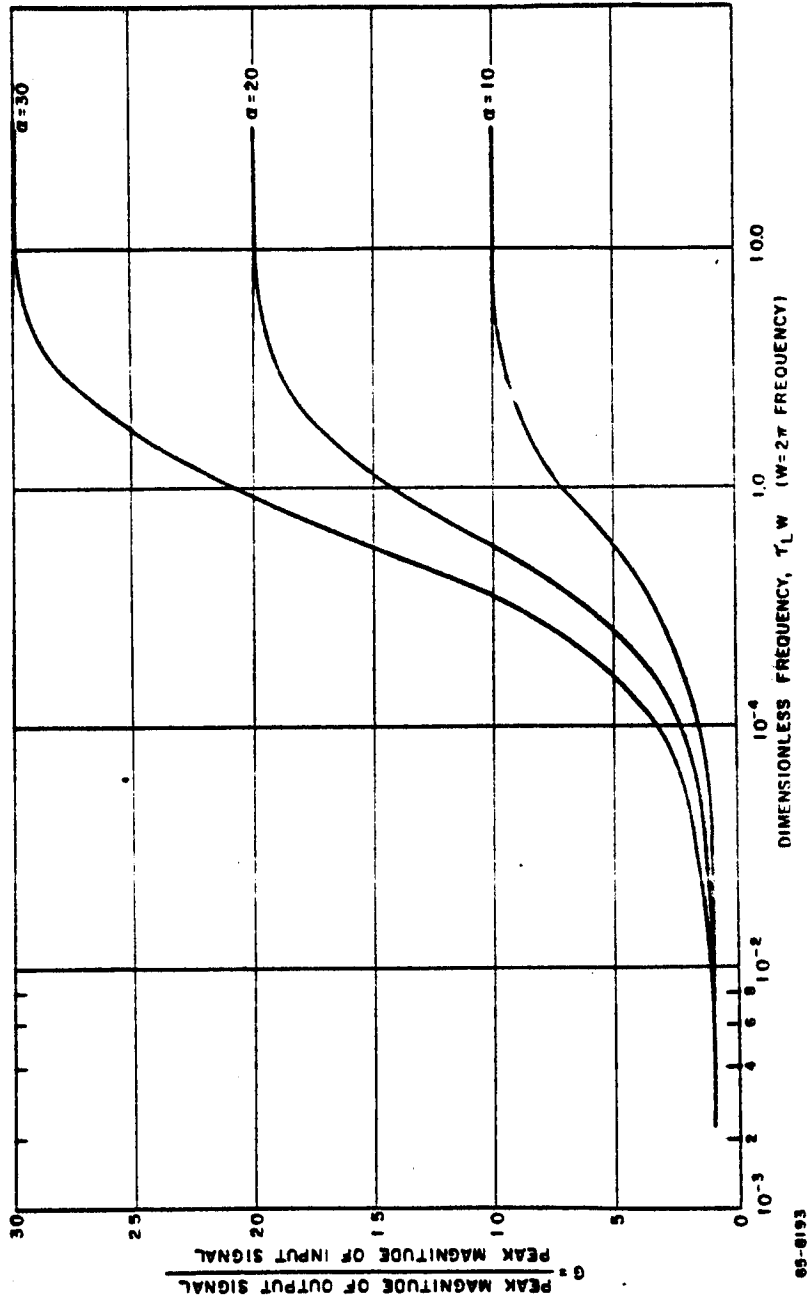$$G \;\cong\; \sqrt{1 + (a\,\tau_L\,\omega)^2} \quad,\quad \tau_L\,\omega \ll 1 \tag{D17}$$

For different a's, the amplitude ratio thus has the same value when:

$$a\,\tau_L\,\omega \;=\; \text{Constant} \tag{D18}$$

or when:

$$f \;=\; \frac{\omega}{2\pi} \;=\; \frac{\text{Constant}}{2\pi\, a\, \tau_L} \tag{D19}$$

From figure A.5, $G = 1.4$ with $\tau_L\,\omega = 0.1$ and $a = 10$; the constant in the above equations for this G is thus $a\tau_L\,\omega = 1$ and:

$$f(G \to 1) \;=\; \frac{1}{2\pi\, a\, \tau_L} \tag{D20}$$

From figure D6, it is apparent that the phase angle increases with increasing a. Also, the frequency of peak phase angle lowers by about a factor of 2 as a is increased from 10 to 30.

The preceding plots illustrated the effect of a; in figure D7, the amplitude ratio is plotted versus cycle time for an a of 10 and for τ_L's of 2 and 5 seconds. The effect of increasing τ_L is to increase the limit cycle time (or decrease the frequency) at which the response of the lead network is strongly rate dependent. In figure A.8, the amplitude ratio is plotted versus ω for an a of 20 and τ_L's of 1, 2, and 5 seconds.

3. CIRCUIT FOR LEAD NETWORK

The control circuit with the transfer function given by equation (D1) consists basically of two resistors and one capacitor wired as illustrated in figure D9. The transfer function of this circuit is

$$\frac{V_{bc}(s)}{V_{ac}(s)} \;=\; \frac{1}{a}\,\frac{1 + a\,\tau_L\,s}{1 + \tau_L\,s} \tag{D21}$$

where

$$a \;=\; 1 + \frac{R_1}{R_2} \tag{D22}$$
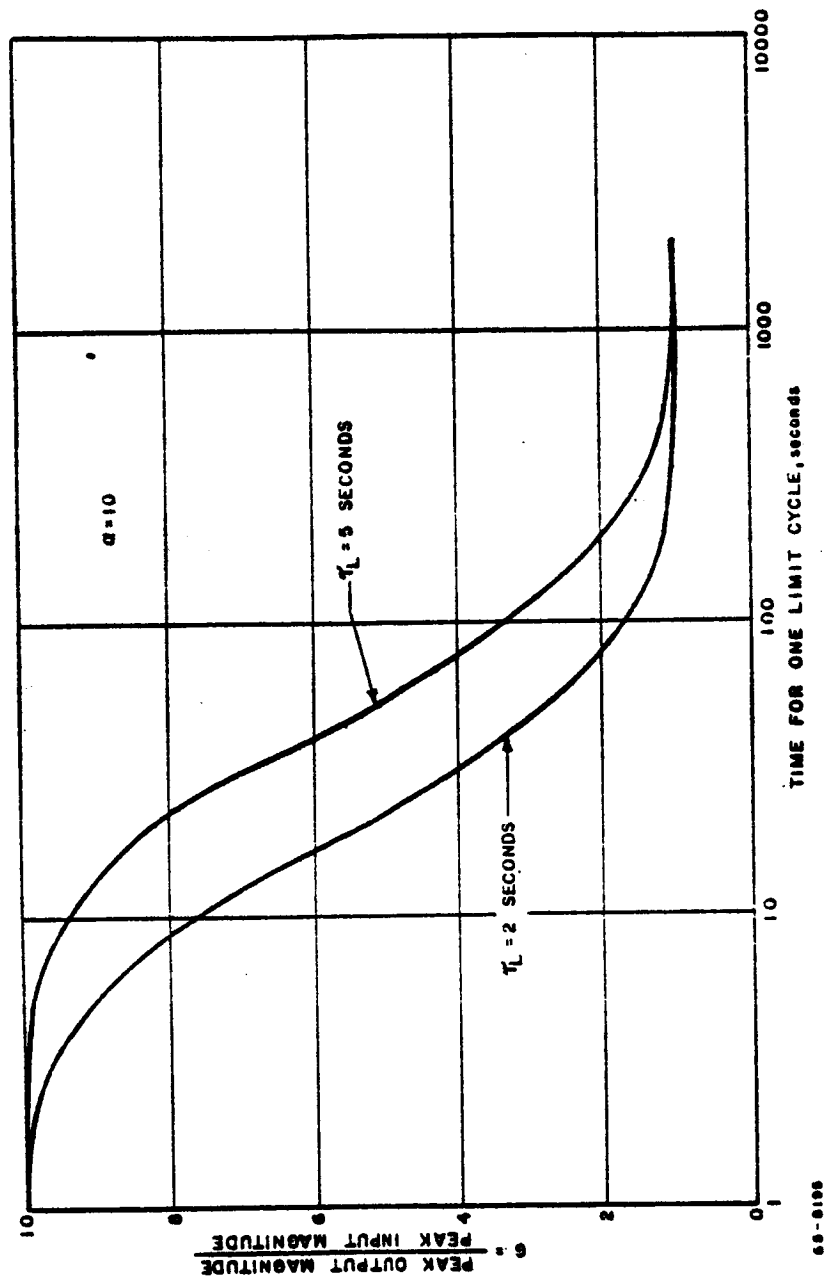
Figure D7 RATIO OF PEAK OUTPUT MAGNITUDE TO PEAK INPUT MAGNITUDE VERSUS
TIME OF ONE CYCLE
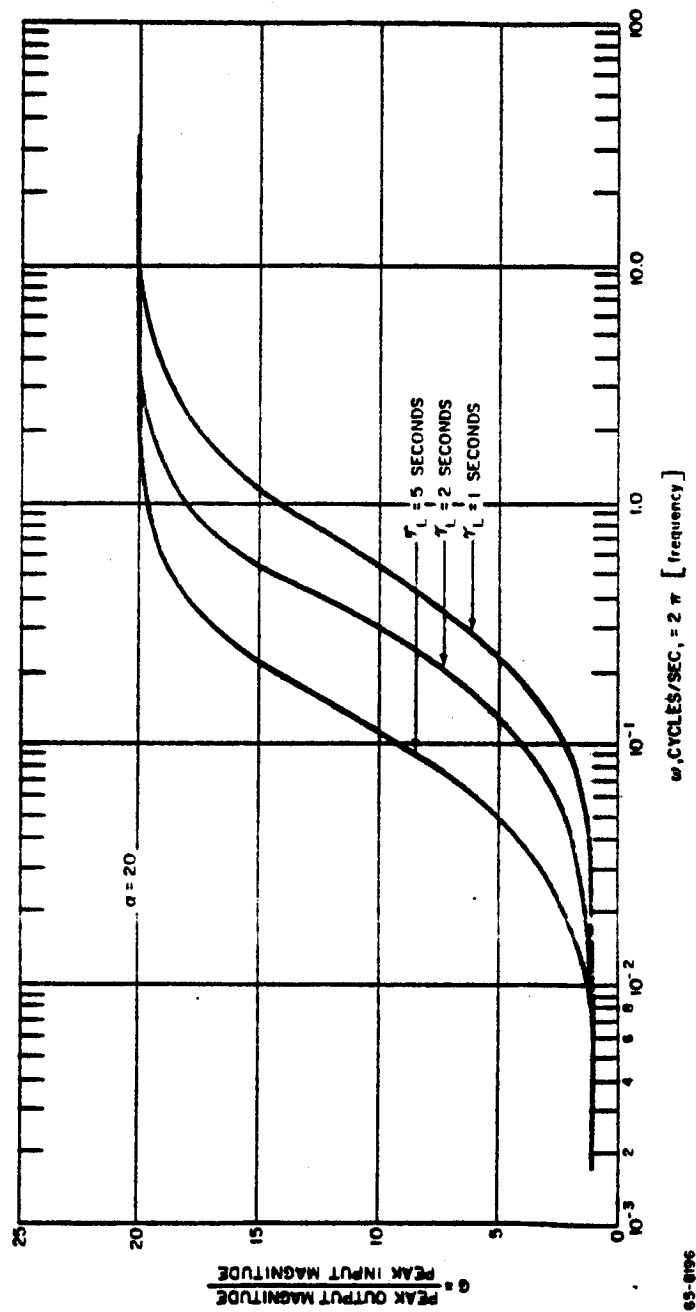
Figure D8 RATIO OF PEAK OUTPUT MAGNITUDE TO PEAK INPUT MAGNITUDE
VERSUS ω

65-8196

-D14-
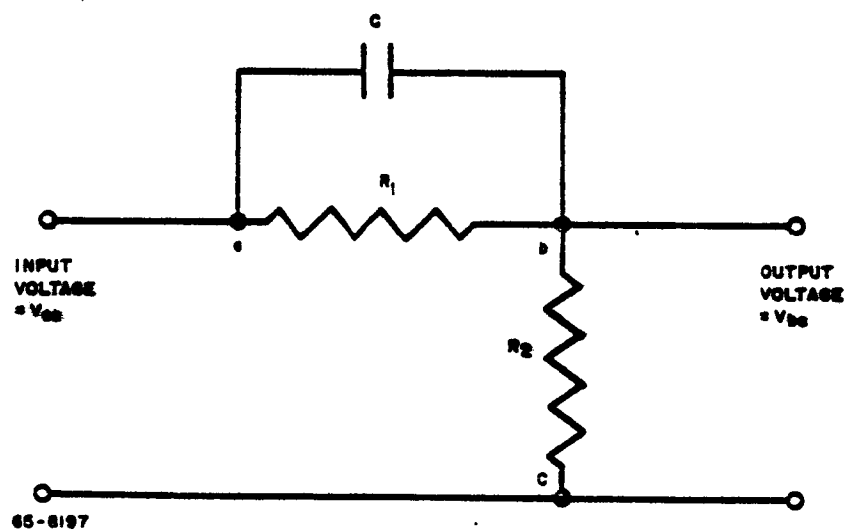
Figure D9 CIRCUIT FOR LEAD NETWORK

$$\tau_L = \frac{R_2 R_1}{R_1 + R_2} C \qquad\qquad\qquad\text{(D23)}$$

This transfer function is identical to that of equation (D1) if an amplifier with a gain of a is added to the input. For the control logic of the Model I and Model II systems, nominal characteristics are:

$C \quad = \quad 100$ microfarads

$R_1 \quad = \quad 200,000 \; \Omega$

$R_2 \quad = \quad 22,000 \; \Omega$

Substitution gives

$a \quad = \quad 10.09$

$\tau_L \quad = \quad 1.982$ seconds

as the nominal lead network constants for the Model I and II resistojet attitude control systems.

APPENDIX E

ANALOG CALCULATIONS OF DUTY CYCLE
VERSUS DISTURBANCE TORQUE

1. INTRODUCTION

To determine more precisely the effect of disturbance torque on the duty cycle for the Model I and II resistojet attitude control systems, additional analog computer calculations have been performed. These calculations were performed for two acquisition angles, 2.25 and 3.40 degrees, with the following other variables:

τ_R = control torque = 0.6×10^{-3} ft-lb = 8130 dyne-cm

J = moment of inertia = 27 slug ft^2

H = hysteresis of switching network = 15 percent

a = lead network constant = 10

τ_L = lead network constant = 2 seconds

t_R = fixed pulse duration for control by inner lines = 4 seconds

For these calculations, three output plotters were used. Two x-y plotters were used, one with a scale to follow in the phase plane the acquisition and the other with a blownup scale to follow in great detail in the phase plane the limit cycle performance. The third plotter was a strip chart recorder on which the following variables were continuously plotted throught a run:

Error Signal

Angular Acceleration, $d^2\theta/dt^2$

Angular Rate, $d\theta/dt$

Angular Error, θ

Total Time

In figures E1, E2 and E3, typical plots from a run are presented.

Figure E1 VEHICLE ACQUISITION IN THE PHASE PLANE

-E2-

Figure E2 VEHICLE LIMIT-CYCLE CONTROL IN THE PHASE PLANE

Figure E3 STRIP CHART RECORD OF SYSTEM PERFORMANCE

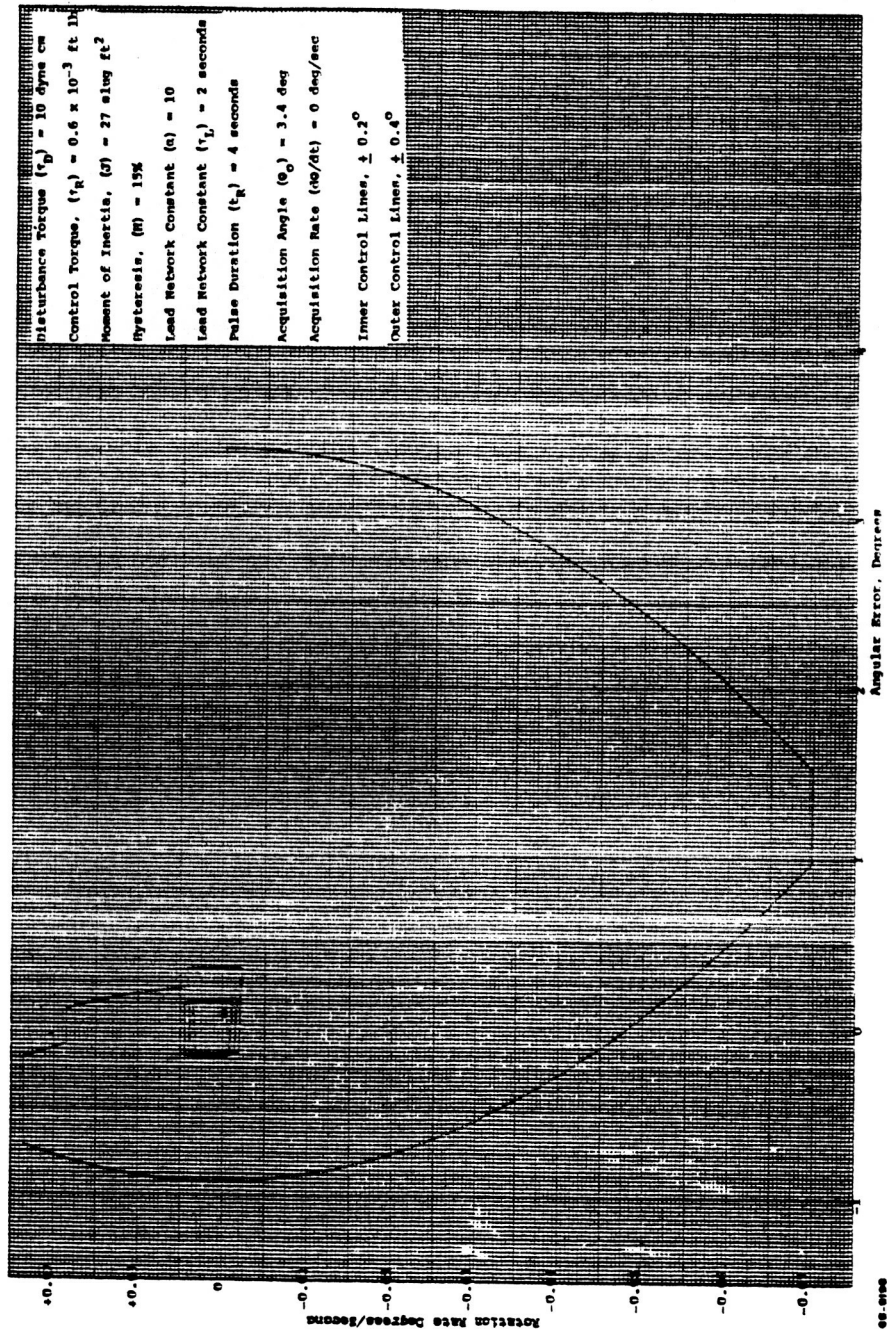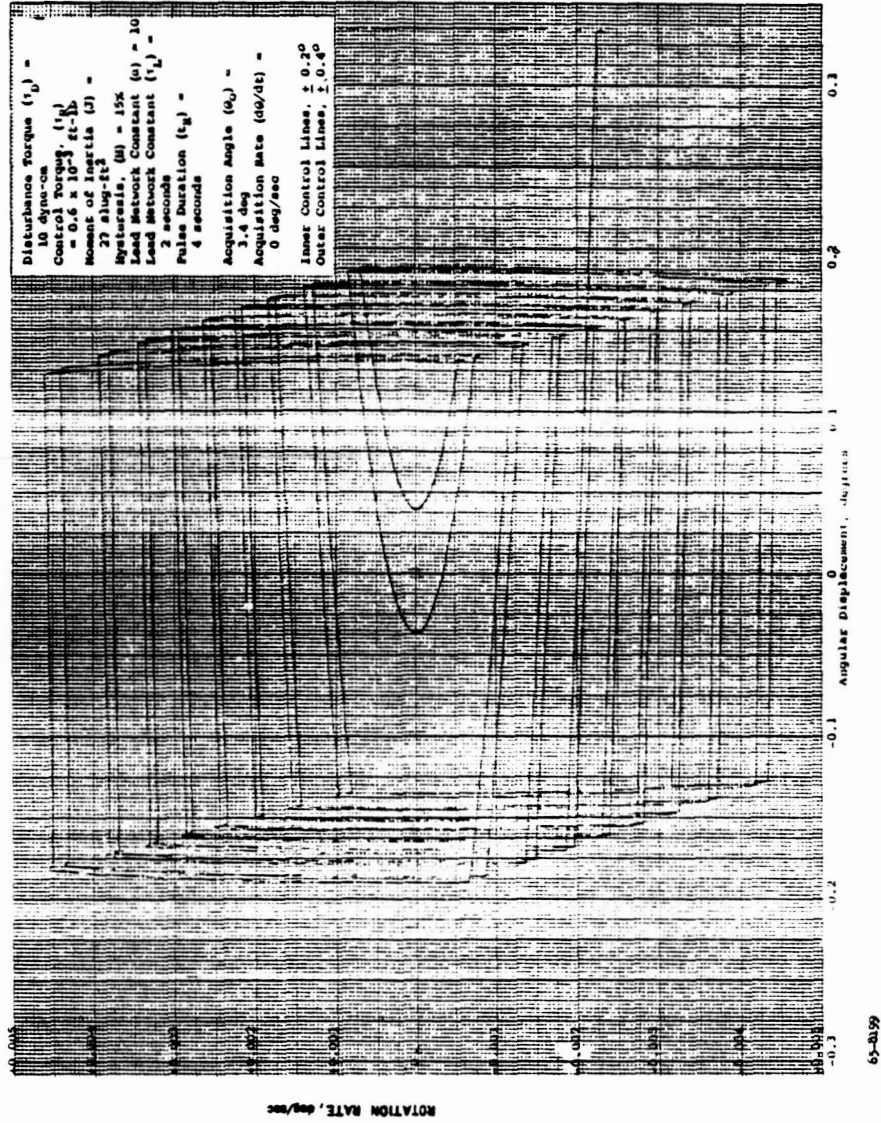## 2. LIMIT-CYCLE PERFORMANCE AS FUNCTION OF DISTURBANCE TORQUE

From the strip chart record, the duty cycle for all runs was calculated; the duty cycle as a function of disturbance torque is presented in figures E4 and E5 for acqusition angles of 3.4 and 2.25 degrees, respectively. The most striking feature of these plots is that real discontinuities exist in the plots of duty cycle versus disturbance torque. In some cases, a change in the disturbance torque of as little as 0.25 dyne-cm resulted in a change in the duty cycle of two to three at the boundary between soft and hard limit-cycle operation. As the disturbance torque decreased, the frequency of occurrence of these discontinuities increases but their amplitude decreases.

The reason for these discontinuities can be seen with reference to some limit-cycle plots for the case of 3.4-degree acquisition angle. In figures E6 and E7 , the phase plane plots are given for disturbance torques of 110 and 90 dyne-cm, between which the control goes from soft limit-cycle control to hard-limit control consisting of basically one hard-limit cycle coupled with one soft-limit cycle. From disturbance torques of 90 to 39, no discontinuities occur and the duty cycle decreases from a peak value of 0.0374 at 100 dyne-cm to 0.0135 at 38 dyne-cm. The limit-cycle plots for disturbance torques of 70, 39, and 37 are presented in figures E8 , E9 , and E10 . For a disturbance torque of 70, the soft limit-cycle branch is larger than at 90 dyne-cm resulting in a decreased duty cycle. In both of these cases, the cycle is slowly nulling to a limit cycle which would retrace itself and have the shape illustrated in figure E11 .

At 39 dyne-cm, the solf-limit part of the cycle has almost reached the opposite control line. The system is now much slower nulling than for the higher disturbance torques (70 and 90); thus, if the run were continued long enough, the two soft-limit and hard-limit branches would approach one another and merge into one retraceable cycle similar to that sketched in figure E11 , except with a larger soft limit-cycle branch.

As the disturbance torque is reduced slightly below 39 dyne-cm, a point is reached where the soft-limit branch just reaches the opposite control line and triggers the opposing resistojet. When this occurs, a step increase in the duty cycle occurs. For a disturbance torque of 37 dyne-cm, this has occurred and a completely different type of limit cycle control occurs. Comparison of the limit cycles for 37 and 39 dyne-cm illustrates dramatically the difference 2 dyne-cm of disturbance torque can make. For 37 dyne-cm, the cycle has not nulled, but appears to be nulling to a cycle with one soft limit branch and two hard-limit branches for a repeating cycle.
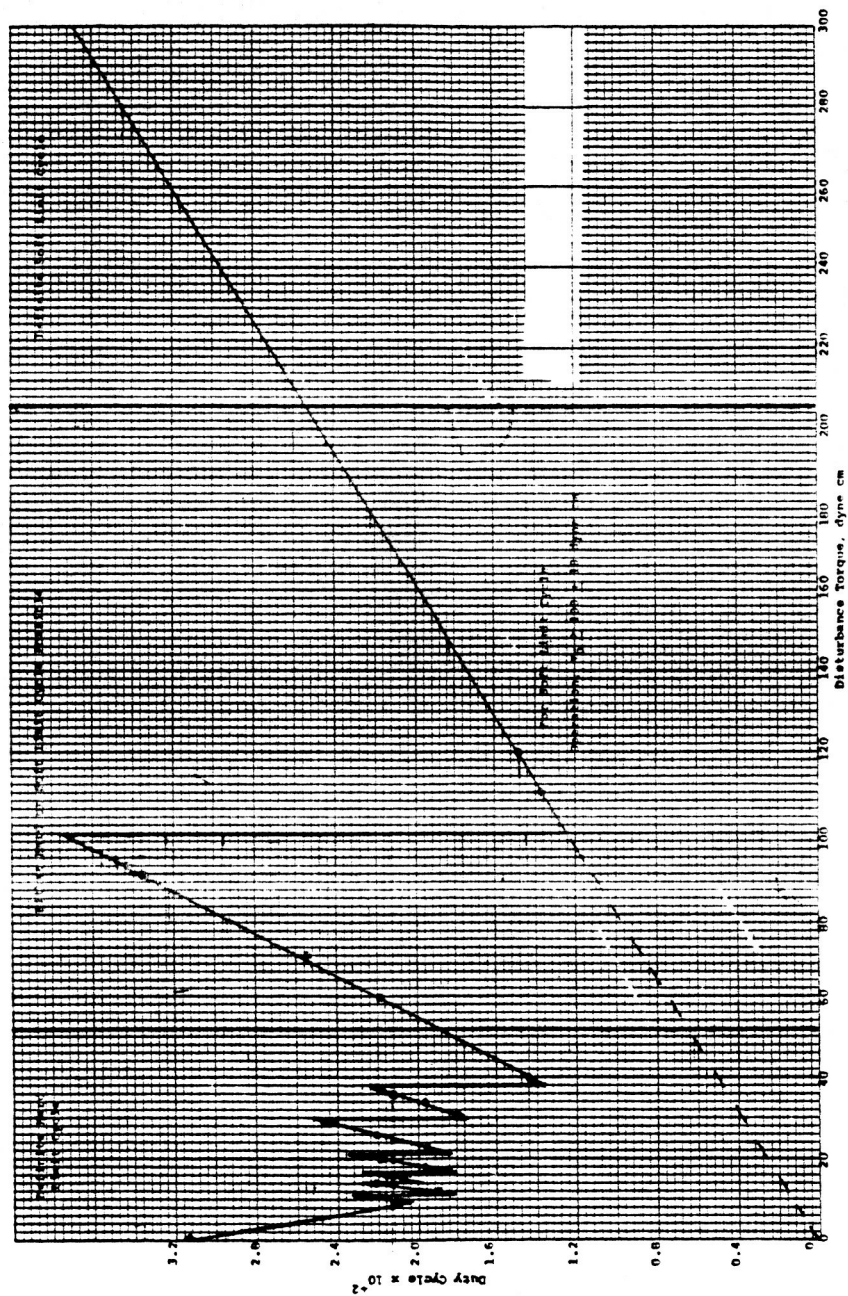
Figure E4 DUTY CYCLE VERSUS DISTURBANCE TORQUE, $\rho_o = 3.4$ DEGREES, $\dot{\rho}_o = 0$
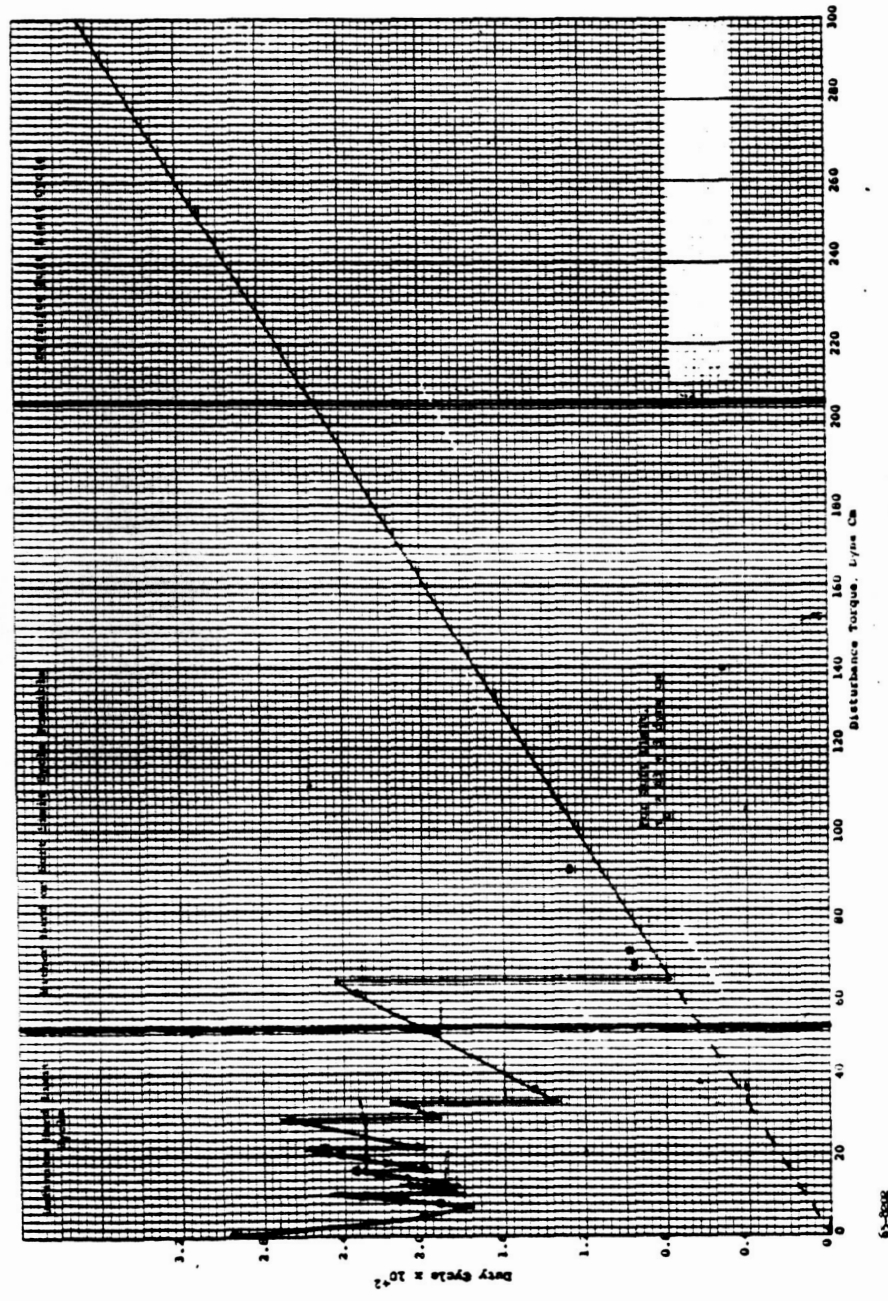
Figure E5 DUTY CYCLE VERSUS DISTURBANCE TORQUE, $\theta_0 = 2.25$ DEGREES, $\dot{\theta}_0 = 0$
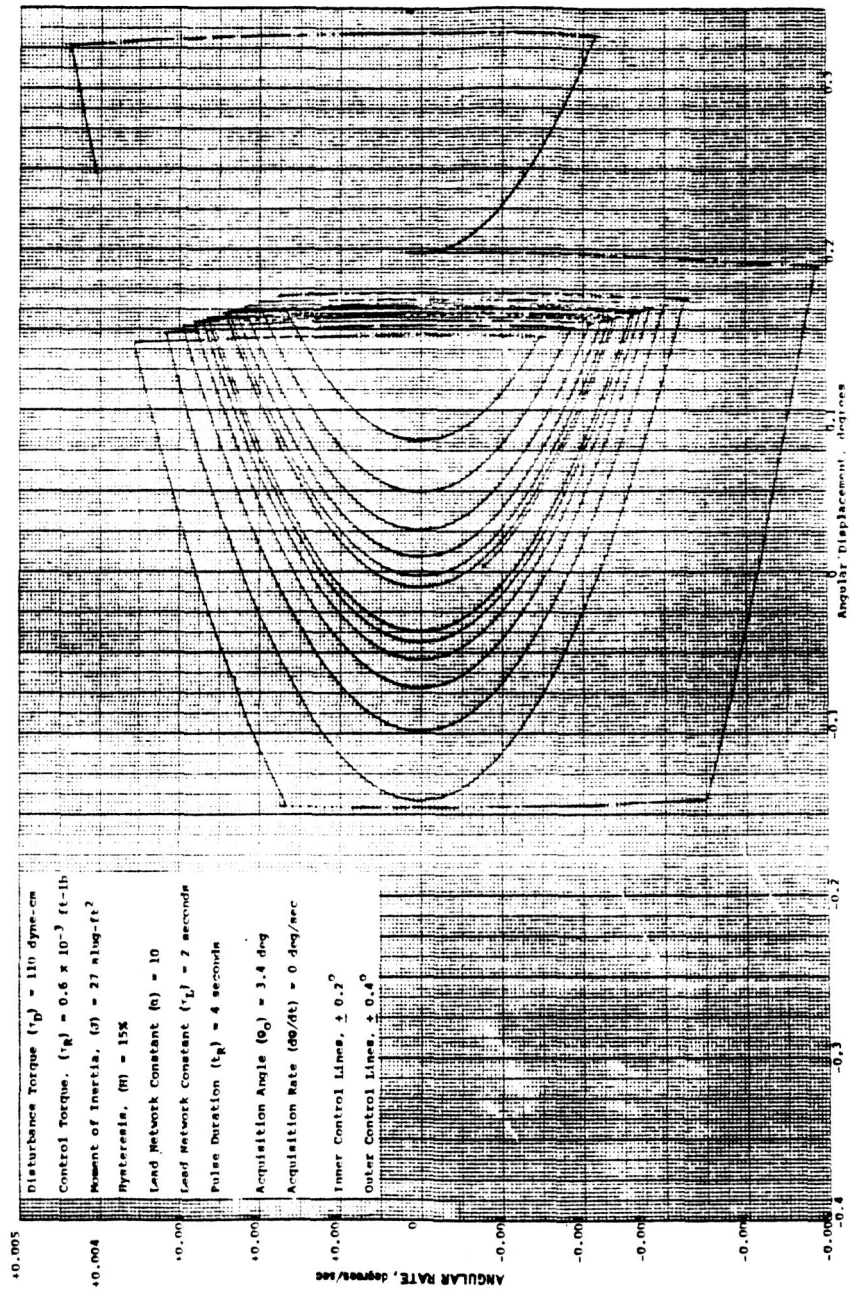
Figure E6 LIMIT CYCLE FOR DISTURBANCE TORQUE OF 110 DYNE-CM

Disturbance Torque (τ_D) = 110 dyne-cm

Control Torque, (τ_R) = 0.6 x 10^{-3} ft-lb

Moment of Inertia, (J) = 27 slug-ft^2

Hysteresis, (H) = 15%

Lead Network Constant (n) = 10

Lead Network Constant (τ_L) = 7 seconds

Pulse Duration (t_R) = 4 seconds

Acquisition Angle (θ_0) = 3.4 deg

Acquisition Rate (deg/ft) = 0 deg/sec

Inner Control Lines, ± 0.2°

Outer Control Lines, ± 0.4°

Angular Displacement, degrees

ANGULAR RATE, degrees/sec

65-B203

Figure E7 LIMIT CYCLE FOR DISTURBANCE TORQUE OF 50 DYNE-CM

Disturbance Torque (T_D) = 50 dyne-cm

Control Torque, (T_R) = 0.6 x 10^{-3} ft-lb

Moment of Inertia, (J) = 27 slug-ft^2

Hysteresis, (H) = 15%

Lead Network Constant (α) = 10

Lead Network Constant (T_L) = 2 seconds

Pulse Duration (t_R) = 4 seconds

Acquisition Angle (θ_a) = 3.4 deg

Acquisition Rate $(d\theta/dt)$ = 0 deg/sec

Inner Control Lines, $\pm$ 0.2°

Outer Control Lines, $\pm$ 0.4°

ANGULAR RATE, deg/sec

Angular Displacement, degrees

65-86A

Figure E9 LIMIT CYCLE FOR DISTURBANCE TORQUE OF 70 DYNE-CM

Disturbance Torque (T_D) = 70 dyne-cm

Control Torque, (T_R) = 0.6 x 10^{-3} ft-lb

Moment of Inertia, (J) = 27 slug-ft^2

Hysteresis, (H) = 15%

Lead Network Constant (a) = 10

Lead Network Constant (T_L) = 2 seconds

Pulse Duration (t_R) = 4 seconds

Acquisition Angle (θ_0) = 3.4 deg

Acquisition Rate (dθ/dt) = 0 deg/sec

Inner Control Lines, ± 0.2°

Outer Control Lines, ± 0.4°

Angular Displacement, degrees

ANGULAR RATE, deg/sec

65-8008

-E10-

Figure E9 LIMIT CYCLE FOR DISTURBANCE TORQUE OF 39 DYNE-CM

-E11-

Figure E10 LIMIT CYCLE FOR DISTURBANCE TORQUE OF 37 DYNE-CM
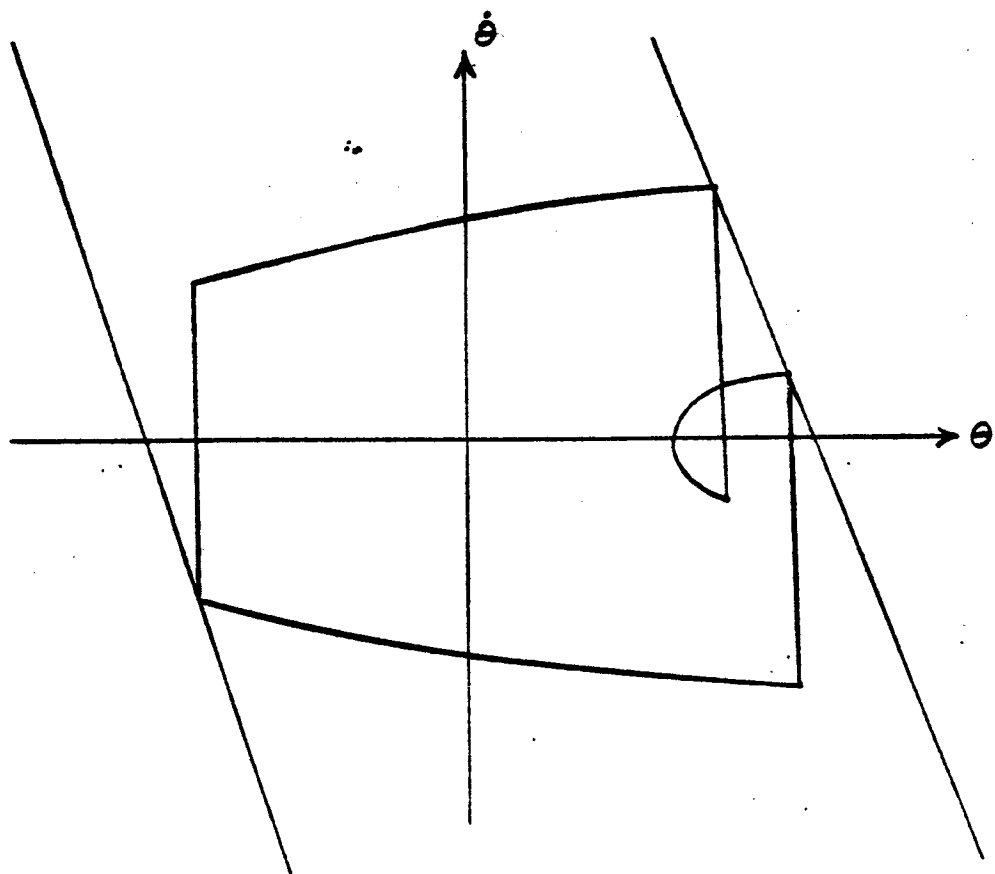
Figure E11 SKETCH OF NULLED LIMIT CYCLE

For lower disturbance torques, very complex cycles are obtained. In figure E2, for example, a plot is presented of a complete repeating cycle for a disturbance torque of 10 dyne-cm. The complete repeating cycle consists of two soft-limit branches and 16 hard-limit branches.
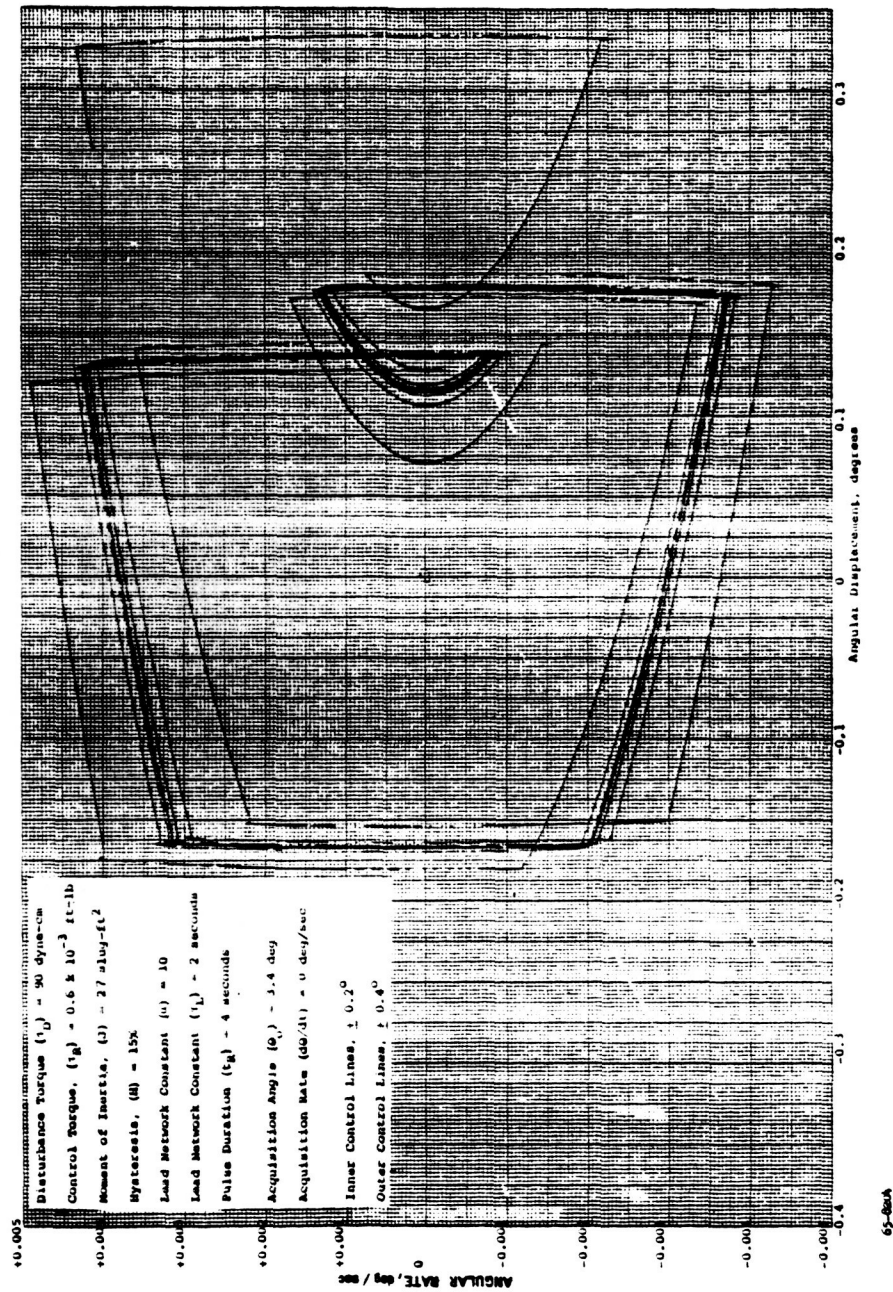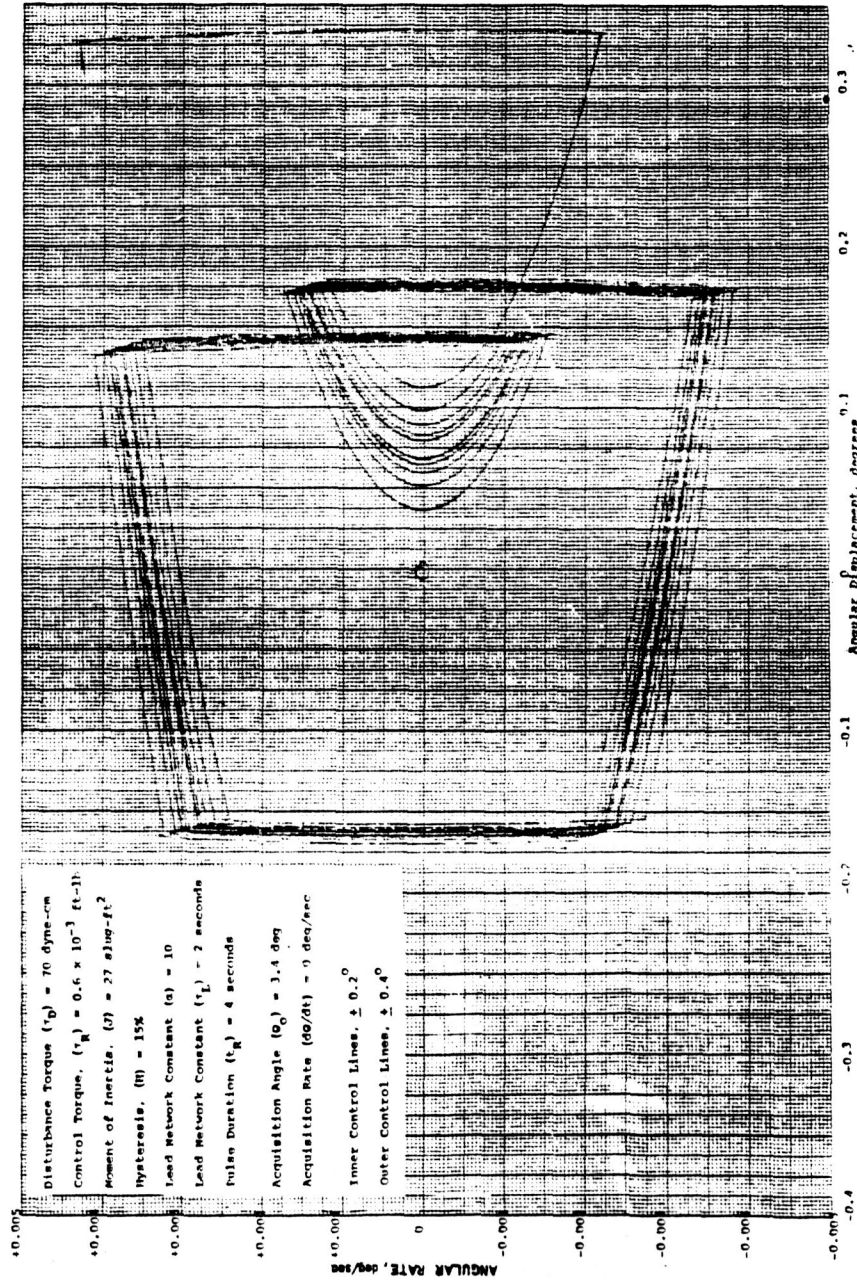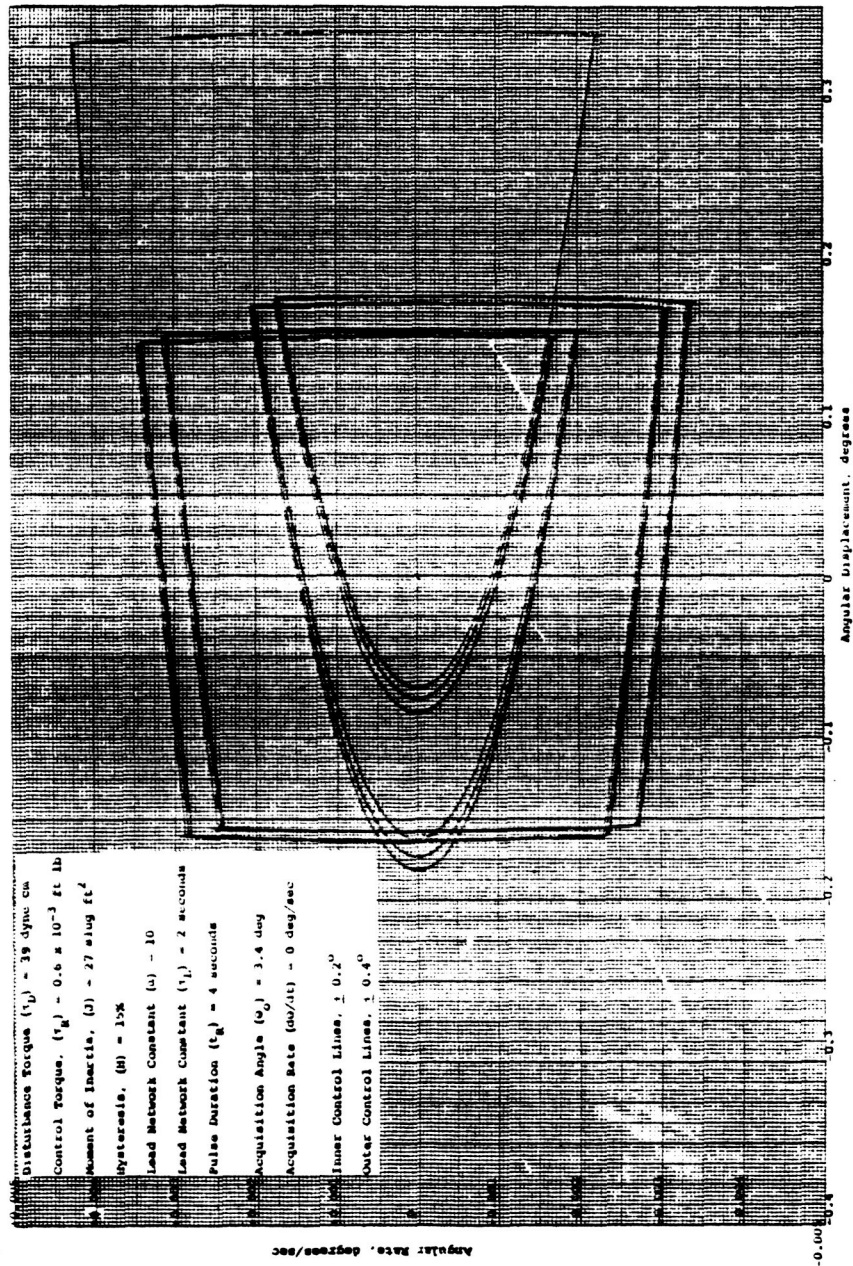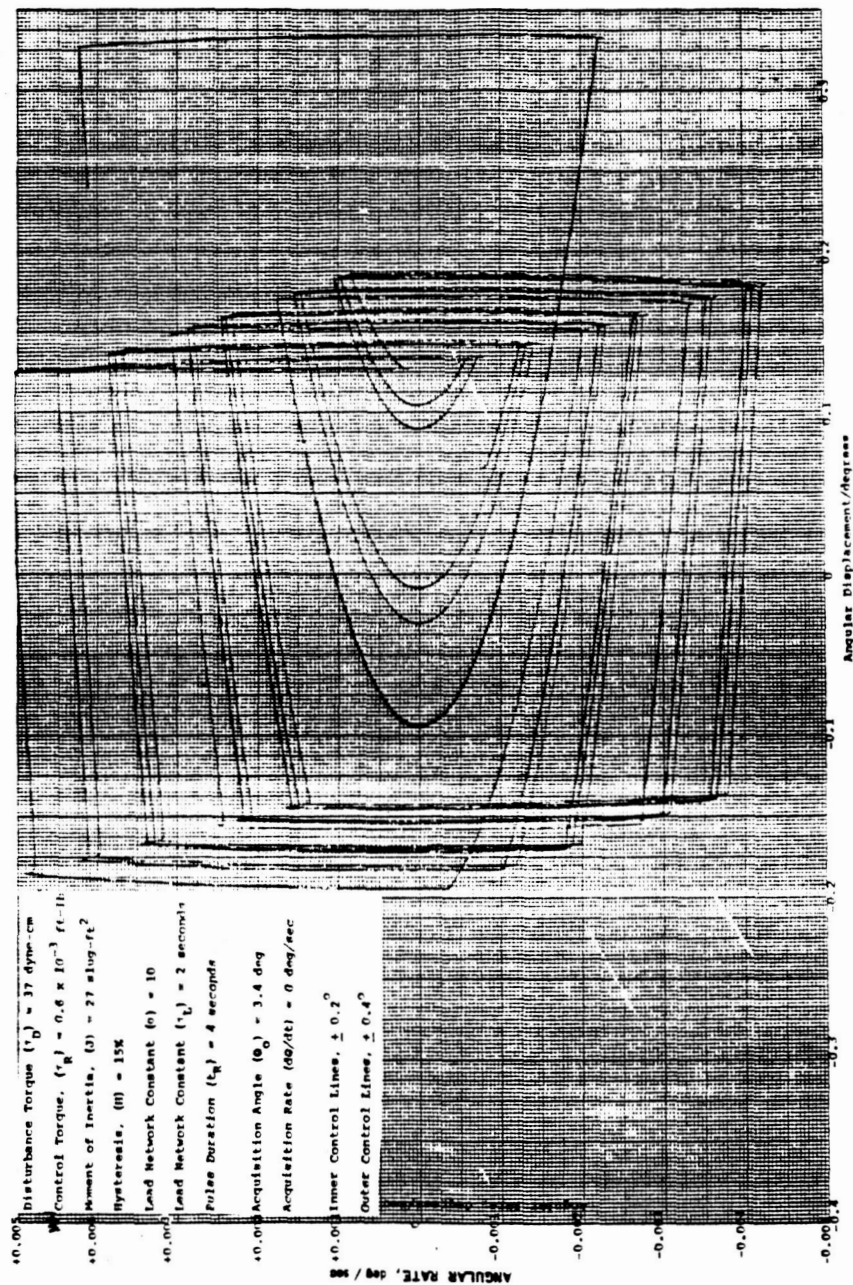
The limit cycle for zero disturbance torque always consists of one repeating hard-limit cycle as would be expected and as illustrated in figure E12.

Comparison of figures E4 and E5 illustrates the effect of acquisition angle on the disturbance torque at which control changes from soft limit-cycle control to hard-limit control. In both plots, the regions of definite hard limit and definite soft limit-control are presented. It is seen that at an acquisition angle of 2.25 degrees, soft-limit cycle is maintained down to 63 ± 3 dyne-cm, while for an acquisition angle of 3.40 degrees, the limit cycle changes from soft to hard at a disturbance torque of 100 ± 10 dyne-cm. The maximum duty cycle is 0.0374 for $\theta_o = 3.4$ degrees, whereas it is only. 0.0294 for $\theta_o = 2.25$ degrees.
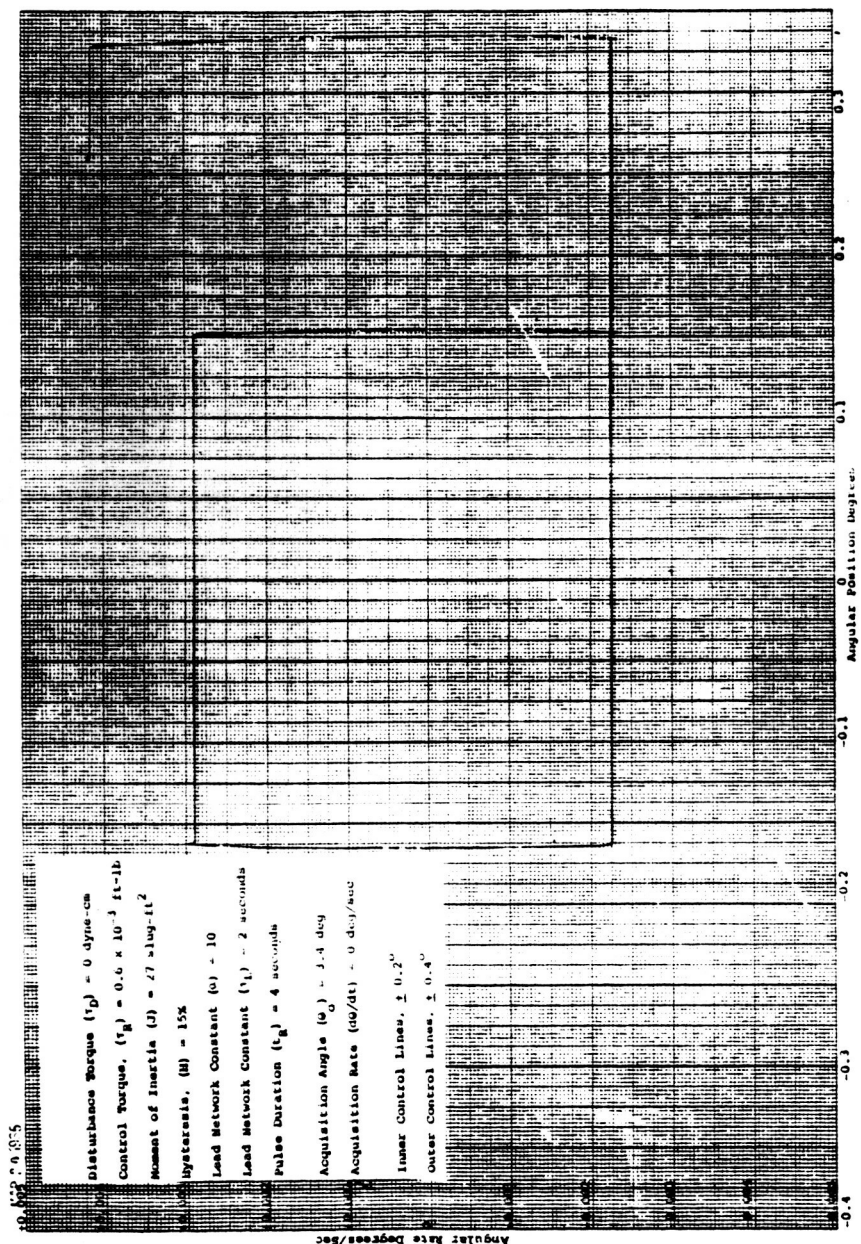
Figure E12 LIMIT CYCLE FOR DISTURBANCE TORQUE OF ZERO DYNE-CM

APPENDIX F

PERFORMANCE OF THE SINGLE AXIS RESISTOJET ATTITUDE
CONTROL SYSTEM ON THE IMPULSE BALANCE

The impulse balance is attractive for checkout of single-axis ACS because of the possibility of systematically varying the acquisition angle, $\theta_{initial}$, acquisition rate, $\dot{\theta}_{initial}$, and disturbance torque, τ_D . In the present test setup, data are transmitted from the table by lightweight wires; the number of wires and thus the amount of data which can be transmitted must be held to a minimum because of the possibility of introducing disturbance torques into the system. For the initial tests only the clockwise and counterclockwise valve signals, and the angular position and total angular error signals have been transmitted.

Figure F1. illustrates a hard-limit cycle, obtained on the impulse table for a negligible disturbance torque ($\tau_D \approx 0$ dyne-cm), and a control thrust of about 124×10^{-6} pound.

HARD LIMIT CYCLE

TABLE MOMENT OF INERTIA 28 lb ft sec²

DISTURBANCE TORQUES   0 dyne cm

THRUST LEVEL   124 µlb

INNER CONTROL LINES ± 0.2 deg rate

CHANNEL 1   VALVE SIGNAL (CLOCKWISE)

CHANNEL 2   VALVE SIGNAL (COUNTERCLOCKWISE)

CHANNEL 3   TABLE TOTAL ERROR θ(t) + dθ(t)/dt
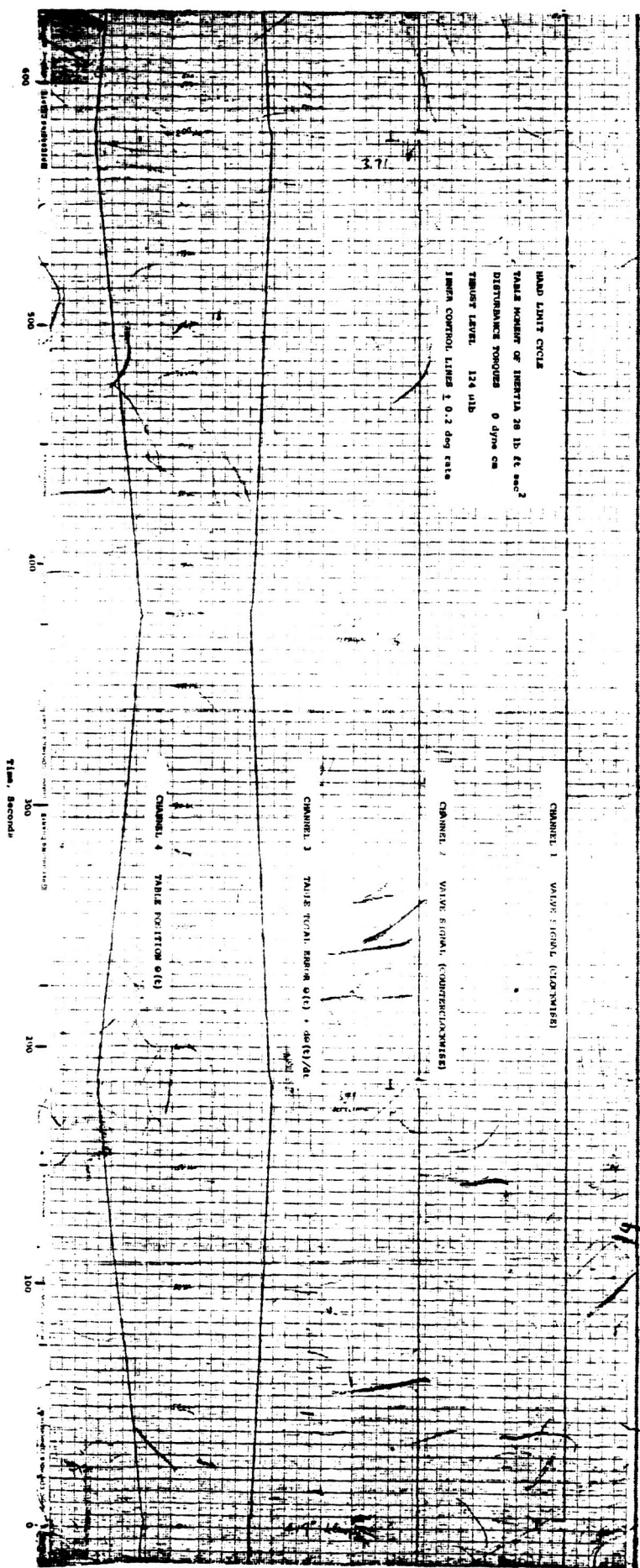
CHANNEL 4   TABLE POSITION θ(t)

Time, Seconds

Figure F1   RECORD OF SINGLE-AXIS RESISTOJET ACS TEST ON IMPULSE BALANCE

F2A

APPENDIX G

ADAPTIVE ATTITUDE CONTROL SYSTEM

1. INTRODUCTION AND BACKGROUND

The disturbance torque which a satellite will encounter cannot be predicted with any precision at the present time. Thus, the attitude control system must be designed to handle a range of disturbance torques extending from zero up to some estimated maximum possible disturbance torque which represents with a high degree of confidence the maximum disturbance torque the system could possibly receive. The objective of an ACS design evaluation is to arrive at the system which provides attitude control over the entire mission duration with a minimum total system mass and maximum reliability. As will be discussed below, this objective requires an adaptive control system, that is, one which automatically changes certain system parameters to provide satisfactory limit cycle operation of the system regardless of what the actual disturbance torque may be.

The adaptive control system should thus be designed to insure that (1) the propellant mass is sufficient for the entire mission for whatevever disturbance torque is encountered between zero and the estimated maximum possible value, and (2) the pulsing frequency of the system is minimized.

The need for an adaptive control system is further illustrated by figure G1 . where a typical plot of duty cycle versus disturbance torque is sketched. With the control torque fixed, the fixed pulse duration for control on the inner lines would be set at a value to give soft limit cycle operation with a minimum pulsing rate with the maximum possible disturbance torque. Analog computer simulation of the control system would then be used to generate the curve of figure G1 . The design point as illustrated is for soft limit cycle operation with the maximum possible disturbance torque. The duty cycle on which the propellant consumption rate, and hence propellant mass required for the entire mission, is based is $(D_{SL})_{max}$. At some disturbance torque lower than the maximum possible value, the limit cycle with $(t_R)_{max}$ will jump into hard limit cycle operation with a corresponding large increase in the duty cycle. As illustrated, the duty cycle with no change in thrust characteristics exceeds $(D_{SL})_{max}$ over a large range of disturbance torques, and if no adaptive control action were taken, that is, both the control torque and the pulse duration remained fixed, the propellant mass in the design would have to be based on $(D_{HL})_{max}$ rather than on $(D_{SL})_{max}$. The ratio of $(D_{HL})_{max}$ to $(D_{SL})_{max}$ (or of the propellant masses) might be as much as a factor of 2 to 3 based on analog computer simulation of the control system (see figures E4 and E5 of appendix E).

Adaptive control action for $\tau_D < (\tau_D)_{max}$ can be applied by reducing either or both the control torque and the pulse duration. The discussion below is based
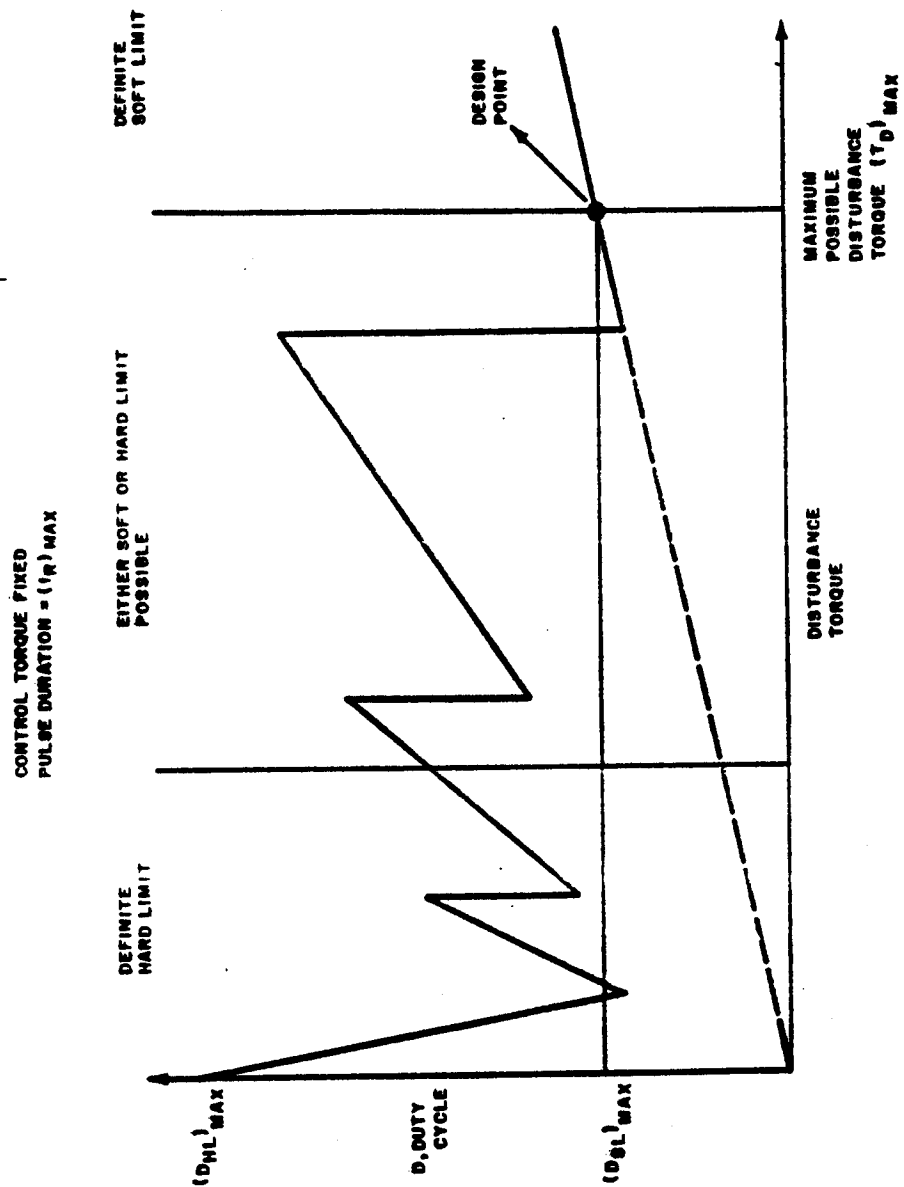
Figure G1 DUTY CYCLE VERSUS DISTURBANCE TORQUE FOR MAXIMUM PULSE DURATION

65-8211

-G2-

on reduction of the pulse duration as the adaptive control mechanism with a fixed control torque. In figure G2, the variation of duty cycle with disturbance torque is illustrated for three pulse durations with the control torque fixed. The curve for $(\tau_R)_{max}$ is the same as that sketched in figure G1. If a disturbance torque of $(\tau_D)_2$ were encountered and no change made in τ_R, a duty cycle of $(D_{HL})_2 > (D_{SL})_{max}$ would occur which is unacceptable. If the pulse duration were automatically decreased to some value $(\tau_R)_v$, soft limit cycle operation would occur with a disturbance torque of $(\tau_D)_2$ and a duty cycle $(D_{SL})_2 < (D_{SL})_{max}$ would occur which is acceptable. With a pulse duration of $(\tau_R)_v$, however, a lower disturbance torque than $(\tau_D)_2$ could still result in hard limit cycle operation with a duty cycle greater than $(D_{SL})_{max}$. At some pulse duration $(\tau_R)_{min}$, however, the duty cycle for the fixed control torque will not be greater than $(D_{SL})_{max}$ for all disturbance torques. Thus, this pulse duration represents the minimum pulse duration required to insure that a propellant mass based on $(D_{SL})_{max}$ is sufficient for the entire mission. Thus, a possible adaptive control system is one which varies stepwise the pulse duration, $(\tau_R)_v$, between two limits, $(\tau_R)_{max}$ and $(\tau_R)_{min}$. Depending on the particular system, it might be desirable to decrease τ_R below $(\tau_R)_{min}$ to minimize the pulsing frequency for low disturbance torques.

The question might be asked as to why the pulse duration was not preset at a constant value of $(\tau_R)_{min}$ since this insures that the propellant mass based on $(D_{SL})_{max}$ is sufficient for the entire mission. Another consideration of importance from a reliability point of view, however, is the pulsing frequency of the resistojets which should be minimized for maximum reliability. Thus, if the pulse duration were set at $(\tau_R)_{min}$ and the actual disturbance torque were $(\tau_D)_{max}$, the limit cycle would follow a path in the phase plane like that illustrated in figure G3A and the pulsing frequency would be very high.

If the pulse duration were $(\tau_R)_{max}$, however, the path followed would be like that illustrated in figure G3B and the pulsing frequency would be minimized. The pulsing frequency for soft limit cycle operation is given by:

$$f = \frac{\tau_D}{\tau_R \, \tau_R} \tag{G1}$$

and thus, for a fixed τ_D and τ_R, f varies inversely with τ_R so long as soft limit cycle operation is maintained. In addition to this factor, a pulse duration $(\tau_R)_{min}$ might not be sufficient to hold the limit cycle control on the inner lines with a disturbance torque $(\tau_D)_{max}$ and the control would jump to the outer back-up lines.

In summary, an adaptive control system is required if it is desired to minimize the propellant mass required for a given mission and, at the same time, minimize the pulsing frequency of the system for any disturbance torque between zero and an estimated maximum possible disturbance torque.
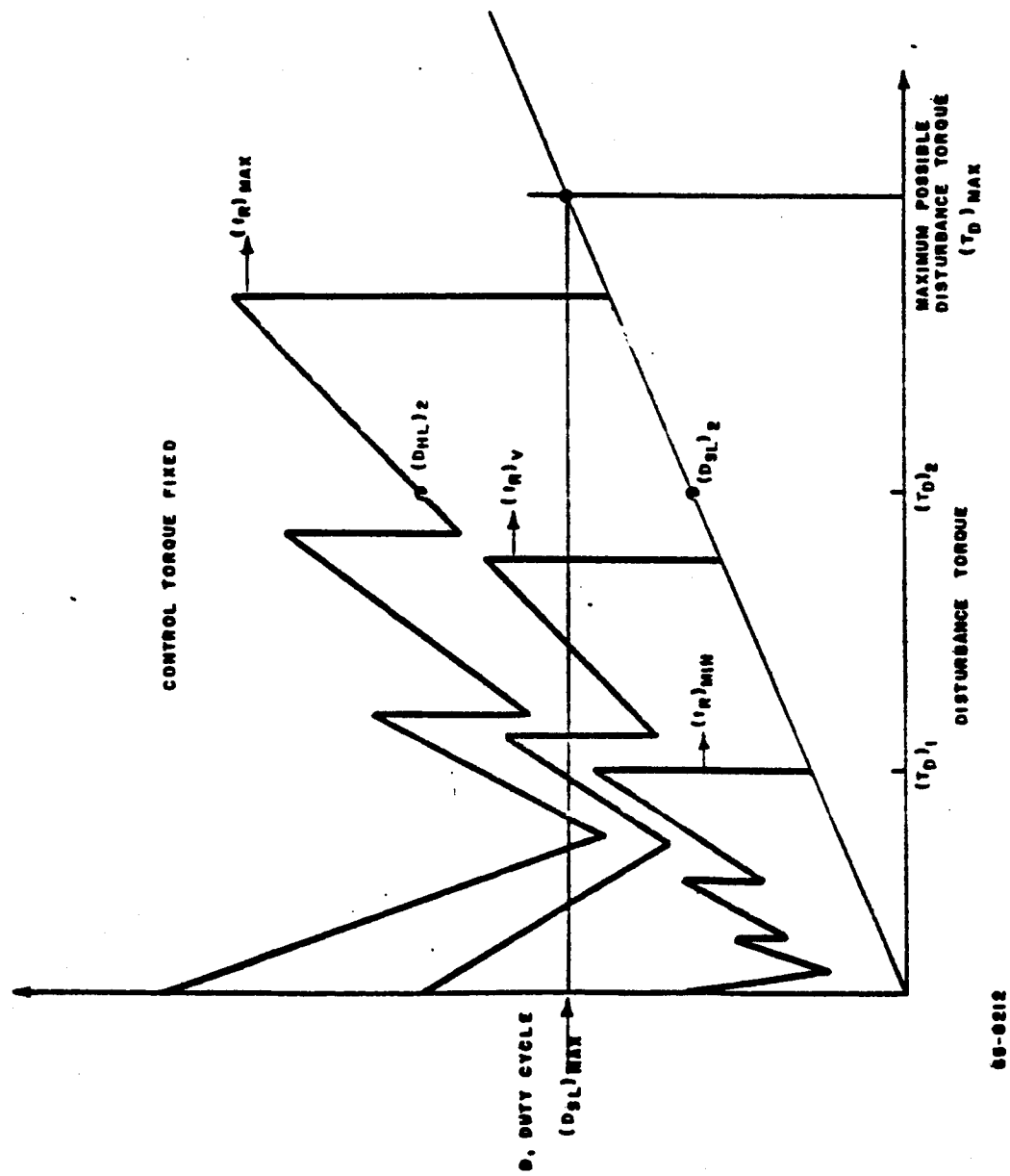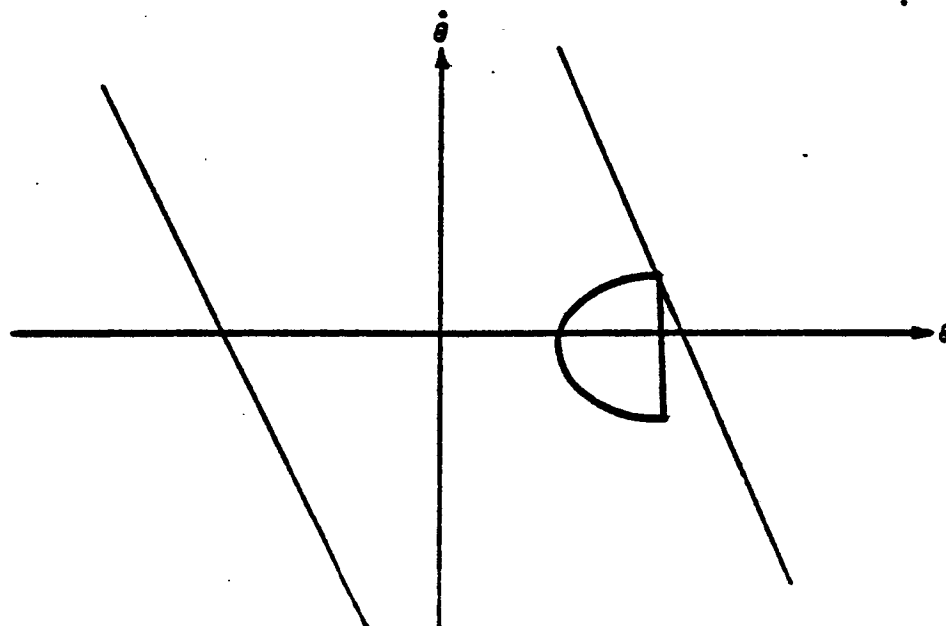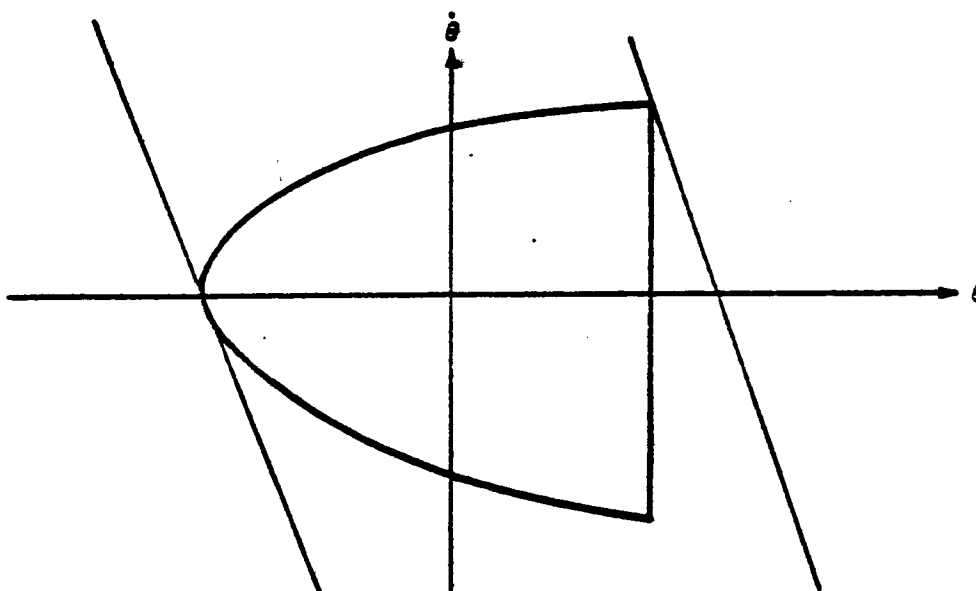
Figure G2 SKETCH ILLUSTRATING MINIMUM PULSE DURATION

68-8812

A. PULSE DURATION = $(t_R)_{MIN}$
DISTURBANCE TORQUE = $(T_D)_{MAX}$

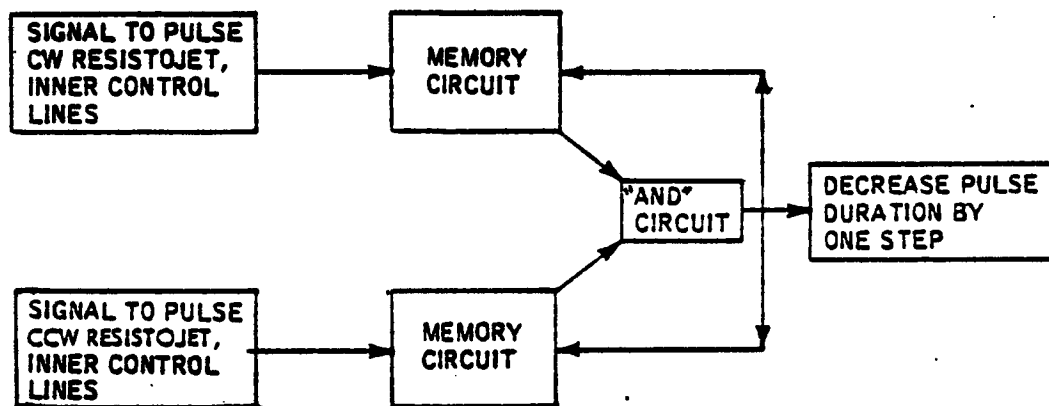B. PULSE DURATION = $(t_R)_{MAX}$
DISTURBANCE TORQUE = $(T_D)_{MAX}$

66-6213

Figure G3   PHASE PLANE PATH FOLLOWED BY SYSTEM WITH DISTURBANCE TORQUE $(T_D)_{MAX}$
AND PULSE DURATIONS OF $(t_R)_{MIN}$ AND $(t_R)_{MAX}$

-G5-

2. PROPOSED ADAPTIVE CONTROL SYSTEM

As discussed above, an adaptive control system is required to insure sufficient propellant mass to fulfill the entire mission and at the same time to minimize the pulsing frequency of the system. The following discussion describes conceptually an adaptive control system for this purpose which would involve some simple additions to the present control logic system as used in the Single Axis Tests. The proposed method involves the stepwise variation of the pulse duration on the inner control lines in response to the mode of resistojet pulsing; the mode of resistojet pulsing in turn depends directly on the disturbance torque for a given set of thrustor characteristics. If preferable, the control action could be variation of the control torque by variation of the plenum pressure or a combination of variation of both the plenum pressure (control torque) and the pulse duration. The pulse duration should be easier to vary however and can be instantaneously changed whereas a decrease in the plenum pressure can be made only gradually as the pressure is reduced by pulsing of the resistojets.

It is assumed that the control torque and maximum pulse duration have been established based on the estimated maximum possible disturbance torque, $(\tau_D)_{max}$. Analog computer calculations have also established a $(t_R)_{min}$ which insures sufficient propellant mass for any disturbance torque between zero and $(\tau_D)_{max}$.

The system during acquisition will have the fixed pulse duration for the inner lines set at the maximum value, $(t_R)_{max}$. This will insure control within the desired error limits, though with a hard limit cycle except for disturbance torques very near $(\tau_D)_{max}$. In the hard limit cycle, the opposing clockwise and counterclockwise resistojets will be pulsed each cycle, an unacceptable condition with a pulse duration of $(t_R)_{max}$. When this occurs, the pulse-on-duration of both resistojets will automatically be decreased by a predetermined amount. A possible circuit to perform this function might conceptually be as illustrated in figure G4. If hard limit cycle operation occurs, both the CW and CCW resistojets will be pulsed. The two memory circuits would then simultaneously pass signals to the "and" circuit which requires both inputs before passing a signal. A signal would then pass to the pulse duration control which would automatically decrease the pulse duration by one step. The memories would simultaneously be erased. If a hard limit cycle still occurred, the above process would be repeated and the pulse duration decreased until either soft limit-cycle operation occurred or the minimum pulse duration, $(t_R)_{min}$ was reached. While $(t_R)_{min}$ would be set at a value low enough to guarantee that the propellant mass was sufficient for the entire mission, it might or might not be desirable to set $(t_R)_{min}$ below this value to minimize the pulsing frequency if very low disturbance torques were encountered. Analog computer calculations would be used to determine a satisfactory value of $(t_R)_{min}$. The minimum possible value of $(t_R)_{min}$ is set by the time for thrust buildup and decay which is about 50 milliseconds for the present system.

SIGNAL TO PULSE CW RESISTOJET, INNER CONTROL LINES → MEMORY CIRCUIT

SIGNAL TO PULSE CCW RESISTOJET, INNER CONTROL LINES → MEMORY CIRCUIT

"AND" CIRCUIT → DECREASE PULSE DURATION BY ONE STEP

65-8214

Figure G4 BLOCK DIAGRAM OF CIRCUIT TO AUTOMATICALLY DECREASE PULSE DURATION BY ONE   STEP WHEN HARD LIMIT-CYCLE OPERATION OCCURS

Suppose now that the system has automatically adjusted t_R either to $(t_R)_{min}$ or to a value where soft limit-cycle operation occurs and an increase in the disturbance torque occurs. This increase in disturbance torque, if no corrective action occurs and the system is in soft limit-cycle operation, produces a decrease in the cycle time resulting in more frequent pulsing. If the disturbance torque becomes sufficiently large, the control may jump out of the inner control lines and transfer to the outer backup lines unless the pulse duration is increased. To handle the situation of a large step increase in the disturbance torque, with transfer of control to the backup lines, the pulse duration produced by the backup lines must always be sufficiently large to handle the estimated maximum possible disturbance torque. Thus, the minimum on-time for a pulse controlled by the backup lines should be set at $(t_R)_{max}$ by selection of the proper value of the lead network delay constant, τ_L. This should insure that control will jump back to the inner control lines even if an unusally large step increase in τ_D occurs so long as τ_D is not larger than $(\tau_D)_{max}$. If the system does jump out of the inner control lines, large disturbance torques will have encountered and t_R on the inner lines should be reset to $(t_R)_{max}$ as illustrated in figure G5.

If the disturbance torque increases slowly or levels off at some higher value, control will not jump out of the inner lines. It will be desirable to increase the pulse duration of the inner lines to minimize the pulsing frequency without leaving soft limit cycle operation. For example, consider the sketch, of figure G6. The limit cycle as sketched with the solid lines would have a very low cycle time and high pulsing rate. The cycle time is given by either:

$$t_t^2 = 8(\theta_c - \theta_o)\left(\frac{\tau_R}{\tau_R - \tau_D}\right)^2 \frac{J}{\tau_D} \tag{G2}$$

or:

$$t_t = t_R \frac{\tau_R}{\tau_D} \tag{G3}$$

It is desirable to increase the pulsing time to give a limit cycle such as that illustrated by the dotted line. As an arbitrary criterion of satisfactory versus unsatisfactory limit cycle behavior, satisfactory operation is defined as a limit cycle in which θ_o (θ at $\dot\theta = 0$) is less than or equal to zero, that is, the limit cycle represented by the dotted line. If $\theta_o \geq 0$ as for the solid line, it is desirable to increase the pulse duration to reduce the pulsing frequency.

The circuit illustrated by the block diagram of figure G7 will accomplish this objective. Referring to the CW resistojet, a quantity $\Delta = \theta_o - \theta$ is calculated continuously. This output goes to a switching network which passes a signal only if $\Delta \geq \theta_c$. The output from the switching network erases a memory circuit as shown. The memory is activated by a signal to pulse the CW resistojet. The signal from the memory passes through a fixed time delay to an "and" circuit. The signal for pulsing the resistojet also passes to this "and" circuit.
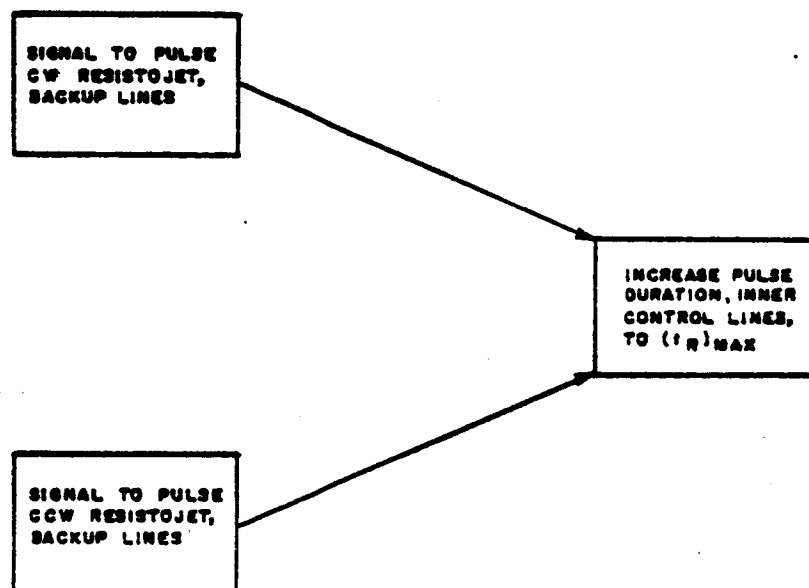
Figure 65   INCREASE IN FIXED PULSE DURATION TO (t_R) MAX
IF CONTROL JUMPS TO BACKUP LINES
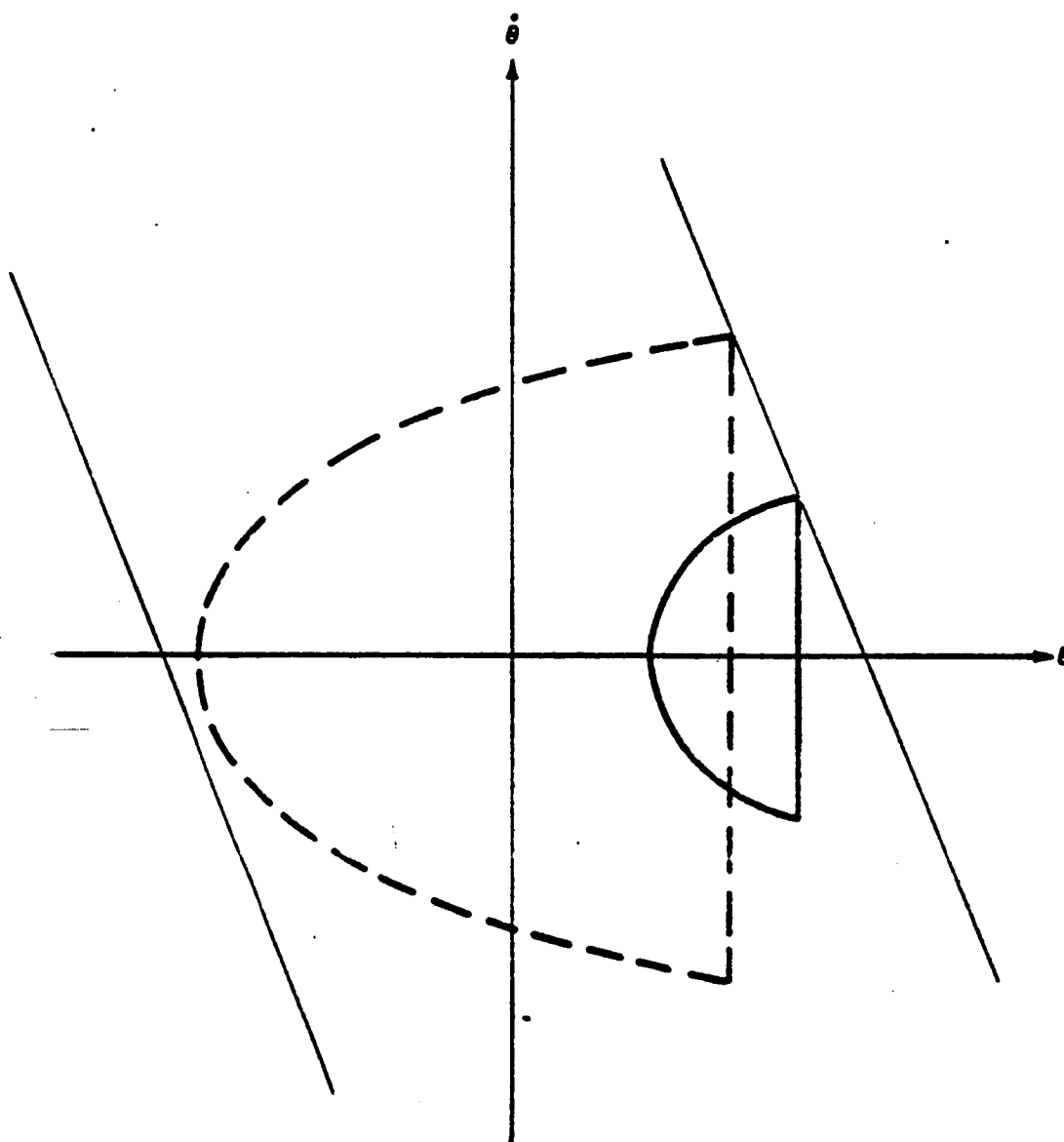
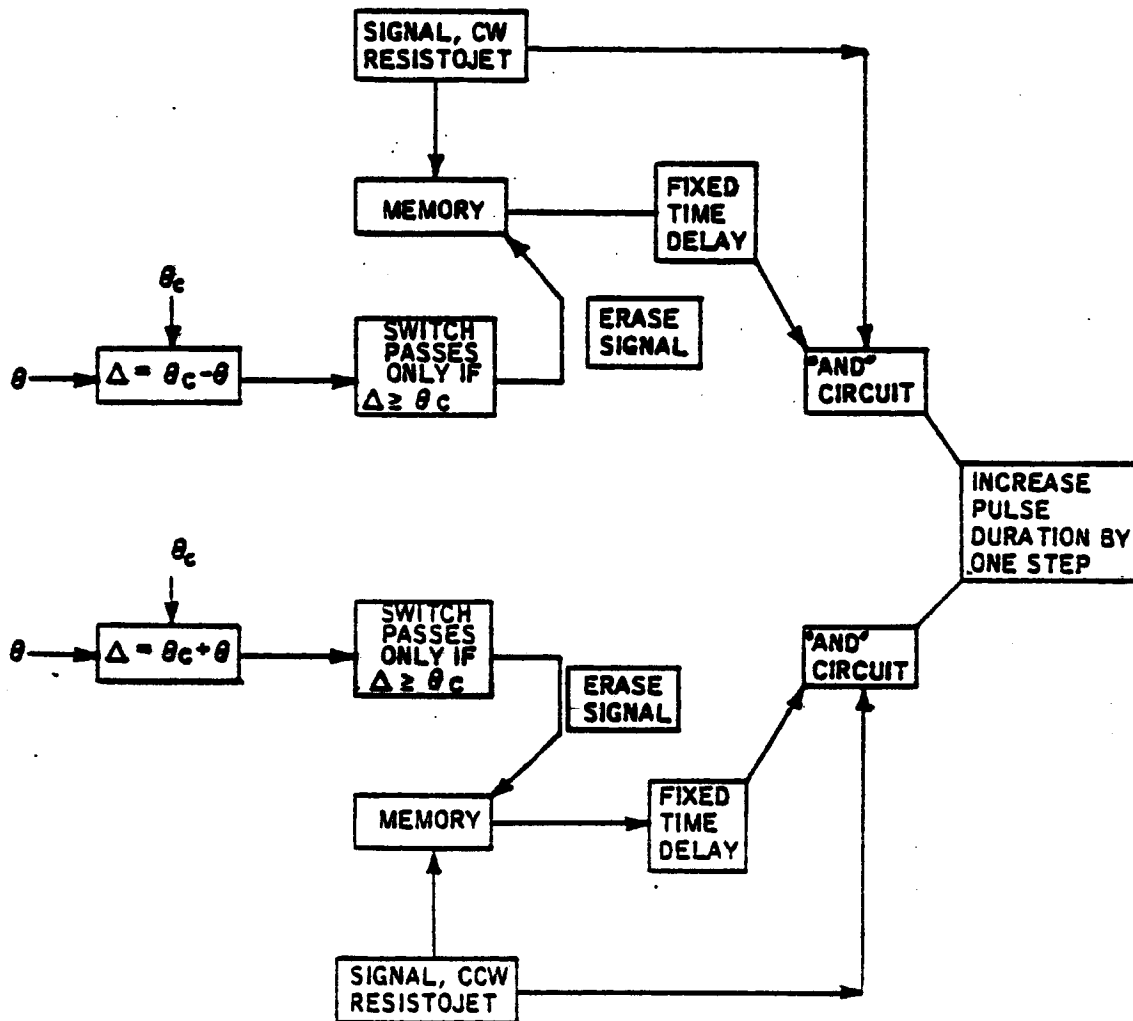Figure G6 SKETCH ILLUSTRATING SOFT LIMIT-CYCLE OPERATION WITH LOW- AND HIGH-PULSING RATES

65-8217

Figure G7 LOGIC FOR INCREASING PULSE DURATION IN SOFT LIMIT-CYCLE
OPERATION TO REDUCE PULSING RATE

If both signals are received simultaneously by this circuit, the pulse duration is increased by one step. Suppose now, the memory is vacant and the CW resistojet pulses ($\theta = \theta_c$, $\Delta = 0$). The memory is activated. After the preset time delay, the "and" circuit is activated by the signal from the memory. The disturbance torque decreases θ thereby increasing Δ. If Δ does not exceed θ_c during the cycle, the memory stays activated and the next signal to pulse the CW resistojet increases the pulse duration by one step. If Δ does exceed θ_c, the memory is erased, the succeeding signal to pulse the CW resistojet cannot pass the "and" circuit, and the pulse duration remains constant. The CCW resistojet operates as above except $\Delta = \theta_c + \theta$.

The stepwise increase in pulse duration cannot be too large; otherwise, the system will be thrown into hard limit cycle operation. It can be shown that θ_c is given by the following relation:

$$\theta_c - \theta_0 = \frac{1}{8} \frac{(\tau_R - \tau_D)^2}{J \tau_D} t_R^2 \tag{G4}$$

Let

t_{R1} = pulse duration when $\theta_0 = 0$

t_{R2} = pulse duration when $\theta_0 = -\theta_c$

Then;

$$\frac{\theta_c}{2\theta_c} = \frac{(t_{R1})^2}{(t_{R2})^2} \tag{G5}$$

or:

$$\frac{t_{R2}}{t_{R1}} = \sqrt{2} \tag{G6}$$

This represents the maximum ratio by which the pulse duration should be increased with the criterion used above for increasing the pulse duration when $\Delta \geq \theta_c$.

3.   SELECTION OF THE CONTROL TORQUE LEVEL

As discussed previously, the attitude control system design should be based on the estimated maximum possible disturbance torque which the satellite could ever encounter. A necessary condition on the control torque is therefore:

$$\tau_R > (\tau_D)_{max} \tag{G7}$$

A system with a control torque just slightly greater than the disturbance torque would not function in a satisfactory fashion however. Consider the sketch of figure G8 . The system drifts with a given disturbance torque, τ_D, across the control line to point (a) as shown. At point (a) the resistojet is either pulsed on for a preset time duration producing an impulse bit (inner control lines for the Model I and II systems) or pulsed on continuously until the system is driven back across the control line (backup lines for the Model I and II systems). In either case, the path followed in the phase plane plot during the time of thrust application is strongly dependent on the difference between the control torque, τ_R, and the disturbance torque, τ_D; the angular acceleration is given by:

$$\frac{d^2\theta}{dt^2} = -\frac{\tau_R - \tau_D}{J}$$ (G8)

Referring to the figure G8 now, if $\tau_R = \tau_D$, the system will follow the path (a) to (b) and the angular error will continue to increase at a constant rate of rotation. If τ_R is only slightly greater than τ_D, the rate of rotation will decrease only slightly with time, and, for continuous thrust, the system will follow the path (a) to (c). Since the control line should be set so that $\pm \theta_{co}$ is only slightly less than the allowable angular error, the allowable error will obviously be exceeded when the control torque is only slightly greater than the disturbance torque. The control torque should thus be set at some level considerably in excess of the maximum expected disturbance torque.

As the control torque is further increased relative to the disturbance torque, a value is reached where the slope in the phase plane initially after thrust start-up is equal to the slope of the control line and the path (a) to (d) is followed. For very large control torques, the path followed will essentially be an almost vertical line on the phase plane plot as represented by the path (a) to (e).

It is suggested that a reasonable criterion for the minimum control torque is given by the condition that the slope in the phase plane of the path followed by the system immediately after thrust is turned on must be equal to the slope of the control line. A relation for the minimum control torque based on this criterion will now be derived. Integrating equation (G8) with $\dot{\theta} = d\theta/dt$ and $\dot{\theta} = \dot{\theta}_1$ at $t = 0$ gives:

$$\dot{\theta} - \dot{\theta}_1 = -\frac{\tau_R - \tau_D}{J} t$$ (G9)

Now,
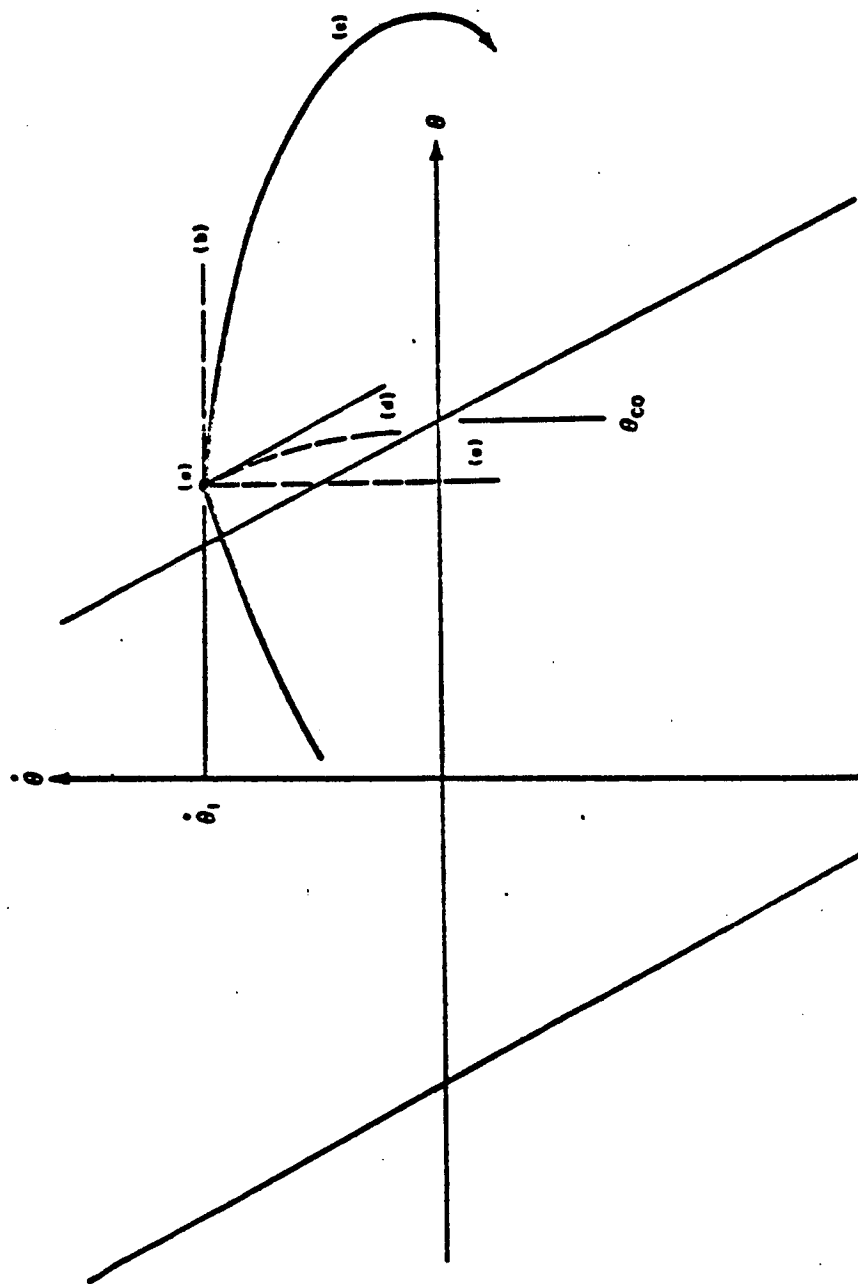
$$\frac{d\dot{\theta}}{d\theta} = \frac{d\dot{\theta}}{dt} \cdot \frac{dt}{d\theta} = \frac{1}{\dot{\theta}} \frac{d\dot{\theta}}{dt}$$ (G10)

Figure G8 SKETCH ILLUSTRATING PHASE PLANE PATHS FOLLOWED FOR DIFFERENT CONTROL TORQUE LEVELS

68-828

Substituting and letting $t = 0$ gives the slope in the phase plane of the path followed by the satellite at the moment thrust is turned on:

$$\left(\frac{d\dot{\theta}}{d\theta}\right)_{t=0} = -\frac{\tau_R - \tau_D}{J \dot{\theta}_1} \tag{G11}$$

A relation for $\dot{\theta}_1$ must now be derived. This relation is based on the maximum value of $\dot{\theta}_1$ for a soft limit cycle which occurs when the impulse delivered is sufficient to just drive the system to the opposite control line as illustrated in figure G9.

Integrating equation (G8) from (2) to (1) with $\tau_R = 0$ and neglecting the small difference between θ_1 and θ_{co} gives:

$$\frac{d\theta}{dt} = \frac{\tau_D}{J} t \tag{G12}$$

$$\theta + \theta_{co} = \frac{\tau_D}{2J} t^2 \tag{G13}$$

When $\theta = +\theta_{co}$, $t = t_c$ and, from (G13):

$$t_c = 2\sqrt{\frac{\theta_{co} J}{\tau_D}} \tag{G14}$$

Substitution of this relation into (G12) gives:
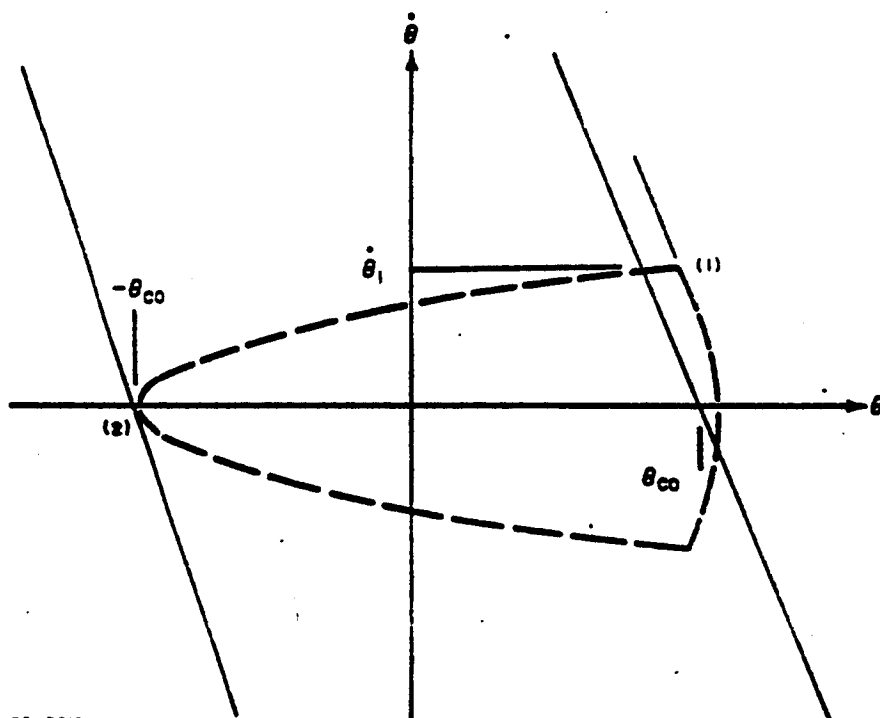
$$\dot{\theta}_1 = 2\sqrt{\frac{\theta_{co} \tau_D}{J}} \tag{G15}$$

Substitution into equation (G11) and setting:

$$\left(\frac{d\dot{\theta}}{d\theta}\right)_{t=0} = -\frac{1}{(a-1)\tau_L} \tag{G16}$$

where $\dfrac{1}{(a-1)\tau_L}$ is the control line slope gives:

$$\tau_R = \tau_D \left[1 + \frac{2\sqrt{\dfrac{\theta_{co} J}{\tau_D}}}{(a-1)\tau_L} \right] \tag{G17}$$

63-8219

Figure G9 ILLUSTRATION OF SOFT LIMIT CYCLE WITH MAXIMUM IMPULSE

With $(r_D)_{max}$ representing the estimated maximum possible disturbance torque, the permissible criterion for the minimum limit of r_R, the control torque, is:

$$r_R \geq (r_D)_{max} \left[1 + \frac{2 \sqrt{\dfrac{\theta_{co} J}{(r_D)_{max}}}}{(a-1) r_L} \right] \tag{G18}$$

As an illustration, for the Model I system:

θ_{co} = 0.2°

J = 27 slug ft^2 = 3.66 x 10^8 gmm cm^2

a = 10

r_L = 2 seconds

Substitution gives:

$$r_R \gtrsim [(r_D)_{max} + 125.8 \sqrt{(r_D)_{max}}] \tag{G19}$$

With $(r_D)_{max}$ of 1600 dyne cm,

$r_R \geq$ 6630 dyne cm

The resistojets supplied to NASA Lewis have a nominal thrust of 0.3 x 10^{-3} pounds which with a moment arm of two feet provides a control torque of 8130 dyne cm and thus meets the criterion of equation (G18).

The maximum control torque will be based on the basic assumptions that an adaptive control system is used and that limit cycle control is maintained by fixed pulse duration operation of the resistojets. The criterion is based on maintaining soft limit cycle control down to some minimum disturbance torque, $(r_D)_{min}$, below which it is satisfactory for hard limit cycle operation to occur. This maximum control torque is directly dependent on the minimum pulse duration built into the control logic, $(r_R)_{min}$. In the 2nd Quarterly Progress Report, it is shown that the criterion for definite soft limit cycle operation is:

$$r_R r_R \leq 2 \sqrt{r_D \theta_{co} J} \tag{G20}$$

Setting:

$$\tau_R = (\tau_R)_{max}$$

$$\tau_R = (\tau_R)_{min}$$

$$\tau_D = (\tau_D)_{min}^{SL}$$

Equation, (D.20) becomes:

$$(\tau_R)_{min} \; (\tau_R)_{max} \leq 2 \sqrt{\theta_{co} \, J \, (\tau_D)_{min}^{SL}} \tag{G21}$$

As an example, with $J = 27$ slug ft^2

$$(\tau_D)_{min}^{SL} = 10 \text{ dyne-cm}$$

$$\theta_{co} = 0.2°$$

$$(\tau_R)_{min} = 0.1 \text{ seconds}$$

the value for $(\tau_R)_{max}$ is computed to be:

$$(\tau_R)_{max} = 286000 \text{ dyne-cm}$$

In summary, the control torque selected for attitude control should lie within the range:

$$\left\{ (\tau_D)_{max} \left[1 + \frac{2\sqrt{\dfrac{\theta_{co} \, J}{(\tau_D)_{max}}}}{(a-1)\,\tau_L} \right] \right\} \leq \tau_R \leq \left\{ \frac{2}{(\tau_R)_{min}} \sqrt{\theta_{co} \, J \, (\tau_D)_{min}^{SL}} \right\} \tag{G22}$$

Within this range, other factors must be considered before a final desired value of the control torque is selected. Among these are the desire to use the same thrustors for despinning, acquisition, and station keeping as well as for attitude control and the desire to operate the resistojet under conditions of pressure, heater diameter, and nozzle configuration and dimensions which give a high specific impulse. These factors and their interrelationship can be considered quantitatively only when a specific satellite and mission are being considered.

APPENDIX H

CELESTIAL SIMULATOR AND TEST RANGE (ASTROLAB)

A celestial simulator or Astrolab is presently under construction at Avco RAD as part of an internally funded program. The purpose of the laboratory will be to evaluate complete spacecraft guidance and control systems. The basic laboratory is shown in figure H1.

Referring to figure H1 the attitude control system to be evaluated will be placed on the internal air bearing table. The table and air bearing are, in turn, located within a vacuum chamber. The attitude control system located on the air bearing table will include: (1) power supply and power conditioning equipment; (2) a reaction system, including propellant storage and feed; (3) control logic package; (4) sensors; and (5) signal conditioning equipment. The test range is 30 feet long and will contain a planet simulator, a star simulator, and a solar simulator. The combination of the three-axis air bearing, vacuum chamber, and celestial simulator will thus permit realistic evaluation of complete attitude control systems.

Figure H1 AVCO RAD CELESTIAL SIMULATOR AND ILS1 RANGE (ASTROLAB)

SK-10333

ASTRO LABORATORY